Contract No:

This document was prepared in conjunction with work accomplished under Contract No. DE-AC09-08SR22470 with the U.S. Department of Energy (DOE) Office of Environmental Management (EM).

Disclaimer:

Solid Secondary Waste Data Package Supporting Hanford Integrated Disposal Facility Performance Assessment

G. P. Flach

D. I. Kaplan

R. L. Nichols

R. R. Seitz

R. J. Serne

May 2016

SRNL-STI-2016-00175, Revision 0

DISCLAIMER

Printed in the United States of America

Prepared for
U.S. Department of Energy

SRNL-STI-2016-00175
Revision 0

Keywords: *PA*
SSW

Retention: *Permanent*

Solid Secondary Waste Data Package Supporting Hanford Integrated Disposal Facility Performance Assessment

G. P. Flach
D. I. Kaplan
R. L. Nichols
R. R. Seitz
R. J. Serne

May 2016

Prepared for the U.S. Department of Energy under contract number DE-AC09-08SR22470.

Savannah River National Laboratory™
OPERATED BY SAVANNAH RIVER NUCLEAR SOLUTIONS

REVIEWS AND APPROVALS

AUTHORS:

G. P. Flach, Environmental Modeling Date

D. I. Kaplan, Environmental Sciences & Biotechnology Date

R. L. Nichols, Geosciences Date

R. R. Seitz, Environmental Modeling Date

R. J. Serne, Pacific Northwest National Laboratory Date

TECHNICAL REVIEW:

W. P. Kubilius, Engineering Process Development, Reviewed per E7 2.60 Date

K. L. Dixon, Geosciences, Reviewed per E7 2.60 Date

D. Li, Environmental Sciences & Biotechnology, Reviewed per E7 2.60 Date

G. P. Flach, Environmental Modeling, Reviewed per E7 2.60 Date

R. J. Serne, Pacific Northwest National Laboratory, Reviewed per E7 2.60 Date

APPROVAL:

_____

D. A. Crowley, Manager Date
Environmental Modeling

_____

J. J. Mayer II, Manager Date
Environmental Sciences & Biotechnology

_____

T. O. Oliver, Manager Date
Geosciences

_____

K. M. Kostelnik, Manager Date
Environmental Restoration Technology

_____

D. J. Swanberg, Manager Date
Technology Maturation and Analysis, Chief Technology Office, Washington River Protection Solutions

This page intentionally left blank

EXECUTIVE SUMMARY

This data package provides recommendations for waste form physical and chemical properties to support the initial analysis of Solid Secondary Waste (SSW) disposals in the 2017 Integrated Disposal Facility (IDF) Performance Assessment (PA). At this time, specific formulations have not been identified for cementitious materials that will be used to encapsulate or solidify SSW, and no IDF-specific experiments were conducted to obtain data for the PA. Thus recommended property values are provided for a range of candidate materials, and based on a review of existing literature.

Four key SSW streams were identified for emphasis due to expected inventories for contaminants of potential concern (COPC): HEPA filters, ion exchange resins, carbon adsorber beds and Ag-mordenite. Based on current disposal plans, compacted HEPA filters were considered as an encapsulated waste form and the other three key waste streams were assumed to be blended and solidified in a cementitious matrix. Considerations for alternative disposal methods were also addressed. The IDF PA team identified specific COPCs expected to be the key contributors for the PA calculations: Tc-99, I-129, Cs-137, Sr-90, uranium isotopes (and total uranium), chromium, mercury and nitrate. These species are the focus of this data package.

The data package includes recommended inputs for the physical properties of the cured cementitious materials (e.g., saturated hydraulic conductivity, bulk density, porosity, moisture characteristic curves), assumptions governing the release of contaminants of concern from the key waste streams, and properties associated with mass transport of the contaminants of concern through the cured cementitious materials (e.g., distribution coefficients, solubility, diffusion coefficients). As would be expected, there were differing amounts of information available for specific input parameters for the different candidate disposal mixes. Variability in the information gathered represents uncertainty due to measurement error, variability from multiple samples using a given mix, and differences in properties associated with different mixes. Depending on available information, some recommendations are provided in the form of best estimates and statistical distributions, others are provided in the form of best estimates with a range of potential values, and others may be addressed based on simplifying assumptions and expert judgment. Collectively the recommendations are representative of the available data and some will need to be confirmed or modified to reflect information specific to the actual mixes that are selected for IDF waste forms.

Developing distributions and recommended values, even with the uncertainty regarding the mix formulations, serves to provide the recommended values in a form that facilitates the development and implementation of the uncertainty and sensitivity analysis tools for the initial stages of the 2017 IDF PA. Sensitivity and uncertainty analyses based on these initial recommendations can be used to gain insights into assumptions and uncertainties that are significant for the conclusions of the PA. This, in turn, provides the ability to identify the range of acceptable conditions and also identify critical areas where refined, mix- and waste form-specific, information is needed to support future iterations of the PA. These insights can guide selection of mixes and prioritize the needs for further specific laboratory or field studies. Initial modeling using this representative data can also be used to identify less sensitive parameters for which further study may be less important and specifications for mixes and waste forms can be more flexible, which will be expected to be beneficial for operations.

ACKNOWLEDGEMENTS

The authors acknowledge the support of Washington River Protection Solutions (WRPS), especially the programmatic and technical support of Dave Swanberg and Paul Cavanah for oversight of the efforts. The work benefitted significantly from active engagement and reviews from the team responsible for preparation of the Integrated Disposal Facility performance assessment. This included Pat Lee (WRPS technical lead) and Bob Andrews, Mick Apted, Randy Arthur, Benoit Paris and Rainer Senger of INTERA. Internal technical checking and reviews for Savannah River National Laboratory were provided by Walt Kubilius, Ken Dixon and Dien Li. The PNNL Letter Report was checked by Wooyong Um. These reviews and inputs were critical during development, but the authors maintain responsibility for the final content of the report.

TABLE OF CONTENTS

LIST OF TABLES

LIST OF FIGURES

LIST OF ABBREVIATIONS

BFS	Blast Furnace Slag
CH-TRU	Contact Handled Transuranic
CSH	Calcium-silicate-hydrate
CSP IX	Clean Salt Processing Ion Exchange
EIS	Environmental Impact Statement
ETF	Effluent Treatment Facility
FA	Fly ash
FFTF	Fast Flux Test Facility
GAC	Granular Activated Carbon
HEPA	High Efficiency Particulate Air
HICs	High Integrity Containers
HTWOS	Hanford Tank Waste Operations Simulator
IDF	Integrated Disposal Facility
ILAW	Immobilized Low-Activity Waste
IX Resin	Ion Exchange Resin
LERF	Liquid Effluent Retention Facility
LLW	Low-Level Waste
MLLW	Mixed Low-Level Waste
OPC	ordinary portland cement
PA	Performance Assessment
RF	Resorcinol-formaldehyde
SALDS	State Approved Land Disposal Site
SRNL	Savannah River National Laboratory
SSW	Solid Secondary Waste
TC&WM	Tank Closure and Waste Management
WAC	Waste Acceptance Criteria
WMA	Waste Management Area
WRAP	Waste Receiving and Processing
WTP	Waste Treatment and Immobilization Plant
XAS	X-ray Absorption Spectroscopy

This page intentionally left blank

1.0 Introduction

This data package addresses solid secondary waste (SSW) destined for disposal at the Integrated Disposal Facility (IDF) located in the 200 East Area at the Hanford Site. Construction of the IDF was undertaken based on a Performance Assessment (PA) performed in 2001 (DOE/ORP-2000-24, *Hanford Immobilized Low-Activity Waste Performance Assessment: 2001 Version*) (ILAW PA). A draft update to the ILAW PA was completed in 2005, but was not finalized. This data package supports the development of an updated PA (referred to as the "2017 IDF PA") that will be used as part of the documentation for the initiation of operations for the IDF.

Data needs that are the focus of this data package were identified based on experience from the 2001 ILAW PA, the draft 2005 PA, and development of conceptual models and modeling approaches to be applied for the current PA. Interactions with the IDF PA team, including development of the inventory data package, have helped to focus detailed efforts for this data package on a few key waste streams, contaminants of concern, and disposal configurations that are expected to be the primary contributors to the dose resulting from SSW disposed at the IDF.

The key waste streams include: High Efficiency Particulate Air (HEPA) filters, ion exchange resins, granular activated carbon, and Ag-mordenite. The key parameters include: initial saturation, saturated hydraulic conductivity and moisture characteristic curves, effective diffusion coefficient, distribution coefficient (K_d), dry bulk density, porosity, and compressive strength. The IDF PA team also identified a set of key contaminants that are expected to be the primary concern for the PA calculations: Tc-99, I-129, Cs-137, Sr-90, uranium isotopes (and total uranium), chromium, mercury and nitrate. These contaminants are the focus of this data package. Other contaminants would be expected to be screened or addressed in a more generic manner. A document was prepared with a proposed modeling approach for the 2017 IDF PA (Lehman et al., 2015). Considerations for cementitious materials are summarized below.

1.1 Use of this data package

The mix specification(s) and final disposal configuration for SSW have not been identified at this time. This data package was developed using available information from existing studies of cementitious materials considered representative of mixes that may be used for SSW encapsulation and/or solidification. No waste form-specific laboratory or field studies were conducted to support this data package. Thus, information is provided in a form that considers uncertainty due to measurement error, variability from multiple samples using a given mix, and differences in properties associated with different mixes. The intent is for the data to support the initial PA calculations for insights on the properties required for the different SSW rather than to recommend specific mixes for the different wastes at this time.

As would be expected, there were differing amounts of available information for specific input parameters for the different mixes. Depending on available information, some data are provided in the form of best estimates and statistical distributions, others are provided in the form of best estimates with a range of potential values, and others may be addressed based on assumptions. Developing the distributions serves to provide the recommended values in a form that facilitates the development and implementation of the uncertainty and sensitivity analysis tools for the initial stages of the 2017 IDF PA. The distributions are representative of the available data and will need to be modified to reflect the actual mixes that are selected.

Although there are limitations, the use of representative data, including uncertainties, provides a means to gain insights into assumptions and uncertainties that are significant for the conclusions of the PA. This, in turn, provides the ability to identify the range of acceptable conditions and also identify critical areas

where refined, mix- and waste form-specific, information is needed to support future iterations of the PA. These insights can guide selection of mixes and prioritize the needs for further specific laboratory or field studies. Initial modeling using this representative data can also be used to identify less sensitive parameters for which further study may be less important and specifications for mixes and waste forms can be more flexible, which will be expected to be beneficial for operations.

1.2 Quality Assurance

The work for this data package is conducted under Savannah River National Laboratory (SRNL) procedures associated with development of information to support PAs. These procedures address documentation and review requirements, including checking and documentation of any calculations. Requirements for performing reviews of technical reports and the extent of review are established in manual E7 2.60. SRNL documents the extent and type of review using the SRNL Technical Report Design Checklist contained in WSRC-IM-2002-00011, Rev. 2. SRNL contributors to the data package were also trained by INTERA on modeling quality assurance requirements for Washington River Protection Solutions.

2.0 Integrated Disposal Facility

The IDF is a near surface disposal facility for low-level (LLW) and mixed low-level radioactive waste (MLLW). The design includes two adjacent expandable cells, each including a double liner with leachate collection and removal, and a leak detection system (see Figure 2-1). All SSW is expected to be containerized prior to disposal and no distinction is made between modeling of LLW and MLLW cementitious waste forms. Glass waste forms are also expected to be segregated from other waste forms to avoid potential concerns with chemical influences of leachate from cementitious materials on potential releases from glass materials. During operations, as each layer of waste is disposed, the containers will be uncovered for a period of time before the leveling backfill is placed over and around the waste packages as a base for the next layer of waste. The data provided in this document are primarily taken from experiments with intact and unaged test specimens. Potential near-term (operations) and long-term (post closure) FEPs that could influence the properties of SSW are also introduced, but specific data for these conditions have not been included.

The choice of backfill will have an influence on the conditions around the waste containers, which can impact aging of the waste forms and the rate of eventual releases from the waste forms. It is assumed that the backfill will be a flow-able material that will fill voids between containers. Hydraulically, the fill will also be expected to facilitate drainage of excess water between containers before the cover is in place. There will be potential for limited moisture accumulation on the top of containers. After the cover is placed, recharge beneath the cover will be very low and the backfill is expected to maintain low moisture contents between the containers consistent with assumed recharge rates that will increase over the long term. The backfill is also expected to have similar geochemistry to the Hanford sediments.

The IDF is planned to receive waste from a variety of operations on the Hanford site (Prindiville 2016, RPP-ENV-58562). The Hanford Waste Treatment and Immobilization Plant (WTP) will be a major generator of waste to be disposed including:

- Immobilized Low-Activity Waste (ILAW) glass
- Low-Activity Waste (LAW) melters
- Solid Secondary Waste
- Effluent Treatment Facility (ETF)-generated SSW.

Additional generators for waste to be disposed at the IDF include:

- Fast Flux Test Facility (FFTF) decommissioning waste
- Secondary Waste Management LLW and MLLW
- Onsite Non-*Comprehensive Environmental Response, Compensation, and Liability Act of 1980* non-tank LLW and MLLW.

More specific information regarding assumptions for the SSW that is the subject of this data package is provided in Section 3.0.

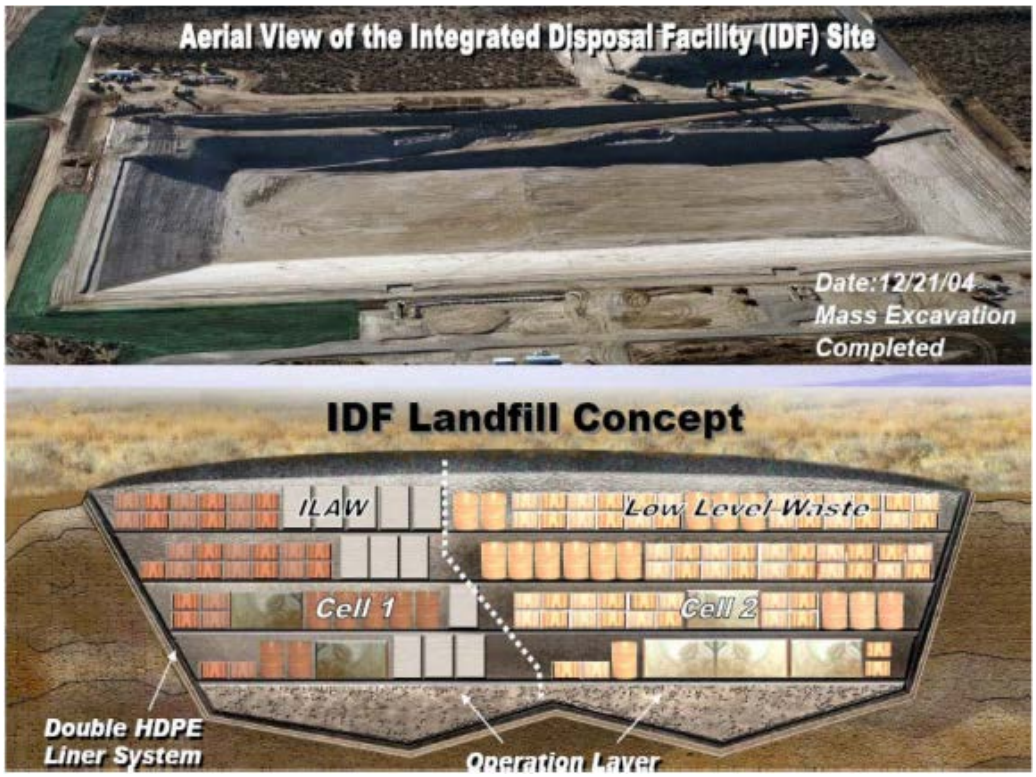

Figure 2-1. Integrated Disposal Facility and example configuration for waste placement (Figure from "Integrated Disposal Facility Performance Assessment Plan," TOC-PRES-14-4880 (Eberlein and Aly, Presented November 18, 2014).

2.1 Performance Assessment considerations

The waste acceptance criteria (WAC) for the IDF must address a number of considerations, including the need to limit potential long-term waste releases to levels that are protective of human health and the environment. DOE Manual 435.1-1, *Radioactive Waste Management*, includes the requirement to conduct a PA to demonstrate the ability to meet performance objectives and to support development of numerical WAC that identify the acceptable concentrations and total activity/mass of contaminants of potential concern to be disposed. A PA uses integrated numerical models, representing the waste forms and engineered and natural systems, to evaluate the long-term performance of the disposal facility. This data package is focused on the information necessary to support the assessment of the SSW forms. A companion data package (Cantrell et al. 2016) addresses the liquid secondary waste that will be disposed at IDF.

During the time since the 2001 ILAW PA, the mission for the IDF has changed; the mission has been expanded from only accepting ILAW glass to include previously mentioned waste forms from WTP operations and other non-WTP waste forms. The non-glass waste forms are the focus of this data package. The non-glass waste streams are expected to rely on cementitious materials for encapsulation and solidification of the waste forms. Cementitious materials are used extensively for waste disposal in the United States and around the world. The literature review in support of this data package included experiences with waste forms and PA modeling approaches for multiple disposal facilities in the United States and in several other countries.

2.1.1 General PA considerations

A PA requires input data specific to the natural and engineered systems. This data package includes the data to support calculations specific to the SSW forms to be disposed at the IDF. Thus, specific emphasis is placed on components of the engineered system, primarily the containers and waste forms. As described above, the broader engineered system has some influence on waste form modeling (e.g., recharge rates, moisture content, local geochemistry). These factors will be considered as part of the basis for this data package, but the primary emphasis will be on the material properties of the SSW waste forms.

Cementitious materials are often used as engineered barriers in waste disposal and other facilities as a means to contain the radioactive waste and/or to limit the migration of radionuclides into the accessible environment. One common form of barrier is the cementitious material as the waste form, that is, the waste is intimately mingled with the cementitious material. Another common form is that of containment, something intended to isolate the waste from the environment, such as a container or a vault. In this form, the waste is segregated from the cementitious material used as a barrier. In either case, the release of radioactive waste can be controlled as a function of initial material properties and barrier dimensions, and the rate at which the cementitious material is assumed to degrade and lose its effectiveness as a chemical and physical barrier.

"Degrade" is often used synonymously with "aging", however, aging does not always result in degraded performance. There are two aspects to be considered in aging, the effect on hydraulic properties and the effect on chemical properties. The timing and extent of the effects of aging is difficult to quantify. In order to take credit for the benefits of cementitious materials in a PA or PA-like analysis, it is necessary to have models and data sufficient to stand up to external reviews. This concern regarding the need to be able to stand up to external scrutiny has often resulted in overly-conservative assumptions being made regarding barrier degradation. Although expedient in the short-term, such approaches can result in more costly or over-restrictive decisions being made. The intent of this data package is to identify aging processes that are expected to impact and not impact long term performance of the SSW forms.

2.1.2 Example considerations for modeling cementitious materials

Modeling of the performance of cementitious materials for very long time frames in support of LLW disposal PAs has been a topic of specific interest for many years. For example, in the late 1980s and 1990s, the US NRC sponsored research directed at leaching of radionuclides from cementitious waste forms (McConnell et al. 1997) and modeling the evolution and performance of cementitious barriers (e.g., Seitz and Walton 1992, Walton et al. 1990). These earlier studies focused on specific mechanisms of aging of cementitious materials and approaches to model intact and degraded cementitious materials for PAs.

A number of specific activities have been undertaken to provide recommendations and improve the modeling of cementitious materials since that time. For example, NRC Staff published NUREG-1573, "A Performance Assessment Methodology for Low-Level Waste Disposal Facilities – Recommendations of NRC's Performance Assessment Working Group" (NRC 2000). The NUREG is not a regulatory document and is not binding, but does reflect NRC Staff perspectives on acceptable approaches and provides insight into expectations for a PA. The performance of engineered barriers was flagged as one of five key issues in the document.

Section 3.3.4 of NUREG-1573 includes more detailed suggestions for addressing performance of engineered barriers. The importance of addressing interactions between different materials is emphasized along with verification of construction quality. Section 3.3.4.4 includes additional information about addressing performance of engineered barriers. The emphasis of the suggestions is on general

characteristics to be considered for intact, degrading and degraded performance (e.g., need to address cracking when considering hydraulic conductivity of a cementitious barrier).

NRC Staff also prepared Draft Final NUREG-1854 in 2007, "NRC Staff Guidance for Activities Related to U.S. Department of Energy Waste Determinations". NUREG-1854 includes recommendations for reviews of PAs conducted for Section 3116 issues. Engineered barriers are addressed in Section 4.3.2 of NUREG-1854. The importance of redox conditions and pH in terms of chemical performance are highlights, but it is also recommended to address the potential impacts of physical changes in a cementitious barrier and the associated impacts on changes in a barrier's effectiveness from a chemical perspective. NRC Staff also refer to NUREG-1573 as a source of information and similar to NUREG-1573, re-emphasized the importance of considering interactions of different materials and also construction quality. Sections 4.3.2.2 and 4.3.3.2 of NUREG-1854 include relatively detailed lists of review considerations for assessments of engineered barriers and source terms. The lists include considerations related to confirming dimensions, functionality expected for barriers (e.g., safety functions), construction methods and materials, assumptions regarding durability, chemical performance and changes in pore water chemistry, waste and barrier compatibility, basis for assumptions, etc.

2.1.3 Performance Assessments for the IDF

The IDF has been addressed in a few modeling efforts leading up to the 2017 IDF PA. The most recent efforts include a draft IDF PA in 2005 and the IDF was also addressed in the *Final Tank Closure and Waste Management Environmental Impact Statement for the Hanford Site, Richland, Washington* (EIS) (DOE 2012). In these analyses, releases from cementitious waste forms were assumed to be controlled by diffusion through the cementitious material. The EIS addressed the potential for aging of the cementitious materials by introducing a factor of about 60 increase in the diffusion coefficient for a degraded waste form.

The proposed modeling approach for the 2017 IDF PA was documented in Lehman et al. (2015). This document served as a starting point to identify the modeling approaches and it was noted that the approaches were expected to evolve as the effort progressed. The glass and cementitious materials waste forms are assumed to be placed in containers or waste packages. Although the containers and waste packages may delay the time before which aqueous solutions may come into contact with the waste forms and hence delay the initiation of waste form degradation and release, the PA is not expected to credit delays resulting from the presence of the containers or waste packages beyond the 100 years of institutional control. However, the potential effect of these features on the near field chemical environment will be considered.

Radionuclide and non-radionuclide release mechanisms from the source are assumed to be generally controlled by the degradation rate of the waste form and diffusion into the pore water in the backfill and waste form. Subsequent fluxes into the subsurface are controlled by advection through the backfill and vadose zone. Alternative release scenarios will be evaluated depending on the results of waste form testing summarized in the glass and cementitious materials data packages.

For the near-field environment (i.e., the region in the disposal facility that includes the waste package and surrounding backfill where coupled chemical and hydrologic processes may affect the alteration and release of contaminants to the aqueous phase), reactive chemistry may, as needed, be simulated to ascertain chemical interactions and to determine how the chemical interactions may affect release rates. A distribution coefficient (K_d) approach may be used to simplify these interactions, once the reactive chemistry analyses have been completed.

Within the facility, the characteristics of the release may include considerations such as chemical reactivity, solubility limited control, corrosion rates of activated metals, advective release and diffusion limited control of radionuclides from solid form. Kinetic controls resulting from dual domain porosity represent another mechanism possibly controlling contaminant release, but the complexity of incorporating these controls into the modeling will necessitate abstraction of the results of such detailed models using appropriate boundary conditions and simpler representations for use in the Performance Assessment. These controls generally result in a diffusive-type release of contaminants contained in pore water that is not located in advection flow paths but that still shares a hydraulic connection to pore water in those paths. The waste material itself and any actions taken to stabilize it, such as grouting, will be examined in the near-field to ascertain whether chemical reactivity is sufficient to warrant more complex release modeling.

3.0 Waste description

The waste streams for the 2017 IDF PA are summarized in RPP-ENV-58738 (Lee 2015) and described in detail in the IDF PA inventory data package, RPP-ENV-58562 (Prindiville 2016). Figure 3-1 provides perspective regarding the different waste streams resulting from operations of the WTP and ETF and the SSW that will be treated and disposed at IDF. For the purposes of the PA, SSW is generally classified into two categories: debris waste (defined in Washington Administrative Code section 173- 303-040 as waste with a particle size greater than 60 mm) and non-debris waste (waste with a particle size less than or equal to 60 mm).

Non-debris waste includes small particulates that can potentially be blended into the cementitious material (e.g., ion exchange resins, granular activated carbon). Debris includes larger materials (e.g., components, filters, etc.) that will be encapsulated in a cementitious material. Figure 3-2 is an example of encapsulation of supercompacted waste drums that may be representative of management of HEPA filters. Modeling approaches to address the option to encapsulate non-debris waste is also addressed in this data package, given that there are examples where dewatered resins are placed into a container without being blended in a cementitious material. Note that there also may be an option to shred filter media into a form that could be disposed as a solidified waste form after blending with a cementitious material. However, the current assumptions for waste volumes and concentrations assume that the filters are supercompacted and encapsulated. Although this is the current assumption, this data package is prepared generally to recognize the different options available to address different waste streams.

The wastes identified in Figure 3-1 have also been categorized based on the concentrations of key contaminants. As noted previously, the IDF PA team has identified the key waste streams that are the focus of this data package: HEPA filters, granular activated carbon, ion exchange resins and Ag-mordenite. These waste streams are planned to be addressed using specific assumptions identified in this data package. Other waste streams are considered lower activity source terms that can be modeled using a more generic approach that will also be described.

3.1 Disposed configurations considered in the PA

In the context of a PA, the terms solidification and encapsulation are used to represent two basic configuration of the disposed waste (Figure 3-3). Solidification may be applied for “non-debris” waste of particulate size that would be mixed into a grout or other solidification media. In this case the properties of the waste form will represent the integrated mixture of waste and solidification media (e.g., ion exchange resins blended in a cementitious matrix). Encapsulation can be applied for waste (may be debris or non-debris) with major voids filled by a clean encapsulating media and a specified thickness of encapsulating media completely surrounding the waste. In the case of resins, the dewatered resins may also be placed into a container made of cementitious materials. The necessary thickness of the encapsulating media around the waste would be determined in an iterative manner based on results of the PA.

The solidification and encapsulation media are selected to limit the release of contaminants into the disposal environment. Cementitious materials offer beneficial physical properties (e.g., low hydraulic conductivity) and geochemical properties (e.g., sorption). The mixes used for the cementitious materials can also be supplemented to enhance the physical or chemical properties (e.g., blast furnace slag). From the perspective of input data for the PA, material properties for the final waste form using a generally applicable formulation can be identified for the encapsulating media, because it is not mixed with the waste stream. For a stabilized waste stream, the input data may depend to some extent on the specific waste mixed with the stabilization media.

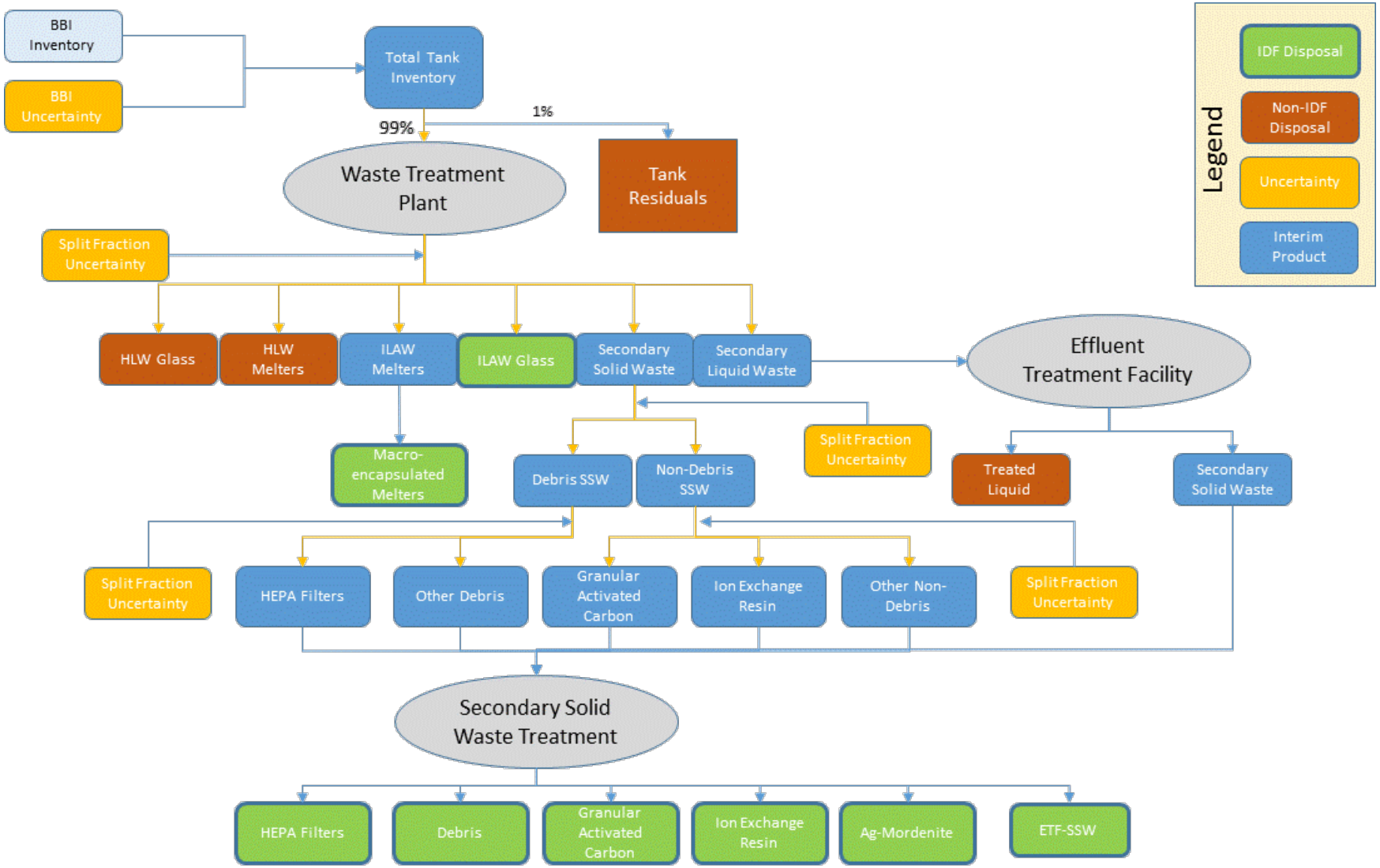

Figure 3-1. WTP and ETF wastes and resulting wastes from SSW treatment.

Figure 3-2. Example of supercompacted drums encapsulated in a cementitious material.

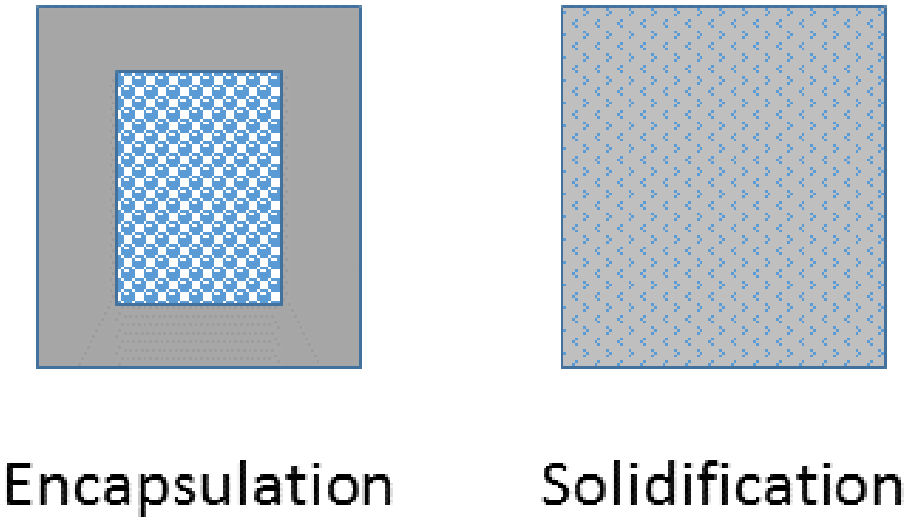

Figure 3-3. Simplified illustration of encapsulation and solidification.

It is expected that debris waste will be encapsulated using a standard disposal grout formulation. The exact formulation is still being investigated but mixtures containing water, ordinary portland cement (OPC), blast furnace slag (BFS), fly ash (FA), and/or aggregate are being considered. It is expected that non-debris waste will be solidified using a dry blend mix of ordinary portland cement, BFS, and/or lime mixed with water. The water to dry blend ratio is expected to 0.4 to 0.6. The addition of grout additives (also known as "getters") to enhance the retention of the more mobile constituents (e.g., technetium and iodine) is also being investigated by Qafoku et al. (2015) in the context of cementitious waste forms for liquid secondary waste.

For PA modeling, encapsulation would potentially include consideration of release/partitioning from the waste form to pore water (reflecting the retention properties of the waste stream) and then migration through the clean media (e.g., diffusion). Solidified waste forms would involve consideration of release/partitioning from the waste stream into the pore solution of the stabilization media and migration through the solidification media (i.e., release/partitioning from the waste stream would be dependent on the solidification media). If solidification is selected, the effects on the retention capability of the waste stream will need to be addressed (e.g., ion exchange resins or activated carbon). For example, changes in the pore solution passing through the cementitious material could also influence the retention capability of the waste stream.

3.2 IDF SSW streams

RPP-ENV-58738 provided a consolidated summary of the waste streams and initial proposals for potential disposal methods. The latest information on plans for waste treatment and disposal are addressed in the Inventory Data Package (RPP-ENV-58562, Prindiville 2016). Summaries for different waste streams from the Inventory Data Package are included here for information.

3.2.1 WTP operations

SSW is generated as the result of WTP operations. It includes low-level and mixed low-level radioactive debris and non-debris waste such as melter consumables, failed process components, analytical laboratory waste, spent resins, spent carbon adsorbent, HEPA filters, and other process-related waste. Compared to other WTP SSW, the spent resins, spent carbon adsorbers, Ag-mordenite, and HEPA filters are expected to contain proportionally higher radionuclide inventories. These MLLW streams will require different treatment methods (based on contaminant types and levels) to meet Land Disposal Restrictions requirements prior to disposal at IDF. All SSW deemed as LLW would be packaged and stabilized (grouted) or compacted prior to being disposed of at IDF.

3.2.2 ETF-generated SSW

The ETF-generated SSW results from treating secondary liquid waste from the 242-A evaporator, the retrieval of CH-TRU tanks, and from WTP operations, which includes low-level and mixed low-level liquid effluent from the melter primary off-gas treatment system, the LAW vitrification secondary off-gas/vessel vent treatment system, process vessel washes, floor drains, sumps, and vessel vent header drains. In addition, liquid waste from Pretreatment Facility sources such as the radioactive liquid disposal vessels and tanks including process condensates from evaporators, caustic waste from the LAW caustic scrubber, and spent reagents from the resin addition process would be routed to the Liquid Effluent Retention Facility (LERF)/ETF for treatment (Bechtel 2013, 24590-WTP-RPT-PT-02-005 Rev. 7). For analysis purposes, these waste streams were assumed to be representative of the ETF-generated SSW to be disposed at IDF[1]. These SSW resulting from ETF are addressed in Cantrell et al. (2016).

[1] Although leachate from the Mixed Waste Trench and other miscellaneous sources are planned for disposal at IDF as part of ETF SSW, the expected concentrations and associated volumes are assumed insignificant compared to the

The current ETF treatment process is similar to the process that existed when the Tank Closure and Waste Management (TC&WM) EIS analysis was performed. Therefore, the differences in the fraction of mobile radionuclides such as ^{99}Tc and ^{129}I that volatilize and are captured in the liquid off-gas system and ultimately end up in the ETF-generated SSW is primarily due to changes in the inventory estimate and changes in the handling of recycle streams at WTP. The earlier HTWOS model that was used in the TC&WM EIS had a simple recycle scheme for the LAW melter off-gas (Figure D-8 in WRPS (2009), RPP-17152, Rev. 1). The more recent model (Figure C-15 in WRPS (2015), RPP-17152, Rev. 12) recycles liquid effluents to more locations for more effective management of the effluents.

After treatment at the ETF, the liquid portion of the treated waste stream would be disposed of at the State-Approved Land Disposal Site (SALDS) while the byproduct waste generated from the ETF solidification process would be packaged and disposed of at the IDF as ETF-generated secondary solid waste. This waste stream originating from the WTP operations is often referred to as WTP secondary liquid waste.

The high temperatures associated with the LAW vitrification process could cause volatilization of mobile radionuclides such as ^{99}Tc and ^{129}I that would not be captured in the liquid off-gas treatment system and would ultimately end up in ETF-generated secondary solid waste. Since the fraction of these constituents ending up in the final waste form is difficult to predict, a wide range of glass retentions have been proposed to test the limits of ^{99}Tc and ^{129}I loadings in cementitious waste forms against established waste form performance characteristics.

3.2.3 FFTF decommissioning waste

In accordance with the *TC&WM EIS ROD* (78 FR 75913), DOE selected FFTF Alternative 2 Entombment, which would remove all above-grade structures, including the reactor building. Below-grade structures would remain in place and be filled with grout to immobilize the remaining radioactive and hazardous constituents, then covered with a RCRA-compliant barrier. The FFTF-generated SSW under the Entombment Alternative includes:

- Any demolition waste from the main Reactor Containment Building and Buildings 491E and 491W that cannot be consolidated in below-grade spaces
- All radioactive and hazardous materials from other ancillary buildings
- The reactor vessel, piping systems, and tanks (drained to the extent practicable of liquid sodium) that would not fit in below-grade spaces
- Solid waste resulting from waste processing

3.2.4 Waste management LLW and MLLW

Secondary waste from general operations includes workers' personal protective equipment, tools, and other contaminated materials from tank farm operations, as well as:

- Secondary LLW and MLLW from operation of LLBG 218-W-5, trenches 31 and 34
- Secondary LLW and MLLW from operation of the Waste Receiving and Processing Facility (WRAP)
- Secondary LLW and MLLW from operation of the T Plant complex.

contributions from WTP. Additionally, IDF leachate contributions are not included to avoid double counting of inventory in the 2017 IDF PA analysis.

3.2.5 Onsite non-CERCLA non-tank LLW and MLLW

Onsite non-CERCLA non-tank LLW and MLLW includes waste from onsite generators such as the Central Waste Complex, Plutonium Finishing Plant, T Plant complex, Waste Encapsulation and Storage Facility, WRAP, groundwater sampling activities, Pacific Northwest National Laboratory, Cold Vacuum Drying Facility, Canister Storage Building, and Liquid Waste Processing Facilities (LERF, ETF, State Approved Land Disposal Sites, and Treated Effluent Disposal Facility).

3.3 Specific waste streams addressed in this data package

Four specific wastes streams were identified by the IDF PA team for consideration in this data package: Granular Activated Carbon (Carbon Adsorber Beds), Ion Exchange Resin (IX Resin), HEPA Filters, and Ag-mordenite. For the purposes of this PA, a generic category of waste is added to capture all debris waste to be disposed at IDF. Each of these wastes is summarized in the following subsections based on descriptions in the IDF Inventory Data Package and other sources.

3.3.1 Carbon adsorber beds

SSW inventory data from the Hanford Tank Waste Operations Simulator shows that the LAW Melter spent adsorber beds and Ag-mordenite (see below) are major contributors of ^{129}I. The carbon adsorber beds are part of the LAW off-gas treatment system and contain activated carbon for mercury and halide (F, Hg) removal as well as ^{129}I abatement. Carbon adsorber beds are considered non-debris MLLW, which from a treatment perspective, contain potentially problematic amounts of Hg and ^{129}I. Although treatment may remove some of the hazard, the conservative recommendation for disposition of this waste is to dispose of it at IDF. The beds would be transported to a local offsite treatment facility where they would be repackaged into suitable disposal containers with a stabilization grout for RCRA metals and Category 3 radioactive waste containment using a Hanford approved grout formulation that meets regulatory criteria.

The option to consider the carbon adsorber beds as an encapsulated waste form not blended in a cementitious matrix is also addressed.

3.3.2 Ion exchange resin

Ion exchange resins and HEPA filters (see next section) are the largest sources of ^{99}Tc for SSW. After being dewatered at WTP, the IX resins (Category 3 non-debris MLLW) would be transported in High Integrity Containers (HICs) offsite for treatment. At the treatment facility, the resin would be repackaged into suitable disposal containers blended with a stabilization grout for RCRA metals and Category 3 radioactive waste containment using a Hanford approved grout formulation meeting regulatory criteria.

The option to consider the ion exchange resins as an encapsulated waste form not blended in a cementitious matrix is also addressed.

3.3.3 HEPA filters

The current assumption is that non-woven glass paper (borosilicate microfiber) HEPA filters would be used and they could be either MLLW or LLW debris depending on their location/function within the WTP facility. All HEPA filters (both Category 1 and Category 3) are expected to be sent to an offsite treatment facility in carbon steel 55-gallon drums where they will be compacted into “pucks” at an approximated compaction ratio ranging from 5:1 to 10:1. Multiple pucks would be placed into suitable disposal boxes and macroencapsulated with grout to meet LDR requirements for RCRA constituents[2].

[2] The work authorization process implemented at the treatment facility determines the allowable number of pucks based on waste stream characterization information provided by the waste generator at the time of shipment to the treatment facility. Disposal

This macroencapsulation process would meet Category 3 stabilization requirements, which exceeds Category 1 requirements making this latter categorization irrelevant.

3.3.4 Ag-mordenite cartridges

Silver impregnated adsorbers (e.g., mordenite) are designed to capture Iodine from off gas systems, and thus, similar to the carbon adsorbers can be one of the primary sources of Iodine in the IDF inventory. The Ag-mordenite waste stream is expected to be non-debris MLLW similar to the carbon adsorber beds, and may include problematic concentrations of Hg and ^{129}I. Although treatment may remove some of the hazard, the conservative recommendation at this time is to assume disposal at IDF without removal of COPCs. The Ag-mordenite would be transported to a local offsite treatment facility where they would be repackaged into suitable disposal containers blended with a stabilization grout for RCRA metals and Category 3 radioactive waste containment using a Hanford approved grout formulation that meets regulatory criteria.

3.3.5 Other debris SSW

For the purposes of this data package, "other debris SSW" includes all "debris" SSW except for HEPA Filters. Debris streams will undergo some type of volume reduction via compaction/supercompaction, sorting, and repackaging at an offsite treatment facility prior to disposal at the IDF (Prindiville 2016). The WTP secondary waste forecast suggests that more than a third of the debris is compactible debris. Approximately 25% of the projected waste is compactible, Category 1 LLW that is expected to have a higher compaction ratio than Category 3 MLLW, but also have lower concentrations prior to compaction. As a result, these waste streams may become somewhat more concentrated at the time of disposal, however, the treatment facility will not generate waste streams that exceed the Waste Acceptance Criteria (WAC) limits at the IDF (i.e., greater-than-Category 3). It is assumed that, after treatment, the debris will be encapsulated in grout and releases will be controlled by the properties of the grout.

box limits (after drums are compacted into pucks at a compaction ratio of approximately 10:1) are closely managed such that Category 3 limits are not exceeded.

4.0 IDF Performance Assessment modeling context

Subsurface moisture flow and solute transport modeling of SSW disposal will be performed as part of the overall IDF PA (Lee 2015, Lehman et al. 2015). Cementitious materials used for SSW waste encapsulation and/or solidification are expected to be explicitly considered in modeling, while external carbon steel and similar limited service-life containers involved in the operational treatment and transport of waste forms will be ignored beyond an institutional control period. For encapsulated debris SSW, the PA is also expected to consider an embedded waste zone with distinct material properties. Contaminant release from SSW waste forms to the natural environment will occur primarily via aqueous transport processes for the radionuclide and chemical species of interest identified in the project work plan: ^{99}Tc, ^{129}I, ^{137}Cs, ^{90}Sr, uranium isotopes (and total U), Cr, Hg and nitrate. The processes affecting liquid phase transport considered here are advection, diffusion, sorption and solubility control. The purpose of this section is to identify the class of flow and transport governing equations and associated parameters that are supported by this data package. Recommended material property values are provided in Sections 6.0 through 8.0 for the relevant encapsulation and solidification cementitious materials, and treated (e.g. compacted) debris SSW materials. Also discussed are the expected post-closure environmental conditions to which SSW waste will be exposed, in preparation for an assessment of initial saturation conditions in Section 9.0 and long-term evolution / degradation of initial material properties in Section 10.0.

4.1 Moisture flow

In the absence of osmotic and gas-phase effects on liquid flow, the pore water flux in an unsaturated and/or saturated porous medium is commonly computed from Darcy's law, written here in one-dimensional form for the vertical direction z as

$$U = -k_r[S(p_c)]K_s\frac{\partial h}{\partial z} \quad (1)$$

where

U = volumetric liquid flux or Darcy "velocity" [L/T]

k_r = relative permeability (function of saturation) [-]

S = liquid saturation [L^3 liquid / L^3 void]

p_c = capillary tension head [L]

K_s = saturated hydraulic conductivity [L/T]

h = hydraulic head [L].

Hydraulic head is defined by

$$h \equiv P/\rho g + z \quad (2)$$

where

P = liquid pressure [F/L^2]

ρ = liquid density [M/L^3]

g = gravitational acceleration [L/T^2]

z = vertical coordinate [L]

Hydraulic head gradient accounts for moisture flow driven by pressure gradients and/or gravitational body forces. Saturation is a function of capillary tension head, which is defined by

$$p_c \equiv -P/\rho g \tag{3}$$

Note from Equations (2) and (3) that

$$h = -p_c + z \tag{4}$$

The porosity of a porous medium is the fraction of the total volume that is void of solid phase material [L^3 void / L^3]:

$$n \equiv \frac{V_v}{V} \tag{5}$$

Saturation in Equation (1) is the fraction of the void space occupied by water (or pore solution) [L^3 liquid / L^3 void]:

$$S \equiv \frac{V_w}{V_v} \tag{6}$$

Moisture content is the fraction of the total volume occupied by water [L^3 liquid / L^3]:

$$\theta \equiv \frac{V_w}{V} = \frac{V_w}{V_v}\frac{V_v}{V} = Sn \tag{7}$$

A differential water balance is

$$\frac{\partial Sn}{\partial t} = -\frac{\partial U}{\partial z} \tag{8}$$

rate of water accumulation = net water influx

Combining Darcy's law from Equation (1) with this mass balance yields a one-dimensional form of Richards (1931) equation:

$$\frac{\partial Sn}{\partial t} = \frac{\partial}{\partial z}\left[k_r K_s \frac{\partial h}{\partial z}\right] \tag{9}$$

The present data package supports porous-medium flow modeling using Equation (9) or equivalent governing equation for moisture flow, for example, the STOMP code in single-phase liquid mode.

The required inputs to Richards equation are

- Total porosity, n (for transient flow analysis)
- Saturated hydraulic conductivity, K_s

- Relative permeability function, $k_r(S)$
- Water retention function, $S(p_c = -h + z)$

The most commonly-used relative permeability and water retention curves are the van Genuchten (1980) / Mualem (1976) functions, which are defined in terms of an "effective saturation"

$$S_e \equiv \frac{S - S_r}{1 - S_r} = \frac{\theta - \theta_r}{\theta_s - \theta_r} \tag{10}$$

where $\theta_s = n$ and the subscripts "r" and "s" denote residual and full saturation conditions respectively. The van Genuchten (1980) / Mualem (1976) functions are

$$S_e = \left[\frac{1}{1 + (\alpha p_c)^{n_{vG}}}\right]^{m_{vG}} \tag{11}$$

and

$$k_r = S_e^L \left[1 - \left(1 - S_e^{1/m_{vG}}\right)^{m_{vG}}\right]^2 \tag{12}$$

where L = 0.5. The input parameters to Equations (10) through (12) number four: θ_r, α [L^{-1}], n_{vG} and m_{vG}. In some cases, L = 0.5 and the conceptual constraint $\theta_s = n$ are relaxed for improved fitting of water retention data, which increases the number of moisture characteristic curve inputs to six. However, a common assumption is

$$m_{vG} = 1 - 1/n_{vG} \tag{13}$$

and this equation together with $L = 1/2$ and $\theta_s = n$ reduce the required inputs to three independent parameters: θ_r, α and n_{vG}. In this three parameter case, residual saturation defines the maximum amount of pore water that can be drained through capillary suction. The α parameter defines the air-entry pressure, the minimum tension needed to lower liquid saturation below 100%. The n_{vG} parameter defines how sharply relative permeability declines after liquid tension exceeds the air entry pressure.

This data package supports moisture flow modeling within SSW waste forms using Richards equation coupled with van Genuchten / Mualem characteristic curves. Recommended values for n, K_s, θ_r, θ_s, α, n_{vG}, m_{vG} and L are developed in Section 6.0.

4.2 Solute transport

Solute transport in a porous medium may occur through advection and/or diffusion. Multiple formulations and terms have been used in the literature to describe diffusion in porous media, often in an incomplete or ambiguous manner, which has led to considerable confusion. For that reason, parameter definitions and terms are carefully presented in this data package using conventions similar to Walton (1992). Note that an equally valid but different set of terms is used by Cantrell et al. (2016). This SSW data package supports advective-diffusive transport of solutes in situations where chemical interactions can be reasonably approximated by linear instantaneous sorption and/or instantaneous solubility control.

The advective flux of a solute is

$$j = Uc \tag{14}$$

where

j = solute flux [mol/L^{2}T]

U = volumetric water flux or Darcy velocity [L/T]

c = solute concentration [mol/L^3]

The one-dimensional form of Fick's law for molecular diffusion of a dilute solute in a quiescent pool of water assuming no inter-ion interactions is

$$j = -D_m \frac{\partial c}{\partial x} \tag{15}$$

where

j = solute flux [mol/L^{2}T]

D_m = molecular diffusion coefficient [L^2/T]

c = solute concentration [mol/L^3]

Fick's law in a saturated porous medium is

$$j = -D_i \frac{\partial c}{\partial x} \tag{16}$$

where

D_i = "intrinsic" diffusion coefficient [L^2/T]

Both diffusion coefficients are empirical factors defined by experimental measurements. The intrinsic diffusion coefficient D_i is significantly smaller than D_m due to multiple porous medium effects. One effect is that only a portion of the porous medium is occupied by water, such that the cross-sectional area available for aqueous diffusion is proportional to porosity n. This area reduction effect can be explicitly represented in Fick's law by decomposing D_i into the product

$$D_i \equiv nD_e \tag{17}$$

which defines "effective" diffusion coefficient D_e for the porous medium. Equation (16) becomes

$$j = -nD_e \frac{\partial c}{\partial x} \tag{18}$$

The effective diffusion coefficient is smaller than D_m because of additional porous medium effects. In open water, diffusion occurs along a straight-line path between two points. In a porous medium, solute diffusion occurs over longer, tortuous, paths through the microstructure. Furthermore, sufficiently narrow

pore throats can constrict solute passage. Tortuosity, constrictivity and any other unaccounted for physical effects of the porous medium are commonly combined into a lumped factor $\tau < 1$ defined by

$$D_e \equiv \tau D_m \tag{19}$$

This dimensionless lumped parameter τ is typically referred to as "tortuosity" or "tortuosity factor" for brevity. Combining Equations (17) and (19) yields

$$D_i = nD_e = n\tau D_m \tag{20}$$

Equation (20) can be extended to unsaturated media by replacing porosity with water content $\theta \equiv Sn$ and assuming that the tortuosity factor does not vary significantly with saturation within the range of interest:

$$D_i = Sn\tau D_m \tag{21}$$

More generally tortuosity can be made a function of saturation when the departure from saturated conditions is larger.

A one-dimensional differential species mass balance using Equations (14), (16) and (21) is

$$\frac{\partial Snc}{\partial t} + \frac{\partial (1-n)\rho_s c_s}{\partial t} = -\frac{\partial}{\partial x}\left[Uc - Sn\tau D_m \frac{\partial c}{\partial x}\right] \tag{22}$$

rate of solute accumulation + rate of species accumulation in the solid phase
= net advective influx of solute + net diffusive influx of solute

where

ρ_s = mass density of the solid phase [M/L^3]

c_s = species concentration in the solid phase [mol/M]

Under the assumption of linear instantaneous sorption, c_s is defined in terms of solute concentration through a distribution coefficient K_d [L^3/M]:

$$c_s \equiv K_d c \tag{23}$$

Combining Equations (22) and (23) and assuming constant properties yields

$$\frac{\partial c}{\partial t} Sn\left[1 + \frac{(1-n)\rho_s K_d}{Sn}\right] = -\frac{\partial Uc}{\partial x} + Sn\tau D_m \frac{\partial^2 c}{\partial x^2} \tag{24}$$

The quantity

$$R \equiv \left[1 + \frac{(1-n)\rho_s K_d}{Sn}\right] \tag{25}$$

known as the "retardation factor", is the ratio of total species mass to solute mass (R = 1 for a nonsorbing species). Combining Equations (24) and (25) and incorporating pore velocity

$$v \equiv \frac{U}{Sn} \tag{26}$$

reduces the species mass balance to

$$R\frac{\partial c}{\partial t} = -\frac{\partial vc}{\partial x} + D_e\frac{\partial^2 c}{\partial x^2} \tag{27}$$

The required inputs to this advection-diffusion-sorption equation are a flow field (v) and

- Effective diffusion coefficient, D_e (=τD_m)
- Porosity, n (to compute R)
- Solid phase density, ρ_s (to compute R)
- Species-specific sorption coefficient, K_d (to compute R)

If solubility control is implemented via the constraint

$$c \leq c_{sol} \tag{28}$$

where c_{sol} is an empirical constant, then c_{sol} is also a required input (species-specific). Sections 7.0 and 8.0 provide recommended values for D_e, K_d, and where applicable c_{sol}, for SSW cementitious and debris waste materials and these chemical species: Tc, I, Cs, Sr, U, Cr, Hg and nitrate.

4.3 Environmental conditions

Sections 6.0 through 8.0 develop recommended input parameter values to support moisture flow and solute transport simulations at the beginning of the PA period following waste disposal operations and facility closure. An understanding of the environmental conditions to which SSW waste forms will be exposed is helpful toward assessing how certain initial parameter values may evolve throughout the PA assessment periods of 1000 years and beyond. Two environmental conditions of interest and discussed in this section are backfill soil tension and soil pore water chemistry.

An upper bound on backfill soil tension can be computed by assuming no surface recharge, that is, gravity equilibrium conditions. When volumetric moisture flow is zero, the hydraulic gradient must also be zero from Darcy's law (Equation (1)) and thus hydraulic head is uniform throughout the vadose zone. Assigning z = 0 to the water table and noting that capillary tension head is zero under saturated conditions implies h = 0 at the water table and thus throughout the unsaturated zone. From Equation (4) the capillary tension head at any position under gravity equilibrium conditions equals the height of the water table:

$$p_c = z \tag{29}$$

The thickness of the vadose zone beneath the IDF is approximately 100 meters or 10,000 cm (Yonkofski 2015, Section 7.2). Therefore the tension head in backfill surrounding SSW waste forms is expected to less than 10^4 cm.

Soil tension can be more accurately estimated by considering the recharge rate expected under post-closure conditions and soil hydraulic properties. Above the capillary fringe adjoining the water table capillary tension head becomes nearly constant (e.g. Wilson 1980 Figure 15, Nimmo et al. 2002 Figure 2), as shown in Figure 4-1 reproduced from Nimmo et al. (2002). Constant p_c implies a unit hydraulic head gradient from Equation (4):

$$\frac{\partial h}{\partial z} = 0 + \frac{\partial z}{\partial z} = 1 \tag{30}$$

From Darcy's law unsaturated hydraulic conductivity K is then equal to the recharge rate I

$$K(p_c) \equiv k_r K_s = -U \equiv I \tag{31}$$

provided $K_s \geq I$; otherwise $K = K_s$. Knowing the recharge rate I and unsaturated hydraulic conductivity function $K(p_c)$, one can back solve for the corresponding capillary tension p_c.

Yonkofski (2015) describes the natural system surrounding the IDF and summarizes recharge estimates and modeling assumptions from relevant studies. The design life of the planned IDF cover system extends to 500 years after facility closure. Most recently a post-closure recharge rate of 0.5 mm/yr through 500 years has been recommended for the Waste Management Area (WMA) C PA "Reference Case" (Yonkofski 2015, Table 6-6). After 500 years the recommended recharge is 1.0 mm/yr for the "Reference Case" and 3.5 mm/yr for "Sensitivity Case 1" (Yonkofski 2015, Table 6-6). A recharge rate of 1.0 mm/yr is assumed here for the purpose of estimating general soil conditions surrounding SSW waste forms. In terms of conventional hydraulic conductivity units, 1.0 mm/yr equals 3.2E-9 cm/s which is well below the saturated hydraulic conductivity of Hanford sediments ($K_s > I$).

Rockhold et al. (2015, Tables 4.9 and 6.6) provide recommended hydraulic properties for natural sediments beneath the Hanford site and IDF near-field engineered system materials; these recommended parameter values are presented in Table 4-1 for selected materials. Unsaturated hydraulic conductivity as a function of capillary tension head in the conventional units of cm/s is plotted in Figure 4-2(a) for native "Sand" and "Gravel" sequences, and "Low-Density Backfill", "High-Density Backfill" and generic "Concrete" materials in the IDF engineered system. Lower density backfill will likely fill space in between IDF waste forms within a waste layer, and higher density backfill will likely separate waste layers (Rockhold et al. 2015, p. 4.9). For the purpose of evaluating Equation (31), these curves are replotted in Figure 4-2(b) in the more convenient units of mm/yr. For each material, the tension head p_c satisfying Equation (31) is the point of intersection of the unsaturated conductivity curve $K(p_c)$ and the horizontal infiltration line I = 1.0 mm/yr. These points of intersection are 500 cm for the Sand sequence and 1200 cm for the Gravel sequence. Although not explicitly shown, the backfill curves intersect 1.0 mm/yr at suctions of roughly 200 and 400 cm. Hence, the post-closure tension head surrounding SSW waste forms is expected to lie well below the upper bound of 10,000 cm, much closer to 1000 cm or lower value.

The tension head range indicated above is specific to the assumed infiltration rate and vadose zone sediment properties. A change to infiltration and/or sediment properties will generally shift the range. For example, increasing the infiltration rate to 3.5 mm/yr (e.g. WMA C "Sensitivity Case 1") for the Hanford Sand and Gravel materials reduces tension head to the range 350 to 750 cm (or 140 to 300 cm for the two backfill materials).

Sulfate and magnesium attack, carbonation, chloride ingress and primary constituent (e.g. calcium) leaching are potential chemical degradation mechanisms of significance to IDF cementitious waste forms and encapsulation barriers (e.g. Pabalan et al. 2009, Samson et al. 2009). Table 4-2 summarizes chemical composition data from Hanford site groundwater (Napier et al. 2005) and vadose zone sediment samples (Thornton 1997, Serne et al. 2002, Napier et al. 2005). These data indicate an alkaline pore solution (pH ≈ 7.2, CO_3^{--} ≈ 400 mg/L ≈ 7 mmol/L) with ionic concentrations on the order of [SO_4^{--}] ≈ 200 mg/L (2 mmol/L), [Mg^{2+}] ≈ 50 mg/L (2 mmol/L) and [Cl^-] ≈ 25 mg/L (0.70 mmol/L).

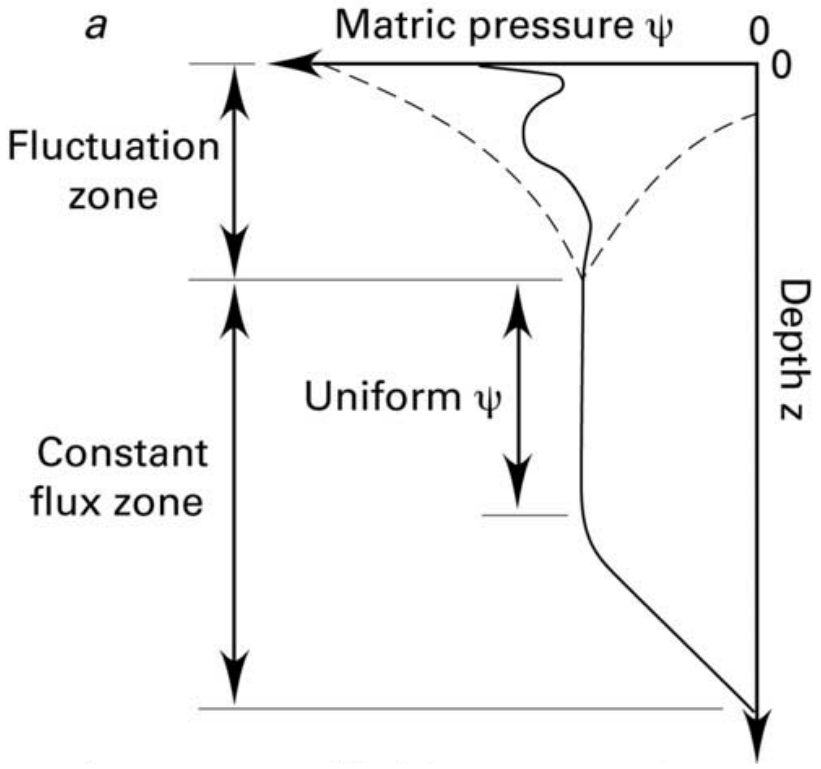

Figure 4-1. Schematic drawing reproduced from Nimmo et al. (2002) depicting zone of constant tension above the capillary fringe.

Table 4-1. Recommended hydraulic properties for selected IDF near-field materials from Rockhold et al. (2015, Tables 4.9 and 6.6).

Parameter	Sand Sequence (anisotropy = 1/3 case)	Gravel Sequence (anisotropy = 1/3 case)	Low-Density Backfill	High-Density Backfill	Concrete
Porosity, n (assumed = θ_s)	0.384	0.174	0.37	0.35	0.067
Saturated hydraulic conductivity, K_s (cm/s)	6.157e-3	7.714e-3	1.86e-2	4.91e-3	1.33e-9
Saturated water content, θ_s (cm^3 water / cm^3)	0.384	0.174	0.37	0.35	0.067
Residual water content, θ_r (cm^3 water / cm^3)	0.029	0.0038	0.03	0.03	0
van Genuchten / Mualem parameter, α_{vG} (1/cm)	0.06419	0.08859	0.057	0.065	3.87e-5
van Genuchten / Mualem parameter, n_{vG} (-)	1.698	1.271	2.8	1.7	1.29
van Genuchten / Mualem parameter, m_{vG} (-)	$1-1/n_{vG}$	$1-1/n_{vG}$	$1-1/n_{vG}$	$1-1/n_{vG}$	$1-1/n_{vG}$
van Genuchten / Mualem parameter, L (-)	0.375	-0.225	0.5	0.5	0.5

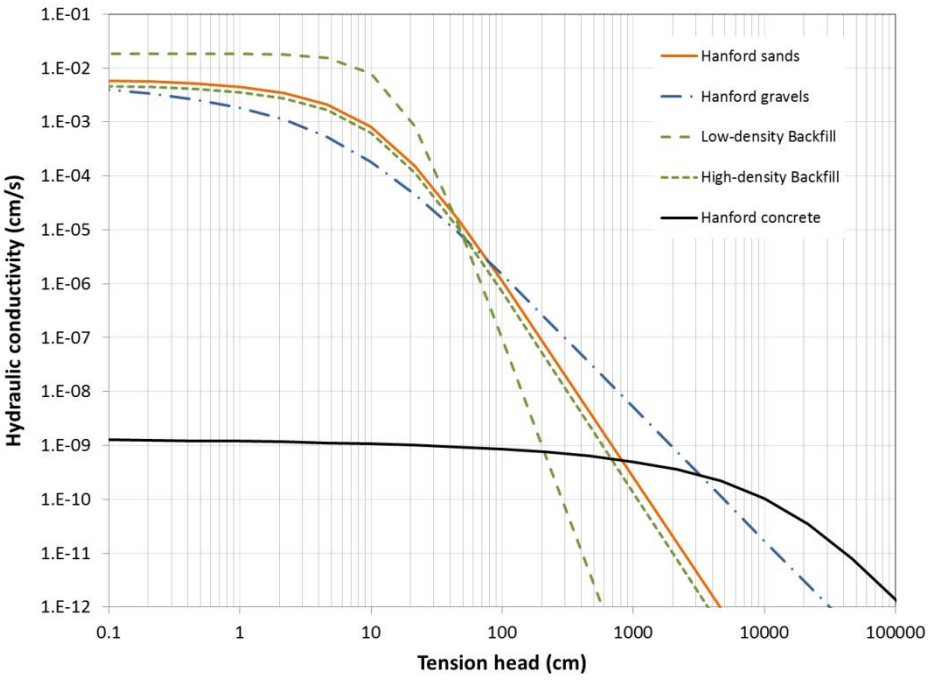

(a)

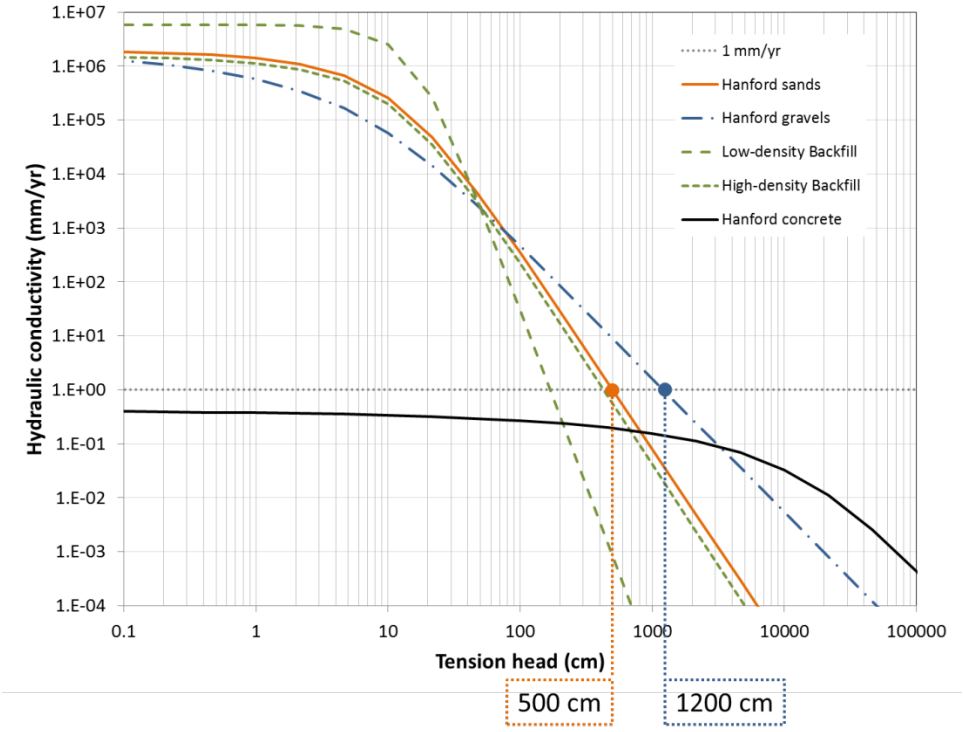

(b)

Figure 4-2. Hydraulic conductivity as a function of tension head for selected IDF near-field materials; (a) *K* in cm/s, (b) *K* in mm/yr.

Table 4-2. Chemical composition of Hanford groundwater and vadose zone moisture.

Sample	pH	CO_3^{--} (mg/L)	SO_4^{-} (mg/L)	Mg^{2+} (mg/L)	Cl^{-} (mg/L)	Reference
Hanford vadose zone based on C-018H disposal site characterization study	-	-	avg: 10.6	-	-	Thornton 1997 PNNL-11633 Section 2.3
Hanford site groundwater	8.43 Table 2.2	222.7 Table 2.4	79.75 Table 2.4	22 Table 2.6	20.07 Table 2.4	Napier et al. 2005 NUREG/CR-6881 PNNL-15244
Hanford site 1:1 soil:water extract	7.48 Table 2.15	2823 Table 2.17	54.63 Table 2.17	208 Table 2.19	<9.452 Table 2.17	Napier et al. 2005 NUREG/CR-6881 PNNL-15244
Clean borehole 299-W22-48	6.93 @ 91.5 ft bgs 7.25 @ 101.5 ft bgs Table 5.23‡	median: 423 range: 184 to 1058 Table 5.25†	median: 195 range: 30 to 493 Table 5.25†	median: 56 range: 13 to 168 Table 5.25†	median: 24 range: 3 to 117 Table 5.25†	Serne et al. 2002 PNNL-13757-1
Clean borehole 299-W22-50	7.21 @ 116 ft bgs 7.49 @ 140 ft bgs Table 5.46‡	median: 364 range: 122 to 1184 Table 5.48†	median: 217 range: 103 to 1163 Table 5.48†	median: 37 range:1 to 111 Table 5.48†	median: 20 range: 7 to 304 Table 5.48†	Serne et al. 2002 PNNL-13757-1

†Theoretically calculated composition of vadose-zone porewater (1:1 sediment-to-water extracts multiplied by dilution factor)
‡ Actual UFA extracted porewater

5.0 Interpretation of diffusion tests

Section 4.2 explicitly presented the diffusion coefficient definitions and terms used in this data package to avoid ambiguity, and confusion with alternative or conflicting parlance used in other literature. In a similar vein, the experimental methods used to measure diffusion coefficients and cited in this data package are discussed herein using the conventions for definitions, symbols and terms in Section 4.2.

5.1 Diffusion cell

A diffusion cell apparatus places the porous test sample between two fluid reservoirs (e.g. Ampadu et al. 1999 Figure 1). One-dimensional solute diffusion between the fluid cells is induced through a concentration and/or electrical gradient. After steady-state conditions are reached, the intrinsic diffusion coefficient D_i is determined using the equivalent of Equation (16) (e.g. Equation (1) in Delagrave 1998). Assuming saturated conditions, the effective diffusion coefficient D_e is computed by dividing by porosity n following Equation (17).

5.2 ANSI/ANS 16.1

The ANSI/ANS 16.1 method (ANSI/ANS-16.1-2003 reaffirmed 2008) places a uniformly-spiked porous test sample in a water bath. The leachant is periodically replaced at prescribed intervals to maintain a low solute concentration, and analyzed to determine the amount of species leached during each exposure period.

In the absence of advection, the general solute transport equation (Equation (27)) reduces to

$$\frac{\partial c}{\partial t} = \frac{D_e}{R}\frac{\partial^2 c}{\partial x^2} \tag{32}$$

The quotient factor can be replaced with an “apparent” diffusion coefficient defined as

$$D_a \equiv \frac{D_e}{R} \tag{33}$$

yielding

$$\frac{\partial c}{\partial t} = D_a\frac{\partial^2 c}{\partial x^2} \tag{34}$$

The adjective “apparent” calls out the fact that D_a is a lumped parameter representing both diffusion and sorption processes, not solely diffusion. Also, be aware that “apparent” diffusion coefficient in this data package is termed “effective” diffusion coefficient in ANSI/ANS 16.1.

The ANSI/ANS 16.1 data analysis method assumes that the leached zone within the porous specimen is thin compared to its overall geometry, such that the semi-infinite region solution to Equation (34) is an accurate representation of the diffusion process. Assuming a uniform initial concentration c_0 within the specimen and zero concentration at the exposed surface, Crank (1975, Equation (2.45)) gives the analytic solution to Equation (34) as

$$c = c_0 \mathrm{erfc}\left(\frac{x}{2\sqrt{D_a t}}\right) \tag{35}$$

where erfc(·) is the complementary error function. The solute flux at any position in the specimen can be computed from Equations (18) and (35):

$$j = -nD_e \frac{\partial c}{\partial x} = -nD_e c_0 \frac{\partial}{\partial x}\left[erfc\left(\frac{x}{2\sqrt{D_a t}}\right)\right] \tag{36}$$

Taking the derivative and using $D_e = RD_a$ from Equation (33):

$$\begin{aligned} j &= -nD_e c_0 \cdot \frac{2}{\sqrt{\pi}} \exp\left(\frac{-x^2}{4D_a t}\right) \cdot \frac{1}{2\sqrt{D_a t}} \\ &= -nc_0 RD_a \cdot \frac{2}{\sqrt{\pi}} \exp\left(\frac{-x^2}{4D_a t}\right) \cdot \frac{1}{2\sqrt{D_a t}} \\ &= -nc_0 R \cdot \sqrt{\frac{D_a}{\pi t}} \cdot \exp\left(\frac{-x^2}{4D_a t}\right) \end{aligned} \tag{37}$$

At the exposure surface x = 0, the solute flux is

$$j = -nc_0 R \cdot \sqrt{\frac{D_a}{\pi t}} \tag{38}$$

Figure 5-1 is an excerpt from the ANSI/ANS 16.1 procedure summarizing much of data analysis method and terminology; "a_n/A_0" is the fraction leached during interval "n". Toward reproducing Equation (1) in Figure 5-1, the following definitions are first adopted:

V = specimen volume [L^3]

A_s= specimen geometric surface area [L^2]

M = species leachable mass within the specimen [M]

The rate of change of species mass in the specimen is equal to the product of surface area and flux

$$\frac{dM}{dt} = A_s j = -Vnc_0 R \cdot \frac{A_s}{V} \cdot \sqrt{\frac{D_a}{\pi t}} = -M_0 \cdot \frac{A_s}{V} \cdot \sqrt{\frac{D_a}{\pi t}} \tag{39}$$

where M_0 is the initial species mass. Continuing

$$\frac{d(-M/M_0)}{dt} = \frac{A_s}{V} \cdot \sqrt{\frac{D_a}{\pi t}} \tag{40}$$

Solving for D_a yields

$$D_a = \pi \cdot \left[\frac{d(-M/M_0)}{dt}\right]^2 \cdot \left(\frac{V}{A_s}\right)^2 \cdot t \qquad (41)$$

Equation (41) is the differential equivalent of the discrete interval equation shown in Figure 5-1. This comparison clearly indicates that ANSI/ANS 16.1 leaching tests measure apparent diffusion as defined by Equation (33). That is, "effective" diffusion coefficient in ANSI/ANS 16.1 parlance is identical to effective diffusion coefficient divided by retardation factor using the terms of this data package. However, for a non-sorbing species (R = 1), the "effective" diffusion coefficients in both naming conventions are the same quantity.

$$D = \pi\left[\frac{a_n/A_o}{(\Delta t)_n}\right]^2\left[\frac{V}{S}\right]^2 T \ , \qquad (1)$$

where:

D is the effective diffusivity (cm^2/s);

V is the volume of specimen (cm^3);

S is the geometric surface area of the specimen as calculated from measured dimensions (cm^2);

T is the leaching time representing the "mean time" of the leaching interval (s) as follows:

$$T = [\tfrac{1}{2}(t_n^{1/2} + t_{n-1}^{1/2})]^2 \ . \qquad (2)$$

A_o is the total quantity of a given contaminant in the specimen at the beginning of the first leaching interval (i.e., after the initial 30-s rinse);

a_n is the quantity of a nuclide released from the specimen during leaching interval n, corrected for radioactive decay (see 3.2);

$(\Delta t)_n = t_n - t_{n-1}$ is the duration, of the n'th leaching interval (s).

Figure 5-1. Excerpt from the ANSI/ANS 16.1 procedure summarizing the data analysis method.

5.3 EPA-1315

The EPA-1315 leaching test is an enhancement of ANSI/ANS 16.1. The data analysis method is summarized in Figure 5-2. Although not obvious from superficial comparison of Figure 5-1 and Figure 5-2, the ANSI/ANS 16.1 and EPA-1315 data calculations can be shown to be functionally equivalent by integrating Equation (39) over the time interval t_{i-1} to t_i:

$$\begin{aligned}
\int_{t_{i-1}}^{t_i} dM &= -M_0 \cdot \frac{A_s}{V} \cdot \sqrt{\frac{D_a}{\pi}} \int_{t_{i-1}}^{t_i} t^{-\frac{1}{2}}\, dt \\
M_i - M_{i-1} &= -M_0 \cdot \frac{A_s}{V} \cdot \sqrt{\frac{D_a}{\pi}} \left[2t^{\frac{1}{2}}\right]_{t_{i-1}}^{t_i} \\
\frac{M_{i-1} - M_i}{M_0} &= 2\frac{A_s}{V} \cdot \sqrt{\frac{D_a}{\pi}} \cdot \left(\sqrt{t_i} - \sqrt{t_{i-1}}\right)
\end{aligned} \qquad (42)$$

Solving for D_a yields

$$D_a = \pi \left[\frac{1}{2} \cdot \frac{V}{A_s} \cdot \frac{(M_{i-1} - M_i)/M_0}{\left(\sqrt{t_i} - \sqrt{t_{i-1}}\right)} \right]^2 \tag{43}$$

In EPA-1315 parlance

$$M_{t_i} = \frac{M_{i-1} - M_i}{A_s} \tag{44}$$

and

$$\rho C_0 = \frac{M_0}{V} \tag{45}$$

Substituting Equations (44) and (45) into Equation (43) produces the result

$$D_a = \pi \left[\frac{M_{t_i}}{2\rho C_0 \left(\sqrt{t_i} - \sqrt{t_{i-1}}\right)} \right]^2 \tag{46}$$

which is the same as shown in Figure 5-2. This comparison clearly shows that the "observed diffusivity" in EPA-1315 parlance is identical to apparent diffusion coefficient as defined by Equation (33), and "effective" diffusion coefficient in ANSI/ANS 16.1.

$$D_i^{obs} = \pi \left[\frac{M_{t_i}}{2\rho C_o \left(\sqrt{t_i} - \sqrt{t_{i-1}}\right)} \right]^2$$

Where:

D_i^{obs} = observed diffusivity of a COPC for leaching interval i (m^2/s)
M_{t_i} = mass released during leaching interval i (mg/m^2)
t_i = cumulative contact time at the end of the current leaching interval, i (s)
t_{i-1} = cumulative contact time at the end of the previous leaching interval, i−1 (s)
ρ = sample density (dry basis) ($kg\text{-}dry/m^3$)
C_0 = initial leachable content (i.e., available release potential) (mg/kg)

Figure 5-2. Excerpt from the EPA-1315 procedure summarizing the data analysis method.

5.4 Half-cell leaching

A half-cell leaching test involves bringing clean and spiked porous specimens into contact, and then monitoring the concentration profile in either or both specimens (Brown et al. 1969, Golovich et al. 2014). The two materials may be dissimilar. Diffusion within each material is governed by Equation (34). Mass diffusion is mathematically analogous to heat conduction (Crank 1975) and analytical solutions for the latter can be readily adapted to the former. Myers (1971, Chapter 6) presents an analytic heat conduction solution for the case of semi-infinite regions contacting with no interfacial resistance. The contact temperature at the material interface is a constant (Myers 1971 Equation (6.4.37), Crank 1975 Equation 3.47). By analogy, the constant interface concentration for mass diffusion can be shown in general to be

$$c_i = \frac{c_{01}\left(nR\sqrt{D_a}\right)_1 + c_{02}\left(nR\sqrt{D_a}\right)_2}{\left(nR\sqrt{D_a}\right)_1 + \left(nR\sqrt{D_a}\right)_2} \tag{47}$$

where $c_{0\ell}$ is the initial concentration in semi-infinite region ℓ (Flach 2009, Equations (6a,b) extended to sorbing species). If c_{02} = 0 and $c_{01} = c_0$, then the analytic solutions in regions 1 and 2 based on Equation (35) are

$$\frac{c_0 - c}{c_0 - c_i} = \text{erfc}\left(\frac{x}{2\sqrt{D_{a1}t}}\right) \tag{48}$$

and

$$\frac{c}{c_i} = \text{erfc}\left(\frac{x}{2\sqrt{D_{a2}t}}\right) \tag{49}$$

respectively. Golovich et al. (2014) describe analysis of half-cell data using a statistical "probit" function that is related to the normal distribution and inverse error function:

$$\text{probit}(p) = \sqrt{2}\cdot\text{erf}^{-1}(2p - 1) \tag{50}$$

The analytic solutions can be written generally as

$$c_r = \text{erfc}\left(\frac{x}{2\sqrt{D_a t}}\right) = 1 - \text{erf}\left(\frac{x}{2\sqrt{D_a t}}\right) \tag{51}$$

where c_r denotes either of the non-dimensional concentration ratios in Equations (48) and (49). If the probit transform is applied to $c_r/2$ the result is

$$y \equiv \text{probit}\left(\frac{c_r}{2}\right) = \sqrt{2}\cdot\text{erf}^{-1}\left[-\text{erf}\left(\frac{x}{2\sqrt{D_a t}}\right)\right] = \frac{-1}{\sqrt{2D_a t}}\cdot x \tag{52}$$

At a given time, $y(x)$ is a linear function with slope:

$$b \equiv \frac{-1}{\sqrt{2D_a t}} \tag{53}$$

Solving for apparent diffusion coefficient yields (Golovich 2014 page 2.7)

$$D_a = \frac{1}{2b^2 t} \tag{54}$$

Note that like ANSI/ANS 16.1 and EPA-1315 leaching tests, half-cell diffusion experiments produce measurements of apparent diffusion coefficient, $D_a = D_e/R$ (Equation (33)).

The above analysis is valid for both saturated and unsaturated conditions provided D_a is a constant and thus not a function of saturation. The equivalent statement is that the tortuosity factor τ does not vary from its saturated value, that is, Equation (21) holds under unsaturated conditions. If that is not the case then the right-hand side of Equation (54) represents the product of D_a and τ_{unsat}/τ_{sat}.

6.0 Hydraulic properties

The grout mix or mixes that will be used for IDF waste encapsulation and solidification have not yet been defined. However, future IDF disposal grouts are anticipated to be similar to grouts currently in use at the Hanford site for radionuclide disposal under similar conditions. Three such examples are identified in Table 6-1 as Mix 18, Mix 19 and Mix 25. American Rock Products "4257020 Grout" is a cement / fly ash dry mix that could be used for waste encapsulation and/or solidification. American Rock Products "4100023 Grout" is cement / fly ash / sand formulation best suited for waste encapsulation. Both of these grout mixes lack larger aggregate that could prevent infilling of smaller voids when used for waste encapsulation. A concrete that has been used to encapsulate Hanford Category 3 waste is also included as a point of reference (Mix 25). This mix is representative of an encapsulation cementitious material suited for casting in forms with reinforcing steel. IDF waste is expected to generally be placed in steel containers such as drums, B-25 boxes or similar handling / shipping container. The two American Rock Products grouts best represent the type of grout expected to fill such containers and see predominant use in SSW disposals. Mix 18 is a mortar (contains sand) and Mix 19 is a paste (no sand). Thus development of material property recommendations in this section focuses on pastes and mortars (no large aggregate), which may or may not include slag cement as a dry ingredient.

6.1 Hydraulic conductivity, porosity and dry bulk density

Values for saturated hydraulic conductivity (K_s), porosity (n) and dry bulk density (ρ_b) were compiled from various reports on cementitious waste forms and barriers (Appendix A). The values were obtained from numerous independently conducted studies and represent 21 mixes (Table 6-1) with various amounts of dry components (portland cement, slag, fly ash, sand, and aggregate) blended with either water or concentrated salt solution. Figure 6-1 shows the dry mix composition of the mixes used in the study. K_s values reported for the mixes in Table 6-1 covered a large range extending from 1.0E-10 to 1.0E-4 cm/s; see Appendix A for all values used in this study. Order statistics, a non-parametric analysis method that does not require data to fit a normal distribution, was used to analyze the K_s data set. Probability theory was combined with order statistics to analyze the cumulative distribution function (cdf) for K_s values in the data set.

Data sets with a wide range of values are commonly plotted on log-probability plots for analysis (Sinclair, 1976). Log-probability plots are generally prepared by plotting cumulative probability as the abscissa on a probability scale and using a log scale for the ordinate. A log-probability plot of the K_s values used in this study was prepared as shown in Figure 6-2. K_s values less than 1.0E-7 cm/s plot along a straight line and K_s values greater than 1.0E-7 cm/s plot along another straight line with a different slope. The two different slopes on the log-probability plot indicate two populations are present in the entire data set and that each set can be described as being log-normally distributed. The K_s values greater than 1.0E-7 cm/s represent two mixes of grout that were considered for decommissioning a reactor building at the DOE Savannah River Site. Because cementitious materials with K_s values greater than 1.0E-7 cm/s are generally not considered viable for waste disposal, these mixes were removed from the data set used for further study. The remaining set of 98 K_s data values from 19 different mixes were divided into three groups based on the dry materials considered to have the greatest effect on hydraulic conductivity and contaminant mobility. These three groups were identified as follows:

1) Mixes with slag but neither sand nor aggregate
2) Mixes with slag and sand and/or aggregate
3) Mixes without slag but with sand and/or aggregate

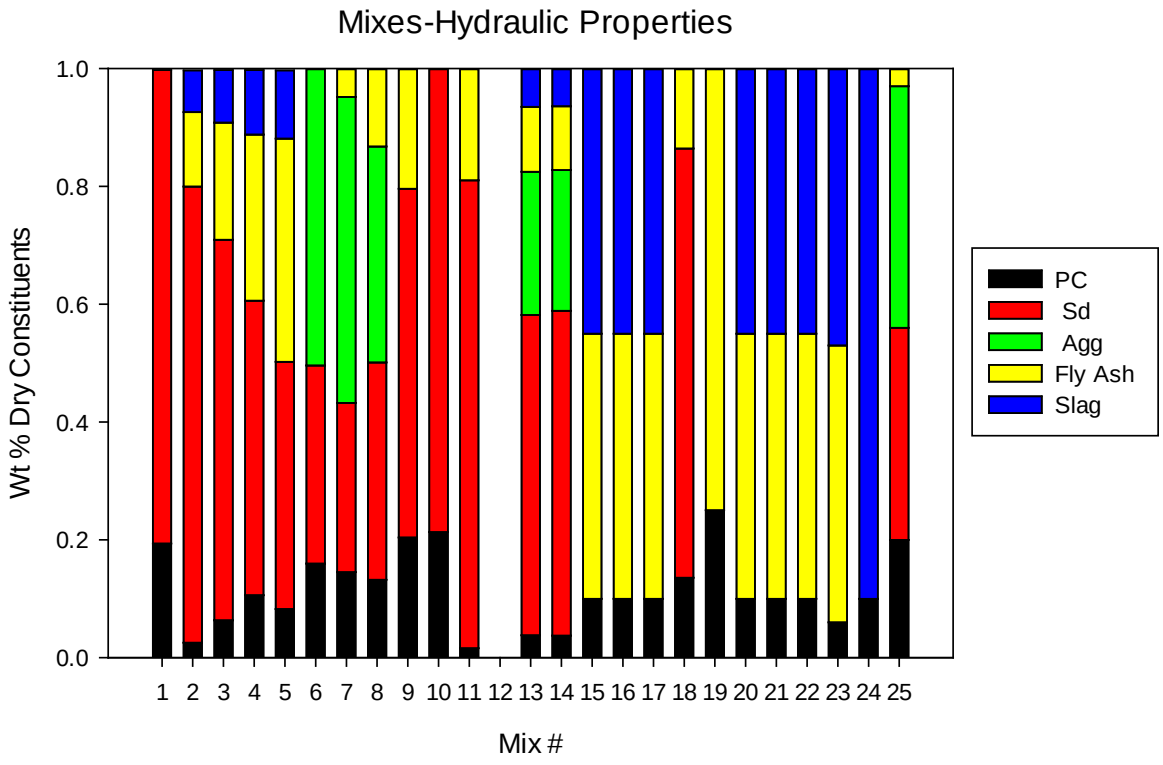

(PC = portland cement, Sd = Sand, Agg = aggregate)

Figure 6-1. Dry components in mixes.

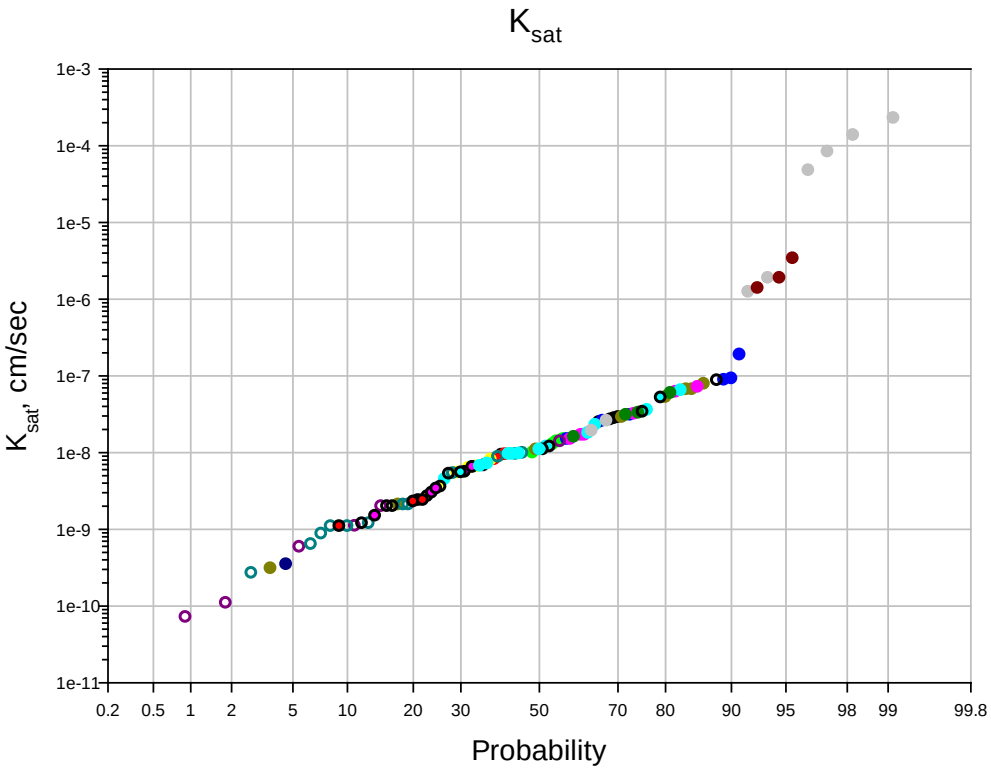

Figure 6-2. Log-probability plot of K_s for all samples.

Table 6-1. Dry mix composition of mixes used in the estimates of saturated hydraulic conductivity, dry bulk density, water exchangeable porosity, and drainage curve parameters.

Mix #	% Dry Weight (w/w)					w/c ratio †	Reference
	Portland Cement	Sand	Aggregate	Fly Ash	Slag		
1	19%	80%	0%	0%	0%	0.98	Dixon and Phifer, 2007a
2	3%	77%	0%	13%	7%	0.75	Dixon and Phifer, 2007a
3	6%	65%	0%	20%	9%	0.49	Dixon and Phifer, 2007a
4	11%	50%	0%	28%	11%	0.37	Dixon and Phifer, 2007a
5	8%	42%	0%	38%	12%	0.39	Dixon and Phifer, 2007a
6	16%	34%	50%	0%	0%	0.51	Dixon and Phifer, 2007b
7	14%	29%	52%	5%	0%	0.38	Dixon and Phifer, 2007b
8	13%	37%	37%	13%	0%	0.39	Dixon and Phifer, 2007b
9	20%	59%	0%	20%	0%	0.42	Dixon and Phifer, 2007b
10	21%	79%	0%	0%	0%	0.97	Dixon and Phifer, 2006
11	2%	79%	0%	19%	0%	0.85	Dixon and Phifer, 2006
13	4%	54%	24%	11%	6%	0.58	Stefanko and Langton, 2011
14	4%	55%	24%	11%	6%	0.55	Stefanko and Langton, 2011
15	10%	0%	0%	45%	45%	0.60	Dixon et al., 2008
16	10%	0%	0%	45%	45%	0.60	Dixon et al., 2008
17	10%	0%	0%	45%	45%	0.60	Dixon et al., 2008
18	14%	73%	0%	14%	0%	0.42	Hanford 4100023 Grout
19	25%	0%	0%	75%	0%	0.29	Hanford 4257020 Grout
20	10%	0%	0%	45%	45%	0.60	Dixon and Phifer, 2008
21	10%	0%	0%	45%	45%	0.45	Patel, 2014
22	10%	0%	0%	45%	45%	0.50	Patel, 2014
23	6%	0%	0%	47%	47%	-	Rockhold et al., 1994
24	10%	0%	0%	0%	90%	0.60	Dixon et al., 2010
25	20%	36%	41%	3%	0%	-	Hanford Category 3 Waste Encapsulation Concrete

† water to cementitious materials ratio

Each group was plotted in a log-probability plot and linear regression was used to identify the best-fit line for each group. The abscissa was replaced by the z-score for ordered values corresponding to the cumulative probability for each data point in the group and plotted on an arithmetic x-axis and $log10(K_s)$ was plotted as the ordinate on an arithmetic y-axis for the linear regression, and as a result, the slope and intercept for each best fit line are estimates of the mean and standard deviation of the $log10(K_s)$ population. The z-score was calculated using the following equation from (Mandel, 1964) after K_s values had been arranged in ascending order (1 to N) based on the value:

$$z - score = \frac{i - {}^{3}/_{8}}{N + {}^{1}/_{4}} \tag{55}$$

where i is the order of an individual sample and N is the total number of samples. This is a modified equation for cumulative probability that takes into account that the values are unique and do not represent probability area in a cumulative distribution function which is the basis of this graphical technique area (Mandel, 1964).

The log-probability plot for each group is shown in Figure 6-3 along with the transformed axes (z-score and log) for the linear regression. In Figure 6-3 each data point is color coded by the group it represents. Each group is considered to approximate a log-normal distribution because the correlation coefficient (r^2) for each group is approximately 0.9 or greater. The group that included slag and did not have either sand or aggregate plotted below the remaining groups indicating it has a lower K_s. This was confirmed to be statistically significant at the 95% confidence interval using a student t-test analysis of the difference between the means. The remaining groups were not statistically different from each other. Based on this data, slag appears to reduce the K_s of cementitious material and inclusion of sand and/or aggregate tends to increase K_s. Probability density functions (pdf) were prepared for each of the groups and are shown in Figure 6-4 to compare the K_s populations of the different groups with the composite of all the groups.

Summary statistics of $log10(K_s)$ for the groups and entire population are listed in Table 6-2. The best estimate value for saturated hydraulic conductivity in Table 6-2 is defined as

$$K_s^{BE} = 10^{mean[log10(K_{s,i})]} \tag{56}$$

Pessimistic/high (K_s^{PE}) and optimistic/low (K_s^{OE}) estimates are defined as the upper and lower 95% confidence interval (±2-sigma) values about the sample mean:

$$K_s^{PE} = 10^{mean[log10(K_{s,i})]+2s_m} \tag{57}$$

$$K_s^{OE} = 10^{mean[log10(K_{s,i})]-2s_m} \tag{58}$$

The sample standard deviation of the $log10(K_s)$ mean is

$$s_m = \frac{s}{\sqrt{N}} \tag{59}$$

where s is the sample standard deviation, and N is the number of samples.

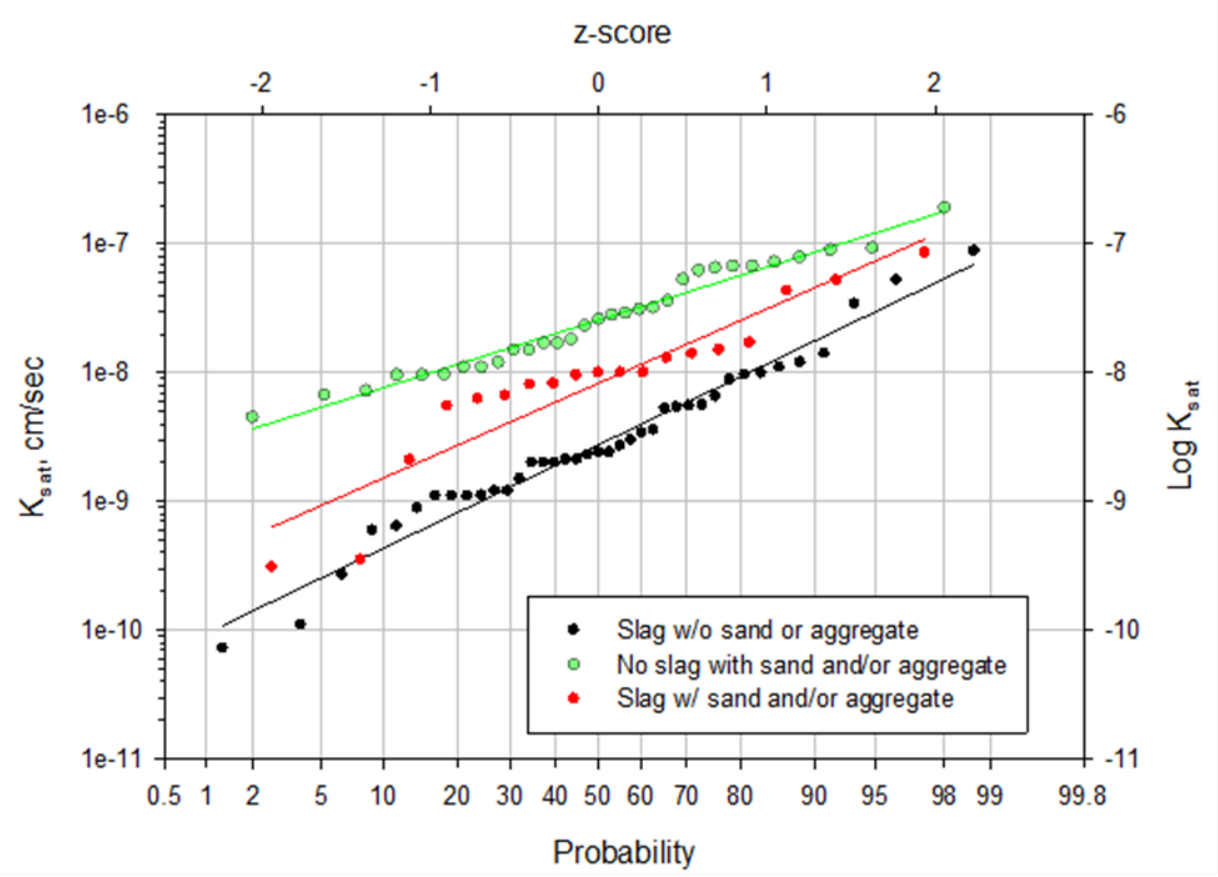

Figure 6-3. Log-probability plot of K_s for subgroupings of mixes.

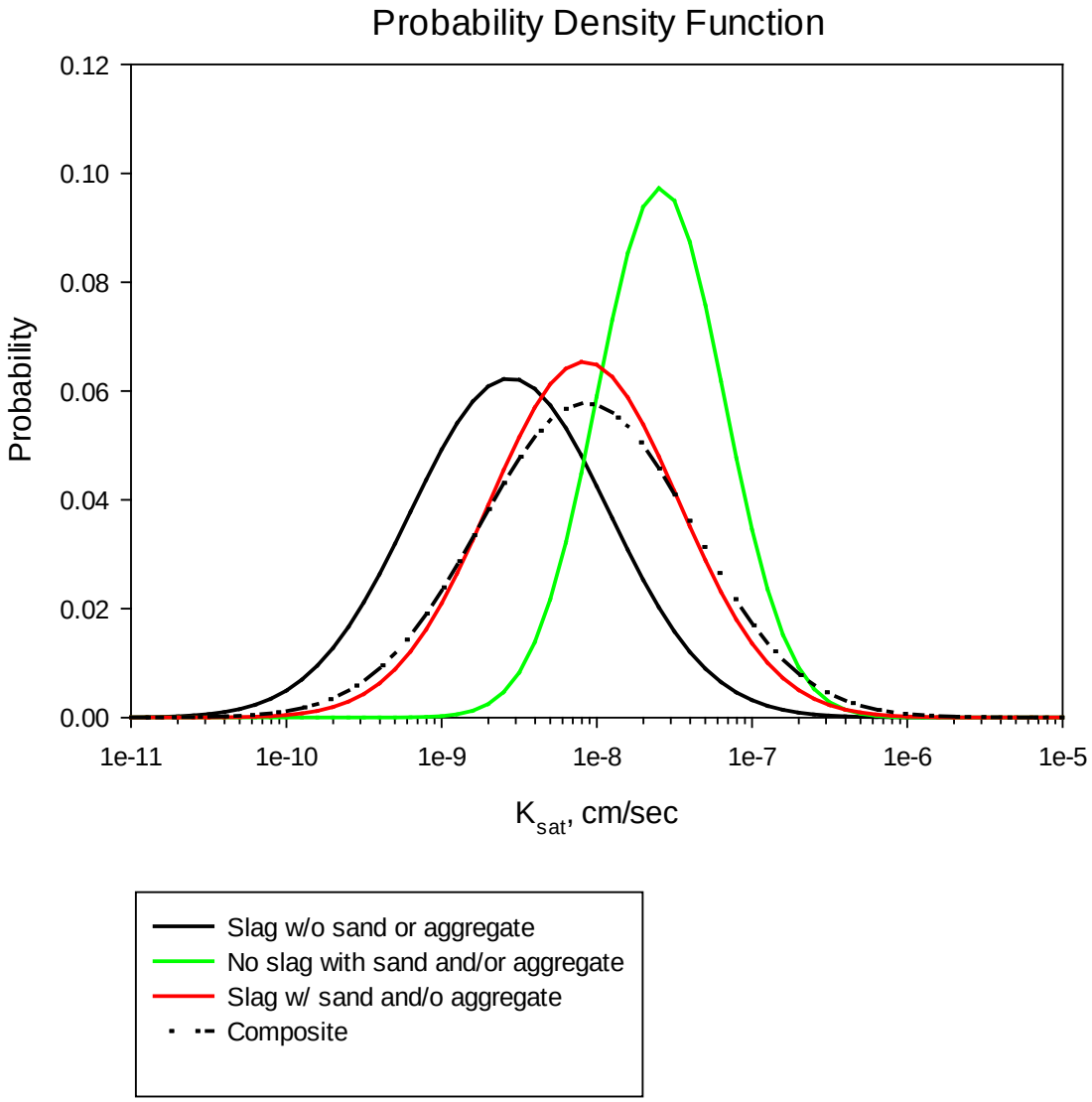

Figure 6-4. Probability density functions for K_s in each subgroup and the overall population.

Table 6-2. Summary statistics for K_s, dry bulk density, water exchangeable porosity.

Statistic	w/ Slag, w/o Sand	w/o Slag, w/ Sand	w/ Slag, w/ Sand	All
Log10[Saturated hydraulic conductivity (cm/s)]				
Count (N)	39	31	19	98
Mean	-8.56	-7.59	-8.08	-8.07
Standard deviation (s)	0.64	0.41	0.59	0.68
Correlation coefficient (r^2)	0.97	0.97	0.87	0.97
Standard deviation of mean (s_m)	0.21	0.15	0.29	0.14
Saturated hydraulic conductivity (cm/s)				
Sample mean upper range (+2s_m); K_s^{PE}	4.5E-09	3.6E-08	1.6E-08	1.2E-08
Sample mean; K_s^{BE}	2.8E-09	2.6E-08	8.3E-09	8.5E-09
Sample mean lower range (-2s_m) ; K_s^{OE}	1.7E-09	1.8E-08	4.3E-09	6.2E-09
Dry bulk density (g/cm^3)				
Count (N)	39	31	18	97
Mean	1.07	1.98	1.88	1.59
Standard deviation (s)	0.13	0.08	0.07	0.44
Sample mean upper range (+2s_m)	1.12	2.01	1.91	1.68
Sample mean lower range (-2s_m)	1.03	1.95	1.84	1.50
Porosity (cm^3 void / cm^3 total)				
Count (N)	28	31	18	86
Mean	0.59	0.18	0.24	0.33
Standard deviation (s)	0.03	0.05	0.03	0.19
Sample mean upper range (+2s_m)	0.60	0.20	0.25	0.37
Sample mean lower range (-2s_m)	0.58	0.17	0.22	0.29
Solid density (g/cm^3)[1]				
Count (N)	29	31	18	86
Mean	2.47	2.43	2.46	2.45
Standard deviation (s)	0.11	0.07	0.06	0.08
Sample mean upper range (+2s_m)	2.68	2.54	2.53	2.62
Sample mean lower range (-2s_m)	2.32	2.27	2.27	2.27

[1] Calculated from dry bulk density and porosity

Estimates of dry bulk density and water exchangeable porosity were similarly derived for the same groups as in the analysis of K_s. Table 6-2 contains the summary statistics for dry bulk density (ρ_b) and water exchangeable porosity (n) assuming normal distributions. Particle density (ρ_s) can be calculated using the following equation

$$\rho_s = \frac{\rho_b}{1-n} \tag{60}$$

Particle density was calculated for each of the samples with reported dry bulk density and porosity and summary statistics were calculated for the resulting particle density values, Table 6-2.

6.2 Moisture characteristic curves

Moisture retention properties of samples were determined using laboratory measurements of pressure head and moisture content. Curve fitting is used to estimate the parameters in the van Genuchten equation defining the moisture retention curve (see Equations (10) and (11)):

$$\begin{aligned} \theta(p_c) &= \theta_r + \frac{\theta_s - \theta_r}{[1 + (\alpha p_c)^{n_{vG}}]^{m_{vG}}} \quad p_c \leq 0 \\ \theta(p_c) &= \theta_s \qquad\qquad\qquad\quad p_c > 0 \end{aligned} \tag{61}$$

The fitted parameters are θ_s, θ_r, α, n_{vG} and m_{vG}. Saturation S is computed from Equation (10) as

$$S = S_r + \frac{1 - S_r}{[1 + (\alpha p_c)^{n_{vG}}]^{m_{vG}}} \tag{62}$$

and relative permeability from Equation (12) with L assumed to be 0.5.

Figure 6-5 shows drainage curves for several of the cement paste and mortar (paste with sand/aggregate) mixes (Mixes 1, 2, 3, 4, 5, 9, 16 and 22) in Table 6-1 and Figure 6-1. Mortars drain easier than pastes as shown by saturation less than 100% for suction pressures above 10 to 100 cm. The paste drainage curves exhibit two behaviors with some beginning to drain at suction pressures of approximately 1.0e+4 cm H_2O and others showing essentially no drainage. Dixon et al. (2010) determined the latter behavior to be a result of insufficient drainage data at higher suctions for curve fitting. The curves with essentially no drainage did not have laboratory measurements with suction pressures above 1.0e+4 cm H_2O for curve fitting while those pastes showing drainage had laboratory measurements with suction pressures to about 6.0e+6 cm H_2O. Paste curves based on data sets lacking high suction measurements were discarded from further consideration.

Table 6-3 presents van Genuchten parameters based on the mortar and paste mixes defined in Table 6-1. Figure 6-5 shows the corresponding moisture retention curves, and "Composite" mortar and paste curves generated by simply averaging the van Genuchten parameters from individual curves. Figure 6-6 plots relative permeability and moisture retention for just the composite materials. The curves in Figure 6-5 have been truncated to correspond to the range of test conditions used to develop data for the water retention curves.

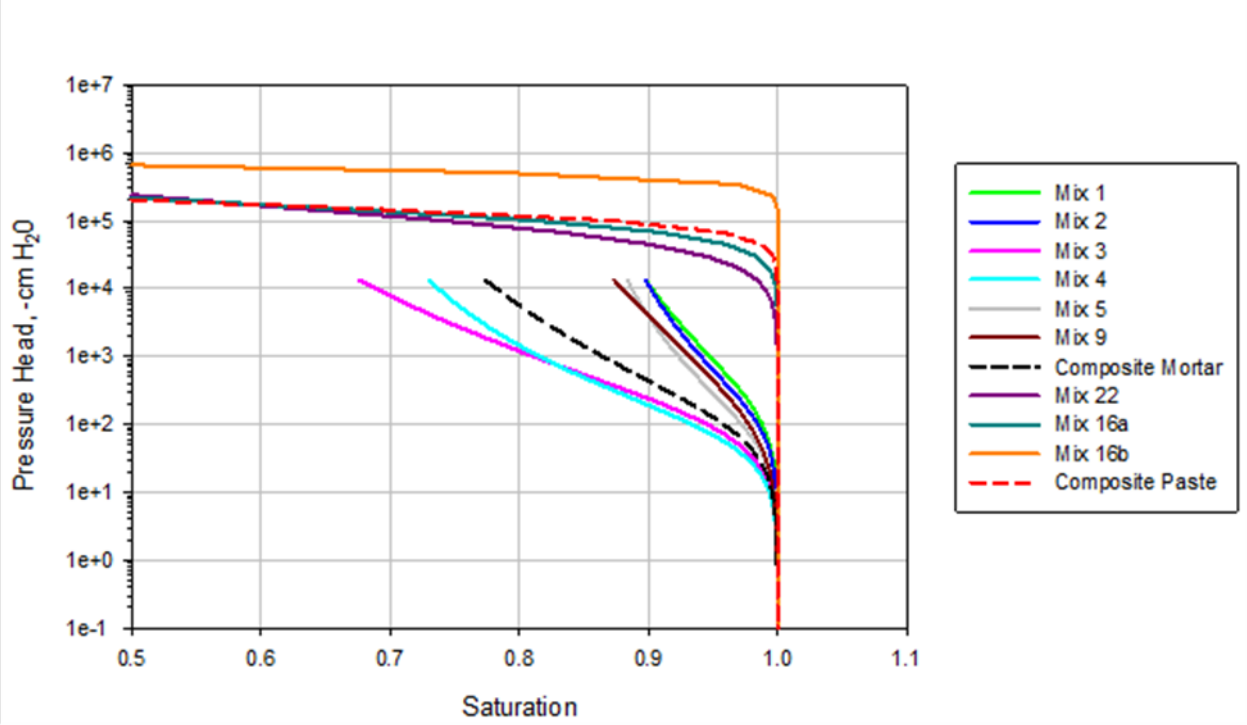

Figure 6-5. Moisture retention curves for mortars and pastes.

Table 6-3. van Genuchten parameters for mortars and pastes.

Mix #	θ_s	θ_r	α (1/cm)	n	m	Reference
1	0.296	0.234	0.006	1.153	0.133	Dixon and Phifer, 2007a
2	0.279	0.234	0.008	1.215	0.177	Dixon and Phifer, 2007a
3	0.222	0.093	0.010	1.167	0.143	Dixon and Phifer, 2007a
4	0.252	0.162	0.015	1.266	0.210	Dixon and Phifer, 2007a
5	0.196	0.162	0.016	1.208	0.172	Dixon and Phifer, 2007a
9	0.220	0.000	0.015	1.026	0.025	Dixon and Phifer, 2007b
15	0.570	0.540	0.150	1.030	0.029	Dixon et al., 2008
16	0.590	0.585	0.150	1.230	0.187	Dixon et al., 2008
17	0.580	0.572	0.150	1.300	0.231	Dixon et al., 2008
20	0.578	0.492	0.008	1.012	0.012	Dixon and Phifer, 2008
23	0.578	0.000	1.08E-05	1.650	0.394	Rockhold et al., 1994
16a	0.615	0.000	7.00E-06	2.223	0.550	Dixon et al., 2010
16b	0.615	0.000	1.60E-06	5.440	0.816	Dixon et al., 2010
Mortar	0.244	0.148	0.012	1.172	0.143	This report
Paste	0.603	0.000	6.47E-06	3.104	0.587	This report

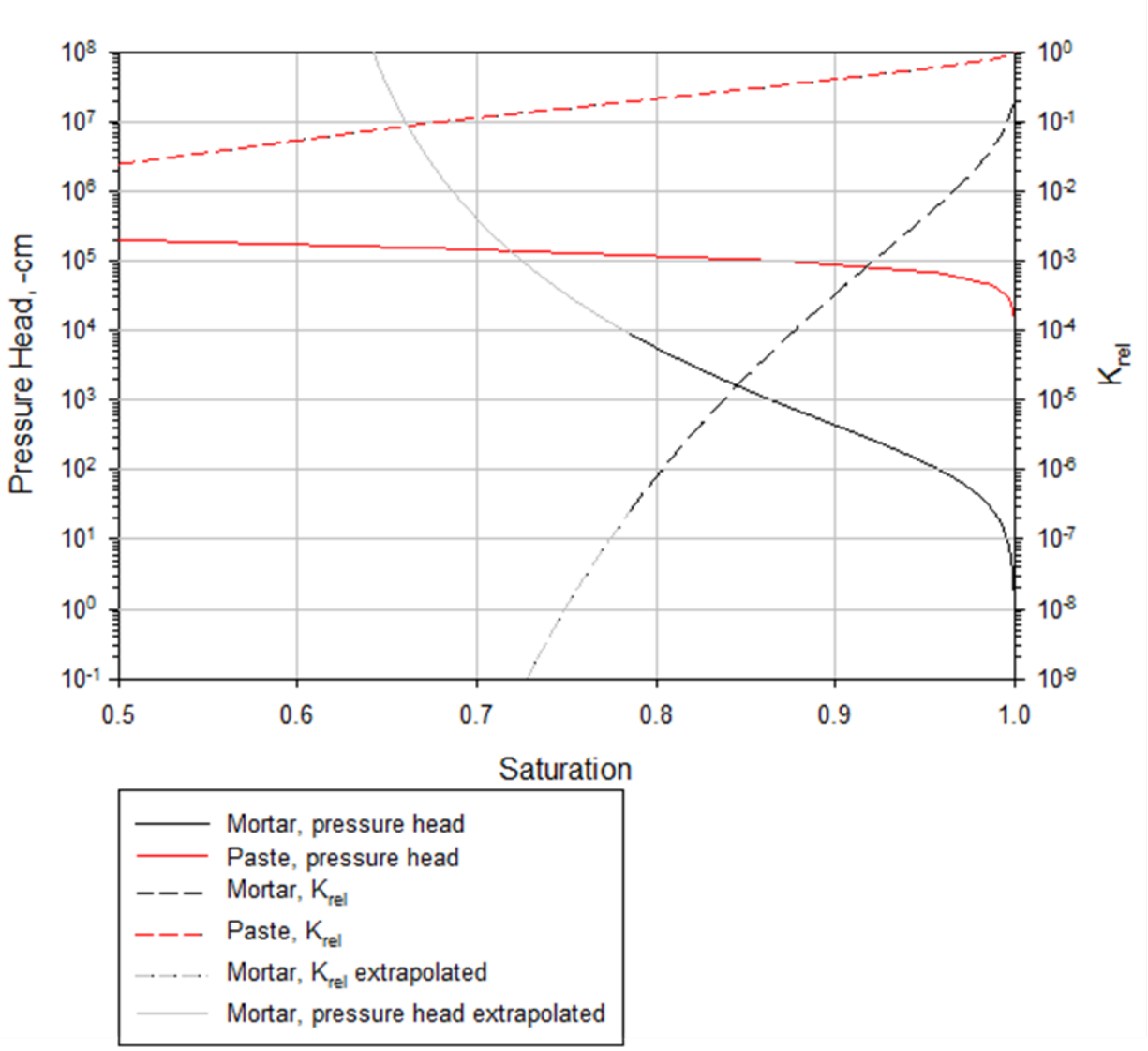

Figure 6-6. Relative permeability and moisture retention composite curves for mortars and pastes.

As discussed in Section 4.3, moisture tension heads under post-closure conditions are expected to be on the order of 1000 cm or lower. The characteristic curves plotted in Figure 6-5 and Figure 6-6 are supported by measurements from saturation ($p_c \leq 0$) through about p_c = 10,000 cm. Thus, the recommended water retention curves for both mortar and paste are considered valid under post-closure conditions. Prior to facility closure, cementitious materials could be exposed to the atmosphere for an extended period, corresponding to drier conditions and higher suctions approaching p_c = 1.0E+6 cm (see Section 9.0). The recommended paste characteristic curve is considered valid under atmospheric exposure conditions, because measurements extended to 6.0e+6 cm. However, the mortar curve is an extrapolation beyond $p_c = 10{,}000$ cm and considered invalid for use in atmospheric exposure scenarios.

From a conceptual perspective, mortars are expected to desaturate in a similar manner as pastes at high suctions. That is, the mortar and paste curves should roughly overlap at some point. The van Genuchten water retention curve for mortar (fitted to 0 < p_c < 2.0E+4 cm data) indicates 75% saturation at 2.0E+4 cm and a residual saturation of 60%. These fractions of the total porosity are likely associated with relatively small pore sizes, characteristic of pure paste, and distinctly smaller than larger pore sizes that produced the initial drainage at much lower suctions. More specifically, the observed drainage behavior of mortar suggests a bimodal pore size distribution. The van Genuchten (1980) functional form implies a unimodal distribution and is not capable of matching water retention curve data from bimodal samples (e.g. Zurmuhl and Durner 1998). However, a linear superposition of two van Genuchten functions can represent the combined effect of two distinct subpopulations of pore sizes (e.g. Durner 1994).

This concept can be used to derive an alternative to the initial mortar characteristic curve shown in Figure 6-6. The specific equations chosen for blending material properties are given in Section 2.1 of Jordan and Flach (2013). For clarity going forward, the original mortar curve shown in Figure 6-6 is identified as the "unimodal mortar" curve, and the alternative as the "bimodal mortar" curve. The following criteria are imposed on the material properties of the bimodal alternative:

1) saturated hydraulic conductivity and water content (porosity) must match those of the unimodal mortar
2) water retention behavior must match that of the unimodal mortar over the range 0 < p_c < 2.0E+4 cm, that is, honor the experimental data
3) water retention behavior should approximate that of pure paste for p_c > 2.0E+4 cm.

Criterion 3) is satisfied by selecting pure paste as one of the blending materials and using properties verbatim from Table 6-2 and Table 6-3. Criterion 2) is satisfied by assuming that the remaining fraction is composed of an semi-empirically defined cemented sand material with pore size distribution characterized by mortar testing over the range 0 < p_c < 2.0E+4 cm. More specifically, we require that the volume of water drained from the cemented sand fraction be identical to that drained from the unimodal mortar ("mortar" for brevity):

$$(n - \theta) = f_{cs}(n_{cs} - \theta_{cs}) \tag{63}$$

Here the "cs" subscript refers to the cemented sand component and f_{cs} is the volume fraction of cemented sand in the total volume. The water retention behavior of each material is defined by the general relationship (see Equations (10) and (11))

$$\frac{\theta - \theta_r}{n - \theta_r} = S_e(\alpha, n_{vG}, m_{vG}) \tag{64}$$

or

$$\theta = \theta_r + S_e(\alpha, n_{vG}, m_{vG})(n - \theta_r) \tag{65}$$

Combining Equation (65) for each material with Equation (63) yields

$$(n-\theta_r)(1-S_e) = f_{cs}(n_{cs}-\theta_{csr})(1-S_e^{cs}) \tag{66}$$

Equation (66) can only be satisfied over a range of suctions if the relative saturation function for the cemented sand fraction is the same function as that for the mortar

$$S_e = S_e^{cs} \tag{67}$$

That is, the van Genuchten parameters for the cemented sand fraction (α^{cs}, n_{vG}^{cs}, m_{vG}^{cs}) must be those for the unimodal mortar (α, n_{vG}, m_{vG}). The van Genuchten parameters for cemented sand are thus taken directly from Table 6-3.

Equation (66) then reduces to

$$f_{cs} = \frac{n-\theta_r}{n_{cs}-\theta_{csr}} \tag{68}$$

The total mortar porosity is composed of contributions from the cemented sand and pure paste fractions.

$$n = f_{cs}n_{cs} + (1-f_{cs})n_p \tag{69}$$

Equations (68) and (69) can be manipulated with the results

$$f_{cs} = \frac{n_p-\theta_r}{n_p-\theta_{csr}} \tag{70}$$

$$n_{cs} = \frac{n\left(n_p-\theta_{csr}\right)+n_p(\theta_{csr}-\theta_r)}{\left(n_p-\theta_r\right)} \tag{71}$$

The saturated hydraulic conductivity of the cemented sand fraction is

$$K_{cs} = \frac{K-(1-f_{cs})K_p}{f_{cs}} \tag{72}$$

The geometric mean of the two mortars in Table 6-2 is taken as the saturated conductivity K. The results of applying the above equations to mortar data are summarized in Table 6-4.

Figure 6-7 compares the alternative bimodal characteristic curves to those for unimodal mortar and pure paste. As designed, the bimodal water retention curve overlaps the unimodal curve over the range of suctions for which experimental data are available, and then mimics the behavior of the paste curve at higher suctions. While the mortar water retention curves are practically identical for p_c < 2.0E+4 cm, the relative permeability curves differ significantly within this lower suction range. The net effect on unsaturated hydraulic conductivity is apparent from Figure 6-8, where the departure is observed to occur between 10 and 100 cm of suction head. At the expected field condition of p_c = 1000 cm the unsaturated hydraulic conductivities for the two mortars differ by about three orders of magnitude. This unexpected observation indicates the choice between unimodal and bimodal material properties to be impactful to subsurface modeling under almost any unsaturated condition (p_c > 10 cm).

Table 6-4. Hydraulic and moisture retention properties for mortar with a bimodal pore size distribution.

Parameter	Paste	Mortar, unimodal	Blend fraction 1	Blend fraction 2	Mortar, bimodal	Comments
Blend material	n/a	n/a	Cemented sand	Paste	n/a	Bimodal mortar constructed as blend of "Paste" and "Cemented sand" fractions
Blend fraction	n/a	n/a	0.755	0.245	n/a	Calculated from Equation (70)
Basis	Table 6-2 Table 6-3	Table 6-2 Table 6-3	semi-empirical	Table 6-2 Table 6-3	blend	Blend material 1 properties are deduced
Porosity, n	0.603	0.244	0.127	0.603	0.244	Porosity set to saturated water content from Table 6-3 for "Paste" and "Mortar, unimodal". "Cemented sand" porosity calculated from Equation (71).
Saturated hydraulic conductivity, K_s (cm/s)	2.8E-09	1.47E-08	1.87E-08	2.8E-09	1.47E-08	"Mortar, unimodal" saturated hydraulic conductivity geometric set to geometric mean of mortars with and without slag from Table 6-3. "Cemented sand" hydraulic conductivity calculated from Equation (72).
Saturated water content, θ_s	0.603	0.244	0.127	0.603	0.244	Table 6-3 or same as porosity
Residual water content, θ_r	0	0.148	0	0	0	"Cemented sand" porosity is assumed to be fully drained for $h_c > 10^4$ cm.
Residual saturation, S_r	0	0.607	0	0	0	Calculated from residual water content
van Genuchten α (1/cm)	6.47E-06	0.012	0.012	6.47E-06	n/a	"Cemented sand" same as "Mortar, unimodal".
van Genuchten n_{vG}	3.104	1.172	1.172	3.104	n/a	"Cemented sand" same as "Mortar, unimodal".
van Genuchten m_{vG}	0.587	0.143	0.143	0.587	n/a	"Cemented sand" same as "Mortar, unimodal".
van Genuchten L	0.5	0.5	0.5	0.5	n/a	"Cemented sand" same as "Mortar, unimodal".

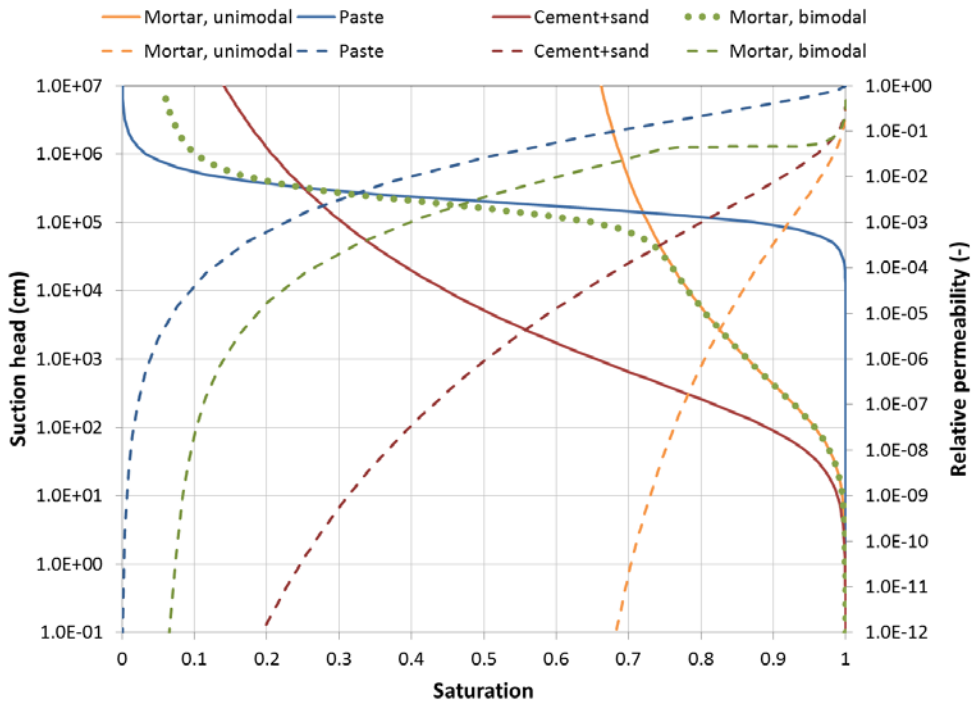

solid and dotted lines = Suction head; dashed lines = relative permeability

Figure 6-7. Moisture retention and relative permeability curves for mortars with unimodal and bimodal pore size distributions.

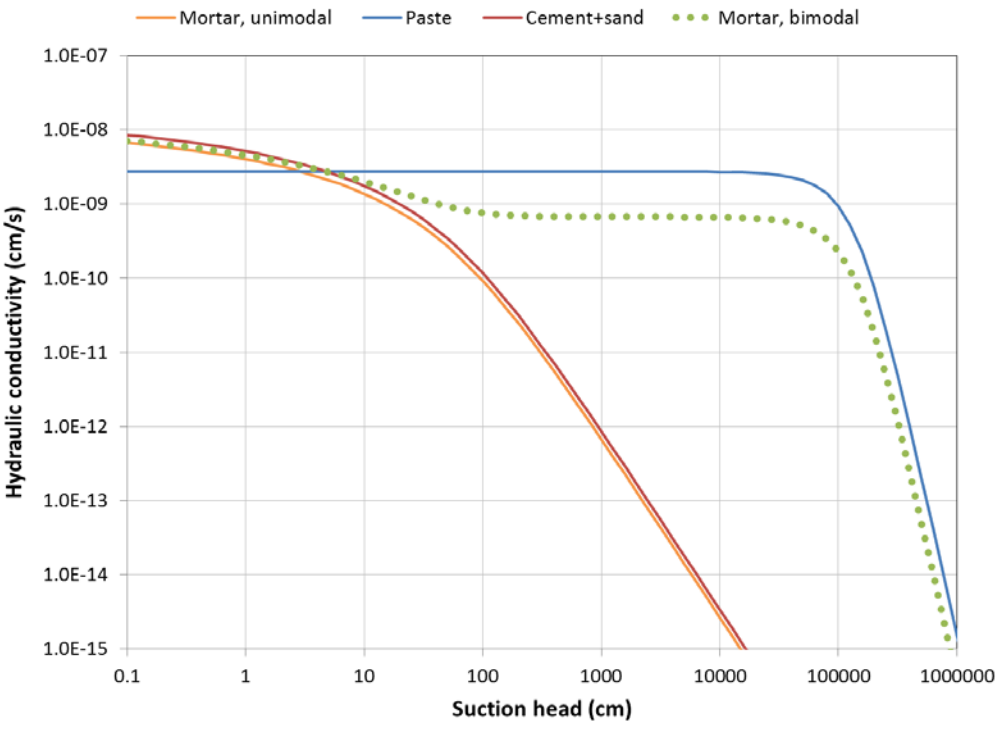

Figure 6-8. Unsaturated hydraulic conductivity for mortars with unimodal and bimodal pore size distributions.

With this consideration, the bimodal mortar properties are recommended over the unimodal properties on the basis that:

- The material properties of the bimodal material honor the available data.
- The bimodal characteristic curves are thought to be representative of mortar over a much broader range of suction heads.
- Unsaturated hydraulic conductivity for the bimodal mortar is similar to that of paste, and other cementitious materials.
- Unsaturated hydraulic conductivity for the bimodal mortar is higher than that of unimodal mortar, and constitutes what is assumed to be a pessimistic assumption.

6.3 Material property recommendations

The specific grout formulations that will be used to encapsulate and solidify SSW streams have not yet been defined (Section 3.1) but can be anticipated to fall within four broad categories: cement + fly ash paste, cement + fly ash + slag paste, cement + fly ash + sand mortar, and cement + fly ash + slag + sand mortar. The recommended hydraulic properties for these four classes of potential SSW grouts are

cement + fly ash paste:	"w/Slag, w/o Sand" paste (Table 6-2 and Table 6-3)
cement + fly ash + slag paste:	"w/Slag, w/o Sand" paste (Table 6-2 and Table 6-3)
cement + fly ash + sand mortar:	"w/o Slag, w/ Sand" mortar (Table 6-2 and Table 6-4)
cement + fly ash + slag + sand mortar:	"w/Slag, w/ Sand" mortar (Table 6-2 and Table 6-4)

For example, "Grout mix 5" (American Rock Products "4257020") in current use at the Hanford site for disposals similar to anticipated SSW in the IDF is a cement + fly ash paste.

A paste dry-mix may be used to solidify non-debris SSW (< 60 mm particle size), producing a cast material that is more similar to mortar than a pure paste. Mortar properties are considered more appropriate than paste properties for IDF PA modeling on this basis, and because mortar properties are assumed to be more pessimistic in terms of the PA. For any SSW debris waste within an encapsulation grout, we recommend taking no potential credit for resistance to advective transport within the waste zone, because of uncertainty in the form and effective properties of the debris waste(s) that will be disposed. Soil properties could be assumed for the waste zone, so that the waste zone represents neither a barrier nor a conduit for moisture transport relative to the backfill surrounding the waste form.

7.0 Effective diffusion coefficient

The term "effective diffusion coefficient" as used within this data package is defined by Equations (16) through (19). Effective diffusion coefficient D_e is a physical property, not dependent on species-specific sorption and/or solubility. Popular experimental techniques for measuring diffusion coefficients are reviewed in Section 5.0. The diffusion cell method measures intrinsic diffusion coefficient defined by Equation (16). A porosity value is required to compute effective diffusion coefficient from intrinsic diffusion coefficient ($D_e = D_i/n$). Ideally porosity is measured for each diffusion cell specimen. The ANSI/ANS 16.1, EPA-1315 and "half-cell" methods all measure a species-dependent apparent diffusion coefficient defined by Equation (33). A retardation coefficient value is required to compute the effective diffusion coefficient ($D_e = RD_a$). Ideally testing is performed using a non-sorbing species such that $R = 1$ and then $D_e = D_a$ directly.

The grout mix or mixes that will be used for IDF waste encapsulation and solidification have not yet been defined. However, IDF disposal grouts are anticipated to be similar to grouts currently in use at the Hanford site for radionuclide disposal under similar conditions. Table 7-1, "Reference Mixes" section, identifies three such examples. American Rock Products "4257020 Grout" is a cement / fly ash dry mix that could be used for waste encapsulation and/or solidification. American Rock Products "4100023 Grout" is cement / fly ash / sand formulation best suited for waste encapsulation. Both of these grout mixes lack larger aggregate that could prevent infilling of smaller voids when used for waste encapsulation. A concrete that has been used to encapsulate Hanford Category 3 waste is also included as a point of reference. This mix is representative of an encapsulation cementitious material suited for casting in forms with reinforcing steel. IDF waste is expected to generally be placed in steel containers such as drums, B-25 boxes or similar handling / shipping container. The two American Rock Products grouts best represent the type of grout expected to fill such containers and see predominant use in SSW disposals.

Table 7-1, "Experimental Data" section, presents effective diffusion coefficient data from 100 cement paste and mortar specimens tested under saturated conditions. Data from concrete specimens were considered less representative than data from pastes and mortars and were excluded. Candidate data were identified from Phifer et al. (2006), Pabalan et al. (2009), DOE Savannah River and Hanford site technical reports, and other literature. Mixes with ground blast furnace slag were included in part because slag may be desirable for reducing permeability (ACI 233R-03) and/or improving ^{99}Tc retention (e.g. Estes et al. 2012). Also, many leaching test results are available for non-sorbing species in slag pastes and mortars. Most of the selected data involve leaching of nitrate (NO_3), nitrite (NO_2) or tritium (HTO), because these species are known to be non-sorbing in cementitious materials such that $D_e = D_a$. Chloride (Cl^-) leaching results were also reported in some studies and these data were included for completeness, with the understanding that chloride is slightly sorbing. Delagrave et al. (1998) and Ampadu et al. (1999) performed diffusion cell tests that generated intrinsic diffusion coefficient values; these were converted to effective diffusion coefficient using porosity, measured or estimated by Phifer et al. (2006, Section 6.1.4), as indicated in the "Porosity" column. All other tests were ANSI/ANS 16.1 or EPA-1315 experiments that generated apparent diffusion coefficient values. All species were initially considered to be practically non-sorbing, such that $D_e = D_a$. Some references report results in terms of a leach index defined by

$$LI = -log10\left[D_e\left(\mathrm{cm}^2/\mathrm{s}\right)\right] \tag{73}$$

In those cases, the "Leach index" column is populated with the reported LI and D_e computed from Equation (73); otherwise, leach index is computed from the measured diffusion coefficient.

Table 7-1. Effective diffusion coefficient reference information and data.

#	Identification label	Cement wt%	Fly ash wt%	Slag cement wt%	Silica fume wt%	Sand wt%	Large aggr. wt%	Lime/ Ca(OH)2 or other wt%	w/cm†	Species	Porosity n	Leach index	Intrinsic diffusion coefficient D_i cm^2/s	Effective diffusion coefficient D_e cm^2/s	Reference
	Reference Mixes														
	4257020 Grout	25%	75%						0.29						American Rock Products
	4100023 Grout	14%	14%			73%			0.43						American Rock Products
	Category 3 Waste Encapsulation Concrete	20%	3%			33%	41%	3% steel fiber	0.42						HNF-1981 Rev. 0
	Experimental Data														
1	Oblath (1986) Reference	20%	80%						0.47	NO3		7.157		7.0E-08	DPST-86-442
2	Oblath (1986) Mix 52		50%	48%				2% lime	0.60	NO3		7.245		5.7E-08	DPST-86-442
3	Langton (1986) Mix 2A/B	20%	80%						0.52	NO3		7.9		1.2E-08	DPST-86-551
4	Langton (1986) Mix 3A/B	13%	61%	26%					0.52	NO3		5.7		2.0E-06	DPST-86-551
5	Langton (1986) Mix 4A/B		47%	47%				5% lime	0.58	NO3		8.3		4.7E-09	DPST-86-551
6	Langton (1987a) Mix 1A/B	20%	80%						0.52	NO3		8.2		6.1E-09	DPST-86-863
7	Langton (1987a) Mix 2A/B		47%	47%				5% $Ca(OH)_2$	0.58	NO3		8.9		1.3E-09	DPST-86-863
8	Langton (1987a) Mix 3A/B	13%	61%	26%					0.52	NO3		8.1		7.4E-09	DPST-86-863
9	Langton (1987b) Slag Mix I Bowen		47%	47%				5% $Ca(OH)_2$	0.58	NO3		9.1		8.5E-10	DPST-87-673
10	Langton (1987b) Slag Mix I Marshall		47%	47%				5% $Ca(OH)_2$	0.58	NO3		9.1		7.2E-10	DPST-87-673
11	Langton (1987b) Slag Mix I Belews Creek		47%	47%				5% $Ca(OH)_2$	0.58	NO3		9.4		4.2E-10	DPST-87-673
12	Langton (1987b) Slag Mix I D-Area		47%	47%				5% $Ca(OH)_2$	0.58	NO3		8.7		1.9E-09	DPST-87-673

#	Identification label	Cement wt%	Fly ash wt%	Slag cement wt%	Silica fume wt%	Sand wt%	Large aggr. wt%	Lime/ Ca(OH)2 or other wt%	w/cm†	Species	Porosity n	Leach index	Intrinsic diffusion coefficient D_i cm²/s	Effective diffusion coefficient D_e cm²/s	Reference
13	Langton (1987b) Slag Mix II Marshall	9%	45%	45%					0.63	NO3		8.5		3.5E-09	DPST-87-673
14	Langton (1987b) Slag Mix II Belews Creek	9%	45%	45%					0.63	NO3		8.6		2.6E-09	DPST-87-673
15	Oblath (1989) Lysimeter - water >8%	20%	80%						0.47	NO3		8.3		5.0E-09	ES&T v23 1989
16	Langton (1988) Mix 1	20%	80%						0.52	NO3		8.3		5.0E-09	MRSSPv112 1988
17	Langton (1988) Mix 2	18%	47%	35%					0.96	NO3		6.1		8.0E-07	MRSSPv112 1988
18	Langton (1988) Mix 3		47%	47%				5% $Ca(OH)_2$	0.58	NO3		8.9		1.3E-09	MRSSPv112 1988
19	Langton (1991) J Mix Mortar	31%				69%			0.46	NO3		7.3		5.0E-08	WSRC-MS-91-073
20	Langton (1991) Z-2 Mix Mortar	19%		12%		69%			0.43	NO3		7.8		1.7E-08	WSRC-MS-91-073
21	Cozzi Pickenheim Sample 2-2	10%	45%	45%					0.60	NO2		8.1		7.9E-09	SRNL-STI-2012-00546
22	Cozzi Pickenheim Sample 3-2	10%	45%	45%					0.60	NO2		8.1		7.9E-09	SRNL-STI-2012-00546
23	Cozzi Pickenheim Sample 4-2	10%	45%	45%					0.60	NO2		8.2		6.3E-09	SRNL-STI-2012-00546
24	Cozzi Pickenheim Sample 6-2	10%	45%	45%					0.64	NO2		8.1		7.9E-09	SRNL-STI-2012-00546
25	Cozzi Pickenheim Sample 7-2	10%	45%	45%					0.64	NO2		8.1		7.9E-09	SRNL-STI-2012-00546
26	Cozzi Pickenheim Sample 8-2	10%	45%	45%					0.64	NO2		8.2		6.3E-09	SRNL-STI-2012-00546
27	Cozzi Pickenheim Sample 2-2	10%	45%	45%					0.60	NO3		8.7		2.0E-09	SRNL-STI-2012-00546
28	Cozzi Pickenheim Sample 3-2	10%	45%	45%					0.60	NO3		8.8		1.6E-09	SRNL-STI-2012-00546
29	Cozzi Pickenheim Sample 4-2	10%	45%	45%					0.60	NO3		8.7		2.0E-09	SRNL-STI-2012-00546

#	Identification label	Cement wt%	Fly ash wt%	Slag cement wt%	Silica fume wt%	Sand wt%	Large aggr. wt%	Lime/ Ca(OH)2 or other wt%	w/cm†	Species	Porosity n	Leach index	Intrinsic diffusion coefficient D_i cm²/s	Effective diffusion coefficient D_e cm²/s	Reference
30	Cozzi Pickenheim Sample 6-2	10%	45%	45%					0.64	NO3		8.7		2.0E-09	SRNL-STI-2012-00546
31	Cozzi Pickenheim Sample 7-2	10%	45%	45%					0.64	NO3		8.5		3.2E-09	SRNL-STI-2012-00546
32	Cozzi Pickenheim Sample 8-2	10%	45%	45%					0.64	NO3		8.5		3.2E-09	SRNL-STI-2012-00546
33	Riegel et al. WP001-A	10%	45%	45%					0.59	NO3		7.0		1.0E-07	SRNL-STI-2012-00558
34	Riegel et al. WP001-B	10%	45%	45%					0.59	NO3		6.9		1.3E-07	SRNL-STI-2012-00558
35	Riegel et al. WP003-A	10%	45%	45%					0.67	NO3		7.3		5.0E-08	SRNL-STI-2012-00558
36	Riegel et al. WP003-B	10%	45%	45%					0.67	NO3		7.4		4.0E-08	SRNL-STI-2012-00558
37	Riegel et al. WP005-A	10%	45%	45%					0.70	NO3		7.0		1.0E-07	SRNL-STI-2012-00558
38	Riegel et al. WP005-B	10%	45%	45%					0.70	NO3		6.9		1.3E-07	SRNL-STI-2012-00558
39	Riegel et al. WP010-A	10%	45%	45%					0.72	NO3		7.3		5.0E-08	SRNL-STI-2012-00558
40	Riegel et al. WP010-B	10%	45%	45%					0.72	NO3		7.3		5.0E-08	SRNL-STI-2012-00558
41	Riegel et al. WP011-A	10%	45%	45%					0.64	NO3		6.9		1.3E-07	SRNL-STI-2012-00558
42	Riegel et al. WP011-B	10%	45%	45%					0.64	NO3		6.9		1.3E-07	SRNL-STI-2012-00558
43	Riegel et al. WP014-A	10%	45%	45%					0.55	NO3		7.3		5.0E-08	SRNL-STI-2012-00558
44	Riegel et al. WP014-B	10%	45%	45%					0.55	NO3		7.5		3.2E-08	SRNL-STI-2012-00558
45	Riegel et al. WP018-A	10%	45%	45%					0.73	NO3		6.6		2.5E-07	SRNL-STI-2012-00558
46	Riegel et al. WP018-B	10%	45%	45%					0.73	NO3		7.3		5.0E-08	SRNL-STI-2012-00558
47	Riegel et al. WP021-A	10%	45%	45%					0.60	NO3		6.8		1.6E-07	SRNL-STI-2012-00558
48	Riegel et al. WP021-B	10%	45%	45%					0.60	NO3		6.6		2.5E-07	SRNL-STI-2012-00558

#	Identification label	Cement wt%	Fly ash wt%	Slag cement wt%	Silica fume wt%	Sand wt%	Large aggr. wt%	Lime/ Ca(OH)2 or other wt%	w/cm†	Species	Porosity n	Leach index	Intrinsic diffusion coefficient D_i cm²/s	Effective diffusion coefficient D_e cm²/s	Reference
49	Riegel et al. WP023-A	10%	45%	45%					0.51	NO3		6.8		1.6E-07	SRNL-STI-2012-00558
50	Riegel et al. WP023-B	10%	45%	45%					0.51	NO3		7.0		1.0E-07	SRNL-STI-2012-00558
51	Riegel et al. WP001-A	10%	45%	45%					0.59	NO2		7.1		7.9E-08	SRNL-STI-2012-00558
52	Riegel et al. WP001-B	10%	45%	45%					0.59	NO2		7.0		1.0E-07	SRNL-STI-2012-00558
53	Riegel et al. WP003-A	10%	45%	45%					0.67	NO2		7.3		5.0E-08	SRNL-STI-2012-00558
54	Riegel et al. WP003-B	10%	45%	45%					0.67	NO2		7.4		4.0E-08	SRNL-STI-2012-00558
55	Riegel et al. WP005-A	10%	45%	45%					0.70	NO2		7.0		1.0E-07	SRNL-STI-2012-00558
56	Riegel et al. WP005-B	10%	45%	45%					0.70	NO2		7.0		1.0E-07	SRNL-STI-2012-00558
57	Riegel et al. WP010-A	10%	45%	45%					0.72	NO2		7.1		7.9E-08	SRNL-STI-2012-00558
58	Riegel et al. WP010-B	10%	45%	45%					0.72	NO2		7.1		7.9E-08	SRNL-STI-2012-00558
59	Riegel et al. WP011-A	10%	45%	45%					0.64	NO2		7.3		5.0E-08	SRNL-STI-2012-00558
60	Riegel et al. WP011-B	10%	45%	45%					0.64	NO2		7.3		5.0E-08	SRNL-STI-2012-00558
61	Riegel et al. WP014-A	10%	45%	45%					0.55	NO2		7.3		5.0E-08	SRNL-STI-2012-00558
62	Riegel et al. WP014-B	10%	45%	45%					0.55	NO2		7.5		3.2E-08	SRNL-STI-2012-00558
63	Riegel et al. WP018-A	10%	45%	45%					0.73	NO2		6.7		2.0E-07	SRNL-STI-2012-00558
64	Riegel et al. WP018-B	10%	45%	45%					0.73	NO2		7.4		4.0E-08	SRNL-STI-2012-00558
65	Riegel et al. WP021-A	10%	45%	45%					0.60	NO2		6.9		1.3E-07	SRNL-STI-2012-00558
66	Riegel et al. WP021-B	10%	45%	45%					0.60	NO2		6.7		2.0E-07	SRNL-STI-2012-00558
67	Riegel et al. WP023-A	10%	45%	45%					0.51	NO2		6.8		1.6E-07	SRNL-STI-2012-00558

#	Identification label	Cement wt%	Fly ash wt%	Slag cement wt%	Silica fume wt%	Sand wt%	Large aggr. wt%	Lime/ Ca(OH)2 or other wt%	w/cm†	Species	Porosity n	Leach index	Intrinsic diffusion coefficient D_i cm²/s	Effective diffusion coefficient D_e cm²/s	Reference
68	Riegel et al. WP023-B	10%	45%	45%					0.51	NO2		7.1		7.9E-08	SRNL-STI-2012-00558
69	Delagrave et al. (1998) M25-0	100%							0.25	HTO	8.7%	7.1	6.3E-09	7.2E-08	Delagrave et al. (1998)
70	Delagrave et al. (1998) M25-50	~50%				~50%			0.25	HTO	7.5%	7.3	3.8E-09	5.1E-08	Delagrave et al. (1998)
71	Delagrave et al. (1998) M25(FS)-0	94%			6%				0.25	HTO	4.0%	7.4	1.6E-09	4.0E-08	Delagrave et al. (1998)
72	Delagrave et al. (1998) M25(FS)-50	~47%			~3%	~50%			0.25	HTO	4.6%	7.6	1.1E-09	2.4E-08	Delagrave et al. (1998)
73	Delagrave et al. (1998) M45-0	100%							0.45	HTO	22.2%	6.4	9.83E-08	4.4E-07	Delagrave et al. (1998)
74	Delagrave et al. (1998) M45-50	~50%				~50%			0.45	HTO	12.2%	6.4	4.58E-08	3.8E-07	Delagrave et al. (1998)
75	Delagrave et al. (1998) M45(FS)-0	94%			6%				0.45	HTO	18.6%	6.7	3.79E-08	2.0E-07	Delagrave et al. (1998)
76	Delagrave et al. (1998) M45(FS)-50	~47%			~3%	~50%			0.45	HTO	11.7%	7.2	7.9E-09	6.8E-08	Delagrave et al. (1998)
77	Johnston and Wilmot (1992)	100%							0.25	HTO	11.3%	7.0		9.12E-08	Johnston and Wilmot (1992)
78	Johnston and Wilmot (1992)	100%							0.25	Cl	11.3%	7.3		5.15E-08	Johnston and Wilmot (1992)
79	Johnston and Wilmot (1992)	100%							0.35	HTO	18.1%	7.1		8.43E-08	Johnston and Wilmot (1992)
80	Johnston and Wilmot (1992)	100%							0.35	Cl	18.1%	7.1		7.18E-08	Johnston and Wilmot (1992)
81	Johnston and Wilmot (1992)	90%			10%				0.25	HTO	14.2%	7.2		5.92E-08	Johnston and Wilmot (1992)
82	Johnston and Wilmot (1992)	90%			10%				0.25	Cl	14.2%	7.8		1.53E-08	Johnston and Wilmot (1992)
83	Johnston and Wilmot (1992)	85%			15%				0.25	HTO	13.0%	7.3		4.86E-08	Johnston and Wilmot (1992)
84	Johnston and Wilmot (1992)	85%			15%				0.25	Cl	13.0%	7.6		2.52E-08	Johnston and Wilmot (1992)
85	Johnston and Wilmot (1992)	90%			10%				0.35	HTO	22.5%	7.3		5.29E-08	Johnston and Wilmot (1992)

#	Identification label	Cement wt%	Fly ash wt%	Slag cement wt%	Silica fume wt%	Sand wt%	Large aggr. wt%	Lime/ Ca(OH)2 or other wt%	w/cm†	Species	Porosity n	Leach index	Intrinsic diffusion coefficient D_i cm²/s	Effective diffusion coefficient D_e cm²/s	Reference
86	Johnston and Wilmot (1992)	90%			10%				0.35	Cl	22.5%	7.5		3.37E-08	Johnston and Wilmot (1992)
87	Johnston and Wilmot (1992)	85%			15%				0.35	HTO	19.8%	7.3		4.64E-08	Johnston and Wilmot (1992)
88	Johnston and Wilmot (1992)	85%			15%				0.35	Cl	19.8%	7.8		1.58E-08	Johnston and Wilmot (1992)
89	Ampadu et al. (1999) OPC 45	100%							0.45	Cl	22.9% est	6.9	2.59E-08	1.1E-07	Ampadu et al. (1999)
90	Ampadu et al. (1999) OPC 55	100%							0.55	Cl	29.2% est	6.9	3.70E-08	1.3E-07	Ampadu et al. (1999)
91	Ampadu et al. (1999) OPC 65	100%							0.65	Cl	35.5% est	6.7	6.34E-08	1.8E-07	Ampadu et al. (1999)
92	Ampadu et al. (1999) FA20 45	80%	20%						0.45	Cl	22.9% est	7.7	5.07E-09	2.2E-08	Ampadu et al. (1999)
93	Ampadu et al. (1999) FA20 55	80%	20%						0.55	Cl	29.2% est	7.7	6.46E-09	2.2E-08	Ampadu et al. (1999)
94	Ampadu et al. (1999) FA20 65	80%	20%						0.65	Cl	35.5% est	7.3	1.73E-08	4.9E-08	Ampadu et al. (1999)
95	Ampadu et al. (1999) FA40 45	60%	40%						0.45	Cl	22.9% est	7.8	4.07E-09	1.8E-08	Ampadu et al. (1999)
96	Ampadu et al. (1999) FA40 55	60%	40%						0.55	Cl	29.2% est	7.9	3.70E-09	1.3E-08	Ampadu et al. (1999)
97	Ampadu et al. (1999) FA40 65	60%	40%						0.65	Cl	35.5% est	7.8	5.09E-09	1.4E-08	Ampadu et al. (1999)
98	SIMCO WS-2	10%	45%	45%					0.60	OH	60.3%	8.1		7.5E-09	SIMCO June (2010) report
99	SREL Saltstone 6 month cure: Oxic	10%	45%	45%					0.60	NO3		7.8		1.5E-08	SREL-R-15-0003
100	SREL Saltstone 6 month cure: Reducing	10%	45%	45%					0.60	NO3		7.8		1.7E-08	SREL-R-15-0003

† Water to dry cementitious materials ratio

Figure 7-1 plots normal distribution z-score versus the base 10 logarithm of the effective diffusion coefficient data. The correlation coefficient for a linear fit to the data is r^2 = 97%, indicating that the D_e data are approximately log-normally distributed. Table 7-2 compares summary statistics for the entire population of data to selected subsets, where the standard deviation of the sample mean is computed as

$$s_m = s/\sqrt{N} \tag{74}$$

where s is the sample standard deviation and N is the number of samples.

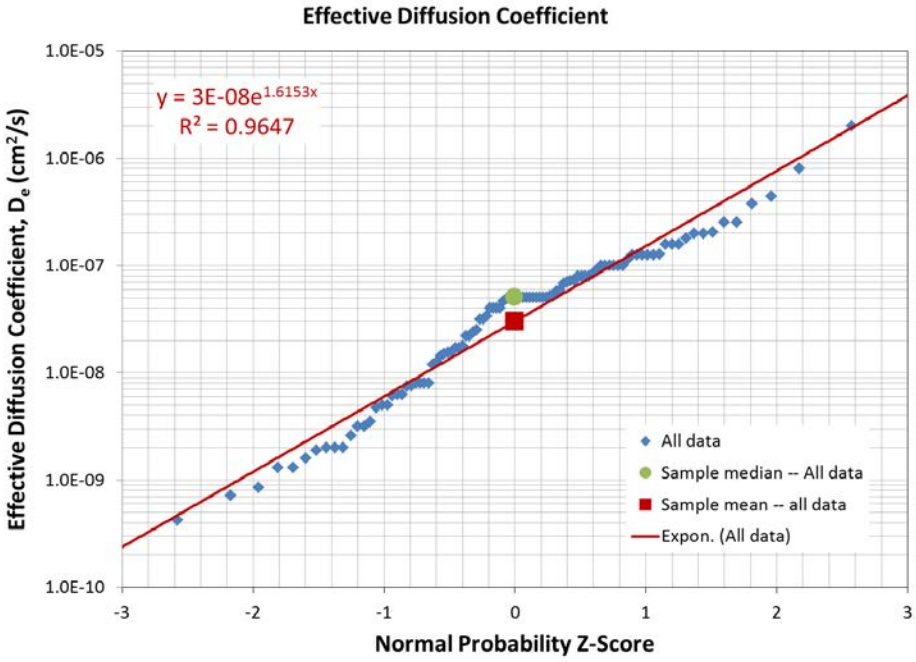

Figure 7-1. Base10 logarithm of effective diffusion coefficient data versus normal distribution z-score.

Table 7-2. Summary statistics for effective diffusion coefficient for different dry mix formulations.

Statistic	All Data	w/o Slag	w/ Slag	w/o Sand (paste)	w/ Sand (mortar)	w/o Slag & w/Sand	Saltstone
Sample count	100	35	65	94	6	5	51
Standard dev. of log10[D_e] (s)	0.71	0.48	0.81	0.72	0.47	0.44	0.62
Std. dev. of mean log10[D_e] (s_m)	0.071	0.080	0.100	0.075	0.191	0.199	0.087
Sample population maximum	2.0E-06	4.4E-07	2.0E-06	2.0E-06	3.8E-07	3.8E-07	2.5E-07
Population upper range (+2s)	8.1E-07	3.7E-07	1.0E-06	8.2E-07	4.7E-07	5.3E-07	6.5E-07
Sample mean upper range (+2s_m)	4.2E-08	6.0E-08	4.0E-08	4.1E-08	1.3E-07	1.7E-07	5.5E-08
Median	5.0E-08	4.9E-08	5.0E-08	4.9E-08	5.0E-08	5.1E-08	5.0E-08
Geometric mean D_e ($10^{\text{mean De}}$)	3.0E-08	4.1E-08	2.5E-08	2.9E-08	5.4E-08	6.9E-08	3.7E-08
Sample mean lower range (-2s_m)	2.2E-08	2.9E-08	1.6E-08	2.1E-08	2.3E-08	2.8E-08	2.5E-08
Population lower range (-2s)	1.1E-09	4.6E-09	6.2E-10	1.0E-09	6.3E-09	8.9E-09	2.1E-09
Sample population minimum	4.2E-10	5.0E-09	4.2E-10	4.2E-10	1.7E-08	2.4E-08	1.6E-09

Little to no change in the median, and small changes in the mean value are observed across the various populations. Modest changes in the sample standard deviation are noted. These comparisons suggest that the variability of the grout diffusion data is not strongly dependent on the formulations considered in Table 7-2, unlike the hydraulic property data considered in Section 6.0. Nonetheless, separate paste and mortar properties can be defined based on the "w/o Sand" and "w/ Sand" classes as noted.

Table 7-3 provides summary statistics for three additional sub-populations focused on eliminating potential data biases. The "No Cl^-" group omits tests performed with chloride which may exhibit sufficient sorption to bias D_e toward lower values. For this grouping, the median is unchanged and the mean is actually slightly lower. Thus no bias due to inclusion of chloride data was detected. The "No Langton (1986) Mix 3A/B" group omits one 2.0E-6 cm^2/s value, which is approaching a value representative of soil. The median is unchanged and the mean is slightly lower indicating minimal impact of this potential outlier. The third group omits chloride data and the Langton (1986) Mix 3A/B value. Again, very minimal changes to summary statistics occur. Table 7-2 and Table 7-3 together suggest that the entire data set can be used to develop recommended values for D_e.

In developing recommended D_e values, we assume that the IDF PA analysis requires a best estimate value that reflects the average behavior of SSW waste forms. The recommended best-estimate value is the mean value from the entire population, D_e = 3.0E-8 cm^2/s. This value is shown in Table 7-4. Also listed are the recommendations of other authors and assumed values in relevant modeling studies as points of reference. Also provided in Table 7-4 are ±2-sigma pessimistic / high and optimistic / low values based on the total variability of the data population; these values define the 95% confidence range for an individual waste form.

Table 7-3. Summary statistics for effective diffusion coefficient excluding potential data biases.

Statistic	All Data	No Cl^-	No Langton (1986) Mix 3A/B	No Cl^- & No Langton (1986) Mix 3A/B
Sample count	100	85	99	84
Standard dev. of log10[D_e] (s)	0.71	0.76	0.69	0.74
Std. dev. of mean log10[D_e] (s_m)	0.071	0.082	0.070	0.080
Sample population maximum	2.0E-06	2.0E-06	8.0E-07	8.0E-07
Population upper range (+2s)	8.1E-07	9.7E-07	7.0E-07	8.3E-07
Sample mean upper range (+2s_m)	4.2E-08	4.3E-08	4.0E-08	4.0E-08
Median	5.0E-08	5.0E-08	5.0E-08	5.0E-08
Geometric mean D_e ($10^{mean\ De}$)	3.0E-08	2.9E-08	2.9E-08	2.8E-08
Sample mean lower range (-2s_m)	2.2E-08	2.0E-08	2.1E-08	1.9E-08
Population lower range (-2s)	1.1E-09	9.0E-10	1.2E-09	9.5E-10
Sample population minimum	4.2E-10	4.2E-10	4.2E-10	4.2E-10

Table 7-4. Recommendations and IDF PA assumptions for effective diffusion coefficient.

Effective Diffusion Coefficient† D_e (cm²/s)	Grout	Paste	Mortar	Comments
Pessimistic / high value considering total (population) uncertainty	8.1E-07	8.2E-07	4.7E-07	Population upper range from Table 7-2
Pessimistic / high value considering mix uncertainty	1.5E-07	1.6E-07	3.0E-07‡	Best-estimate value + $2s_{mix}$ from Equation (78)
Best-estimate value	3.0E-08	2.9E-08	5.4E-08	Means from Table 7-2
Optimistic / low value considering mix uncertainty	6.2E-09	5.3E-09	1.0E-08‡	Best-estimate value - $2s_{mix}$ from Equation (78)
Optimistic / low value considering total (population) uncertainty	1.1E-09	1.0E-09	6.3E-09	Population lower range from Table 7-2
Recommendations of others				
Phifer et al. (2006) recommendation: Low quality concrete	8.0E-07			Phifer et al. (2006) Table 6-44
Phifer et al. (2006) recommendation: Medium/ordinary quality concrete	1.0E-07			Phifer et al. (2006) Table 6-44
Phifer et al. (2006) recommendation: High quality concrete	5.0E-08			Phifer et al. (2006) Table 6-44
Meyer and Serne (1999) recommendation (Table 5.2 NO3)	5.0E-08			PNNL-13035
Pierce et al. (2004) recommendation: Any cement/grout (Table 13 N)	5.0E-09			PNNL-14805
2003 Risk Assessment	2.5E-08			As reported in PNNL-24022, Table 3.3
TC&WM EIS: Nitrate (non-sorbing species) effective diffusion coefficient through 500 years	3.04E-08			As reported in PNNL-24022, Table 3.5
Cantrell (2015)	2.0E-09 to 1.0E-08			PNNL-24081, Table 3.1
Cantrell et al. (2016): LAW Waste Cast Stone	2.0E-09 to 1.0E-08			PNNL-25194, Table 3.1, Nitrate
Cantrell et al. (2016): Secondary Waste Fly-Ash-Based Cast Stone	2.0E-10 to 9.0E-10			PNNL-25194, Table 3.1, Nitrate
Cantrell et al. (2016): Secondary Waste Lime-Based Grout	3.0E-11 to 8.0E-10			PNNL-25194, Table 3.1, Nitrate
Past IDF PA assumptions				
2003 Supplemental LAW Waste RA	2.5E-08			As reported in PNNL-24022, Table 3.7
2005 IDF PA Secondary Waste	5.0E-09			As reported in PNNL-24022, Table 3.7
2012 TC&WM EIS LAW and Secondary Waste	3.04E-08			As reported in PNNL-24022, Table 3.7

† equal to apparent or observed diffusion coefficient for a non-sorbing species
‡ calculation assumes s_{mix} same as for log10[De] for paste (= 0.37)

A range defining the uncertainty of average waste form behavior may also have value for the IDF PA analysis. In this case the pessimistic value for D_e should account for uncertainty in the grout formulation(s) that will be used for SSW burials, but not container-to-container variability for the grout formulation(s) that will ultimately be used. The total variability in the $log10(D_e)$ data set can be decomposed into "between-mix" and "within-mix" variability (e.g. Walpole and Myers 1978, Theorem 10.1) as:

$$\sigma^2_{total} = \sigma^2_{between-mix} + \sigma^2_{within-mix} \quad (75)$$

The total variance of the $log10(D_e)$ population is estimated from Table 7-2 (or Table 7-3) as

$$s^2_{total} = (0.72)^2 = 0.51 \quad (76)$$

The most reliable within-mix statistics available from Table 7-1 data are those from the 10% cement / 45% fly ash / 45% slag mix known as "Saltstone". This mix comprises one half of the available data (51 values). The within-mix $log10(D_e)$ variability for Saltstone from Table 7-2 is

$$s^2_{saltstone} = (0.62)^2 = 0.39 \quad (77)$$

Assuming that all mixes have approximately the same within-mix variability as Saltstone, Equations (75) through (77) can be combined yielding the estimate

$$s_{mix} \cong \sqrt{s^2_{total} - s^2_{saltstone}} = \sqrt{0.51 - 0.39} = 0.35 \quad (78)$$

Table 7-4 provides recommended pessimistic / high (1.5e-7 cm^2/s) and optimistic / low (6.2e-9 cm^2/s) values for effective diffusion coefficient based on mix uncertainty estimated by Equation (78). Assuming a log-normal distribution for the between-mix variability, the pessimistic and optimistic values correspond to a ±95% confidence interval about the best-estimate value.

The summary statistics in Table 7-4 for generic grout are also provided for paste and mortar mixes. These values are computed in the same manner as described above for grout, with one exception. The total variance of the mortar data is less than the variance of the Saltstone data, which would produce a negative between mix variance. This outcome may be a result of a small mortar sample size (N = 6) and/or limited test mixes. As a remedy, the between-mix standard deviation for mortar is assumed to be the same as that for paste ($s_{mix} = 0.37$). The table also provides examples from other studies for information. Note that values for similar COPC from Cantrell et. al (2016) are not included due to the fundamental differences in the mixes considered.

A paste dry-mix may be used to solidify non-debris SSW (< 60 mm particle size), producing a cast material that is more similar to mortar than a pure paste. Mortar properties are considered more appropriate than paste properties for IDF PA modeling on this basis, because mortar properties are pessimistic-tending. For any SSW debris waste within an encapsulation grout, we recommend taking no credit for resistance to diffusive transport within the waste zone, because of uncertainty in the form and effective properties of the debris wastes that may be disposed. An appropriate effective diffusion coefficient for the waste zone is 5.0E-6 cm^2/s for soil-like conditions (Phifer et al. 2006 Table 5-18).

Implicit in the above discussion is an assumption that the grout samples were fully saturated during testing. Full or practically 100% saturation was likely the case for multiple reasons:

- To avoid self-desiccation and associated early-age cracking, grout formulations are generally designed to provide more mix water than the minimum necessary to support hydration reactions; excess water occupies the pore space.
- While curing, additional external water is typically made available to the pore structure through water contact or a high humidity atmosphere, which ensures 100% saturation at least adjoining exposed surfaces.
- All of the test methods considered herein exposed sample surfaces to a water bath, that would have quickly saturated any near surface unsaturated portions of the sample (where early diffusion occurs), if not the entire sample.
- EPA-1315 requires periodic sample weighing, creating the opportunity to observe mass gain due to water imbibition; the source references do not report such observations.
- Evolving saturation conditions leading to a non-constant apparent diffusion coefficient would have produced results deviating from the expected square-root-of-time behavior in experimental data plots; the source references do not report concerns about sample saturation state.

For these reasons, the effective diffusion coefficient values in Table 7-4 are thought to be fully reflective of saturated conditions.

8.0 Geochemistry

This section includes a general discussion of the three parameters used to describe solute interaction with the solid phase:

- distribution coefficient (K_d values),
- apparent solubility concentration (k_s), and
- apparent diffusion coefficient (D_a).

Additionally, the impact of the following parameters on these geochemical parameters was evaluated:

- cementitious material composition (OPC+FA, OPC+FA+BFS, OPC+FA+aggregate, OPC+FA+BFS+aggregate),
- cementitious material age (Stage I, Stage II, and Stage III),
- longevity of reducing conditions in cementitious materials with BFS,
- conceptual model and parameterizing COPC desorption from secondary waste (Granular activated carbon (GAC), resin, HEPA filters, and Ag-mordenite),
- disposal design (encapsulated vs. solidification)

The basic philosophy used to develop and to parameterize the geochemical models involved using: 1) basic mechanistic studies primarily reported in the literature to provide guidance for the conceptual geochemical models, and 2) empirical studies, preferably with site-specific materials and conditions, to provide input values to help quantify the conceptual models. COPC partitioning between the aqueous and solid phases was described using the K_d value and the apparent solubility concentration (defined in Section 8.1). A series of look-up tables (Tables 8-4 – 8-7) were prepared containing these parameters that vary with the type of porous media, the age of the cementitious material, and the presence or absence of BFS. Additionally, upper and lower limits are recommended. Given the size of these look-up tables, they are placed at the end of the Section 8.0 rather than integrated with the text.

Sections 8.2 and 8.3 describe the apparent solubility concentrations and the apparent diffusion coefficient, D_a, and how they differ from K_d values. Importantly, it was decided not to employ more mechanistic surface complexation models, which are discussed in these sections. While such models have been used to address limited conditions, their widespread application for PAs has not yet been widely used primarily because an extraordinarily large number of model-input values would need to be generated to support the large number of COPCs and wide range of environmental conditions existing in disposal environments. Iterative PAs is the appropriate approach to support a decision on the possible need for more complex sorption models. Section 8.4 defines and describes the approach used to select the best, minimum, and maximum input parameters for K_d, k_s, and D_a values.

The conceptual models describing COPC release from reducing cementitious materials, non-reducing cementitious materials, various secondary waste (GAC, spent ion-exchange resin, HEPA filters, and Ag-mordenite), and the two types of waste form (encapsulated and solidified) are also described (Sections 8.5 through 8.8). Section 8.9 culminates in a series of tables with recommended input values and justification for their selection (Section 8.9).

8.1 Distribution Coefficients (K_d values)

The radionuclide-solid phase interactions are complex, and include adsorption (surface binding), absorption (incorporated into the structure of the solid phase), partitioning into organic matter,

complexation, precipitation, and co-precipitation. The magnitude of this interaction for a given contaminant may vary greatly depending on solid phase composition or pore water chemical composition. Each of the types of interaction between the contaminant and cementitious material has a unique numerical representation. However, the most common approach used in coupled reactive-transport modeling is to incorporate all of these reactions into one K_d value. The K_d value is the simplest construct describing contaminant sorption to cementitious materials. Sorption is used here in a manner consistent with the definition provided by Stumm and Morgan (2012), that is, all processes that remove solutes from the aqueous phase. The K_d value (mL g^{-1}), as discussed in Section 4.2 in relation to Equation (23), is the ratio of the contaminant concentration sorbed to the solid phase (c_s (mol g^{-1})) divided by the contaminant concentration in the liquid surrounding the solid phase (c (mol mL^{-1}). It is important to note that sorption, as expressed by K_d values, is normalized by mass, and not volume, as transport modelers often use, or surface area, as surface chemists use. First and foremost, it is assumed that steady state is achieved and that kinetic, the necessary time required for sorption to be complete, is not limiting sorption. Sorption kinetics is typically not an issue for water movement within cementitious materials, thereby providing long aqueous/solid phase contact times. The K_d construct also describes a process that is reversible, i.e., the rate at which it adsorbs is equal to the rate that it desorbs. The K_d construct also describes sorption within the lower range of a sorption isotherm (Figure 8-1) where sorption is linear, i.e., where changes in aqueous concentration do not impact the extent of sorption.

As COPC concentration on the solid phase increases, the sorption isotherm becomes non-linear, i.e., it takes on a Freundlich sorption profile. An alternative sorption process, in which a sorption maximum is obtained, the Langmuir model, also exists, but is less likely to be a concern in repository conditions where COPC concentrations are relatively low. The non-linearity has been attributed to the number of available sorption diminishing to a point that it becomes less likely for the solute to find an available sorption site. The aqueous phase concentration where this transition occurs varies with solute and sorbent. For example, in a carbonate sandy soil, the transition between linear and non-linear sorption for Sr was 10^{-5} M Sr and for Cs was 10^{-6} M Cs (Krupka et al. 1999). Upon adding more solute to the system, as may occur near or in the source term, precipitation may occur and solubility can control the release of the solute from the aqueous phase. This is discussed in more detail in Section 8.2.

An important limitation of the K_d construct is that, in theory, it describes sorption under a very limited set of aqueous and solid phase conditions. Changes in either may alter the K_d value. The extent of this change varies greatly with the solute, such that some solutes, such as Cs and nitrate/nitrite are much less prone to changes in magnitude of sorption than other solutes, such as U and Hg. Other ions in solution can compete with COPCs for sorption sites and may form complexes with the COPC resulting in a complex species that has unique binding affinities to mineral surfaces (Stumm and Morgan 2012). To account for the impact of aqueous ions on COPC sorption, it is common practice to use an appropriate aqueous proxy in the K_d laboratory measurement (Krupka et al. 1999).

As pointed out above, the K_d construct assumes the reaction is reversible, i.e, that the rate of adsorption is equal to the rate of desorption. However, it has been frequently demonstrated in laboratory studies that the rate of desorption is much slower than the rate of adsorption (Rumynin et al. 2005). The implication of this discrepancy is that the desorption process is rate limiting and therefore K_d values measured using the desorption method provide a better estimate for transport modeling. This is discussed in more detail in regards to how data was selected (Section 8.4).

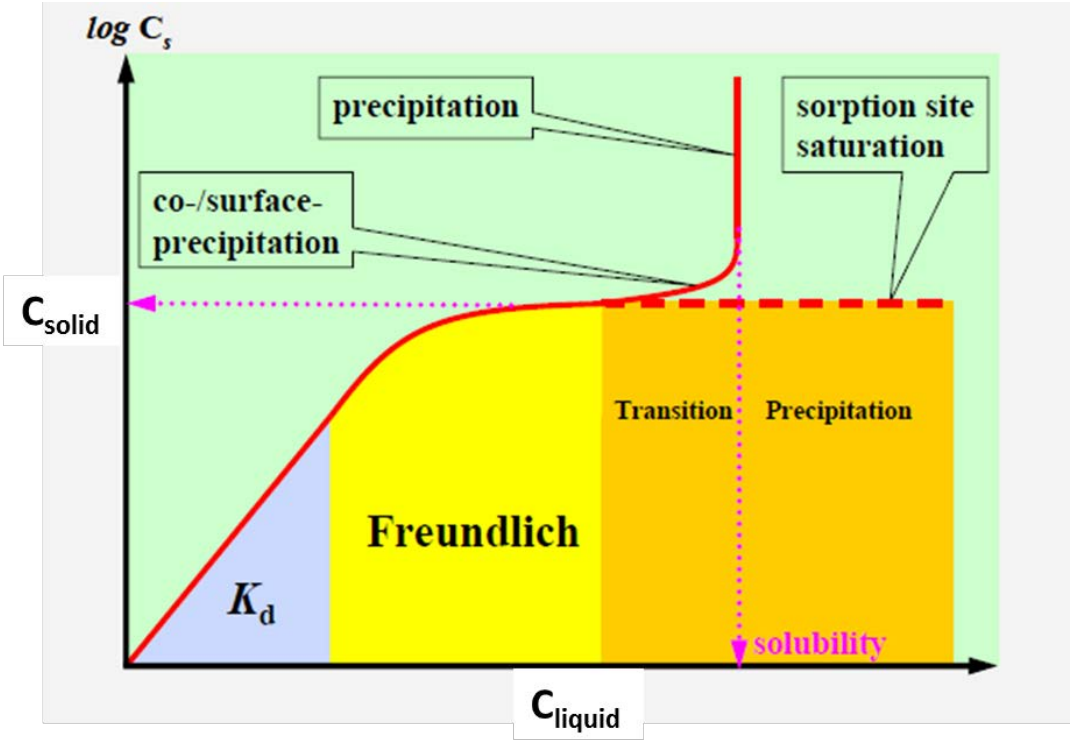

Figure 8-1. Sorption isotherm (aqueous COPC concentration, C_{liquid}, versus surface bound COPC, C_{solid}) identifying the linear range (K_d equation), non-linear range (Freundlich sorption equation), and the apparent solubility product (k_s) (based on figure from (Wang et al. 2009).

Identifying the processes that govern COPC chemical behavior is the single most important task necessary for estimating K_d values for a PA. Once the dominant geochemical process is identified for a specific geological and chemical environment, the range of relevant "empirical" K_d values can be narrowed. COPC geochemical processes have been ascertained primarily through experiments in which a key parameter is systematically varied, *e.g.*, suspension pH or COPC concentration. The trends displayed during these experiments provide key information regarding COPC behavior and also shed light on which processes may be controlling the COPC interaction between the solid and liquid.

In summary, the reasons for selecting the K_d construct for the PA are listed below.

1) The majority of the data in the literature describes sorption using K_d values (or percent sorbed that can be converted to K_d values with knowledge of the amount of solids and liquids used in the experiment).
2) Under the expected low concentrations of the contaminants, sorption is expected to be linear, i.e., sorption is independent of contaminant concentration and, therefore, K_d is a constant for a given contaminant/geological material/water composition combination under identical (geo)chemical conditions.
3) K_d can be used directly in common PA transport codes, including STOMP, PORFLOW, and GoldSim.
4) There is presently no thermodynamically-based conceptual model or numerical code that is robust enough to predict accurately the degree of COPC adsorption/desorption as the solid phase and aqueous phases evolves during the period of interest of the PA.

8.2 Apparent Solubility Concentrations (k_s)

In addition to the K_d construct, the apparent solubility concentration, k_s, (mol/L) can be used to describe COPC partitioning between the solid and aqueous phases, especially within disposal sites and within waste forms (Figure 8-1). k_s values are used for conditions where the concentrations of the COPCs exceed the solubility of an assumed solubility-controlling mineral phase. Such conditions are identified based on a combination of thermodynamic calculations and laboratory microscopy and wet chemistry studies involving COPC of varying concentrations (Stumm and Morgan 2012). Selection of controlling solid phases for the SSW PA activities is based on laboratory experiments, calculations, and the literature. It is anticipated that when COPC concentrations exceed the solubility concentration value for a given mineral, precipitation or more likely coprecipitation occurs and subsequent COPC aqueous concentrations are controlled by k_s. These coprecipitated phases are not pure end-member mineral phases, i.e., they include trace impurities in them that alter thermodynamic estimates of the solubility concentration. Consequently, it is more accurate to use empirical, laboratory-derived measurements of k_s values, referred to as apparent solubility concentrations. At concentrations below the solubility limit, the COPC concentration is assumed to be controlled by the K_d construct. When the solubility-controlling solid could not be identified but empirical solubility tests indicated that some unidentified phase was controlling solution concentration, then an empirical solubility relationship was used.

Apparent solubility concentrations are proposed for use under reducing cementitious conditions for Tc and Cr. Theoretically, these COPCs have been shown to be solubility controlled (Cantrell and Williams 2012; Li and Kaplan 2012; Rai et al. 1987; Bajt et al. 1993), and equally important, laboratory data are available.

8.3 Apparent Diffusion Coefficients (D_a)

Apparent diffusion coefficients (D_a) are described in detail in Section 5.0 and defined in Equation (33). The D_a construct is a combination of hydrology and geochemistry as compared to D_e, which does not include geochemistry (diffusion of a non-reactive COPC). The advantage of this parameter is that it reflects directly the process of concern. It also provides a measure of desorption, as opposed to (ad)sorption, which typically is the rate limiting step. However, the application of the D_a for PA purposes is rather limited because it is not a robust parameter; slight changes in the experimental set up, such as sampling interval and leachate chemistry, can yield vastly different results (EPA 2013). Consequently, a standard method, Method EPA 1315 (EPA 2013) has been established that does not necessarily represent the conditions of interest, but importantly, permits comparing measured values between tests and laboratories. Such a test is very important for example when evaluating different cement formulations for their capacity to immobilize COPCs. To provide site-specific information, researchers have developed modified EPA 1315 methods. For example, for PA purposes, the ideal D_a test for an oxidizing cementitious waste form might be an EPA 1315 method modified to include oxidizing partially saturated conditions and various cementitious leachate chemistries. Another important limitation of the D_a parameter is that, as noted above, it's a compound construct including both hydrological and chemical conditions. As cementitious materials age, both these parameters will change independently. Decoupling these processes, through the combined use of D_e and K_d/k_s provides greater robustness and the opportunity to capture expected hydrological and mineral changes in the evolution of cementitious materials.

The laboratory derived D_a estimate assumes that linear reversible sorption conditions (i.e., K_d conditions) exist. For reducing cementitious solids, this assumption is reasonable for NO_2^-, NO_3^-, I, Cs, and Sr, but not for Cr or Tc, which have been shown to precipitate under these conditions (Section 8.2). The implications of estimating D_a values by assuming K_d-like conditions when k_s conditions exist is that the magnitude of D_a is in part controlled by the initial Cr or Tc concentrations used in the monolith (larger initial spikes above solubility limits will result in unrealistically low estimated D_a values).

There have been several D_a measurements primarily of nitrate, nitrite, iodine, and technetium using a wide range of Hanford specific cementitious formulations. Lockrem et al. (2005) and Pierce et al. (2010) report Hg D_a values of Hanford waste forms. Because not all needed D_a values are available for the range of cementitious conditions anticipated during the PA's period of interest, it was necessary to use both literature values, and values calculated based on the recommended values for D_e adjusted using the recommended K_d values ($D_a(calc)$) (Appendix E). A comparison of the $D_a(calc)$ values and measured D_a indicates the former are either within an order of magnitude (nitrate, nitrite) or are larger (pessimistic; Cr and Tc) than the measured values. This is not surprising, given that Cr and Tc are not controlled by K_d and therefore the assumptions used in $D_a(calc)$ would be biased in an overly pessimistic manner with respect to the measured values.

8.4 Approach to Selection of Geochemical Parameters

Ideally, all input data would be derived from experiments conducted using Hanford-specific materials and under the appropriate environmental conditions. That is not possible. For example, it is not possible to measure U leaching from Cast Stone that has been aged 100s to 1000s of years because there is not any of this material available. However, where site-specific data was not available, literature K_d values using non-Hanford solid and aqueous phases were used. Careful selection of these literature values was required to ensure that the experimental conditions used to generate the K_d, k_s, *or* D_a values were reasonably appropriate for Hanford conditions. Finally, when Hanford-specific and literature values were not available, expert judgment was used to estimate values based on chemical analogue information. The intent is to provide data that can be used for the initial PA calculations, which can then provide insights regarding areas where further refinement is needed.

In summary, a ranking of the data pedigree used for selecting the best K_d, k_s, and D_a values follow:

1. Hanford-specific measured data,
2. literature experimental data, and
3. expert judgment based on analogue.

Furthermore, K_d data pedigree ranking was further ranked in decreasing pedigree:

1. desorption measurements of appropriate analogue waste form samples,,
2. desorption measurements of laboratory COPC-amended samples, and
3. literature derived values.

There have been several compendiums of COPC K_d values for cementitious materials (Bradbury and Sarott 1995; Bradbury and VanLoon 1997; Cronstrand and Power 2005; Krupka and Serne 1998; Wang et al. 2009; Kaplan 2016; and Ochs et al. 2016).

Furthermore, k_s data pedigree was further ranked by:

1. laboratory measurements, and
2. thermodynamic calculations.

Finally, perspective on the impact of aggregate (aggregate of sand) on measured K_d results. The most chemically reactive fraction of cementitious materials is the cement itself and not the aggregate. Within cement there are various minerals that are especially reactive to some COPCs, while other minerals are more reactive to other COPCs. Most COPC sorption studies are conducted with either cements or specific mineral phases within cement; they typically do not include any aggregate. There are also several other studies where they report only the paste used, even though the formulation includes

aggregate (e.g., a cementitious material made with OPC and sand is simply referred to as OPC). There have not been any systematic studies conducted to quantify the impact of aggregate on K_d values. Previous compilations of cementitious material K_d values have not accounted for the presence of aggregate (Krupka and Serne 1998; Cronstand and Power 2005; Wang et al. 2009; Kaplan 2016; Och et al. 2016). One set of studies provides information supporting the conclusion that aggregate has minimal impact on the K_d was reported by Wang et al. (2009) (and summarized in less detail in Ochs et al. 2016). These reports compile cement K_d values agreed upon by an international panel of experts for use in PA calculations.[3] Among the data included in this compilation was a full suite of COPC sorption data for two site-specific formulations, CEM I and CEM III. CEM I included 75% aggregate and CEM III, a reducing mortor, included 64% aggregate. The K_d values from a dozen COPCs were included in graphs and tables containing K_d data in the literature, many of which originated from tests with pure paste/cement samples. The CEM I and CEM III, data did not stand out and the experts did not conclude the need to differentiate between K_d values originating from studies with and those without aggregate.

While the notion that aggregates do not dilute K_d values may seem counter intuitive, it should be kept in mind that few sorption phenomena are additive, stemming from unique physical (size) and distribution (coatings) properties of the cement phases that are not accounted for in component additivity models (dilution effect). Cement forms coatings along aggregate and as such, it is spread out in places where the water is most likely to travel. In this conceptualization, it is therefore possible for a concrete containing 10% cement to have water flow in regions that come into contact dominated by cement particles and the aggregate would be hydraulically isolated.[4] By analogy, many, if not all soils have coatings. In the southeastern US, the bulk mineralogy is very unreactive (kaolinite, quartz, gibbsite, and trace levels of illite). They derive essentially all of their reactivity from surface coatings of iron oxyhydroxides or organic matter. The presence of 3% iron in the soil, which exists primarily as iron-oxyhydroxide coatings, converts a largely inert solid phase to a moderately reactive soil (with respect to highly reactive geologically younger soils). Similarly, the presence of 2 to 4 percent natural organic matter, again as particle coatings, completely changes the tendency of these soils to bind solutes.

In summary, as noted above, selection for K_d values for the IDF PA will be biased towards results based on site-specific measurements. Where data is missing literature values will be used for guidance. As was done with previous Hanford cement data packages (Krupka et al. 2004), literature K_d values, including studies conducted with pastes, will also be used to provide guidance where lack of sufficient site-specific data is available.

8.4.1 Best Estimates

The best estimates present the most likelyK_d, k_s, *or* D_a values for a given condition. These values are based primarily on some central value of relevant data, Hanford or SRS site-specific experimental data, or on expert judgment. Furthermore, the professional judgment used in selecting the best estimates is based on the best available data. Best estimates are not necessarily a numerical mean of all available values, but instead represent a critical review of the available data and are based heavily on the quality of the experiments used to generate the data (Section 8.4). Identifying best estimates also relied greatly on consideration of geochemical theory and geochemical modeling. For example, measured k_s values that approached values calculated based on thermodynamic consideration were assigned high pedigree. In the case of D_a, there is limited available data using a wide range of potential cement formulations (Um et al. 2016; Westsik et al. 2013; Cantrell et al. 2016). The authors summarized the D_a data by providing a

[3] These values are designed to provide guidance and understanding for how to select K_d values for a specific site and they note the need for site specific measurements.

[4] D. Kaplan corresponded with Dr. M. Ochs (ARCADIS, Schlieren, Switzerland) regarding this subject and Dr. Ochs mentioned he was not aware of any studies quantifying the influence of aggregates on K_d values. He also noted "I feel that the real question is whether a radionuclide moving through a cement barrier would actually ever encounter an aggregate surface or whether all surfaces are effectively covered by cement minerals – and where cracks would be located."

minimum and maximum D_a values (Cantrell et al. 2016). The D_a best estimates were calculated as the mean of these two extreme recommended values, and as such represent the central value of this limited data set.

8.4.2 Data Range

The data ranges were based on estimates of the 95th percentile, not all data. A key problem with this approach is that there is not sufficient data in all cases to provide these estimates. Such information is needed for all three cement stages for each COPC for the appropriate geochemical parameter (K_d, k_s, and/or D_a). As with the best estimates (Section 8.4.1), the preferred option is to base this estimate on Hanford-specific measurements. But where such data was not available, it was based on an approach applied at the SRS (Almond and Kaplan 2011). As is summarized in (Almond and Kaplan 2011), this approach is based on Cs, Sr, and I K_d measurements made on 22 aged saltstone samples of widely different states of oxidation, and composition. Furthermore, the measurements were made under conditions that were approaching those of oxidizing conditions, i.e., on a bench top. Based on these measurements, the authors concluded that the 95-percentile range was best estimated by a log normal distribution (non-zero-truncated log normal in the case of I) and could be estimated using

$$K_{d,min} = K_d - (1.5 * 0.5K_d) = 0.25K_d \quad (79)$$

$$K_{d,max} = K_d + (1.5 * 0.5K_d) = 1.75K_d \quad (80)$$

where K_d is the best estimate. Because the details of the wasteform are still not certain, the range and distribution for this PA need to be changed. The range will be increased compared to that recommended by Almond and Kaplan (2011), and the recommended distribution will be changed from log-normal to triangular. The latter distribution makes no assumption about how the data is distributed, which is necessary because of the lack of experimental data. To capture these differences, the ranges were calculated using

$$K_{d,min} = K_d - (1.5 * 0.6K_d) = 0.1K_d \quad (81)$$

$$K_{d,max} = K_d + (1.5 * 0.6K_d) \cong 2\,K_d \quad (82)$$

For example, if the Best Estimate K_d is 100 mL/g, the K_d (*min*) would be 10 mL/g (based on Equation (81)) and the K_d (*max*) would be 200 mL/g and the distribution would be triangular. While this approach provides consistency in the treatment of the variability, ideally enough data would be available under each cement stage and for each COPC to create COPC specific distribution ranges.

For k_s data, the min and max values were set to plus or minus one order of magnitude. As will be discussed in Section 8.9, this range is based on a critical review of the large number of Tc-reducing cementitious material measurements that have been reported. For consistency, the same range for Tc, was applied for Cr, which has far fewer reported measurements in reducing cementitious material conditions.

The range for D_a values was derived primarily from a large data set reviewed by Cantrell et al. (2016). The ranges they assigned for Cr, I, N, Tc, and U were consistently about 1 order of magnitude (see Table 8-7 at end of section). An order of magnitude range was used for the other COPCs not considered by Cantrell et al. (2016), Cs, Hg, and Sr. As is the case with K_d and k_s the D_a distribution was assigned a triangular distribution.

8.5 Cementitious Materials Conceptual Model

The core of the conceptual model used to describe COPC geochemistry in cementitious environments was taken from Atkinson et al. (1988) and has been proposed in previous Hanford data packages (Krupka et al. 2004; Last et al. 2015; Cantrell et al. 2016), as well as at the SRS (Kaplan 2016), and in Europe (Ochs 2016; Wang et al. 2009; Cronstrand and Power 2005). There is extensive research supporting the underpinnings of this model, which describes three types of physicochemical aging environments, or stages, that all cementitious materials generally progress through (Figure 8-2).[5] The duration of each stage is controlled by how much recharge water, measured in units of pore volumes (or exchange cycles) passing through the cementitious material, thereby promoting cement degradation. The advantage of using Figure 8-2 and the concept of exchange cycles is that it is generic to a wide range of cement configurations and compositions. Once flow models have been established for a specific facility, the exchange cycles for that facility can be quantified. Facilities with more concrete will have larger exchange cycles (larger pore volumes) than those with less concrete. An exchange cycle can be converted quickly into units of time once the water travel rate through a specific cementitious facility is established.

A key difference between the Hanford and the European and SRS systems is that the Hanford system is much drier. This has a number of important geochemical consequences that deal with the interaction (coupling) of processes. The two most important differences are: 1) there will be far fewer pore volumes passing through the system and 2) the cement system may be unsaturated with respect to water. While the first issue can be addressed with the existing conceptual physiochemical aging model, the second issue cannot. The potential presence of an interconnected gas pathway is not captured in this model. Among the key geochemical processes that are especially influenced by a gas pathway is accelerated carbonation of cement as a result of providing a faster pathway for $CO_2(g)$ to come into contact with the cementitious material and accelerated oxidation of reducing cements as a result of providing a faster pathway for $O_2(g)$ to oxidize the reducing cement. Aside from their concentrations being different in air and porewater, they also diffuse 10^5 times faster through air than in porewater. Carbonation of cement by porewater or air has been extensively studied in relation to the construction industry and several books have been written on the subject (reviewed by Bertos et al. 2004; Parrott 1987). To our knowledge there is no quantitative or qualitative information about the oxidation of reducing cement through an air pathway. This lack of knowledge introduces uncertainty to the conceptual model. There will be a need to modify the existing conceptual geochemical cement model to account for the drier environment unique to Hanford. The general approach is described Section 8.7.3.

8.6 Cementitious Material Aging Resulting from Porewater Leaching

Development of this conceptual model was based on laboratory studies as well as on natural analogue and ancient cement/concrete characterization studies. One of the key aqueous parameters used to identify when one stage starts and ends is pH (Figure 8-2). Changes in pH have been used as an indicator of more widespread changes in cement mineralogy and porewater aqueous chemistry (Krupka et al. 2004; Cantrell et al 2016; Ochs et al. 2016; Wang et al. 2009; Kaplan 2016; Cronstrand and Power 2005). The pH changes are the result of mineralogical transformations that occur as the cement ages. The cement solids present in each stage are assumed to have unique sorption properties and for this reason, unique K_d, k_s, *or* D_a values are assigned to each stage. As noted above, the IDF system is expected to have relatively few exchange cycles stemming from the arid environment and the unsaturated flow conditions expected in the cementitious waste forms. Consequently, it is possible that this three stage conceptual model of the system may be simplified to fewer stages. Initial PA modeling results will provide guidance for deciding whether a simplified model is justified.

[5] Ochs et al. (2016) and the original report by Wang et al. (2009) divide what is referred to here and by others as Stage III into two stages, resulting in four stages of cement aging. It was elected here not to follow their example because it requires another set of data that is very difficult to measure, and as such, does not provide added accuracy.

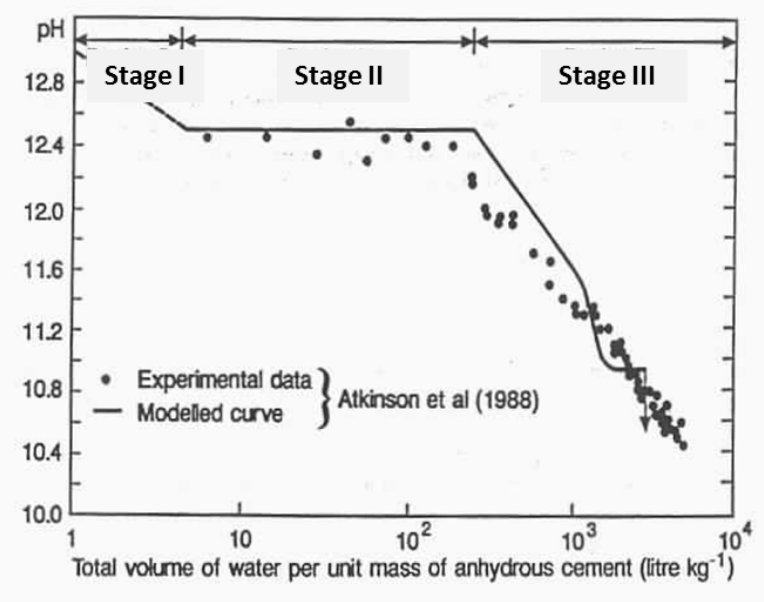

Figure 8-2. Conceptual model used by Krupka et al. (2004) describing the influence of exchange cycles (X-axis) on pH and the designated Stages (Atkinson et al. 1988).

A brief description of each of the three stages is described below in Sections 8.6.1 through 8.6.3, while a more detailed discussion is presented in Krupka et al. 2004. Recommended assumptions are summarized in Table 8-1. Geochemical COPC input values for oxidizing and reducing cementitious materials are provided in Section 8.9.

8.6.1 Young Cementitious Materials (Stage I)

Stage I is the youngest stage of the cementitious solids that occurs immediately after the cement hardens and infiltrating water passes through it. The cement porewater is characterized as having a high pH (>12.5), high ionic strength, and high concentrations of potassium and sodium. The high concentrations of these monovalent cations result from the dissolution of alkali impurities in the various constituents comprising the solids (e.g., lime, ordinary Portland cement, fly ash, and aggregate). Hydration continues during Stage I with the formation of calcium-silicate-hydrate gels (a common shorthand for this gel is calcium-silicate-hydrate (CSH), which is a $CaO\text{-}SiO_2\text{-}H_2O$ amorphous material that hardens and constitutes "cement") and portlandite [$Ca(OH)_2$]. The composition of the cement pore fluid is at equilibrium with portlandite during this time.

Based on the modeling estimates provided by Berner (1992), Stage I may last between 1 and 100 exchange cycles. Unfortunately, assuming a low exchange cycle value for this stage may be pessimistic for some elements, such as Pb, while not pessimistic for other elements that tend to form precipitates at high pH values (*i.e.*, have low solubility concentration values). Therefore, it is recommended that the Stage I duration be set to values that reflect a pessimistic bias for the elements considered.[6]

[6] This pessimistic approach is recommended if a project-specific value is not calculated using a reactive transport model. For example, for calculations associated with the SRS Liquid Waste Tanks Closure PA, a reactive transport model was used with site specific data to estimate transitions between Stages I, II and III (Denham 2007). These Geochemist's Workbench calculations, based on pH (and Eh) transformation indicated that the first stage ended after about 30 pore volumes through Saltstone.

Table 8-1. Best Estimates of Duration of Cementitious Stages for IDF

Stage	Best Estimate (pore volumes)	Range (Pore volumes) [(a)]	Comments
Oxidized Stage I	50	1 to 100	The pessimistic estimate can be either high or low pore volume estimates, depending on the COPC. For I and Tc, assuming a long duration would be pessimistic because their oxidized K_d values are lower during Stage I than Stage II.
Oxidized Stage II	600	100 to 1000	Taking into consideration the less aggressive dissolving attributes of the moderately high carbonate and Ca and Mg concentrations of the Hanford groundwater, in comparison to the SRS groundwater, the Stage II duration was assumed to be 600 exchange cycles. By way of comparison, the SRS groundwater is very low in carbonate concentrations due to its acidic nature (pH ~5.5) and has a Stage II duration of 500 cycles (Kaplan 2016).
Oxidized Stage III	8000	1000 to 10,000	Berner (1992) suggested that the duration of Stage III is between 1000 and 10,000 cycles. Because Hanford groundwater is moderately high in carbonate concentrations, a relatively longer duration for this stage is appropriate: 8000 cycles. Again, by way of comparison, the SRS groundwater is very low in carbonate concentrations due to its acidic nature (pH ~5.5), and therefore would be more prone to promote carbonate dissolution and therefore the duration of Stage III was set by Kaplan (2016) to be 7000 cycles.

[(a)] Suggested range by Berner (1992)

8.6.2 Moderately-aged Cementitious Materials (Stage II)

During Stage II, the soluble salts of the alkali metals are dissolved and washed from the cement solids. The aqueous chemistry is controlled largely by portlandite and calcium-silicate-hydrate gel. The total dissolved calcium concentration is ~20 mM, the pH is strongly buffered at pH ~12.5, and the silica concentration is very low, <0.03 mM/L. The flux of water must dissolve all the slightly soluble portlandite before the leachate chemistry changes.

Berner (1992) determined that Stage II lasts between 100 and 1000 cycles. According to Krupka et al. (2004) and adopted here, most COPC have higher K_d values and higher or lower solubility concentration limits in Stage II than in Stage III. Therefore, a shorter Stage II lifespan would be pessimistic. Stage II K_d values tend to be greater and k_s values tend to be lower than those in Stage I. Notable exceptions include when cation (Sr) or anion (I, Tc, Se) adsorption are expected to be the dominant mode of solid phase uptake, in which case the K_d values in Stage I will be lower due to high salt concentrations, which increase ion exchange competition. Taking into consideration the less aggressive dissolving attributes of the moderately high carbonate and Ca and Mg concentrations of the Hanford groundwater, in comparison to the SRS groundwater, the duration of Stage II was assumed to be 600 exchange cycles. By way of

comparison, the SRS groundwater is very low in carbonate concentrations due to its acidic nature (pH ~5.5) and is assumed to have a Stage II duration of 500 cycles (Kaplan 2016).

8.6.3 Aged Cementitious Materials (Stage III)

In Stage III, the portlandite has been fully dissolved / reacted and the solubility or reactions of calcium-silicate-hydrate gel with the infiltrating water controls the pH of the cement porewater / leachate (Figure 8-2). The calcium-silicate-hydrate gel starts to dissolve incongruently[7] with a continual decrease in pH until it reaches the pH of the background sediment, pH 7 to 8. CSH solubility controls the aqueous pH; its composition starts with a calcium-silicate ratio of about 1.7 and by the end of Stage III, only silicate (SiO_2) remain. The ionic strength of the cement leachate during this stage is relatively low (Reardon 1992). Solution calcium concentrations decrease to 1 to 5 mM and silica concentrations increases to 2- to 6-mM. At very high cycle numbers, other sparingly soluble solids, such as brucite [$Mg(OH)_2$], may buffer the solution pH and dissolved cation concentrations.

Berner (1992) suggested that the duration of Stage III is between 1000 and 10,000 cycles. Because Hanford groundwater is moderately high in carbonate concentrations, a relatively longer duration of 8,000 cycles for this stage is deemed appropriate. Again, by way of comparison, the SRS groundwater is very low in carbonate concentrations due to its acidic nature (pH ~5.5), and therefore would be more prone to promote carbonate dissolution and therefore the duration of Stage III was set by Kaplan (2010) to be 7000 cycles.

The time frame required for the cement pore fluid pH to change from 13.5 to that of the native recharge water is determined by the rate at which water infiltrates to and through the cement system. For example, calculations by Atkinson et al. (1988) indicate that the pH of the near-field pore water would remain above 10.5 for several hundred thousand years (groundwater flow rate of 0.32 cm/yr) for designs of radioactive waste disposal systems being considered in the United Kingdom. Criscenti et al. (1996) performed calculations for three rows of 55-gallon cement-filled drums stacked on top of each other in a shallow land burial ground in the arid Hanford environment for various scenarios. For all scenarios modeled, the system pH did not decrease below 10 for 10,000 years because CSH gel remained to buffer the pH. For a scenario of one barrel filled only one-third with cement at the highest recharge rate (5 cm/yr), the CSH gel was completely depleted after 4,000 years, and the pH dropped to below 10. It is acknowledged that the computer generated predictions by Atkinson et al. (1988) and Criscenti et al. (1996) did not address the potential for significant cement waste form degradation, aside from a few simple thermodynamically controlled weathering reactions for the major cement phases. Thus the results showing such long times for pH to be maintained at alkaline values should be carefully considered.

The network of chemical reactions (both thermodynamic and kinetically controlled) as well as the computer codes capable of solving the complex network of cement weathering reactions have vastly improved over the 20 to 25 years since these studies were performed (see Yabusaki et al. 2015 for more discussion). Despite this ‘warning’, the low recharge rates expected for the IDF subsurface environment and the mass of cementitious secondary wastes to be buried are similar to those modeled by Criscenti et al. (1996); as a result, the IDF near-field cementitious waste form leachate pH might be expected to remain caustic for millennia. This hypothesis is also offered by the Saltstone PA documents for the much wetter SRS site. Savannah River has a nominal infiltration rate through a degraded closure cap of 31.6 cm/yr (SRR, 2013). It has been shown in the FY2013 Special Analysis for the Saltstone Disposal Facility at the SRS (SRR 2013), that the transition from the high pH buffered by CSH to the lower pH buffered by calcite occurs between approximately 24,000 years for Saltstone Disposal Unit (SDU) 4 and

[7] Incongruent dissolution is the non-stoichiometric dissolution to a solid, resulting in the release of dissolved materials into the aqueous that have different proportionalities than would be expected based on the stoichiometry of the solid phase.

>100,000 years for SDU 1 and SDUs that have diameters greater than 150 feet. IDF is expected to have a post-design infiltration rate of about 0.35 cm/yr[8]), which would be expected to further delay this transition.

8.7 Reducing Cementitious Materials

8.7.1 General Approach to Describing Oxidation of an Unsaturated Reducing Cementitious Material

It is anticipated that a cementitious waste form in a Hanford vadose zone may be unsaturated with respect to water. As such, there may be two pathways by which O_2 can enter the waste form and oxidize the system.

1) A porewater pathway, where $O_2(g)$from the vadose zone partitions into porewater (via Henry's Law), and delivers $O_2(aq)$ into the cementitious waste. The oxidation reaction of $O_2(aq)$ with the reducing agents within the cementitious waste form are described by the Shrinking Core Model (Section 8.7.2).

2) An air pathway, where $O_2(g)$from the vadose zone enters directly into the cementitious waste form as the exterior of the waste form desiccates along the edges (Section 8.7.3).

If necessary, these processes would be modelled as coupled processes. This approach requires advanced computational resources and developmental work. An alternative would be to decouple these processes and evaluate each process by itself that is to conduct a porewater pathway analysis and a separate air pathway analysis. The porewater pathway will be conducted assuming fully saturated conditions. The air pathway analysis would involve unsaturated flow modeling and will assume that the oxidation front will advance instantaneously through the cementitious waste form as it desiccates from the exterior towards the interior. The rate determining process will then be determined by identifying which process resulted in the oxidation front moving the fastest. As noted in Section 8.5, there is significant uncertainty regarding how the dynamics of saturated/partially saturated conditions in the cementitious waste forms and surrounding backfill of the IDF will impact air pathway modeling and its impact on spatial evolution of the oxidation front.

8.7.2 Porewater Pathway for Oxidizing Reduced-Cementitious Materials - Shrinking Core Model

There are several cementitious material formulations under consideration that include BFS to promote the reductive precipitation of the COPC, thus decreasing the tendency of some redox-sensitive COPCs (notably Tc) to leach from the solid waste form. There has been a large body of recent research conducted at the Hanford and Savannah River Sites to optimize formulation of this process, and quantify and estimate the longevity of this immobilization process (among the most pertinent to COPC immobilization are: Almond et al. 2012; Langton et al. 2014; Kaplan et al. 2011; Um et al. 2011; Um et al. 2013; Um et al. 2016; Cantrell et al. 2016). A discussion of the nature of the reductant within BFS and quantification of the reduction capacity is provided below in Section 8.7.4.

The reductive capacity of the BFS-cementitious material is expected to decrease over time that the waste form is buried in the subsurface environment. As the waste form ages and becomes increasingly oxidized, it is expected that the capacity of the waste form to immobilize targeted contaminants will decrease. One geochemical approach to modeling the advancement of the oxidation front within reducing cementitious materials is the Shrinking Core Model (Smith and Walton 1993). This model describes the advancement of the oxidized front as resulting from oxidized water diffusing into cement and then chemically

[8] Technical Guidance Document for Tank Closure Environmental Impact Statement Vadose Zone and Groundwater Revised Analyses, Revision 0, March 25, 2005. United States Department of Energy.

consuming (oxidizing) the unspecified reductant in the cementitious material. Application of this model in cementitious waste forms has been described previously (Kaplan 2016).

Electron milli-equivalents (meq e^-/L) are the units used to describe the concentration (more precisely, the activity) of free electrons that can participate in an oxidation-reduction, or redox, reaction. The generalized redox equation is

$$O + e^- = R \tag{83}$$

where:

O	oxidizing agent, meq e^-/L,
R	reducing agent, meq e^-/L, and
e^-	electron.

The greatest concentration of reductant will exist in the waste form when it will be initially placed in the ground. Over time, the concentration of reductant will slowly decrease as more dissolved oxygen in the groundwater, $O_{2(aq)}$, consumes the grout reductant. Once the reduction capacity is exhausted, the reducing cementitious waste form will no longer sequester the targeted COPC, such as ^{99}Tc.

The total oxidizing capacity should be set equal to the amount of dissolved oxygen introduced into the system by infiltrating water. The concentration of reductant present in the slag will decrease over time as more dissolved oxygen in groundwater consumes the grout's reduction capacity. The consumption of the reduction capacity is presented in the following reaction.

$$O_{2(aq)} + R_{(grout)} \rightarrow RO_{2(grout)} \tag{84}$$

where:

$O_{2(aq)}$	O_2 dissolved in water (meq e^-/cm^3 of the fluid),
$R_{(grout)}$	reduction capacity of the grout (meq e^-/gram of solid), and
$RO_{2(grout)}$	oxygenated grout (meq e^-/gram of solid; shown in traditional stoichiometric chemistry as a product of the two reactants, rather than as an oxidized species).

The expression used to calculate the rate of oxidation (R_O; (meq/gram of solid)/yr) for the above reaction is:

$$R_o = kC_{O2}C_R \tag{85}$$

where k is the oxidation rate coefficient in units of 1/(yr·meq/cm^3), C_{O2} is the concentration of $O_{2(aq)}$ (meq/cm^3) and C_R is the concentration of reductant in the grout (meq/g).

Previous data indicates that oxidation of slag is a fast reaction (Estes et al. 2012; Lukens et al. 2005; Shuh et al 2000). Kaplan and Hang (2003) showed that the k value of 1.0 x 10^6 (1/(yr · meq e-/cm^3)) adequately represents a fast reaction.

Perhaps one of the key attributes of this model is that it can be parameterized and as such, it has immediate appeal from a practical point of view. While models based on thermodynamic and reactive transport used to describe this process in SRS disposal systems (Denham 2007; Denham and Millings

2012) are theoretically more acceptable, they require more assumptions and many more input values that are often not available for cementitious waste form conditions. As an example of the type of information needed in these more theoretically acceptable calculations, it is not only necessary to know what the reduction capacity is, you must also know what phases are responsible for redox status and the kinetic information about how they change to other phases as a result of oxidation. These more theoretical models have an important role in understanding the geochemical and contaminant system and can, if needed, provide necessary ancillary information to the broader PA type calculations.

There are a number of simplifying assumptions about the geochemistry that are associated with the shrinking core model (Table 8-2). As with any model, it is important to identify them so that we can direct efforts to substantiate, dismiss, or improve upon them. They also provide direction towards future research needs. Some of the assumptions exist because experimental data is not presently available to offer alternative guidance. For instance, there are conflicting results about the merits of the Ce(IV) method for measuring reduction capacity, yet an alternative method has not been identified (Assumption 2 in Table 8-2). Similarly, the potential role of waste form oxidation directly by air intrusion has not been validated or quantified (Assumption 1 in Table 8-2).

Lukens et al (2005) presented experimental data that was largely in agreement with calculations based on the shrinking core model (Kaplan and Hang, 2003). Lukens et al. (2005) provided an estimate of the rate that the oxidation front moved through saltstone based on spectroscopy considerations. Using a simulant saltstone sample that was cured under reducing conditions for about two years, followed by 120 days of exposure to air, they measured Tc(VII) concentrations using XANES measurements and estimated that the oxidized front had moved 0.28-mm during the 120 days (or 0.85 mm/yr). They went on to evaluate this estimate by comparing it to estimates based on reduction capacity consumption as a result of O_2 diffusion during the 120 day exposure period. They concluded that their spectroscopy-based estimate was reasonable (specifically, assuming $D_{m(O2)}$ = 2e-5 cm^2/s, sample density of 1.7 g/cm^3, $O_2(aq)$ concentration of 2.7e-7 mol/cm^3, and reduction capacity of 0.82 meq/g; and knowledge of Tc total concentration in their sample). It is important to note, that the spectroscopic approach and the diffusion method they used to compare the results have categorically different assumptions, providing additional credence to the estimate.

The oxidation-front rate value generated by Lukens et al. (2005) was compared with calculations made regarding the Saltstone Disposal Facility (Kaplan and Hang 2003) (Figure 8-3). A comparison was made by using the facility geometry, time of exposure, and the 0.85 mm/yr oxidation front value (Lukens et al. (2005). Both the Shrinking Core Model calculations based on Kaplan and Hang (2003) and Lukens et al. (2005) data indicate about ~16% of the saltstone reduction capacity would be consumed after 213,000 years. It is noted that this value of ~16% is very dependent on the dimensions of the facility, and therefore is not directly applicable to Hanford disposal systems.

Table 8-2. Key geochemical assumptions associated with the use of the porewater pathway to describe the oxidation of a reducing cementitious waste form.

1	The only oxidants in the porewater pathway is $O_2(aq)$ that enters the reducing cementitious waste form with recharge water. **(**The air pathway will need to be invoked to introduce $O_2(g)$ into an unsaturated system.) Based on X-ray Absorption Spectroscopy (XAS) measurements, Shuh et al. (2000) concluded that nitrate and nitrite do not oxidize Tc(IV) at any appreciable rate in reducing cementitious materials. After 9 months, saltstone samples amended with nitrate and nitrite had a greater proportion of Tc in the +4 state than saltstone samples amended with Cl^- (a non-redox active anion) without nitrate or nitrite. They note that while NO_3^- and NO_2^- are capable of oxidizing reduced Tc species at low pH environments, the oxidizing species, NO_2^+ and HNO_2, respectively, were not formed in high pH systems. The authors concluded that "The results clearly implicate oxygen as the species responsible for the oxidation of Tc(IV) to TcO_4^-. In addition, these results strongly suggest that nitrate and nitrite do not appreciably oxidize Tc(IV) in the cement."
2	The Ce(IV) method of measuring reduction capacity is representative of the available reduction capacity. It is believed that this method measures essentially all the reduction capacity in the system. The assumption is that over time, all of the reductant would eventually be consumed and that grain rimes do not stop the electrons from coming into contact with the dissolved solute (e.g., Tc and Cr). By way of analogy to another reducing system, it has been shown that when Fe(0) forms oxidized coatings when placed in oxygenated water, the rusted-Fe(0) particle continues to be effective at promoting solute reduction (Henderson and Demond 2007). This was attributed to semi-conductor properties of the iron system and/or cracks in the coatings that permitted underlying electrons from the Fe(0) to enter the aqueous phase. No research supports the idea that a similar process occurs with reducing cementitious waste forms.
3	The source of the reduction capacity does not change with time (i.e., there is no loss of sulfides or ferrous iron as water moves through the waste form. Cantrell and Williams (2012) in a flow through test with saltstone measured loss of S in the leachate, contrary to this assumption. However, many potential forms and sources of sulfur exist in reducing cementitious waste forms (e.g., Harbour et al. (2006) reported that OPC and BFS can each contain a few percent of S while fly ash has an order of magnitude less). It is not clear whether all of these sources of S contribute to the reduction capacity. Furthermore, it is not clear whether just the oxidized S species were selectively washed out during the early part of the study, and as such would not necessarily adversely affect the reduction capacity.
4	The potential oxidizing agents in simulant liquid waste do not lower the reduction capacity to a measurable extent. This assumption was supported by recent measurements by Um et al. (2015) and calculations by Kaplan and Hang (2003).
5	Porewater is fully saturated with $O_2(aq)$. This value is based on measurements made at the SRS and calculations based on Henry's Law (Kaplan and Hang 2003). It is expected that the Hanford recharge water $O_2(aq)$ concentration will be much lower. $O_2(aq)$ concentrations are expected to decrease upon contact with soil due to microbial activity and abiotic reduction by the relatively high concentrations of Fe(II) in Hanford clay fractions (Fredrickson et al. 2004). For example, the SRS subsurface sediment has a reduction capacity of 5.1 meq/kg (Kaplan and Hang 2003). A SRS simulation of saltstone disposal revealed that the overlying horizontal moisture barrier accounts for 14% of the reduction capacity of the disposal system (Kaplan and Hang 2003; page v, Table 2). The Hanford subsurface sediment is expected to have a greater reduction capacity than SRS sediment. SRS vadose zone sediment clay-fraction has <1% Fe(II) (Kaplan et al. 2016), Hanford vadose zone sediment clay-fraction can be >10% Fe(II) (Fredrickson et al. 2004; Dong et al. 2003).
6	There is a 100% efficiency in the reaction of $O_2(aq)$ oxidizing the reduction capacity of the reducing cementitious waste form (i.e., for each equivalent of O_2 there are 4 equivalents of reduction potential consumed (i.e., 4 e^- per $O_2(aq)$ molecule)). 100% efficiency of $O_2(aq)$ oxidizing the BFS will not happen.

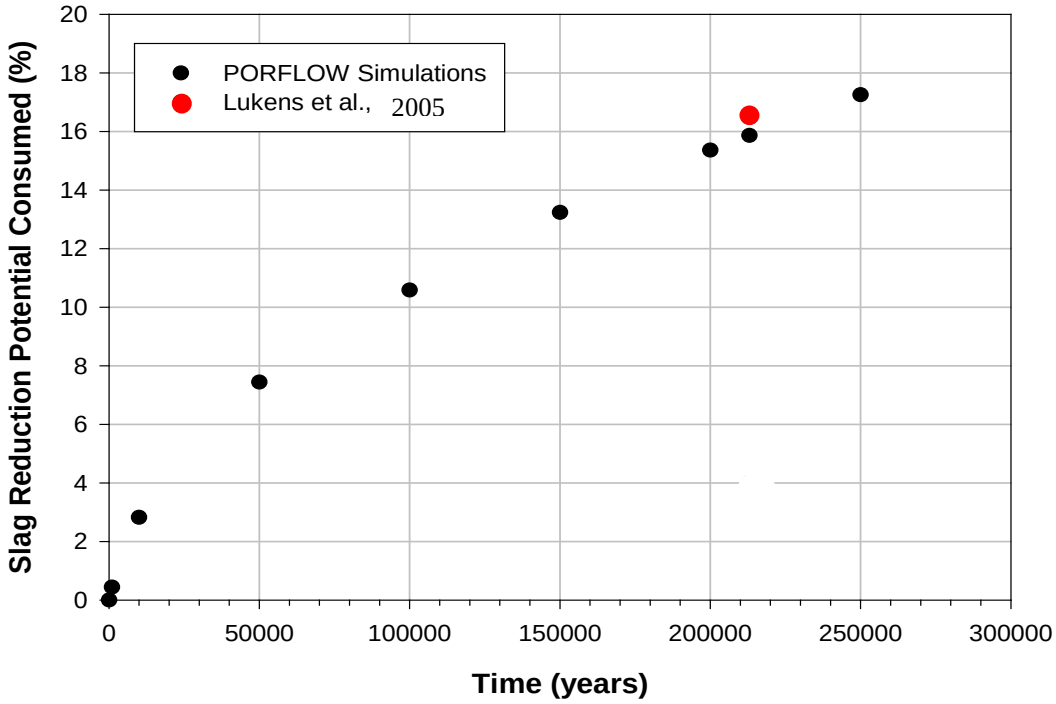

Figure 8-3. Consumption of slag reduction potential by diffusing dissolved oxygen in infiltrating water into the Saltstone Disposal Facility (Kaplan and Hang 2003). Results from Lukens et al. (2005) estimate of oxidation rate (0.85 mm/year) based on spectroscopic measurements were used to estimate reduction potential consumed after correcting for the dimensions of the SDF facility dimensions (red data point).

There are also laboratory results that contradict aspects of the shrinking core model (Langton et al. 2014). Langton et al. (2014) noted that the oxidation front of saltstone cores left exposed to air for 118 days moved faster than expected based on $O_2(aq)$ diffusion calculations (additional details related to the saltstone experiments are provided by Almond et al. 2012). While the authors did not explain the observed contradiction, it is possible that it may in part be due to the fact that they used partially desiccated saltstone samples in their experiment. As described above, the shrinking core model assumes that oxidation of the reducing cementitious material occurs only by $O_2(aq)$ entering through the porewater pathway. In desiccated samples, the air pathway would also be expected to promote oxidation. O_2 diffusion through air is 10^4 faster (not accounting for tortuosity) than through water and would explain the unpredicted rapid oxidation reported by Langton et al. (2014). The saltstone samples used in Langton et al. (2014) were collected from a container left outside with neither temperature nor humidity controls (they reported that temperatures ranged from 14 to 41^{o}C and relative humidity ranged from 26 to 100% during two spring months). Almond et al. (2014) noted color changes between the exterior and interior of the sample that were attributed to oxidation and/or sample desiccation. Cracks in the sample were also noted. These studies support the need to develop an alternative pathway, such as the air pathway, to describe the oxidation of partially saturated reducing cementitious materials. Furthermore, it demonstrates the need for more moisture-controlled and redox-controlled studies, permitting the distinction and the quantification of the two pathways.

Langton et al. (2014) also reported a poor correlation between reduction capacity and Cr and Tc leached from depth discrete samples recovered from partially saturated saltstone and Cast Stone samples. (The Cast Stone sample was not left outside in the open environment for 2 months like the saltstone sample. The Cast Stone sample was likely fully saturated and was covered by rather dry Hanford sediment that had exposure to air before being sectioned and water leached.) This is discussed in more detail below in conjunction with reduction capacity measurements (Section 8.7.4).

8.7.3 Air Pathway for Oxidizing Reduced-Cementitious Materials

Oxidation by the air pathway will be described by modeling the advancement of unsaturated conditions from the outer edge toward the interior of the waste form. As the system becomes unsaturated, it will instantly oxidize redox-sensitive COPCs. This conceptual model pessimistically assumes an infinite source of $O_2(g)$ and that reaction kinetics are instantaneous. Furthermore, unsaturated conditions will be defined as when the volumetric water content decreases to the point where oxygen can effectively diffuse through continuous gas-phase pathways. There is a possibility of continuous gas pathways forming at relatively high liquid saturations, perhaps 90% to 95%. We are not aware of any studies that provide insight into this air pathway. As such, additional work is necessary to refine this conceptual model and to remove implicit pessimistic bias.

8.7.4 Reduction Capacity of Reducing Cementitious Materials

There have also been recent reviews of the redox chemistry involved in cementitious materials containing BFS (Pabalan et al. 2009; Um et al. 2013; Um et al. 2011). These reports indicate that the source of the reduction is the presence of sulfides and to a lesser extent ferrous iron in the BFS. Sulfides play a more important role because they are more soluble than ferrous iron under the alkaline pH conditions of cementitious materials. The phase in the slag responsible for its reducing properties has been assumed to be pyrrhotite with a stoichiometric formula of FeS (Denham 2009). Pyrrhotite is a high temperature highly reduced phase potentially formed under conditions expected during the formation of BFS and has been identified in various smelting slag (Zainoun et al. 2003; Muszer 2006; Gupta et al. 2007). Additionally, there are microbial processes that impact redox behavior in cementitious systems (Smith et al. 2016; West et al. 2009; Humphreys et al. 2009; West et al. 2008).

The reduction capacity measurements have been measured by two methods, the Ce(IV) method (Agnus and Glasser 1985) and the Cr(VI) method (Lee and Batchelor 2003). These methods are described and compared in Kaplan and Hang (2003), and more recently in Um et al. (2015). The key conclusion from these studies was that it is not known whether all or some percentage of the total reduction potential in the cementitious wasteform is “available” for maintaining reducing conditions. Conceptually, the Cr(VI) method provides a measure of only the reduction capacity on the surface of particles, whereas the Ce(IV) method provides a measure more representative of the total reducing capacity. Use of the Ce(IV) method implicitly assumes that during the course of extended durations (i.e., thermodynamic assumptions that steady state is achieved) all the reduction capacity will be eventually be chemically active in the system.

Recently several reduction capacity measurements were made of a wide range of reducing secondary waste form formulations using varying sources of BFS (Um et al. 2015). Um et al. (2015) used two sources of BFS, the SRS source (Holcium Corporation) and a second source from western Canada, labelled “NW BFS.” The Ce(IV) reduction capacity ranged from 0.541 to 1.490 meq/g and the Cr(VI) reduction capacity ranged from 0.404 to 1.389 meq/g. Cast Stone samples made with an average simulant had a reduction capacity of 0.609 to 0.763 meq/g. Reduction capacity measurements were also measured in Cast Stone secondary waste simulants; they ranged from 0.399 to 0.596 meq/g (Um et al. 2011). In general, the reductive capacities measured by the Ce(IV) method were slightly greater than those measured by the Cr(VI) method. They also reported different reduction capacities based on the waste simulant and the cement formulation. Using a single source of BFS, Roberts and Kaplan (2009) reported

that the BFS reduction capacity measured by the Ce(IV) method was 0.819 meq/g, which was near identical to previous measurements 0.832 (Kaplan et al. 2008), 0.817 (Kaplan et al. 2005), and 0.820 meq/g (Lukens et al. 2005). These values of the BFS used at SRS are largely in agreement and within the range of values reported by Um et al. (2015).

Langton et al. (2014) noted a poor correlation between Ce(IV) reduction capacity and the release of Tc and Cr released from Cast Stone and Saltstone. In their study, simulated saltstone cores were left exposed to air for several months, then depth-discrete samples were collected and analyzed for leachable (oxidized) Cr/Tc and reduction capacity. They did not find any relationship between the concentration of oxidized Cr/Tc and reduction capacity. This study underscores the need for additional research to identify an appropriate method to quantify the reduction capacity of reducing grout.

In summary, a great deal of uncertainty exists around the reduction capacity parameters. This uncertainty stems from several sources, including: 1) it is not known whether all or some fraction of the reduction potential is in fact actively involved in immobilizing redox-sensitive COPCs, 2) reduction capacity changes with formulation and type of waste and the final grout formulation has not been determined, and 3) the only test to comparing redox-active COPCs leaching from reducing cementitious materials with measured reduction capacity showed no correlation. Table 8-3 includes recommended inputs for modeling the oxidation state of reducing waste forms.

Table 8-3. Additional input values for modeling oxidation state of IDF reducing cementitious waste forms (discussed in Section 6.6.4)[(a)]

Parameter	Best	95 Percentile Range	Discussion
Reduction capacity (meq/g)	0.6	0.2 to 0.8	Um et al. (2015) reported a range of 0.541 to 1.490 meq/g in a wide range of reducing cementitious materials. Cast Stone samples made with an average simulant had a reduction capacity of 0.609 to 0.763 meq/g. Roberts and Kaplan (2009) reported values using saltstone samples closer to 0.8 meq/g. The SRS PAs use the lowest value measured for present saltstone formulations, 0.607 meq/g. Because of the uncertainty surrounding the final wasteform formulation, a wide range of uncertainty is proposed. This range is based on the range reported in Um et al. (2015) and professional judgment.
Groundwater $O_2(g)$ (meq/L)	1	0.1 to 2	Best value taken from Kaplan et al. (2005; Table 2); based on Henry's Law calculations (2.65e-4 M; assuming $O_2(atm)$ = 0.21 atm; Henry's Law Constant = 0.00126 mol/am; 4 electrons per O_2 molecule). This is a assumed to be a pessimistic estimate because subsurface pore O_2 atmospheric concentrations are expected to be lower than above ground concentrations because of biotic and abiotic processes. Direct measurements of vadose zone groundwater may provide less pessimistic estimates.

[(a)] These values are for IDF waste forms containing a relatively high percentage of BFS in the dry blend. If the Solid Secondary Waste contains less BFS, than values less then these Best values should be used.

8.8 Potential Role of Microorganisms on the Isolation of Radioactive Waste Under Cementitious Disposal Conditions

The potential role of microorganisms on the isolation of radioactive waste in geological disposal systems has long been recognized (e.g. Chapman and McKinley, 1987; Alexander et al., 1992; Stroes-Gascoyne and West, 1996). For cementitious disposal systems such as IDF, the initial pore fluid pH (pH ~13) may be too high to facilitate microbial activity at early times (Rizoulis et al. 2012). Decreases in pH over time as a result of $Ca(OH)_2$ removal will, however, provide conditions more favorable for microbial growth. Assessing the potential impact of microbial populations and processes on the transport and biogeochemical properties of cementitious radioactive waste disposal systems has been guided and informed by consideration of analogy with naturally occurring alkaline systems (e.g., Alexander et., 1992), combined with laboratory testing using naturally occurring alkalitolerant bacteria (e.g., Smith et al., 2016).

Studies focused on the microbial-community viability and composition found in highly alkaline springs (e.g., Smith et al., 2016) show a variation in microbial-community structure across spatially separated sample points of contrasting pH values (ranging from pH 7.5-13). Communities containing alkaliphilic and alkalitolerant bacteria were observed, including at pH 13. Bacterial communities from such natural analogue sites have demonstrated the ability to reduce Fe(III) in microcosm experiments up to pH 10.5 to 11.4 (Pollock et al., 2007; Smith et al., 2016). This supports the potential catalytic role of bacteria to reduce redox-sensitive COPCs under conditions relevant to cement-based radioactive waste disposal facilities.

With respect to potential consequences from microbial processes, microbial processes may alter transport properties of disposal facilities and surrounding host rock. Potential impacts include the formation of biofilm across pore throats causing porosity and permeability changes (Coombs et al. 2010), and altering the size and shape of pore spaces and roughness of grain surfaces (Atekwana et al. 2006). The temporal and spatial extent to which microbial processes will occur in radioactive waste disposal facilities depend on numerous factors, including flow velocity and grain size (Surasani et al. 2013), angularity and surface roughness (Crawford et al. 2012), hydraulic pressure gradient (Ginn et al. 2005), and biological factors involving the metabolic state of cells, the isoelectric point of cell surface polymers, and processes such as filtration and dispersion (Ginn et al. 2005). Microorganisms may also directly influence COPC migration through biochemical effects, most notably by redox-state alteration (West et al., 2008; 2009), or interactions between extracellular biofilm components (e.g. polysaccharides) and COPCs (Kazy et al. 2008).

In summary, studies of naturally occurring hyper-alkaline springs and laboratory testing of hyper-alkaline bacteria provide relevant and useful analogues to high-pH, cement-based disposal facilities. Evidence from such analogue studies provides insights into the viability and consequences of biogeochemical processes that could occur as the infiltration of surficial water leads to the formation of hyper-alkaline conditions within the cementitious disposal facility. Based on observed viability and potential impacts on the conclusions of the PA, consideration of potential microbial effects may need to be part of assessing near- and longer-term transport and redox properties of near-surface, cementitious disposal systems.

8.9 COPC Desorption from SSW Materials

8.9.1 Spent Ion-Exchange Resins

For this analysis, it is assumed that all the resin in the solid secondary waste stream are Spherical Resorcinol-formaldehyde (RF), originating from the CSP IX facility. This resin was designed for Cs uptake. After the ion-exchange resin has been used to remove ^{137}Cs from the liquid tank waste for several cycles and becomes degraded, it is stripped of ions using 0.5 M nitric acid before being disposed. After

this acid treatment, the resin has been shown to still retain 0.321 μCi/g Tc, 0.352 μCi/g Cs, 338 μg/g Cr, and 193 μg/g U (Jenkins et al. 2013). Therefore, the resin-bound Tc, Cr, Cs, and U must be in a form that is extremely tightly bound to the resin; consequently, a very high K_d is warranted.

However, the effectiveness of the resin is very sensitive to oxygen degradation (Jenkins et al. 2013). Extensive research has gone into understanding and quantifying this process (Jenkins et al. 2013; Thorson 2008). The resins are shipped to the Hanford Site under N_2 gas to protect against such degradation. As the resins degrade, their capacity to bind Cs rapidly degrades. The degradation process is chemically described as 1 mole of O_2 oxidizing (destroying) one mole of RF (RF formula weight = 122 g/mol). Therefore, 1 mmol O_2 will oxidize all the active sites on 0.122 g dry weight resin (or 1 mmol O_2/g dry-weight resin will reduce the resin capacity of 12.2%).

While the COPC remaining on the resins after acid washing are likely strongly bound to the resin, the resins themselves may undergo extensive degradation. These two antagonistic processes can release COPCs into the aqueous phase. If the resins are not stored prior to disposal under reducing conditions, then it seems reasonable to assume that the resins will have no long-term binding capacity, i.e., the K_d values for the Tc, Cs, Cr, and U should be set to 0 mL/g. However, if procedures are in place that assure the storage of the resins under reducing conditions, or additional experimental evidence can be provided, then it may warrant assigning some initial very high COPC binding constants. These initial very high K_d values would decrease in a manner proportional to the amount of O_2 that comes into contact with the resins, such that the resin's binding capacity would decrease by 12.2% after exposure to 1 mmol O_2, as described above. However, until such data (i.e., the effect of O_2 introduced via the porewater and air pathways on RF degradation) is collected, K_d values for all COPC should be set to 0 mL/g.

8.9.2 Granulated Activated Carbon

A literature review dealing with the leaching of radioiodine from GAC under PA conditions is provided in Appendix B. Among the key conclusions from this review are that:

1. There is no existing data using site-specific, spent-GAC to quantify the tendency for radioiodine to desorb from the GAC.
2. The best approximation is provided from experiments conducted with two actual spent GAC samples generated from SRS facilities (Kaplan et al. 1999; Kaplan and Serkiz 2000). The static and column flow experiments included leaching with simulated rainwater and simulated cementitious leachate, the latter would be especially appropriate for encapsulated and solidified waste forms.
3. The SRS studies also demonstrated that ionic strength greatly influenced the desorption K_d values. Using rainwater leachate, desorption K_d values were 58,100 to 132,500 mL/g. Using cement leachate, desorption K_d values decreased to 320 to 880 mL/g.

Based on these conclusions, it is recommended that iodine-K_d values for spent GAC have a mean of 600 mL/g and the 95 percentile range be set at 100 to 2000 mL/g. The wide range is to account for the uncertainty associated with the type of GAC being disposed and the long term interaction of GAC with cementitious leachate. It is not clear if iodine oxidation state influences uptake by GAC. But based purely on inorganic chemistry first principles, it would be expected that IO_3^- would bind stronger than I^- to GAC because GAC has hard O-containing surface binding sites, which would preferentially bind with the harder IO_3^- than the I^- species. (Conversely, I^- binds much more strongly to softer metals, such as Ag Pb, and Hg.)

8.9.3 Ag-mordenite

No studies measuring the desorption of ^{129}I from silver-amended mordenite (mordenite is a type of zeolite) were identified. There have been several studies conducted to engineer the material and quantify its efficiency as a sorbent of gaseous radioiodine (Scheele et al. 1983; Scheele et al. 2002; Patton et al. 2014; Jubin et al. 2014). They have shown that the silver is highly effective at binding both I_2, I^-, and methyl-iodine, forming the sparingly soluble AgI precipitate. Chapman et al. (2010) did some XAS analysis, combined with some molecular modeling of iodine capture by Ag-mordenite. In addition to testing the as received form of Ag-mordenite (Ag^+-MOR), they also tested a reduced form of the same material (Ag^0-MOR). They took these materials and exposed them to I_2. They observed that two different form of AgI existed on the reduced Ag^0-MOR sample. One form of the precipitate remained on the mineral surface, while a much smaller sub-nanoprecipitate with a unique structure existed within the pores of the mordenite. Additionally they noted that the Ag of the Ag^0-MOR sample, prior to expose to the I_2, existed on the surface of the mordenite as 3-nm particles. This implies that the material migrates into the zeolite pores during the I_2-treatment. For the oxidized Ag^+-MOR, the AgI was confined to the pores as sub-nanometer AgI clusters. Encouragingly, this may represent a more secure route for radioactive iodine retention. Furthermore, it indicates that under oxidizing conditions, the ^{129}I may become more secure. So while these test conditions are not directly parallel to what might be expected in reducing cementitious repository conditions (specifically the order of addition/treatment), the results provide some insight into the potential behavior of AgI under varying redox conditions.

There have been iodine desorption studies done with commercial Ag-GAC. Kaplan et al. (2000) measured the desorption of ^{129}I from a Ag-GAC (Nucon International, Inc, Columbus OH) under cementitious conditions. They conducted an $^{129}I^-$ adsorption experiment and permitted the system to equilibrate for 2 weeks, then used these materials in a desorption experiment with groundwater and a simulated cement leachate. They reported near identical K_d values for both leachates: 1226 ± 19 mL/g for groundwater and 1426 ± 1244 mL/g for cement leachate. Hoskins et al. (2002) conducted some adsorption tests as a function of pH. They used a Ag-GAC purchased from Calgon Corporation (TOG-NDS-20x50) and exposed it to $I^-(aq)$ prepared in varying pH simulated groundwater solutions (pH 5, 7, and 8). They fitted the data to a Freundlich isotherm (Section 8.1). The Freundlich constant, K_F,[9] which is a ratio of the proportion of iodine on the Ag-GAC vs. that in the aqueous phase, decreased with pH: at pH 5, K_F = 148,500 mL/g, pH 7, K_F = 111,800 mL/g, and at pH 8, K_F = 88,100 mL/g. If we assume for the moment that this trend continues to pH 12, the K_F would be expected to be 10,114 mL/g (R^2 = 0.998, $P \leq 0.05$; intercept = 248,657, slope = -19,879). This suggests that at pH 12, that iodine sorption to the Ag-GAC is extremely high. This is not surprising given that AgI remains sparingly soluble at high pH levels.

A recommended best-estimate I K_d value for the Ag-mordenite is 1000 mL/g, and a minimum value of 100 and a maximum of 10,000 mL/g. This unusually wide range is to capture uncertainty in association to differences in substrate (mordenite vs. GAC), lack of site-specific material experimentation, and the influence of aging on desorption rates. With experimentation directed at quantifying this process under PA relevant conditions, it is likely that extremely low solubility values will be identified.

8.9.4 HEPA filters

No studies were found with data describing the tendency of COPCs to desorb from the HEPA filters expected to be disposed at the IDF. These HEPA filters are composed of non-woven glass paper

[9] Fruendlich isotherm model is $C_{solid} = K_F C_{aq}^{\ n}$, where C_{solid} is the concentration of iodine on the surface (μg/kg), K_F is the Fruendlich constant (ml/g), C_{aq} is the aqueous iodine concentration (μg/mL), and n = the expediential term that reflects the sorption intensity and is theoretically related to the adsorbent site energy distribution.

(borosilicate microfiber) encased in stainless steel. The non-woven glass paper is commonly a type of nylon. To estimate these K_d values, it was assumed:

- That only the particles trapped on the HEPA filters can bind the COPCs, and that the HEPA non-woven glass paper and the filter encasement do not possess any binding capacity. The nylon within the HEPA filters are not designed to adsorb dissolved/aerosol COPC directly from the air.
- The particles trapped on the HEPA filters are composed of fine textured soil.
- K_d values of the fine textured soil were based on the "Soil K_d in Zone 2b – Unimpacted far field sand sequence" as identified in the Hanford Geochemical Data Package (Krupka et al. 2004; Table 5.6). The best estimate K_d values were used in these estimates. Best estimates rather than minimum estimates were used because the fine grain particles are expected to have an especially large binding affinity for COPCs due to their large surface area. Best estimates are assumed to be pessimistic because they represent sorption estimates to bulk vadose zone sediments (sand/silt/clay).
- The filter consists of 1% trapped particles (particle weight/ total compressed filter weight). In the absence of any data, this estimate was used and should be replaced when better values are identified.

As an example, if the recommended soil K_d = 100 mL/g, then the HEPA filter K_d value would be 1 mL/g. Given the uncertainty of this calculation, only one significant figure is assigned to the K_d values mL/g (Table 8-8).

8.9.5 Debris/Non-debris

There is no information presently available about debris K_d values. Until more information is available about the types of materials and their relative proportions existing as debris/non-debris waste, it is recommended that K_d values be set to 0 mL/g for this solid waste.

Much of the debris waste is described as metal, and as such it may be reasonable to assign K_d based on COPC binding to rusted metal, or to Fe-oxyhydroxide minerals, for which there is an extensive data base. For example, a K_d database exists for COPC desorption from the steel tank walls of dispositioned SRS tanks filled with cementitious materials (Li and Kaplan 2012). These K_d values are based on COPC sorption/desorption to various iron oxyhydroxides at ~10.5 pH.

Some debris waste may also contain cellulosic materials, such as wood or cardboard. The impact of cellulose degradation products has been reviewed by Wang et al. (2009). They note that under alkaline conditions of a cementitious disposal facility, cellulose (e.g., cardboard, wood) is unstable will degrade to water-solubilte, low molecular weight compounds. Under anaerobic conditions and in the presence of Ca^{2+}, as is the case for cement porewater, isosaccarinic acid (a polyhydroxy carboxy ligand) has been shown to be the main degradation product (Bourbon and Toulhoat 1996, Glaus et al. 1999). These compounds have been shown to form strong complexes with various COPCs, especially under alkaline conditions. This might promote the release of COPCs from a disposal facility. The presence of cellulosic degradation products might adversely affect two important processes: 1) promote solubilization of precipitated compounds, and 2) diminish the ability of the concrete to sorb a complexed COPC (van Loon and Glaus 1998). Because COPCs generally exist in low concentrations in LLW, the enhancement of COPC solubility by cellulosic degradation products is not of major concern. More concerning, is the lower tendency for organic-complex COPCs to bind to surfaces.

Kaplan and Serkiz (2004) and Kaplan and Serkiz (2006) evaluated the effect of cellulosic degradation products on soil K_d values for a wider range of COPCs. They reported that the presence of the cellulosic degradation products tended to increase sorption of some COPCs, most cations, while decreasing sorption

of other COPCs, including most anions. The enhanced K_d values were attributed to the organic material binding to the poorly sorbing soil, and enhancing the binding capacity (increasing the CEC) of the soil, and this in turn promoted COPC binding. The soils tested had a weak anion exchange capacity, but in the presence of cellulosic degradation products, there was no sorption of the anionic COPCs. Serne et al. (1993) also noted diminished K_d values in the presence of cellulosic degradation products.

8.10 COPC Leaching from Encapsulated and Solidified Waste Forms

8.10.1 Encapsulated Waste Form

No specific experimental information about how COPC desorb from encapsulated waste forms was identified. It is recommended that a simplified approach be used. The K_d of the waste material will be used within the container, and the K_d of the cement will be used as the COPC move into the encapsulating cementitious material. It is assumed that no sorption occurs directly to the container itself. For example, if the encapsulated container hold GAC and the GAC/iodine K_d is 600 mL/g, and the iodine/cement K_d is 8 mL/g, then a K_d of 600 mL/g would be used within the encapsulated container and a K_d of 8 mL/g would be used in the encapsulating cement.

8.10.2 Solidified Waste Form

No specific experimental information about how COPC desorb from solidified waste forms was identified. The simplifying approach advocated here is to assume: the solid waste is well mixed in the cementitious waste form, the sorption to each of the two components (the solid waste and the cementitious material) can be weight or volume averaged, and that the presence of the mixture of the cement or solid waste does not influence K_d values. Regarding the last assumption, this assumes that the cementitious leachate does not alter, such as promote degradation, of the SSW. Ideally, the desorption test of the SSW would be conducted under the appropriate cementitious chemical conditions. For example, if GAC with an iodine K_d of 600 mL/g is mixed 60:40 into the solidified waste form with a iodine K_d of 8 mL/g, then the $K_{d\text{-}solidified}$ would be about 400 mL/g ((0.6 x 600)+(0.4 x 8)) = 363.2 mL/g).

8.11 Data Tables

Detailed data tables from the preceding sections are provided in this section:

- Table 8-4. Distribution Coefficients ($\boldsymbol{K_d}$ values, mL/g): Oxidizing Cementitious Solids
- Table 8-5. Distribution Coefficients ($\boldsymbol{K_d}$ values, mL/g): Reducing Cementitious Solids
- Table 8-6. Apparent Solubility Concentrations (mol/L; *ks*): Reducing Cementitious Materials
- Table 8-7. Iodine $\boldsymbol{K_d}$ Values (mL/g) with Granular Activated Carbon (GAC)
- Table 8-8. Estimated $\boldsymbol{K_d}$ Values (mL/g) for HEPA Filters

Table 8-4. Distribution Coefficients (K_d values, mL/g): Oxidizing Cementitious Solids

Rad	Best Min Max	Oxidizing Cement Stage I	Oxidizing Cement Stage II	Oxidizing Cement Stage III	Comments and References
Cr	Best Min Max	3 0 6	3 0 6	3 0 6	CrO_4^{2-} immobilization as a result of carbonation (the natural process by which concrete becomes coated with $CaCO_3$) has been documented (Macias et al. 1997). Cr(VI) can also be substituted for sulfate in ettringite (Gougar et al. 1996) and can participate in ion-exchange with OH^-. It is anticipated that divalent CrO_4^{2-} will not be as readily exchanged by monovalent anions, such Cl^- and F^-. Ochs et al. (2002) reported CrO_4^{2-} K_d values were between 10 and 100 mL/g when put in contact with various non-reducing cement pastes. They developed a predictive model of CrO_4^{2-} uptake by correlating K_d values to cement sulfate concentrations. Because the composition of the solid secondary waste form has not been finalized, recommended value K_d values are lower than reported values.
Cs	Best Min Max	2 0 4	20 2 40	10 1 20	Krupka et al. (2004) recommended "reasonably conservative" Cs K_d values for IDF for Stages I, II, and III of 2, 20, and 20 mL/g, respectively. Ochs et al. (2016) in a detailed review of the general literature recommended best CsK_d values for Stages I, II, and III of "insufficient data", 2, and 20 mL/g, respectively. Cs K_d values in hardened HTS cement discs, pH 13.3 were close to 3 mL/g (Sarott et al. 1992). Wieland and Van Loon (2003) reviewed Cs K_d values onto various cementitious materials and they had a very narrow range: from 0.2 to 5.0 mL/g. In 1st Stage K_d values were decreased because high ionic strength likely results in competitive exchange (desorption). This has been shown experimentally (Wieland and Van Loon 2003). Kaplan and Coates (2007) measured Cs^+ K_d values in Ca(OH)-saturated and $CaCO_3$-saturated solutions in ground, 40-yr old concrete, simulating 1st/2nd and 3rd Stages, respectively. The measured K_d values were 21 and 17.6 mL/g, respectively. Using an actual aged saltstone core sample recovered the Saltstone Disposal Facility, Almond and Kaplan (2011) reported desorption K_d values using a cement leachate simulate under bench top oxidizing conditions of 18 mL/g, and under inert glovebag conditions of 21 mL/g. The recommended values here are largely in agreement with the previous values selected by Krupka et al (2004).
Hg	Best Min Max	300 30 600	300 30 600	100 10 200	For a more in depth discussion of the Hg-cement literature, please see Table 8-5. Kaplan and Coates (2007) measured Hg K_d values in three cementitious materials (50 year old aged concrete sample recovered from a demolition site, saltstone sample, and a highly oxidized saltstone sample) in which $^{230}Hg^{2+}$ was spiked to a suspension of ground material, permitted to equilibrate, and then desorption K_d values were measured under atmospheric conditions. In the non-reducing aged cement, K_d values ranged from 289 to 568 mg/L; in the saltstone sample (again, measured under oxidizing conditions), the K_d values ranged from 1095 to 1173 mg/L. In the highly oxidized saltstone samples, the K_d value was 841 mL/g. More recently, Bannochie (2015) reported Hg speciation measurements of SRS Tank 50 samples and the TCLP results when that solution was used to make a laboratory saltstone sample. The Tank 50 sample had 126 mg/L total Hg, the saltstone had a total Hg concentration of about 50.4 mg/kg Hg, and the TCLP (conducted in oxidizing

Rad	Best Min Max	Oxidizing Cement Stage I	Oxidizing Cement Stage II	Oxidizing Cement Stage III	Comments and References
					conditions) had a total Hg concentration of 0.151 mg/L. As a first approximation, a K_d value based on these values is 334 mL/g. The likely K_d would be greater under reducing conditions. The key finding by Bannochie (2015) was that 80% of the leached Hg from the TCLP tests was in the methyl-Hg form, demonstrating the importance of speciation on Hg leaching from cementitious materials. It is unknown what the Hg speciation is in Hanford secondary solid waste. Especially low K_d values are recommended here because of the uncertainty regarding the waste form and status of the Hg in the various types of solid secondary waste. Furthermore, solubility controls are likely very important in predicting Hg leaching given the highly reactive nature of Hg towards solids and in high sulfur concentration environments. The recommended values here are less than those generally reported in the literature because the final formulations of the cementitious waste forms have not been finalized and the impact of mercury speciation is not known.
I	Best Min Max	4 0 10	8 1 20	2 0 4	Iodine can exist as either iodide (I^-) or iodate (IO_3^-) in nature. Based on thermodynamic considerations, iodine is expected to exist as a mixture of iodate and iodide under oxidizing conditions and only as iodide under reducing conditions. This is important because iodide sorbs less than iodate to cementitious materials (Evans 2008; Allard et al. 1984). After a detailed review of the literature, Krupka et al. (2004) recommended "reasonably conservative" K_d values for the Hanford IDF for Stages I, II, and III of 10, 5, and 1 mL/g, respectively. The recent results of Last et al. (2015) of iodide and iodate K_d values using various site-specific cement formulations contradict the conclusions of Krupka et al. (2004); they reported iodide and iodate K_d values -0.12 to 0.38 mL/g. However, it is difficult to interpret the results of Last et al. (2015) given the caveats associated with iodide and iodate ICP-MS detection issues and the unrealistically high iodine concentrations used in these experiments, and poor model fits using CXTFIT. I- K_d measured on 7 types of concrete samples increased gradually over 3-mo, then leveled off at 25 to 130 mL/g (Allard et al. 1984; Dayal et al. 1989). Iodide sorption to cement is highly reversible when chloride is in the aqueous phase, suggesting that iodide is reversibly adsorbed and not precipitated onto the surface of the cement (Atkins and Glasser 1992). The impact of chloride concentrations on iodine sorption is important because chloride generally exists in much greater concentrations, ~10^{-5} M, than iodine, ~10^{-8}M (Wang et al. 2009). Increasing pH above pH 12.5 resulted in decreased iodide sorption, likely as a result of decreasing number of surface positive-charged site. (Atkins and Glasser 1992). Iodide sorption increased with increased Ca/Si ratios of CSH (Atkins and Glasser 1992), (which is at its maximum during the 2nd Stage and initial part of the 3rd Stage). K_d values are lower in the 1st Stage because of high concentration of aqueous salts. Iodide sorbed stronger to cement than Cs Allard et al. (1984). A recent review of I cement K_d values showed that in Stage 1, when the pH range was >12.5, that I K_d generally varied between 10 and 300 mL/g (Wang et al. 2009). Jakob et al. (1999) reported I *Kd* values that ranged between 10 and 50 mL/g, based on diffusion tests. Allard et al. (1984) suspected that the high sorption of iodine on cements was probably due to the sorption of iodate. Pointeau et al. (2008) noted that K_d values to hardened

Rad	Best Min Max	Oxidizing Cement Stage I	Oxidizing Cement Stage II	Oxidizing Cement Stage III	Comments and References
					cement increased by an order of magnitude as experimental conditions changed from those representing Stage I to those representing Stage II. As the pH decreases further, to values expected during Stage III and less CSH (the most iodine reactive phases) concentrations continue to decrease, the I K_d decreased again. Kaplan and Coates (2007) measured iodide K_d values in Ca(OH)-saturated and $CaCO_3$-saturated solutions in ground, 40-yr old SRS concrete, simulating $1^{st}/2^{nd}$ and 3^{rd} Stages, respectively. The measured K_d values were 14.8 and 14.4 mL/g, respectively. Finally, Serne et al. (1992) measured effective diffusion coefficients, $D_{a,}$ in reducing and oxidizing cementitious waste formulations. The oxidized samples had D_a values of 1E-10 to 3E-9 cm^2/s and the reduced samples had D_a values 2 E-8 to 8E-8 cm^2/s. The oxidized, but not the reduced samples were retarded with respect to the D_a of Na. Given these geochemical consideration of pH, ionic strength, and changes in solid phase mineralogy, iodine K_d values are expected to be greatest during the 2^{nd} Stage. (A discussion of basing selection of K_d values on measurement involving cement paste, rather than cementitious materials with aggregate, is presented in Section 8.4.) Kaplan (2016) recommends best K_d values for SRS oxidized cementitious materials for Stages I, II, and III of 8, 15, and 4, respectively (they have a much more specified waste and buried scenario than presently exists for IDF secondary waste and therefore has less uncertainty). Ochs et al. (2016) recommended best I K_d values for Stages I, II, and III of 1, 10, and 1 mL/g, respectively for a wide range of oxidizing and reducing cementitious conditions. The slightly lower values recommended by Ochs et al. (2016) can be attributed in part to them not distinguishing between reducing and oxidizing conditions, as is done here. Tests conducted under oxidizing conditions, measured non-zero I K_d values, generally between 10 and 300. Because the formulation of the cementitious waste form has not been finalized, lower values for oxidizing conditions than the SRS are being proposed here. As will be discussed below, recommended I K_d values under reducing conditions are 0, 2, and 0 mL/g for Stages I, II, and III, respectively.
NO_3^- NO_2^-	Best Min Max	0 0 0	0 0 0	0 0 0	Nitrate and nitrite are assumed to be non-reactive (non-sorbing) to cement paste
Sr	Best Min Max	90 10 200	15 2 30	90 10 200	Stable Sr, exists in very high concentrations with respect to radiostrontium in cements, ranging from 100 to 1000 ppm, ~10^{-3} M. The presence of large amounts of an isotope is expected to influence radiostrontium geochemical behavior. Wieland et al (2007) showed that radiostrontium was reversibly and linearly sorbed to cement. Furthermore, they showed that radiostrontium and stable Sr had similar K_d values; stable Sr had K_d values between 80 to 110 mL/g and ^{85}Sr had K_d values of 100 to 120 mL/g. They also noted that varying natural Sr concentrations did not influence radiostrontium K_d values. Several researchers (Tits et al. 2003; Evans 2008; Tits et al. 2006) concluded that CSH phases in hardened Portland cement sorbed Sr^{2+} via cation exchange. More specifically, the silanol groups ($\equiv SiO^-$) are responsible for Sr exchange sites. Therefore, as the Ca:Si ratio of CSH decreases during the 3^{rd} Stage, Sr sorption increases (Ochs et al. 2016). Wieland et al. (2007) showed that the

Rad	Best Min Max	Oxidizing Cement Stage I	Oxidizing Cement Stage II	Oxidizing Cement Stage III	Comments and References
					CSH phases have equal affinities for Ca and Sr, i.e., they have selectivity coefficient = ~1. Some Sr-cementitious material K_d values follow. Sr K_d values were influenced by aqueous Ca concentrations, which steadily decreases during the 2nd Stage while CSH phases loses Ca and the Ca:Si ratio steadily decreases (Tits et al. 2004; Sugiyama and Fujita 1999). Presumably, the Ca^{2+} competes with the Sr^{2+}; consequently Sr K_d values would tend to increase during the 3rd Stage. In pH environments of >12.5 (1st Stage): Wieland et al. (2007) reported K_d values of 80 to 110 mL/g for sulfur resistant Portland cement and between and 300 to 400 mL/g for CSH phases; Tits et al. (2004) reported K_d values of 100 to 4000 for CSH phases. In pH environments of ~12.5 (2nd Stage): Kaplan and Coates (2007) reported Sr K_d value of 28.1 mL/g in 40-yr old concrete with a $CaOH_2$-saturated background solution. Wieland et al. (2007) reported a K_d value of 28 mL/g to CSH phases in a alkali-free background solution; Hietanen et al. (1984) reported K_d values of 1 to 5 for concrete samples. For pH environments of 10.5 to 12 (3rd Stage): Sugiyama and Fujita (1999) reported K_d values between 5 to 170 mL/g for OPC/BFS and 50 to 2000 mL/g for CSH of varying Cs:Si ratios. Kaplan and Coates (2007) reported a K_d of 39 mL/g for 40-years old concrete with a $CaCO_3$-saturated background solution. In summary, it appears that Sr K_d values decreased during 2nd Stage and can be attributed to elevated aqueous Ca levels (Tits et al. 2004). Because CSH slowly decreases the Ca:Si ratios during the 3rd Stage (competing aqueous Ca concentrations decrease), it is expected that Sr K_d values will increase again during the 3rd Stage. Ochs et al. (2016) recommended Sr K_d values of 100, 30, and 100 mL/g for Stages I, II, and III, respectively. The recommended values here also include a decrease in Stage II, to reflect greater competition for sorption sites by Ca^{2+}. Because the formulation of the IDF cementitious waste forms have not been finalized, lower K_d than those recommended by Ochs et al. (2016) were selected to account for this uncertainty.
Tc	Best Min Max	0.8 0 2	0.8 0 2	0.5 0 1	TcO_4^- adsorption to cementitious material has been measured between 1 and 10 mL/g (Allard et al. 1984). Kaplan and Coates (2007) measured TcO_4^- K_d values in Ca(OH)-saturated and $CaCO_3$-saturated solutions in ground, 40-yr old concrete, simulating 1st/2nd and 3rd Stages, respectively. The measured K_d values were 0.8 and 1.4 mL/g, respectively. Lilley et al. (2009) measured TcO_4^- *Kd*: to 50 year old aged cement of 3.30 mL/g; to Vault 2 (25% slag) of 5.08 mL/g; and two Saltstone simulants of 4.77 & 2.75 mL/g (the latter three measurements were under oxidizing conditions). Baker et al. (2000) measured Tc(VII) K_d values of <1 mL/g for NRVB (Nirex Reference Vault Backfill: 25% OPC, 10% Limestone, 30% hydrated lime, 35% water) cementitious materials at pH 12.8. Serne et al (1992) conducted a large number of diffusion tests involving Tc(VII) and nitrate in grout waste forms. Seven apparent diffusion (D_a) values were measured on a slag-free blend (CRW); the average D_a for Tc was 5 x 10^{-9} cm^2/s and for NO_3^- was 3 x 10^{-8} cm^2/s. Assuming NO_3^- has a K_d = 0 mL/g, $D_a = D_e/R_f$, and $R_f = 1 + K_d$ *density/porosity, than Tc K_d in these tests were ~0.8 mL/g. All of the D_a values reported by Westsik et al. (2013) and Um et al. (2016) were conducted with slag-containing formulations, and were therefore not considered here. After a comprehensive review of the cement literature, Ochs et al. (2016) concluded that TcO_4^- K_d values do not change between

Rad	Best Min Max	Oxidizing Cement Stage I	Oxidizing Cement Stage II	Oxidizing Cement Stage III	Comments and References
					Stages I, II, and III, and a best estimate is 1 mL/g. The recommended values account for the observation that most Tc sorption studies have measured a non-zero pertechnetate K_d value. Because the formulation of the IDF cementitious waste forms have not been finalized, lower K_d than those recommended by Ochs et al. (2016) were selected to account for this uncertainty.
U	Best Min Max	1000 100 2000	5000 1000 10000	5000 1000 10000	Ochs et al. (2016), recommended U(VI) K_d values for Stages I, II, and III of 2,000, 40,000, and 30,000 mL/g, respectively. The two primary factors controlling U(VI) sorption to cementitious materials is aqueous Ca and pH conditions (Ochs et al. 2016). There are few studies in which U oxidation state were systematically investigated. The only exception is the study by Bayliss et al. (1996), in which both U(IV) and U(VI) sorption were measured in otherwise identical conditions. No major differences in K_d were reported. Harfouche et al. (2006) used EXAFS to identify U(VI) incorporated into CSH phases. Several authors have reported the formation of calcium urinate (Evans 2008; Wellman et al. 2007). Wellman et al. (2007) reported that U(VI) precipitates in concrete without BFS as insoluble uranyl-oxyhydroxide phases initially, and over time these phases transform to uranyl-silicate phases and then ultimately to uranyl phosphate phases as long as adequate phosphate is present. Together these results indicate that solubility is an important controlling process in the release of aqueous U. Pointeau et al. (2004) reported that U uptake by degraded cement and CSH was linear between 10^{-13} to 10^{-7} M. This suggests two things, sorption is linear in this range and that CSH is the phase controlling U sorption. Sorption on silanol groups ($\equiv SiO^-$) that changed with variable charge (pH) and Ca:Si ratios were reported to be important factors controlling U uptake. They noted increases in U K_d values with decreasing pH, which was in part attributed to the coincidental release of Ca to the aqueous phase. Between pH 12.2 to 10 (within the pH range of the 3rd Stage), the measured U K_d values increased from 30,000 to 150,000 mL/g. More recently, Pointeau et al. (2008), reported that during the 1st and 2nd Stage, U K_d values in hardened cement paste ranged from 1,000 to 4,000 mL/g. It was not until the Portlandite was dissolved (the start of the 3rd Stage), that U K_d values increased significantly by at least an order of magnitude. The observed increase in K_d with degradation of cement towards lower pH and lower Ca concentration range seems to be consistent with the theory that Ca is competing with sorbing sites on cement for uranium. Similarly, Tits et al. (2008) measured U K_d values of CSH phases over a wide range of pH values and reported values in the range of 1000 to 1,000,000 mL/g. It is noteworthy that while the values reported by Tits et al. (2008) were similar to those of Pointeau et al. (2004), they used different cementitious materials: CSH and hardened cement paste, respectively. Because pH and aqueous Ca concentrations change in a systematic manner, it is not possible to separate their respective influences on U uptake (Ochs et al. 2016). Also, opposing observations have been noted regarding the influence of Ca on U uptake: some experiments report that Ca compete with U for sorption sites, whereas other experiments indicate that Ca promote the precipitation of U-Ca solid solution endmembers. Regarding U oxidation state, Bayliss et al. (1996) measured U(IV) and U(VI) sorption under otherwise identical conditions. No major differences in K_d were reported. Evans (2008) concluded

Rad	Best Min Max	Oxidizing Cement Stage I	Oxidizing Cement Stage II	Oxidizing Cement Stage III	Comments and References
					that sorption to silanol groups ($\equiv SiO^-$) likely controls uptake at total U concentration less than 10^{-6} to 10^{-5} molar, beyond which solubility of either $CaUO_4$ (Tits et al. 2008) or CaU_2O_7 (Valsami-Jones and Ragnarsdottir 1997) control aqueous U concentrations. Ochs et al. (2016) recommended K_d values of 2000, 30,000, and 30,000 mL/g for Stages I, II, and III, respectively. Because the formulation of the IDF cementitious waste forms have not been finalized, lower K_d than those recommended by Ochs et al. (2016) were selected to account for this uncertainty. It is anticipated that much of the pessimistic-bias built into these recommended best estimates will be eliminated once measurements are conducted under site specific conditions.

Table 8-5. Distribution Coefficients (K_d values, mL/g): Reducing Cementitious Solids

Rad	Best Min Max	Reducing Cement Stage I	Reducing Cement Stage II	Reducing Cement Stage III	Comments/References
Cs, NO_3^- /NO_2^-					Same values as reported for Oxidizing Cementitious Solids (Table 8-4)
Hg	Best Min Max	500 50 1000	500 50 1000	100 10 200	BFS-containing cements will have elevated sulfur concentrations and the sulfur will include sulfides, which can form sparingly soluble precipitates with Hg. Lockrem et al. (2005) reported D_a values for 41 formulations of Cast Stone with and without getters of <3E-11 to <7E-10 cm^2/s (LI = >10.5 to >9.1, respectively), indicating significant Hg attenuation. They also conducted TCLP batch desorption test that indicated that Hg failed the Universal Treatment Standards (UTS limits), however for longer desorption periods, no detectable Hg was observed to leach from the waste forms. This suggested to Serne and Westsik (2011) that there may be two forms of Hg in the Cast Stone, a readily leachable, perhaps as salts on the surface of the Cast Stone, and a less leachable fraction, perhaps bound to the matrix of the cement in association with sulfur. In the literature, immobilization of Hg in cementitious materials is well studied (Svensson and Allard 2008; Razzell 1990; Svensson and Allard 2007; Svensson et al. 2006). Mercury does not form sufficiently insoluble (hydr)oxides, and a sulfur source needs to be added to promote the formation of the sparingly soluble HgS phase. While many researchers have pointed to cinnabar, a crystalline form of HgS, as a natural analogue of HgS leaching from cementitious materials, this may be an oversimplification because there are many less crystalline, and meta-stable forms of the mineral, resulting in a wide range of solubilities. Furthermore, redox status of the waste monolith is a crucial parameter for the formation of HgS. In samples where only slag was used as a sulfur source, Svensson and Allard (2008) reported D_a values of 1.5E-19 to 3.7E-18 cm^2/s. In the same trial with slag-free formulations (OPC and sand), the D_a values were 3.8E-18 to 1.8E-15 cm^2/s (based on long-term test results). These studies indicate that Hg is strongly bound by cementitious materials, and that reducing conditions may be expected to decrease D_a values (increase sorption) by at least an order of magnitude. Another important general conclusion from this work is that Hg D_a values vary greatly with the speciation of Hg in the waste form. If HgS is not likely formed, e.g., Hg(0) and Hg(II) are present, than D_a values may increase to 1E-9 to 1E-11 cm^2/s. More recently, Bannochie (2015) reported Hg speciation measurements of SRS Tank 50 samples and the TCLP results when that solution was used to make in the laboratory a saltstone sample. The Tank 50 sample had 126 mg/L total Hg, the saltstone had a total Hg concentration of about 50.4 mg/kg Hg, and the TCLP (conducted in oxidizing conditions) had a total Hg concentration of 0.151 mg/L. As a first approximation, a K_d value based on these values is 334 mL/g. This K_d value would have been greater had it been measured under reducing conditions. The key finding by Bannochie (2015) was that 80% of the leached Hg from the TCLP tests was in the methyl-Hg form, underscoring the importance of speciation on Hg leaching. In summary, the presence of sulfides in reducing cementitious waste forms is extremely effective at immobilizing ionic forms of Hg (K_d

Rad	Best Min Max	Reducing Cement Stage I	Reducing Cement Stage II	Reducing Cement Stage III	Comments/References
					>10,000 mL/g or extremely low solubility values). However, because the Hg speciation in the IDF is unknown, additional pessimistic-bias needs to be added to the recommended values.
Tc[(a)]	Best Min Max	1000 100 2000	1000 100 2000	1000 100 2000	Under reducing conditions, it is recommended that Tc(IV) sorption be characterized with a solubility term; K_d values are provided here to offer alternative modeling approaches and to accommodate any potential numerical models that cannot use k_s values. $Tc^{VII}O_4^-$ gets reduced to Tc(IV), which like other tetravalent cations sorbs strongly to surfaces. Lukens et al. (2005) conducted fundamental studies using SRS slag and grout mixtures. In their study, they added Tc(VII) to a reducing grout and using X-ray Absorption Spectroscopy, specifically, XANES, they observed the slow transformation of Tc(VII) to $Tc^{VII}O_2$-H_2O to $Tc^{IV}S_x$. This process was monitored in the grout over a course of 45 months. See a discussion of Tc solubility values under reducing conditions in Table 8-6. The high K_d values selected for these conditions reflect in part the low solubility of Tc under these conditions. Lilley et al (2009) measured $Tc^{VII}O_4^-$ sorption to two SRS Saltstone simulants containing 45% slag, but did not reach steady state. In one experiment they measured a K_d of 18 mL/g and in the other a K_d of 3660 mL/g. Estes et al. (2012) measure Tc K_d values for four types of cement recovered from the SRS in an inert glovebag. After 319 days, two formulations containing BFS had K_d values ranging between 2001 and 8300 mL/g (samples Vault 2 and TR545). Um et al. (2016) measured desorption K_d values for three LSW grout formulations including two with hydrated lime, OPC, and BFS and one with fly ash, OPC and BFS. Under oxidizing conditions, the recommended desorption K_d was 24.0 mL/g. Under reducing conditions, the measured Tc desorption K_d values were ~269 mL/g. They concluded that solubility and not K_d were likely controlling Tc release from reducing cementitious materials samples, but under oxidizing conditions, K_d desorption controlled Tc release. There have been several recent reviews of Tc redox and binding chemistry in cementitious materials (Pabalan et al. 2009; Icenhower et al. 2010; Westsik et al. 2013; Westsik et al. 2014; Ridge 2015). Ochs et al. (2016) recommended best Tc(IV) K_d values of 3000, 3000, and 3000 mL/g for Stages I, II, and III, respectively. Because the formulation of the IDF cementitious waste form has not been finalized, additional pessimistic-bias was included in the selection of K_d values.
Sr	Best Min Max	1000 100 2000	1000 100 2000	100 10 200	Stable Sr, exists in very high concentrations with respect to radiostrontium in cements, ranging from 100 to 1000 ppm. The presence of large amounts of stable Sr is expected to be especially important in systems with high sulfur concentrations, as exists in BFS-blends. When stable sulfate concentrations are sufficiently high, $SrSO_4$ precipitates. $SrSO_4$ has a solubility of 3.2×10^{-7} M (strontium sulfite solubility product is even lower, $SrSO_3$ k_s = 4E-8 M). This process was observed in samples recovered by the Saltstone Disposal Facility (SDF). Almond and Kaplan (2010) measured very high apparent Sr K_d values in an actual SDF core sample contacted with an artificial cement leachate: K_d values of 5728 mL/g under oxidizing conditions and 737 mL/g under inert gas (reducing) conditions. Reigel and Hill (2016) measured appreciably lower apparent Sr K_d values in a second SDF core sample: ~40 mL/g under oxidizing conditions, and ~50 mL/g under inert gas conditions. The cause for the discrepancy of these results compared to earlier results and literature results is not known.

Rad	Best Min Max	Reducing Cement Stage I	Reducing Cement Stage II	Reducing Cement Stage III	Comments/References
					While radionuclide immobilization in the presence of slag is commonly attributed to the reduction of the radionuclide to a less mobile oxidation state, in the case of Sr (and Ba), the presence of sulfur, the reducing agent, is responsible for immobilization through the formation of sulfate/sulfide precipitates. These latter results using site specific materials are especially representative of conditions expected under disposal conditions. Therefore, larger K_d values are warranted for Sr (and Ba) OPC/BFS-blends than in traditional OPC blends.
Cr[(a)]	Best Min Max	1000 100 2000	1000 100 2000	1000 100 2000	Under reducing conditions, it is recommended that Cr(III) sorption be characterized with a solubility term; K_d values are provided here to offer alternative modeling approaches and to accommodate any potential numerical models that cannot use k_s values. Kindness et al. (1994) reported that <0.01 ppm Cr leached from a well cured OPC/BFS monolith prepared with water and spiked with 5000 ppm Cr(III). Using these values, a K_d value is >500,000 mL/g, and an apparent solubility concentration, k_p of <2E-7 mol/L. Bajt et al. (1993) observed XAS spectra of the reduction of Cr(VI) in SRS reducing grout to Cr(III). Rai et al. (1987) measured the solubility of Cr(III) at varying pH and ionic strengths and as varying solid phases. Evans (2008) reported that Cr(III) is structurally incorporated into numerous cement phases, including hydrogarnet, and CSH phases, where the Cr^{3+} replaces octahedrally coordinated Al^{3+}. Polettini et al. (2002) reported that Cr^{3+} could substitute into Si sites of CSH. Westsik et al. (2013) reported Cr apparent diffusion coefficients for 26 Cast Stone (BFS-cement) samples with a wide range of formulations. Cr apparent diffusion coefficients (10^{-12} to 10^{-14} cm^2/sec) were 4 to 6 orders-of-magnitude slower than nitrate, nitrite, and Na (assumed to be conservative tracers with no retardation; 10^{-8} cm^2/s), indicative of significant retardatation. Cr effective diffusion rates were also 2 to 4 orders-of-magnitude lower than Tc. Assuming reversible and linear sorption is responsible for the Cr retention to the Cast Stone, the D_e value are inversely related to retardation factor, which in turn is directly related to K_d (i.e., $D_e = D_0/R_f$). Cr K_d values may be as much as 6 orders of magnitude greater than nitrate/nitrite/Na K_d values, and 2 to 4 orders of magnitude greater than Tc K_d values. While these studies were conducted using a wide range of site-specific cementitious formulations, and there is significant technical understanding of the cement binding process of Cr(III), lower values are recommended here to account for uncertainty associated with final formulation of the cementitious materials that will be used for solid secondary waste at the IDF.
I	Best Min Max	0 0 0	2 0 4	0 0 0	Three studies have shown that I K_d values under reducing conditions are much less than under oxidizing condition. Westsik et al. (2013) and Serne et al. (1993) showed that I had diffusion coefficients similar to nitrate, nitrite and Na, suggesting that no I retardation occurred. Atkins and Glasser (1992) showed that I K_d values for reducing cement was 5 mL/g and for OPC-cement was 40 mL/g. Similarly, Allard et al. (1984) report I K_d values of 3 mL/g for slag-containing cements and for slag-free cement (ordinary Portland cement) they reported an I K_d value of 125 mL/g. Serne et al. (1992) showed a lower apparent diffusion coefficient (greater retardation) for BFS cement than a BFS-free cement. It is likely that part of the reason for the differences between I K_d values can be

Rad	Best Min Max	Reducing Cement Stage I	Reducing Cement Stage II	Reducing Cement Stage III	Comments/References
					attributed to changes in I speciation; reducing conditions will have a greater percentage of iodide, the weakly sorbing species, and oxidizing conditions with have a greater percentage of iodate, the more strongly sorbing species and the species most likely to coprecipitate in various CSH phases. This is further discussed in Appendix C. Reigel and Hill (2016) measured desorption ^{129}I K_d values in an inert glovebag of saltstone cores recovered from the Saltstone Disposal Facility of -1, 5, 4, and 2 mL/g under conditions that would most closely approximate those of Stage II. These latter K_d measurements represent the highest pedigree data because they were conducted with aged samples that actual tank waste. Kaplan and Coates (2007) measured on the benchtop (exposed to air) iodide I^- (iodide) K_d values in $Ca(OH)_2$ saturated and $CaCO_3$-saturated solutions in ground, SRS reducing grout, simulating $1^{st}/2^{nd}$ and 3^{rd} Stages, respectively. The measured I^- K_d values were 6.2 and 11 mL/g, respectively. With the exception of one measurement, all other I K_d measurements found in the literature were non-zero K_d value. The best estimate K_d value in Stage I is set to 0 mL/g because of high ionic strength and low redox. K_d values in the Stage II are slightly increased to capture the results from actual Saltstone samples noted above and the relatively more favorable chemical/mineral environment (Reigel and Hill 2016). In Stage III, the I K_d value is reduced again because all CSH phases (the primarily sorbing phases) have been exhausted, as well as the higher ionic strength, compared to background, of the aqueous phase.
U	Best Min Max	5000 1000 10000	5000 1000 10000	5000 1000 10000	Precipitation and coprecipitation are important U immobilization processes under oxidizing and reducing cementitious conditions. Most studies of U immobilization have been conducted with non-reducing grout. The only exception is the study by Bayliss et al. (1996) in which both U(IV) and U(VI) sorption were measured in otherwise identical conditions. They reported no major differences in U(IV) and U(VI) K_d values. Another indication of the strong U binding potential of potential BFS-containing cementitious materials was reported by Cantrell et al. (2016), where they concluded that the best U D_a value for Cast Stone is <6E-16 cm^2/s (which is approximately equivalent to K_d value >1,000,000 mL/g), which was the slowest noted diffusion of all radionuclides investigated. As part of an extensive review of the literature Ochs et al. (2016), concluded that there were no significant differences between recommended U K_d values for the three cement stages; for Stages I, II, and III, they recommended 30,000, 30,000, and 30,000 mL/g, respectively. The recommended values here have been set lower than those recommended by Ochs et al. (2016) other values to capture the uncertainty associated with the disposal of several waste forms and the fact that the formulation of the waste form has not yet been finalized.
[(a)] Tc and Cr should be modeled using k_s values, K_d are provided for guidance in the event numerical models that cannot handle k_s values is used in the future.					

Table 8-6. Apparent Solubility Concentrations (mol/L; k_s): Reducing Cementitious Materials

		Reducing Cement Stage I	Reducing Cement Stage II	Reducing Cement Stage III					
Cr	Best Min Max	10^{-7} 10^{-8} 10^{-6}	10^{-7} 10^{-8} 10^{-6}	NA NA NA	Bajt et al. (1993) observed XAS spectra of the reduction of Cr(VI) in SRS reducing grout to Cr(III). Rai et al. (1987) measured the solubility of Cr(III) at varying pH and ionic strengths and as varying solid phases (at elevated pH environments, he reported Cr(III) solubilities of <1E-8 M. Kindness et al. (1994) reported that <0.01 ppm Cr leached from a well cured OPC/BFS monolith prepared with water and spiked with 5000 ppm Cr(III). Using these values from Kindness et al. (1994), the K_d value is >500,000 mL/g, and an apparent solubility concentration, k_s, is <2E-7 mol/L.				
Tc	Best Min Max	10^{-9} 10^{-10} 10^{-8}	10^{-9} 10^{-10} 10^{-8}	NA NA NA	Two recent Tc solubility values were made on actual aged Saltstone cores recovered from the Saltstone Disposal Facility; as such, these measurements represent values with high pedigree. Actual saltstone solubility values measured under largely reducing conditions (in both cases some O_2 was detected in the glovebag) were 2E-10 M (Almond and Kaplan 2011) and 3E-8^{-8} M (Reigel and Hill 2016). There were also three experimental Tc solubility values measured under reducing conditions with simulated saltstone samples. A flow-through experiment showed that Tc solubility ranged from 2E-6 to 1E-7 M in saltstone leachate (pH was 12.66 and Eh was -0.38 V) (Cantrell and Williams 2012). In a batch experiment conducted in an inert environment with simulated saltstone, Tc solubility after 319 days was between 9E-9 and 5E-10 M in a simulated saltstone leachate of pH ~11.8 and Eh -0.44 V (Estes et al. 2012). In the same study, but using reducing vault concrete (a slag-containing cement), Estes et al. (2012) measured a solubility in the pH 10.9 and Eh -0.40 V leachate of 4.5E-10 M Tc. Um et al. (2016), using a hydrated lime, 35% OPC, and 45% BFS formulation, reported a Tc solubility of 4.3E-9 M, Thermodynamic modeling captured the data trends and the magnitude of these experimental data from the SRS reasonably well (Li et al. 2012). The Tc solubility in the 3rd stage has a lower solubility to account for the general transformation of Tc into a more soluble phase (as observed through spectroscopy; (Um et al. 2013; Lukens et al. 2005; Arai and Powell 2015) as the Eh of the system gradually becomes increasingly oxidized and the solid phase Tc speciation transitions to more soluble species. Um et al. (2016) measured Tc(IV) solubility in a reducing grout formulation, LSW waste (20% hydrated lime, 35% OPC, 45% BFS) and reported a best values of 3.4 x 10^{-9} M. Pinkston (2013) reviewed and conducted thermodynamic calculation related to some early experiments, but did not review results from actual Saltstone Facility studies. Bayliss et al. (1991) adsorbed Tc onto Portland cement or concrete in an anoxic glove box with 0.05 M dithionite in 1.5 M NaCl (simulating Stage I) for 28 days in 50:1 water:crushed cement: K_d = 5000 mL/g and measured Tc solubility was 10^{-11} M. Assuming Tc_2S_7 as the solubility controlling phase, MMES (1992; Appendix D) calculated that reducing grout used in the SRS saltstone program would maintain Tc at a concentration of 1.4 x 10^{-20} M (2.4E-8 pCi/L). Allard et al. (1984) calculated that reducing concrete would maintain Tc at a concentration <1E-10 M. The selected represented the lower range of values in the literature. The only lower solubility values were reported by Cantrell and Williams (2012), however, their flow through test may not have been at steady state.				

Table 8-7. Iodine K_d Values (mL/g) with Granular Activated Carbon (GAC)

K_d	Oxidized or Reduced Stage I	Oxidized or Reduced Stage II	Oxidized or Reduced Stage III	Comment
Best	600	600	600	There is a general lack of waste specific K_d values for GAC under cementitious environments. The values here are based largely on experiments conducted with spent GAC recovered from two SRS facilities (Kaplan et al. 1999; Kaplan et al. 2000; Kaplan and Serkiz 2000). Using rainwater leachate, desorption K_d values were 58,100 to 132,500 mL/g. Using cement leachate, desorption K_d values decreased to 320 to 880 mL/g. It is recommended that iodine-K_d values for spent GAC have a mean of 600 mL/g.
Min	100	100	100	The 95-percentile range was set at 100 to 2000 mL/g. The wide range is to account for the uncertainty associated with: 1) the type of GAC being disposed, 2) changing water chemistry, and 3) the long-term interaction between GAC in a high pH cementitious environment.
Max	2000	2000	2000	The 95-percentile range was set at 100 to 2000 mL/g. The wide range is to account for the uncertainty associated with: 1) the type of GAC being disposed, 2) changing water chemistry, and 3) the long-term interaction between GAC in a high pH cementitious environment.

Table 8-8. Estimated K_d Values (mL/g) for HEPA Filters

Element		"Far Field K_d Sand Sequence"[a] (mL/g)	Recommended HEPA Filter K_d (mL/g)[b]
Cr	Best	0	0
	Min	0	0
	Max	0.6	0
Cs	Best	2000	20
	Min	500	5
	Max	4000	40
Hg	Best	300	3
	Min	50	0.5
	Max	2500	30
I	Best	0.25	0
	Min	0	0
	Max	15	0.2
NO_3^-/NO_2^-	Best	0	0
	Min	0	0
	Max	0	0
Sr	Best	14	0.1
	Min	5	0.1
	Max	200	2
Tc	Best	0	0
	Min	0	0
	Max	0.6	0
U	Best	1	0
	Min	0.1	0
	Max	4	0

[a] Best, minimum, and maximum K_d values were taken from Krupka et al. (2004), Zone 2b, Table 5.6. They reported Conservative, Best and Range of K_d values. Hg K_d values taken from reported Ni and Sr values reported in table.
[b] Recommended HEPA Filter K_d = "Far Field K_d Sand Sequence" x 0.01

9.0 Initial saturation state of SSW grout

The initial saturation state of buried SSW grout used for encapsulation and/or solidification will influence moisture flow and solute transport until the material equilibrates with its surroundings. Unsaturated hydraulic conductivity and effective diffusion coefficient are reduced for lower moisture content, thus resulting in reduced release rates from the waste form compared to saturated conditions. Also, if the initial saturation in the waste form is below the equilibrium value, then the waste form will imbibe moisture from the surrounding backfill, further hindering liquid phase releases. Thus, an assumption of near saturation in a waste form would tend to be conservatively-biased from the perspective of releases in the liquid phase. However, from the perspective of gas phase migration, higher saturation values would lead to decreased gaseous phase diffusion through a waste form. This could potentially be non-conservative, for example, in the case of assumptions regarding oxidation of a reducing waste form.

A number of uncertain factors will influence the initial saturation level(s) of cured SSW waste form(s) at PA time zero. These include:

- mix design, including the water to cementitious materials ratio (w/cm)
- initial and final curing conditions
- potential longer term exposure to the atmosphere and/or subsurface environment during facility operations and institutional control

Furthermore, little information is available on the initial saturation state of cementitious materials in general, especially materials cured under the conditions similar to those expected at the IDF. While these factors preclude a precise prediction of initial saturation, the range of possibilities can be somewhat narrowed.

An ample supply of water to support cement hydration is critical to achieving optimal structural and transport performance. Limited water availability during initial and/or final curing usually results in degraded properties (e.g. ACI 308R-01, Bonavetti et al. 2000, Shafiq and Cabrera 2004, Ozer and Ozkul 2004, Burlion et al. 2005, Termkhajornkit et al. 2006, Guneyisi et al. 2007). Thus by standard practice (e.g. ASTM C192/C192M-16, ACI 308R-01), cementitious materials are typically cured in manners that prevent significant moisture loss during initial curing and provide additional water to support remaining hydration during final curing. Common examples of the latter are contact with liquid water through ponding, immersion, fogging, sprinkling and wet covers, and curing in a high-humidity environment (relative humidity approaching 100%). At the same time, higher water to cementitious material ratios than required to support hydration also lead to degraded material performance such as compressive strength. Therefore, cementitious mixes are generally designed to achieve an optimal middle ground with respect to w/cm.

Grout mixes best suited for IDF SSW encapsulation and solidification can be expected to incorporate a higher w/cm to improve flowability and filling of void spaces, and because high structural strength is not required to meet expected waste acceptance criteria. Another consideration is the likely curing conditions at the IDF treatment facility. Wet SSW grouts are expected to be poured into containers (e.g. drums, B-25 boxes) which are then largely sealed off from the environment. Water available for hydration will likely be limited to that provided in the wet slurry. With this consideration, SSW grout formulations can be designed with higher water to cementitious material ratios than would be optimal under more common curing conditions, where external water is supplied during the final curing stage. These observations suggest the as-cured saturation of SSW grouts will lie toward the upper end of the 0% to 100% bounding range.

However, an SSW grout that is 100% saturated immediately after hardening and then isolated from any additional source of water may self-desiccate and become only partially saturated. One point of reference is characterization of Saltstone grout (10% cement / 45% fly ash / 45% slag / w/cm=0.69) in a mesoscale mock-up facility at the Savannah River Site (SRR 2015). Simulated saltstone was poured into a B-25 waste container in daily lifts of 8-9 inches to a total height of approximately 42 inches in separate FY2013 and FY2014 mock-up tests. Cored samples were acquired after 2 months of monolith curing in FY2013 and at least 7 months in FY2014. The FY2014 summary report (SRR 2014) states that "B25 lid incorporated a seal to maintain a humid curing environment". The test conditions align with those anticipated in future IDF SSW disposals:

- B-25 box (relevant container size, geometry, material, and closure state)
- Monolith curing within a sealed container at ambient temperatures over months

Gravimetric moisture content (w) measurements were acquired from samples subsequently cored from the monolith using both wet and dry drilling techniques. Gravimetric moisture was reported to be 36 to 37% regardless of the coring technique used (SRR 2015 Page 36, SRR 2014 Section 3.10). Volumetric moisture content can be computed from w using the expression

$$\theta = \frac{\rho_b}{\rho_\ell} w \tag{86}$$

where ρ_ℓ is the density of the pore fluid. For saltstone ρ_b ~ 1.0 g/cm^3 and ρ_ℓ ~ 1.2 g/cm^3 (SIMCO 2010), leading to estimated volumetric water contents of 30% to 31% compared to a porosity of 58% (SRR 2009 Table 4.2-16), which corresponds to an as-cured saturation of 53%. Additional measurements of "as-cured" saturation were not readily identified within this limited scoping study.

After initial curing, SSW waste forms may be exposed to the atmosphere and/or subsurface soil moisture depending on container integrity and future IDF waste handling, storage, and burial practices. SSW grout would generally dry out in response to atmospheric exposure, but gain moisture with exposure to the subsurface (unless already fully saturated). The range of possible saturations for exposed SSW grout at PA time zero, can be estimated based on two equilibrium scenarios. A lower bound on saturation can be derived from the assumption that grout reaches equilibrium with the atmosphere. A higher bound corresponds to buried waste and equilibrium with soil moisture.

Relative humidity and saturation are related through thermodynamic relationships and a material specific water retention curve. Total suction head is related to water vapor pressure through an equilibrium thermodynamic relationship known as the Kelvin relationship (Richards 1965, cited in Fredlund and Rahardjo 1993, Equations 4.1 and 4.3)

$$\psi = \left(P_g - P_\ell\right)/\rho g + \pi = p_c + \pi = -\frac{\mathcal{R}T}{gM_w} ln\left(\frac{P_v}{P_0}\right) = -\frac{\mathcal{R}T}{gM_w} ln(RH) \tag{87}$$

where

ψ = total suction [m]

P_g = gas pressure [Pa]

P_ℓ = liquid pressure [Pa]

ρ = liquid density [kg/m^3]

g = gravitational acceleration [m/s^2]

π = osmotic suction [m]

p_c = capillary or matric suction [m]

$\mathcal{R}$ = universal (molar) gas constant [J/mol-K = m^{3}Pa/mol-K]

T = temperature [K]

M_w = molar mass of water [kg/mol]

P_v = water vapor pressure [Pa]

P_0 = vapor pressure at saturation [Pa]

RH = relative humidity, P_v/P_0 [-]

In light of this expression, water vapor pressure can be viewed as a master variable defining the pressure state of both the gas and liquid phases (Hall and Hoff 2002). The osmotic suction can be estimated from the Morse equation

$$\rho g \pi = iM\mathcal{R}T \tag{88}$$

where

i = van't Hoff factor [-]

M = molarity of the solution [mol/m^3]

The dimensionless van't Hoff factor is approximately one when the molarity of the solution is defined in terms of total ion concentration. For the purpose of defining a lower bound on SSW grout saturation, osmotic suction is ignored so that capillary tension is maximized as $p_c = \psi$. Grout saturation is then computed from the van Genuchten / Mualem characteristic curve defined by Equations (10) and (11) using parameter settings from Section 6.2.

An upper bound on equilibrium saturation can be derived by assuming the waste form is buried quickly and reaches equilibrium with the moist subsurface. In Section 4.3 three post-closure capillary tension conditions were identified: (a) 10,000 cm upper bound based on a gravity equilibrium assumption, (b) 1200 cm assuming the vadose zone is composed of the Hanford "Gravel" sequence (Rockhold et al. 2015), and (c) 500 cm assuming the vadose zone is composed of the Hanford "Sand" sequence (Rockhold et al. 2015). For these specified suction heads, equilibrium grout saturation is computed directly from Equations (10) and (11) using parameter settings from Section 6.2.

Table 9-1 (paste) and Table 9-2 (mortar) present calculated saturation results for four scenarios: atmospheric exposure, and p_c = 10^4, 1200 and 500 cm. The atmospheric conditions correspond to long-term averages inferred from Hoitink et al. (2005 Table 2.1). Relative humidity values equivalent to the

three designated p_c values are also shown for comparison purposes. The saturation calculation for mortar exposed to the atmospheric uses the "bimodal" composite properties from Section 6.2. The equilibrium saturation for atmospheric exposure is 5% for paste and 11% for mortar. Under the expected post-closure condition of $p_c \cong$1000 cm, SSW paste will be fully saturated at equilibrium, while SSW mortar will be moderately unsaturated (86 to 89%).

The range of equilibrium values is larger than desired, but not surprising considering the arid conditions of the Hanford site. The range of expected saturations can be narrowed by considering the degree of waste form exposure to the environment, time scales required to reach equilibrium, and the as-cured saturation state of SSW grouts. During facility operations through burial, SSW grout (paste or mortar) will reside inside steel containers and be largely isolated from the atmosphere (notwithstanding the above hypothetical bounding calculation). Furthermore, drying time scales as the square of the characteristic length. For example exposure conditions that would dry a centimeter-scale specimen over one day would require three decades (100^2 days) to dry a meter-scale SSW waste form in the same manner. These observations and the expectation that as-cured saturation will exceed 50% indicate the lower bound equilibrium saturations to be highly unlikely. Equilibrium saturations projected for SSW grouts in communication with backfill are similar to, but higher than, projected as-cured saturations: 50% < S < 100%. Although the time required for buried SSW grout to reach equilibrium with subsurface moisture will be very slow (time scale ~ characteristic length squared), eventual equilibrium would drive waste saturation closer to the range: 85% < S < 100%.

In summary, the as-cured saturation state of SSW grouts will likely exceed 50% and then slowly approach 85% < S < 100% after burial, if not already highly saturated in the as-cured state. Very low saturations are possible but very unlikely, as long as contact with the atmosphere is limited due to intact waste containment and/or relatively short above-ground storage times.

Table 9-1. Equilibrium saturation for paste under selected exposure conditions.

Parameter	Atmosphere	Gravity Equilibrium	Hanford Gravel	Hanford Sand	Units
temperature, T	12.5	12.5	12.5	12.5	C
	54.5	54.5	54.5	54.5	F
	285.65	285.65	285.65	285.65	K
relative humidity, RH	55%	99.26%	99.91%	99.96%	
saturation pressure, P_0	14.48	14.48	14.48	14.48	millibar
	1448	1448	1448	1448	Pa
water vapor pressure, P_v	797	1438	1447	1448	Pa
gas constant, R	8.314	8.314	8.314	8.314	J/K-mol
molecular weight of water, M_w	18	18	18	18	g/mol
gravitational acceleration, g	9.81	9.81	9.81	9.81	m/s^2
density of water, ρ	998	998	998	998	kg/m^3
ρg	9790.38	9790.38	9790.38	9790.38	Pa/m
total suction, ψ	8041	100	12	5	m
	8.0E+05	1.0E+04	1200	500	cm
	7.9E+07	9.8E+05	1.2E+05	4.9E+04	Pa
	78720	979	117	49	kPa
	777	10	1	0	atm
	787.2	9.8	1.2	0.5	bar
van't Hoff factor, i	1	1	1	1	
molarity, M	0	0	0	0	mol/L
osmotic suction, Π	0.0E+00	0.0E+00	0.0E+00	0.0E+00	Pa
	0	0	0	0	m
	0.0E+00	0.0E+00	0.0E+00	0.0E+00	cm
	0.0E+00	0.0E+00	0.0E+00	0.0E+00	Pa
	0	0	0	0	atm
	0	0	0	0	bar
matric suction, p_c	8041	100	12	5	m
	8.0E+05	1.0E+04	1.2E+03	5.0E+02	cm
	7.9E+07	9.8E+05	1.2E+05	4.9E+04	Pa
	777	10	1	0	atm
	787	10	1	0	bar
saturated water content, θ_s	0.6027	0.6027	0.6027	0.6027	
residual water content, θ_r	0	0	0	0	
van Genuchten (1980) α	6.467E-06	6.467E-06	6.467E-06	6.467E-06	cm^{-1}
van Genuchten (1980) n_{vG}	3.1042	3.1042	3.1042	3.1042	
van Genuchten (1980) m_{vG}	0.586727	0.586727	0.586727	0.586727	
capillary suction head, p_c	804055	10000	1200	500	cm
saturation	0.049	1.000	1.000	1.000	

Table 9-2. Equilibrium saturation for mortar (bimodal) under selected exposure conditions.

Parameter	Atmosphere	Gravity Equilibrium	Hanford Gravel	Hanford Sand	Units
temperature, T	12.5	12.5	12.5	12.5	C
	54.5	54.5	54.5	54.5	F
	285.65	285.65	285.65	285.65	K
relative humidity, RH	55%	99.26%	99.91%	99.96%	
saturation pressure, P_0	14.48	14.48	14.48	14.48	millibar
	1448	1448	1448	1448	Pa
water vapor pressure, P_v	797	1438	1447	1448	Pa
gas constant, R	8.314	8.314	8.314	8.314	J/K-mol
molecular weight of water, M_w	18	18	18	18	g/mol
gravitational acceleration, g	9.81	9.81	9.81	9.81	m/s^2
density of water, ρ	998	998	998	998	kg/m^3
ρg	9790.38	9790.38	9790.38	9790.38	Pa/m
total suction, ψ	8041	100	12	5	m
	8.0E+05	1.0E+04	1200	500	cm
	7.9E+07	9.8E+05	1.2E+05	4.9E+04	Pa
	78720	979	117	49	kPa
	777	10	1	0	atm
	787.2	9.8	1.2	0.5	bar
van't Hoff factor, i	1	1	1	1	
molarity, M	0	0	0	0	mol/L
osmotic suction, Π	0.0E+00	0.0E+00	0.0E+00	0.0E+00	Pa
	0	0	0	0	m
	0.0E+00	0.0E+00	0.0E+00	0.0E+00	cm
	0.0E+00	0.0E+00	0.0E+00	0.0E+00	Pa
	0	0	0	0	atm
	0	0	0	0	bar
matric suction, p_c	8041	100	12	5	m
	8.0E+05	1.0E+04	1.2E+03	5.0E+02	cm
	7.9E+07	9.8E+05	1.2E+05	4.9E+04	Pa
	777	10	1	0	atm
	787	10	1	0	bar
saturated water content, θ_s	Table 6-4 †	Table 6-4 †	Table 6-4 †	Table 6-4 †	
residual water content, θ_r	Table 6-4 †	Table 6-4 †	Table 6-4 †	Table 6-4 †	
van Genuchten (1980) α	Table 6-4 †	Table 6-4 †	Table 6-4 †	Table 6-4 †	cm^{-1}
van Genuchten (1980) n_{vG}	Table 6-4 †	Table 6-4 †	Table 6-4 †	Table 6-4 †	
van Genuchten (1980) m_{vG}	Table 6-4 †	Table 6-4 †	Table 6-4 †	Table 6-4 †	
capillary suction head, p_c	8.0E+05	10000	1200	500	cm
saturation	0.115	0.783	0.857	0.893	

† See composite properties for bimodal mortar.

10.0 Material property evolution / degradation

Physical degradation in cementitious materials typically takes the form of cracks / fractures, although porosity-opening is possible in the case of primary constituent (calcium) leaching. Before identifying and assessing the likelihood and significance of various mechanisms leading to physical degradation, we first assess the likely impact of cracks on moisture flow and solute transport should they occur. The following discussion is based on the expected environmental conditions in the vadose zone at the Hanford site defined in Section 4.3.

10.1 Effect of potential cracks / fractures on flow and transport

Saturated cracks will significantly alter the permeability and diffusion coefficient of a cementitious material, except for apertures below a certain threshold size discussed below. On the other hand, only modest capillary tension is typically required to dewater cracks and greatly reduce or even negate their influence on bulk flow and transport properties under unsaturated conditions. In this section we consider the likely influence of potential cracks on advection and diffusion through SSW grouts (paste or mortar).

A fracture / crack aperture will be liquid-filled under the condition (Wang and Narasimhan 1985)

$$-\frac{P}{\rho g} = p_c < \frac{2\sigma}{\rho g b} \tag{89}$$

where

b = aperture width [L]

σ = surface tension [F/L]

and the other symbols are defined in Section 4.1. The largest capillary pressure head for which a fracture can be saturated corresponds to the smallest aperture width. While apertures may approach zero width, only apertures above a certain threshold size and influencing transport are of interest.

In contrast to larger cracks, Wang et al. (1997) found that crack openings less than 50 μm had "little effect on concrete permeability". In agreement with the latter, Ismail et al. (2004) found that apertures less than about 50 μm did not produce accelerated chloride penetration in cracked concrete. In another chloride propagation study, Sahmaran and Yaman (2008) report that "for crack widths less than about 135 μm, the effect of crack width on the effective diffusion coefficient … was found to be marginal when compared to virgin specimens". Ismail et al. (2008) found that “results obtained with 80–100-μm cracks indicate that the diffusion process still occurs, but at a much slower rate” relative to larger apertures. These studies suggest that the minimum aperture width influencing permeability and aqueous diffusion coefficient is on the order of 100 μm. From Equation (89), any fractures of 100 μm or larger size will be unsaturated at capillary pressures exceeding 15 cm. From Section 4.3, the expected exposure condition for buried IDF waste forms is on the order of 1000 cm. Thus any cracks of potential significance to flow and/or transport, should they occur in SSW grout, are expected to be unsaturated.

Although not fully saturated, cracks can still transport moisture and solutes through film flow on fracture faces. Film thickness and transport decrease as capillary pressure head increases in the adjoining matrix. At sufficiently high tension head, film flow may become insignificant compared to matrix flow. In the following comparison, we use 1.0E-9 cm/s as an optimistically low hydraulic conductivity for the matrix (Table 6-2), which is expected to be saturated or nearly so (Table 9-1 and Table 9-2). Or and Tuller (2000) present an analytic method for estimating film thickness and flowrate through fractures with a specified, idealized, geometry. This theoretical solution can be recast into hydraulic conductivity for the

fracture network, and blended with intact matrix properties to achieve a composite hydraulic conductivity for a fractured cementitious material (Flach et al. 2009 Section 3.7, Jordan and Flach 2013 Section 2.1). Figure 10-1 illustrates two examples for a degraded concrete using Or and Tuller (2000) estimates of fracture properties: 5 mil (127 μm) fractures spaced at 1 cm, and 50 mil (1.27 mm) fractures spaced at 10 cm. Unsaturated hydraulic conductivity is observed to fall below 1.0E-9 cm/s when capillary tension head exceed 200 to 500 cm.

Alternatively, a highly-permeable, coarse-grained material such as gravel can be used as a surrogate for a fracture network (Pruess 1998). Figure 10-2 is an example from Jordan and Flach (2013). Here conductivity falls below 1.0E-9 cm/s at about p_c = 700 cm. Either backfill material shown in Figure 4-2(a) could be adopted as a surrogate for a fracture network. The unsaturated hydraulic conductivity of these materials falls below 1.0E-9 cm/s in the 200 to 600 cm range. Flach et al. (2015) present estimated unsaturated hydraulic conductivity curves for fractured Saltstone (paste) specimens based on experimental measurements. These results are presented in Figure 10-3(a) and (b) depending on whether saturated conductivity was used as a fitting parameter. Unsaturated conductivity for the cracked specimens is estimated to fall below 1.0E-9 cm/s in the 200 to 500 cm range.

The above theoretical (Or and Tuller 2000), conceptual (Pruess (1998), granular materials as fracture surrogates) and experimental (Flach et al. 2015) results indicate that the hydraulic conductivity of a fractured grout will not exceed roughly 1.0E-9 cm/s under the expected post-closure exposure conditions (Section 4.3). That is, any cracks in SSW grout are expected to have minimal impact on unsaturated advective flow and solute transport, certainly compared to full or near saturation conditions.

Although the above analysis focused quantitatively on hydraulic conductivity, effective diffusion coefficient is expected to behave in a similar manner; that is, the same physical conditions leading to insignificant water transport through cracks are expected to also lead to insignificant solute diffusion. The concept underlying this statement is that when water films coating fracture faces become too thin to support significant advection, these films will likewise be too thin to support significant aqueous diffusion.

A more decisive conclusion can be reached by performing a quantitative analysis of diffusion coefficient variability with changing moisture conditions and appealing to surrogate materials. Rockhold et al. (2015, Table 4.3) define van Genuchten water retention parameters for densely fractured immobilized low-activity waste (ILAW) glass. Taking this fracture network as representative of potential cracking in SSW grout, one can estimate the moisture content of the fracture system at specified suction heads. For example, the moisture content of the fracture network at p_c = 0, 100, and 1000 cm is estimated to be 2% (equal to porosity), 0.57%, and 0.13% respectively. The latter water content corresponds to the tension head expected in the Hanford vadose zone as discussed in Section 4.3.

Rockhold et al. (2015, Section 5.2) summarize measurements of intrinsic diffusion coefficient by Conca and Wright (1990, 1991), and themselves using coarse sand samples acquired near the IDF site. Intrinsic diffusion coefficient for a wide variety of materials was observed to vary with moisture content following the power law expression

$$D_i = aD_m\theta^b \tag{90}$$

where D_m= 1.84e-5 cm^2/s, a = 1.49 and b = 1.96 (Rockhold et al. 2015, Figure 5.1).

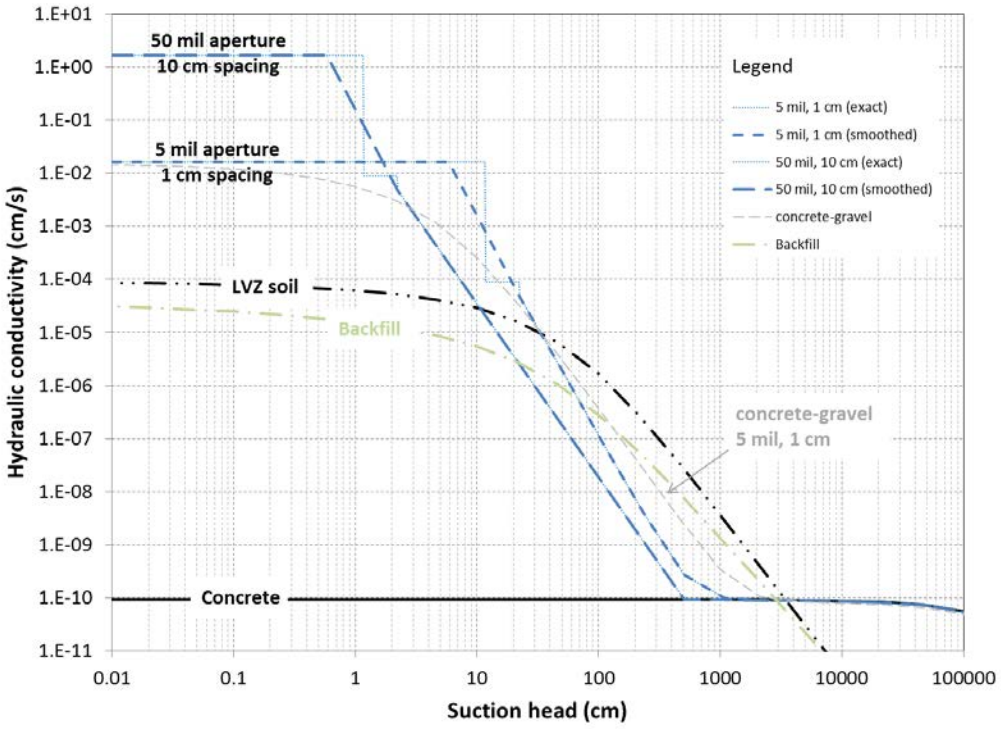

Figure 10-1. Hydraulic conductivity for two fracture-concrete blends based on Or and Tuller (2000); figure adapted from Jordan and Flach (2013, Figure 2-7).

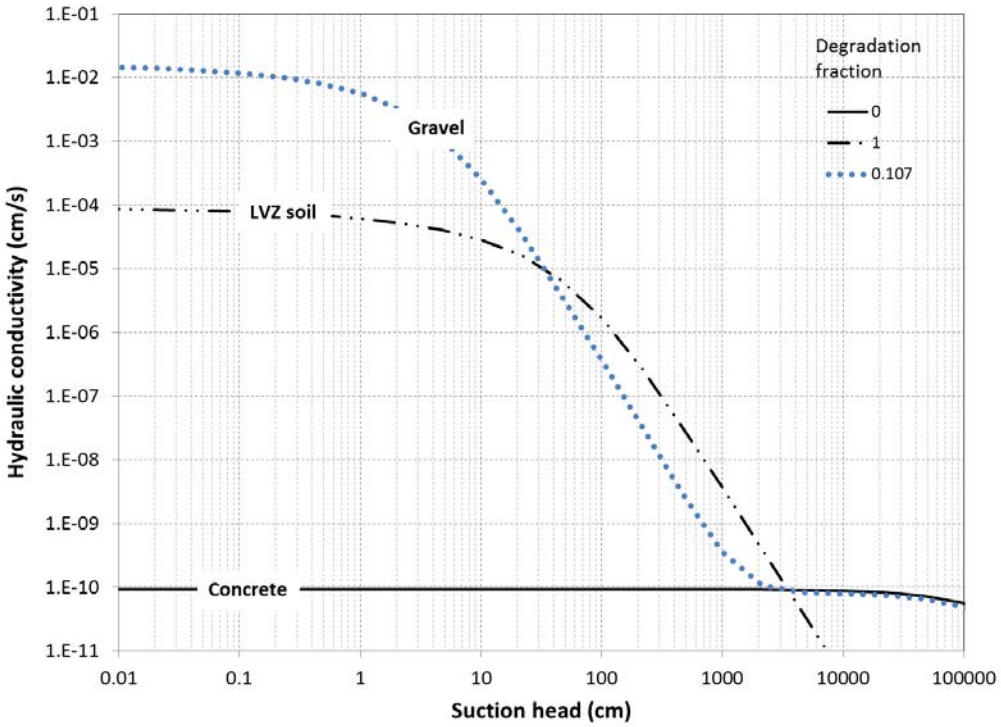

Figure 10-2. Hydraulic conductivity for a gravel-concrete blend; figure adapted from Jordan and Flach (2013, Figure 2-5).

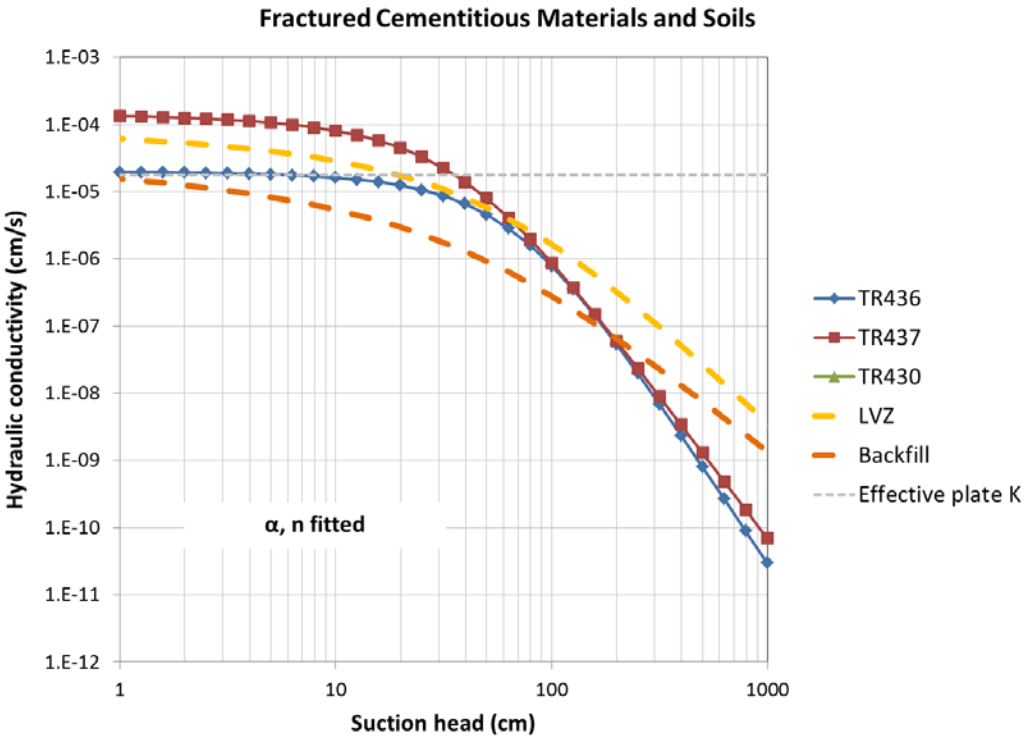

(a)

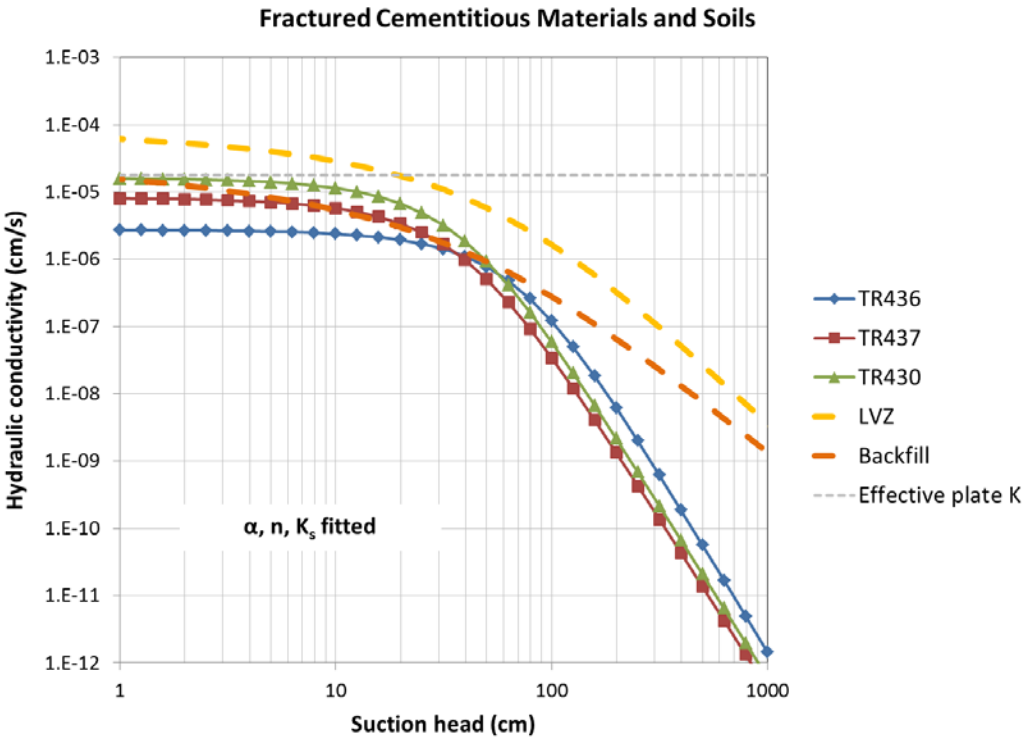

(b)

Figure 10-3. Measured unsaturated hydraulic conductivity for fractured Saltstone specimens; figures reproduced from Flach et al. (2015).

The effective diffusion coefficient of a saturated rough wall fracture network in SSW grout is assumed to be 5.0e-6 cm^2/s, the same as saturated Hanford gravel using Equation (90) and van Genuchten parameters from Table 4-1. Retaining D_m= 1.84e-5 cm^2/s and b = 1.96 and adjusting a to reflect lower tortuosity and constrictivity in the fracture network compared to granular materials yields

$$a_{fracture} = 11.6 \quad (91)$$

or

$$D_i = 2.14 \times 10^{-4}\theta^{1.96} \quad (92)$$

At the expected Hanford exposure condition of p_c = 1000 cm and θ = 0.13%, the result is

$$D_i = 4.7 \times 10^{-10}\ cm^2/s \quad (93)$$

compared to an intrinsic diffusion coefficient of approximately 10^{-8} cm^2/s for saturated grout (Equation (7) and Table 7-4). Thus the flux contribution from the fracture matrix is estimated to be more than an order of magnitude smaller than that of a saturated matrix at p_c = 1000 cm. At p_c = 100 cm however, the result is $D_i = 8.6 \times 10^{-9}$ cm^2/s (~10^{-8} cm^2/s), comparable to a saturated matrix.

Another point is reference is the behavior of gravels under low saturation conditions. Film flow over gravel surfaces is analogous to film flow over rough fracture faces. Conca and Wright (1990) stated that "volumetric water contents are expected to be between 0.5 and 2% in nonporous gravel in a vadose zone that is in equilibrium with a 100% humidity environment and that has no advective flow through gravel" and that an intrinsic “diffusion coefficient of 10^{-8} cm^2/s can be regarded as an upper limit to diffusion coefficients in gravel under these conditions". The expected IDF infiltration rate of 1 mm/yr (up to 3.5 mm/yr) is very low and approaches the “no advective flow” condition stipulated by Conca and Wright (1990).

With respect to hydraulic property and effective diffusion coefficient assignments, the above statements imply that the intact properties recommendation from Sections 6.0 and 7.0 will remain largely valid under physical degradation conditions, provided the capillary tension head in the subsurface exceeds approximately 1000 cm. However, it should also be noted that unsaturated cracks will enhance gas-phase transport, which could indirectly influence aqueous transport through altered Eh or pH conditions affecting sorption and/or solubility. Also note that at modestly lower capillary suctions, even p_c equal to a few hundred centimeters, a different conclusion is reached. Specifically, the effects of fractures are projected to be significant compared to an intact matrix under those conditions.

Considering the sensitivity of the above analyses to capillary tension, general uncertainty in the analysis methods, and appeals to analog behaviors rather than direct measurements, the conclusion that cracks will have little direct impact on aqueous transport for $p_c \geq$ 1000 cm should be considered tentative.

10.2 Assessment of potential physical degradation mechanisms

Pabalan et al. (2009 Section 4) present a recent and thorough review of potential degradation mechanisms relevant to radionuclide and chemical waste disposal in grouted systems. Chemical and physical mechanisms leading to physical damage are discussed separately below.

10.2.1 Chemical attack

Tables 4-4 and 4-5 in Pabalan et al. (2009) provide a qualitative indication of cementitious material susceptibility to chemical attack due to pH, carbon dioxide, magnesium, and sulfate exposure. The exposure concentrations identified in Section 4.3 of this report correspond to at most "Weak" or "Mild" susceptibility using their descriptive terms.

One means of chemical degradation is dissolution and leaching of the calcium-bearing minerals binding the cementitious material together, known as primary constituent leaching. The concentration of Ca^{2+} varies through the leaching process; alkali metals leach first, followed by $Ca(OH)_2$, and then CSH (Walton et al. 1990). In this assessment dissolution of CSH is assumed to control the concentration of Ca^{2+} over most of the leaching process, considering the relative abundance of CSH. CSH dissolves incongruently in that calcium leaches preferentially in comparison to silica. SIMCO (2012, Table 11) measured $[Ca^{2+}]$ = 1.8 - 2.0 mmol/L in a Savannah River Site concrete, which is similar to Clodic and Meike (1997, Table 15, Ca/Si = 0.9) with $[Ca^{2+}]$ = 1.1 - 1.8 mmol/L. At this low concentration (< 2.0E-6 mol/cm^3) and assuming diffusive transport, decalcification proceeds very slowly and is typically insignificant compared to other chemical degradation processes (e.g. Flach and Smith 2014). Cantrell et al. (2016) similarly concluded that "the IDF near-field Cast Stone leachate pH might be expected to remain caustic for millennia."

Carbonation and chloride ingress may not directly damage cementitious materials, but can lead to accelerated corrosion of reinforcing or other embedded steel. Steel corrosion products (rust) are expansive and can cause cracking or spalling in sufficient volume. SSW encapsulation and solidification grout is not expected to contain any steel near environmental exposure surfaces, assuming a minimum thickness of encapsulation grout on the order of 10 cm (4 inches). Furthermore, reactive transport simulations performed by Brown et al. (2013) indicate that a carbonation front effectively stops advancing after initial penetration due to dissolved calcium migrating to the reaction front from unreacted zones. Also, SSW grouts are expected to fully saturated once equilibrated with surrounding backfill. Carbonation via dissolved CO_2 transport alone is extremely slow (Flach and Smith 2014) and typically neglected outright (e.g. Papadakis et al. 1989). Chloride concentrations are low in Hanford vadose zone pore water (Table 4-2).

The rate of sulfate penetration into Saltstone Disposal Unit concrete was estimated by Flach and Smith (2014 Table 2-6) and Flach (2015 Table 4-4) to be approximately 0.02 cm/yr for an exposure concentration of 100 mmol/L. From Section 4.3 the sulfate concentration typical of Hanford vadose zone pore water is about 2 mmol/L, or 50 times lower, which suggests a prorated sulfate attack rate of roughly 0.0004 cm/yr. At this rate 10,000 years of exposure would result in a sulfate penetration depth of only 4 cm. Sulfate penetration does not necessary produce physical damage. Low sulfate exposure concentrations and high porosity in SSW paste materials may lead to no damage from sulfate ingress.

10.2.2 Deformation cracking

In general, deformation cracking of concrete can occur from stresses resulting from both environmental effects and applied short-term and/or long-term mechanical loading. In addition, the shape and size of the specimen affect the expression of the deformation. Examples of environmental conditions which result in stresses include:

1. moisture gain or loss, resulting in expansion or shrinkage, respectively
2. ingress of carbonate ions, which results in shrinkage
   (separate from potential influences of carbonation on embedded steel corrosion)
3. thermal cycling and gradients, and applied stresses
4. physical restraint

5. ingress of chemical species that result in formation of expansive phases (e.g. sulfate attack addressed above)

Each of the above mechanisms, along with damage from mechanical loading, is discussed further below.

Deformation related to moisture: The size and shape of the specimen will influence the rate of moisture loss and the degree of overall restraint provided by the central core, which will generally have higher moisture content than the surface regions. Non-uniform drying and shrinkage will result in differential strains and hence shrinkage-induced tensile stresses near the surface and compressive stresses in the center. Drying shrinkage can occur while the material is in the plastic state prior to setting and also after the material is rigid over more than one year. Drying shrinkage of concrete and grouts with fine aggregate is less than that of grouts without aggregate and Portland cement pastes because of the restraining influence of the aggregates (assuming the aggregates are dimensionally stable under changing moisture states).

Plastic shrinkage occurs when these materials are in the plastic prior to setting and results from mass loss due to evaporation of bleed water from the surface when the rate of water loss is faster than rate of replenishment by water migrating from the interior to the surface. Restraint of the mass by the interior will cause tensile strains in the near-surface region which in turn result in surface crazing/cracking. Depending on the evaporation rate or water loss rate, the nature of the hydrated phases, and the shape of the body, plastic settlement may also occur in pastes and waste forms if excessive water is lost, e.g. draining while the material is in the plastic state. Plastic settlement cracking is typically expressed as deep vertical cracks and sagging of the surface.

Drying also affects cured hydrated cement-based materials. Relative susceptibility of these materials to post-setting drying shrinkage and shrinkage cracking can be estimated based on measurements of the 105°C evaporable water loss of cured material which includes the free water, capillary water, and adsorbed water. The large surface area of the gel phase, which makes up a large portion of hydrated Portland cement materials, results in material that is sensitive to water. The water that can be lost by ambient drying is in the following types of voids in pastes and waste forms:

- The larger voids may only be partially filled with “free” water and water vapor in equilibrium with the relative humidity and temperature of the surrounding environment.
- Capillary pores smaller than about 50 nm and large gel pores wider than about 5 nm contain capillary water which is subject to capillary tension forces. Removal of this water at ambient temperatures and humidities may result in shrinkage.
- Water is also adsorbed onto solid surfaces in up to five molecular layers (about 1.3 nm). Most of this water can be lost on drying and the loss of this water is the main contributing factor to drying shrinkage.

Deformation related to carbonation: Carbonation shrinkage differs from drying shrinkage in that the material gains mass and is densified. Water is released when calcium hydroxide is dissolved from presumably more highly stressed regions resulting in shrinkage and calcium carbonate crystallizes in the pores. The strength is typically increased and the hydraulic conductivity decreased as the result of carbonation.

Deformation related to thermal expansion and thermal gradients: Cement pastes are waste forms that expand when heated. Stresses arise from thermal gradients generated during early hydration and curing and from overall dimensional changes in the material due to variations in ambient temperatures and

temperature gradients of cured material. These stresses can cause cracking and also water loss which can cause severe drying cracking.

Deformation related to restraint: Irregular restraint of the grout or concrete mass by randomly spaced objects will cause tensile strains in the near-field region and throughout the body of the material which in turn can result in cracking. This is typically associated with formation of hydrated phases in the matrix in relation to moisture gradients and resulting stresses.

Mechanical loading: SSW waste forms will be subjected to dynamic loading during disposal operations and cover system placement, and at least several meters of static overburden in the post-closure state. Differential settlement and/or seismic activity could also induce stresses during the post-closure period.

10.2.3 Overall assessment

SSW grout degradation from external chemical exposure appears to be a minimal concern (Section 10.2.1). Physical degradation mechanisms may be significant depending on the specific geometries of SSW waste forms and environmental exposure conditions (Section 10.2.2). However, the adverse effect of cracks is expected to be minimal from the perspective of moisture and solute transport (Section 10.1) for Hanford vadose zone conditions compared to higher saturations. However, cracks may lead to enhanced migration of oxygen and carbon dioxide into the waste form that could influence chemical properties (e.g., if reducing conditions are assumed in the waste form).

11.0 Discussion

This data package includes recommendations for physical and chemical input parameters to support the initial calculations for SSW for the 2017 IDF PA. At this time, a specific formulation has not been identified for cementitious materials that will be used to encapsulate or solidify SSW and no specific experiments were conducted to obtain data for the PA. The recommendations reflect existing information and represent a starting point on which to base the initial PA calculations.

Four key SSW streams were identified as the emphasis: HEPA filters, IX resins, Carbon Adsorber Beds, and Ag-mordenite. Compacted HEPA filters were considered as an encapsulated waste form and the other three key waste streams were assumed to be blended and solidified in a cementitious matrix. Recommended inputs were provided for the physical properties of the cured cementitious materials (e.g., Ks, bulk density, porosity, moisture characteristics), assumptions governing the release of contaminants of concern from the key waste streams, and properties associated with mass transport of the contaminants of concern through the cured cementitious materials (e.g., distribution coefficients, solubility, diffusion coefficients).

The recommendations were developed using available information for a variety of different mix formulations. When sufficient data were available, statistical distributions were developed to enable the full implementation of sensitivity and uncertainty analysis tools for the PA. If the data suggested different distributions depending on the mix (e.g., saturated hydraulic conductivity), a composite distribution and independent distributions were provided to represent the property for the different mixes, respectively. For cases with limited available information, recommendations were provided in the form of a central tendency and range of reasonably expected values.

The recommendations reflect uncertainty in the data on which they were based. The uncertainty includes measurement error, variability from sample to sample for a given mix, and variability across different mixes. Thus, the data package supports an evaluation of the expected performance for a variety of assumptions regarding the formulation that would be used. This provides a means to evaluate the performance for different mixes to aid in the identification of performance requirements to support the selection of an appropriate mix rather than implying at this stage that the PA represents an evaluation of a specific mix for each of the waste forms. Such an approach provides a means to iteratively establish an envelope of acceptable properties and identify key areas of uncertainty requiring further evaluation.

Emphasis was placed on physical properties of the cured samples. Based on conditions at the Hanford site, it is expected that the physical performance of the materials will remain relatively stable (from the perspective of water flow) for very long time frames. There is potential for cracking of the cementitious materials due to a variety of factors. However, the presence of cracks is not expected to significantly impact water flow for the low recharge rates and soil moisture content at the Hanford site, unless there is an increase in soil moisture content that would result in the cracks becoming a preferential pathway. Recommendations were provided to address the evolution of pore solutions and the associated transitions in the geochemical properties of the cementitious materials over time.

11.1 Recommended initial properties for specific IDF SSW grout formulations

The specific grout formulations that will be used to encapsulate and solidify SSW streams have not yet been defined (Section 3.1) but can be anticipated to fall within four broad categories: cement + fly ash paste, cement + fly ash + slag paste, cement + fly ash + aggregate mortar, and cement + fly ash + slag + aggregate mortar. The recommended initial hydraulic (Section 6.0), effective diffusional (Section 7.0) and geochemical (Section 8.0) properties for these four classes of potential SSW grouts are

1. OPC + FA paste
    a. hydraulic: "w/Slag, w/o Sand" paste (Table 6-2 and Table 6-3)
    b. effective diffusion: "Paste" (Table 7-4)
    c. geochemical: oxidizing conditions (multiple tables)
2. OPC + FA + BFS paste
    a. hydraulic: "w/Slag, w/o Sand" paste (Table 6-2 and Table 6-3)
    b. effective diffusion: "Paste" (Table 7-4)
    c. geochemical: reducing conditions (multiple tables)
3. OPC + FA + aggregate mortar
    a. hydraulic: "w/o Slag, w/ Sand" mortar (Table 6-2 and Table 6-4)
    b. effective diffusion: Mortar (Table 7-4)
    c. geochemical: oxidizing conditions (multiple tables)
4. OPC + FA + BFS + aggregate mortar
    a. hydraulic: "w/Slag, w/ Sand" mortar (Table 6-2 and Table 6-4)
    b. effective diffusion: Mortar (Table 7-4)
    c. geochemical: reducing conditions (multiple tables)

For example, "Grout mix 5" (American Rock Products "4257020") in current use at the Hanford site for disposals similar to anticipated SSW in the IDF is an OPC + FA paste; recommended properties for this grout are those listed under item 1. above.

A paste dry-mix may be used to solidify non-debris SSW (< 60 mm particle size), producing a cast material that is physically more similar to mortar than a pure paste, with non-debris particulates playing the role of sand. Mortar properties are considered more appropriate than paste properties for IDF PA modeling on this basis, and because mortar properties are assumed to be pessimistic. For any SSW debris waste within an encapsulation grout, we recommend taking no credit for resistance to advective or diffusive transport within the waste zone, because of uncertainty in the form and effective properties of the debris wastes that may be disposed. Generic soil properties could be assumed for the waste zone (e.g. D_e 5.0E-6 cm^2/s), so that the waste zone represents neither a barrier nor a conduit for moisture and solute transport relative to the backfill surrounding the waste form.

12.0 Recommendations

In the course of developing this data package, a number of knowledge gaps were identified. Primarily, as noted in Section 11, the material property recommendations were constrained by uncertainty in the formulations of cementitious materials that will be used for SSW encapsulation and solidification, and in several instances, limited published data / information from which to develop representative property values. There are also a number of physical and environmental processes that could influence the initial properties of the materials that need to be addressed.

In the near-term, we recommend documenting the waste forms and cementitious mix designs used for similar waste streams within the United States and internationally. A number of references were identified during the literature review for this data package that can serve as a starting point for this effort. This effort may constrain the range of formulations and disposal approaches that should be considered going forward into IDF material selection and characterization. In parallel, general recommendations need to be developed regarding desirable and undesirable attributes for a formulation given specific needs for the waste streams to be disposed at the IDF. Part of this effort would focus on identifying key challenges specific to the four waste streams that were the focus of this data package.

The desirable and undesirable attributes will also need to consider features, events and processes that could influence performance of the disposed waste form. Factors that could result in changes in the initial state of the waste form (e.g., redox, initial physical properties) that could compromise performance need to be identified and prioritized based on the conditions expected at IDF. A number of potential considerations have been identified that could influence the cementitious materials that will need to be addressed (e.g., initial saturation of a cured cementitious material, freeze-thaw, cellulose materials, microbial influences, impact of non-debris waste streams on the properties of a solidified cementitious waste form, controlling factors for release of Tc from a solidified waste form).

The result of the near-term activities will be to help support decisions regarding formulations to be recommended. In the longer-term, the selected formulations will then be tested for the properties of interest identified in this data package and to address key factors that could influence the properties. The priorities and level of refinement needed for testing for each of the different properties can be informed using initial sensitivity and uncertainty analysis results from the IDF PA modeling.

13.0 References

Alexander, R., Dayal, R., Eagleson, K., Eikenburg, J., Hamilton, E., Linklater, C., McKinley, I., and Tweed, C. (1992). A natural analogue of high pH cement pore waters from the Maqarin area of northern Jordan II: results of predictive geochemical calculations. *Jour. of Geochemical Exploration*, 46, 133-146.

Allard, B., Eliasson, L., Hoglund, S., and Andersson, K. (1984). "Sorption of Cs, I and Actinides in Concrete Systems," Rep. No. SKB/KBS Technical Report, SKB/KBS-TR 84-15 SKB, Stockholm, Sweden.

Almond, P. M., and Kaplan, D. I. (2011). "Distribution coefficients (K_d) Generated from a Core Sample Collected from the Saltstone Disposal Facility," Rep. No. SRNL-STI-2010-00667, Savannah River National Laboratory, Aiken, SC.

Almond, P. M., Kaplan, D. I., Langton, C. A., Stefanko, D. B., Spencer, W. A., Hatfield, A., and Arai, Y. (2012). "Method Evaluation and Field Sample Measurements for the Rate of Movement of the Oxidation Front in Saltstone," Rep. No. SRNL-STI-2012-00468, Savannah River National Laboratory, Aiken, SC.

American Concrete Institute. “Slag cement in concrete and mortar,” ACI 233R-03.

American Concrete Institute. “Guide to Curing Concrete,” ACI 308R-01.

Ampadu, K.O., K. Torii and M. Kawamura (1999). “Beneficial effect of fly ash on chloride diffusivity of hardened cement paste,” *Cement and Concrete Research* **29**, 585–590.

ANSI/ANS-16.1-2003. “Measurement of the leachability of solidified low-level radioactive wastes by a short-term test procedure,” Reaffirmed August 2008.

Arai, Y., and Powell, B. A. (2015). "Examination of Tc, S, and Fe Specation within Saltstone.," Rep. No. SRRA042328. Clemson University, Clemson, SC.

ASTM International. “Standard Practice for Making and Curing Concrete Test Specimens in the Laboratory,” C192/C192M − 16.

Atekwana EA, Werkema DD and Atekwana EA. (2006). “Biogeophysics: The effects of microbial processes on geophysical properties of the shallow subsurface,” Applied Hydrogeophysics, Chapter 6. *In Applied Hydrogeophysics*, Vereecken H, Binley A, Cassiani G, Revil A, Titov K. Eds. Springer: The Netherlands, 2006; 161-193.

Atkins, M., and Glasser, F. P. (1992). “Application of portland cement-based materials to radioactive waste immobilization,” *Waste Management* **12**, 105-131.

Atkinson, A., Everett, N., and Guppy, R. (1988). “Evolution of pH in a Radwaste Repository: Internal Reactions Between Concrete Constituents,” Rep. No. AERE-R12939. UKAEA, Harwell, UK.

Bajt, S., Clark, S. B., Sutton, R. S., Rivers, M. L., and Smith, J. V. (1993). “Synchrotron X-ray microprobe determination of chromate content using X-ray Absorption Near-Edge Structure,” *Analytical Chemistry* **65**, 1800-1804.

Baker, S., Baston, G. M. N., Manning, M. C., McCrohon, R., and Williams, S. (2000). "The Aqueous Solubility Behviour of Selenium, Technetium and Tin," Rep. No. AEAT/R/ENV/0233. AEA Technology, Harwell, Didcot UK.

Bannochie, C. J. (2015). "Results of Preliminary Hg Speciation Testing on 4Q14 Tank 50, 1Q15 Tank 50, and SRNL 14-day TCLP Leachate," Rep. No. SRNL-L3100-2015-00054 Rev 0. Savannah River National Laboratory, Aiken, SC.

Bayliss, S., McCrohon, R., Oliver, P., Pilkington, N. J., and Thomason, H. P. (1996). "Near-field Sorption Studies: January 1989 to June 1991," Rep. No. NSS/R277, AEA-ESD-0353.

Bayliss, S., Haworth, A., McCrohon, R., Moreton, A. D., Oliver, P., Pilkington, N. J., Smith, A. J., and Smith-Briggs, J. L. (1991). "Radioelement Behavior in a Cementitious Environment," *In* "Scientific Basis for Nuclear Management XV - Materials Research Society Symposium Proceedings" (C. G. Sombret, ed.), Vol. 257, pp. 641-648. Materials Research Society, Pittsburgh, PA.

Bechtel (2013). "Flowsheet Bases, Assumptions, and Requirements," 24590-WTP-RPT-PT-02-005, Rev. 7, Bechtel National Inc., Richland, WA.

Berner, U. R. (1992). "Evolution of Pore Water Chemistry during Degradation of Cement in a Radioactive Waste Repository Environment," *Waste Management* **12**, 201-215.

Bertos, M. F., Simons, S., Hills, C., and Carey, P. (2004). A review of accelerated carbonation technology in the treatment of cement-based materials and sequestration of CO 2. *Journal of Hazardous Materials* **112**, 193-205.

Bonavetti, V., H. Donza, V. Rahhal and E. Irassar (2000). "Influence of initial curing on the properties of concrete containing limestone blended cement," *Cement and Concrete Research* **30**, 703-708.

Bourbon, X., and Toulhoat, P. (1996). "Influence of Organic Degradtion Products on the Solubilisation of Radionuclides in INtermediate and Low Level Radioactive Wastes," *Radiochim. Acta* **74**, 315-319.

Brown, D. A., J. E. Dunn and B. Fuqua (1969). "Multiple-ion diffusion-I. Techniques for measuring and calculating apparent self-diffusion coefficients in heteroionic systems," *Clays and Clay Minerals* **17**, 271-277.

Brown, K. G., J. Arnold, S. Sarkar, G. Flach, H. van der Sloot, J.C.L. Meeussen and D. S. Kosson (2013). "Modeling Carbonation of High-Level Waste Tank Integrity and Closure," *EPJ Web of Conferences* **56**, 05003.

Burlion, N., F. Bourgeois and J.-F. Shao (2005). "Effects of desiccation on mechanical behavior of concrete," *Cement & Concrete Composites* **27**, 367-379.

Cantrell, K. J. (2015). "Secondary Waste Cementitious Waste Form Data Package for the Integrated Disposal Facility Performance Assessment," Rep. No. PNNL-24081, RPT-SWCS-002, Rev. 0. Pacific Northwest National Laboratory, Richland, WA.

Cantrell, K. J., J. H. Westsik, Jr., R. J. Serne, W. Um and A. D. Cozzi (2016). "Secondary Waste Cementitious Waste Form Data Package for the Integrated Disposal Facility Performance Assessment," Rep. No. PNNL-25194. Pacific Northwest National Laboratory, Richland, WA.

Cantrell, K. J., and Williams, B. D. (2012). "Equilibrium Solubility Model for Technetium Release from Saltstone Based on Anoxic Single-Pass Flow Through Experiments," Rep. No. PNNL-21723. Pacific Northwest National Laboratory, Richland, WA.

Chapman, K. W., Chupas, P. J., and Nenoff, T. M. (2010). "Radioactive iodine capture in silver-containing mordenites through nanoscale silver iodide formation," *Journal of the American Chemical Society* **132**, 8897-8899.

Chapman, N. A. and I.G. McKinley (1987). *The Geological Disposal of Nuclear Waste*, John Wiley & Sons, Chichester, UK.

Clodic, L. and A. Meike (1997). "Development of a Database to Model Concrete Dissolution at 25ºC Using the EQ3/6 Geochemical Modeling Code," Rep. No. UCRL-ID-132088. Lawrence Livermore National Laboratory, Livermore , CA.

Conca, J. L and J. Wright (1990). "Diffusion Coefficients in Gravel Under Unsaturated Conditions," *Water Resources Research* **26**, 1055-1066.

Conca, J. L and J. Wright (1991). "Aqueous Diffusion Coefficient in Unsaturated Materials," *Mat. Res. Soc. Symp. Proc.* **212**.

Coombs, P., Wagner D., Bateman K., Harrison H., Milodowski A.E., Noy D., and West J.M. (2010). "The role of biofilms in subsurface transport processes," *Quarterly Journal of Engineering Geology and Hydrogeology* 43, 131-139.

Cozzi, A. D. and B. R. Pickenheim (2012). "Impact of Standing Bleed Water on Saltstone Placement," Rep. No. SRNL-STI-2012-00546 Rev. 0. Savannah River National Laboratory, Aiken, SC.

Crank, J. (1975). *The mathematics of diffusion*. Second edition. Clarendon Press, Oxford.

Crawford, R.J., Webb, H.K., Truong, V.K., Hasan, J., and Ivanova E.P. (2012). "Surface topographical factors influencing bacterial attachment," *Advances in Colloid and Interface Science* 179-182: 142-149.

Criscenti, L., Serne, R., Krupka, K., and Wood, M. (1996). "Predictive calculations to assess the long-term effect of cementitious materials on the pH and solubility of uranium (VI) in a shallow land disposal environment," Rep. No. PNNL-1182. Pacific Northwest National Laboratory, Richland, WA.

Cronstrand, P., and Power, S. (2005). "Assessment of Uncertainty Intervals for Sorption Coefficients," Rep. No. R-05-75. Swedish Nuclear Fuel and Waste Management Company, Stockholm, Sweden.

Dayal, R., Johnston, H., and Zhou, Z. (1989). "Reactor Operating Waste Disposal Program, 1989 Progress Report," Rep. No. 89-226-K, Ontario Hydroelectic, Ltd., Ontario Canada.

Delagrave, A., J. Marchand, and M. Pigeon (1998). "Influence of Microstructure on the Tritiated Water Diffusivity of Mortars," *Advn. Cem. Bas. Mat.* **7**, 60-65.

Denham, M. E. (2007). "Conceptual model of waste release from the contaminated zone of closed radioactive waste tanks," Rep. No. WSRC-STI-2007-00544, Savannah River National Laboratory, Aiken, SC.

Denham, M. E., and Millings, M. R. (2012). "Evolution of chemical conditions and estimated solubility controls on radionuclides in the residual waste layer during post-closure ageing of High-Level Waste Tanks," Rep. No. SRNL-STI-2012-00404. Savannah River National Laboratory, Aiken, SC.

Dixon. K., J. Harbour and M. Phifer (2008). "Hydraulic and Physical Properties of Saltstone Grouts and Vault Concretes," Rep. No. SRNL-STI-2008-00421, Rev. 0. Savannah River National Laboratory, Aiken, SC.

Dixon. K., J. Harbour and M. Phifer (2010). "Hydraulic and Physical Properties of ARP/MCU Saltstone Grout," Rep. No. SRNL-STI-2009-00419, Rev. 0. Savannah River National Laboratory, Aiken, SC.

Dixon, K. and M. Phifer (2007a). "Hydraulic and Physical Properties of Tank Grouts and Base Mat Surrogate Concrete for FTF Closure," Rep. No. WSRC-STI-2007-00369, Rev. 0. Savannah River National Laboratory, Aiken, SC.

Dixon, K. and M. Phifer (2007b). "Cementitious Material Selection for Future Component-In-Grout Waste Disposals," Rep. No. WSRC-STI-2007-00207, Revision 0. Savannah River National Laboratory, Aiken, SC.

Dixon, K. and M. Phifer (2008). "Hydraulic and Physical Properties of MCU Saltstone," Rep. No. WSRC-STI-2007-00649, Revision 0. Savannah River National Laboratory, Aiken, SC.

Durner, W. (1994). "Hydraulic conductivity estimation for soils with heterogeneous pore structure," *Water Resour. Res.* **30**, 211–233.

Dong, H., Kukkadapu, R. K., Fredrickson, J. K., Zachara, J. M., Kennedy, D. W., and Kostandarithes, H. M. (2003). "Microbial reduction of structural Fe (III) in illite and goethite," *Environmental Science & Technology* **37**, 1268-1276.

EPA-1315. *Mass transfer rates of constituents in monolithic or compacted granular materials using a semi-dynamic tank leaching procedure*, U. S. Environmental Protection Agency.

Estes, S. L., Kaplan, D. I., and Powell, B. A. (2012). "Technetium sorption by cementitious materials under reducing conditions," Rep. No. SRNL-STI-2012-00596. Savannah River National Laboratory, Aiken, SC.

Evans, N. (2008). "Binding mechanisms of radionuclides to cement," *Cement and Concrete Research* **38**, 543-553.

Fiskum, S. K., Arm, S. T., Steele, M. J., and Thorson, M. R. (2008). "Spherical Resorcinol-Formaldehyde Performance Testing with Hanford Tank Waste," *Solvent Extraction and Ion Exchange* **26**, 435-452.

Flach, G. P. (2009). "Approximate solutions for diffusional release from saltstone vaults," Rep. No. SRNL-STI-2009-00114, Rev. 0. Savannah River National Laboratory, Aiken, SC.

Flach, G. P. (2015). "Verification of Sulfate Attack Penetration Rates for Saltstone Disposal Unit Modeling," Rep. No. SRNL-STI-2015-00236, Revision 0. Savannah River National Laboratory, Aiken, SC.

Flach, G., K. Dixon and R. Nichols (2015). "Characterization of Unsaturated Hydraulic Conductivity in Fractured Media Using the Multistep Outflow Method – 15461," *WM2015 Conference*, March 15 – 19.

Flach, G. P., J. M. Jordan and T. Whiteside. (2009). "Numerical flow and transport simulations supporting the saltstone disposal facility performance assessment," Rep. No. SRNL-STI-2009-00115, Rev. 1. Savannah River National Laboratory, Aiken, SC.

Flach, G. P. and F. G. Smith, III. (2014). "Degradation Of Cementitious Materials Associated with Saltstone Disposal Units," Rep. No. SRNL-STI-2013-00118, Rev. 2. Savannah River National Laboratory, Aiken, SC.

Fredlund, D. G. and H. Rahardjo (1993). *Soils Mechanics for Unsaturated Soils*. John Wiley, New York.

Fredrickson, J. K., Zachara, J. M., Kennedy, D. W., Kukkadapu, R. K., McKinley, J. P., Heald, S. M., Liu, C., and Plymale, A. E. (2004). "Reduction of TcO_4^- by sediment-associated biogenic Fe(II)," *Geochimica et Cosmochimica Acta* **68**, 3171-3187.

Ginn, T.R., Camesano, T., Scheibe, T.D., Nelson, K.E., Clement, T.P. and Wood, B.D. (2005). "Microbial transport in the subsurface," *In* Anderson MG. (Ed.), *Encyclopedia of Hydrological Sciences.* 2005, 1603-1626.

Glaus, M. A., Loon, L. R. V., Achatz, S., Chodura, A., and Fischer, K. (1999). "Degradation of Cellulosic Materials Under the Alkaline Conditions of a Cementitious Disposal Facility for Low and Intermediate Level Radioactive Waste, Part I: Identification of Degradation Products," *Analytica Chimica Acta* **398**, 111-122.

Golovich, E. C., L. J. Powers, S. V. Mattigod, G. A. Whyatt, M. M. V. Snyder and D. M. Wellman (2014). "Radionuclide Migration through Sediment and Concrete: 16 Years of Investigations," Rep. No. PNNL-23841. Pacific Northwest National Laboratory, Richland, WA.

Gougar, M., Scheetz, B., and Roy, D. (1996). "Ettringite and C-S-H Portland cement phases for waste ion immobilization: A review," *Waste Management* **16**, 295-303.

Grandy, A. S., and Neff, J. C. (2008). "Molecular C dynamics downstream: The biochemical decomposition sequence and its impact on soil organic matter structure and function," *Science of The Total Environment* **404**, 297-307.

Guneyisi, E., T. Ozturan and M. Gesoglu (2007). "Effect of initial curing on chloride ingress and corrosion resistance characteristics of concretes made with plain and blended cements," *Building and Environment* **42**, 2676-2685.

Gupta, S., Dubikova, M., French, D., and Sahajwalla, V. (2007). "Effect of CO_2 gasification on the transformation of coke minerals at high temperatures," *Energy & Fuels* **21**, 1052-1061.

Hall, C. and W. Hoff (2002). *Water Transport in Brick, Stone and Concrete*. Spon Press, New York.

Harbour, J. R., Hansen, E. K., Edwards, T. B., Williams, V. J., Eibling, R. E., Best, D. R., and Missimer, D. M. (2006). "Characterization of slag, fly ash and portland cement for saltstone," Rep. No. WSRC-TR-2006-00067, Savannah River National Laboratory, Aiken, SC.

Harfouche, M., Wieland, E., Dähn, R., Fujita, T., Tits, J., Kunz, D., and Tsukamoto, M. (2006). "EXAFS study of U (VI) uptake by calcium silicate hydrates," *Journal of Colloid and Interface Science* **303**, 195-204.

Henderson, A. D., and Demond, A. H. (2007). "Long-term performance of zero-valent iron permeable reactive barriers: a critical review," *Environmental Engineering Science* **24**, 401-423.

Hietanen, R., Kamarainen, E.-L., and Aluusua, M. (1984). "Sorption of Cesium, Strontium, Iodine, Nickel and Carbon in Concrete," Rep. No. YJT--84-04. Nuclear Waste Commission of Finnish Power Companies, Helsinki, Finland.

Hinsinger, P., Plassard, C., Tang, C., and Jaillard, B. (2003). "Origins of root-mediated pH changes in the rhizosphere and their responses to environmental constraints: a review," *Plant and soil* **248**, 43-59.

Hoitink, D. J., K. W. Burk, J. V. Ramsdell, Jr. and W. J. Shaw (2005). "Hanford Site Climatological Summary 2004 with Historical Data," Rep. No. PNNL-15160. Pacific Northwest National Laboratory, Richland, WA.

Hoskins, J. S., Karanfil, T., and Serkiz, S. M. (2002). "Removal and sequestration of iodide using silver-impregnated activated carbon," *Environmental Science & Technology* **36**, 784-789.

Humphreys, P., West, J., and Metcalfe, R. (2010). "Microbial effects on repository performance," Rep. No. http://eprints.hud.ac.uk/7613/. University of Huddersfield, Harwell, Didcot, Oxfordshire, UK.

Icenhower, J. P., Qafoku, N. P., Zachara, J. M., and Martin, W. J. (2010). "The biogeochemistry of technetium: A review of the behavior of an artificial element in the natural environment," *American Journal of Science* **310**, 721-752.

Ismail, M., A. Toumi, R. Francois and R. Gagne (2004). "Effect of crack opening on the local diffusion coefficient of chloride in inert materials," *Cement and Concrete Research* **34**. 711-716.

Ismail, M., A. Toumi, R. François and R. Gagné (2008). "Effect of crack opening on the local diffusion of chloride in cracked mortar samples," *Cement and Concrete Research* **38**, 1106–1111.

Jakob, A., Sarott, F.-A., and Spieler, P. (1999). "Diffusion and Sorption on Hardened Cement Pastes-Experiments and Modelling Results," Rep. No. NTB 99-06. Paul Scherrer Institut, Villigen, Switzerland.

Jenkins, K. D., Chen, R. C., Gimpel, R., Deng, Y., Gross, M. R., and Peredo, C. (2013). "Flowsheet Bases, Assumptions, and Requirements," Rep. No. DE-AC27-01RV14136. Bechtel, Richland, WA.

Johnston, H. M. and D. J. Wilmot (1992). "Sorption and diffusion studies in cementitious grouts," *Waste Management* **12**, 103-297.

Jordan, J. M. and G. P. Flach (2013). "PORFLOW Modeling Supporting the FY13 Saltstone Special Analysis," Rep. No. SRNL-STI-2013-00280, Rev. 0. Savannah River National Laboratory, Aiken, SC.

Jubin, R., Bruffey, S., and Patton, K. (2014). "Expanded Analysis of Hot Isostatic Pressed Iodine-Loaded Silver-Exchanged Mordenite," Rep. No. FCRD-SWF-2014-000278, ORN L/LTR-2014/476. Oak Ridge National Laboratory, Oak Ridge, TN.

Kaplan, D. I. (2010). "Geochemical Data Package for Performance Assessment Calculations Related to the Savannah River Site," Rep. No. SRNL-STI-2009-00473. Savannah River National Laboratory, Aiken, SC.

Kaplan, D. I. (2016). "Geochemical Data Package for Performance Assessment Calculations Related to the Savannah River Site," Rep. No. SRNL-STI-2009-00473, Rev 1. Savannah River National Laboratory, Aiken, SC.

Kaplan, D. I., and Coates, J. (2007). "Partitioning of Dissolved Radionuclides to Concrete Under Scenarios Appropriate for Tank Closure Performance Assessments," Rep. No. WSRC-STI-2007-00640. Savannah River National Laboratory, Aiken, SC.

Kaplan, D. I., and Hang, T. (2003). "Estimated Duration of the Subsurface Reducing Environment Produced by the Z-Area Saltstone Disposal Facility," Rep. No. WSRC-RP-2003-00362, Rev. 2. Westinghouse Savannah River Company, Aiken, SC.

Kaplan, D. I., and Serkiz, S. M. (2000). "^{129}Iodine Desorption from Resin, Activated Carbon, and Filtercake Waste Generated from the F- and H-Area Water Treatment Units," Rep. No. WSRC-TR-2000-00308. Westinghouse Savannah River Company, Aiken, SC.

Kaplan, D. I., and Serkiz, S. M. (2004). "Influence of Dissolved Organic Carbon and pH on Contaminant Sorption to Sediment," Rep. No. WSRC-RP-2004-00593, Westinghouse Savannah River Company, Aiken, SC.

Kaplan, D. I., and Serkiz, S. M. (2006). "Influence of Dissolved Organic Carbon and pH on Iodide, Perrhenate, and Selenate Sorption to Sediment," Rep. No. WSRC-STI-2006-00037, Washington Savannah River Company, Aiken, SC.

Kaplan, D. I., Lilley, M. S., Almond, P. M., and Powell, B. A. (2011). "Long-term Technetium Interactions with Reducing Cementitious Materials," Rep. No. SRNL-STI-2011-00668, Savannah River National Laboratory, Aiken, SC.

Kaplan, D. I., Mattigod, S. V., Parker, K., and Iversen, G. (2000). "I-129 Test and Research to Support Disposal Decisions," Rep. No. WSRC-TR-2000-00283, Savannah River National Laboratory, Aiken, SC.

Kaplan, D. I., Roberts, K., Coates, J., Siegfried, M., and Serkiz, S. (2008). "Saltstone and concrete interactions with radionuclides: Sorption (K_d), desorption, and reduction capacity measurements," Rep. No. SRNS-STI-2008-00045, Savannah River National Laboratory, Aiken, SC.

Kaplan, D. I., Serkiz, S. M., and Bell, N. C. (1999). "I-129 Desorption from SRS Water Treatment Media From the Effluent Treatment Facility and the F-Area Groundwater Treatment Facility," Rep. No. WSRC-TR-99-00270. Westinghouse Savannah River Company, Aiken, SC.

Kaplan, D., Hang, T., and Aleman, S. (2005). "Estimated duration of the reduction capacity within a high-level waste tank." Rep. No. WSRC-RP-2005-01674, Revision 0. Washington Savannah River Company, Aiken, SC.

Kazy, S.F., Sar, P. and D'Souza, Sf. (2008). "Studies on uranium removal by the extracellular polysaccharide of a *Pseudomonas aeruginosa* strain," *Bioremediation Journal* **12**, 47-57.

Kindness, A., Macias, A., and Glasser, F. (1994). "Immobilization of chromium in cement matrices," *Waste Management* **14**, 3-11.

Krupka, K. M., and Serne, R. J. (1998). "Effects on Radionuclide Concentrations by Cement/Ground-water Interactions in Support of Performance Assessment of Low-level Radioactive Waste Disposal Facilities," Rep. No. NUREG/CR-6377, PNNL-11408.

Krupka, K. M., Kaplan, D. I., Whelan, G., Serne, R. J., and Mattigod, S. V. (1999). "Understanding variation in partition coefficient, K_d, values. Volume II: Review of geochemistry and available K_d values for cadmium, cesium, chromium, lead, plutonium, radon, strontium, thorium, tritium (^3H), and uranium," Rep. No. EPA 402-R-99-004. USEPA, Washington, DC.

Krupka, K. M., Serne, R. J., and Kaplan, D. I. (2004). "Geochemical Data Package for the 2005 Hanford Integrated Disposal Facility Performance Assessment," Rep. No. PNNL-13037, Rev. 2. Pacific Northwest National Laboratory, Richland, WA.

Langton, C. A. (1986). "Reduced technetium leaching in slag - Class F fly ash saltstone formulations," Rep. No. DPST-86-551. Savannah River National Laboratory, Aiken, SC.

Langton, C. A. (1987a). "Reduced chromium leaching in slag-based saltstone formulations," Rep. No. DPST-86-863. Savannah River National Laboratory, Aiken, SC.

Langton, C. A. (1987b). "Physical properties of slag saltstone," Rep. No. DPST-87-673. Savannah River National Laboratory, Aiken, SC.

Langton, C. A. (1988). "Slag-based saltstone formulations," *Mat. Res. Soc. Symp. Proc.* **112**.

Langton, C. A., Almond, P. M., Stefanko, D. B., Miller, D. H., Healy, D. P., and Minichan, R. L. (2014). "Comparison of depth Discrete Oxidation Front Results and Reduction Capacity Measurements for Cementitious Waste Forms," Waste Management WM14, Phoenix, AZ.

Langton, C. A. and P. B. Wong (1991). "Properties of slag concrete for low-level waste containment (U)," Rep. No. WSRC-MS-91-073. Savannah River National Laboratory, Aiken, SC.

Last, G. V., Snyder, M. M. V., Um, W., Stephenson, J. R., Leavy, I. I., Strickland, C. E., Bacon, D. H., Qafoku, N. P., and Serne, R. J. (2015). "Technetium, Iodine, and Chromium Adsorption/Desorption K_d Values for Vadose Zone Pore Water, ILAW Glass, and Cast Stone Leachates Contacting an IDF Sand Sequence," Rep. No. PNNL-24683. Pacific Northwest National Laboratory, Richland, WA.

Lee, K. P. (2015). "Cementitious Waste Form Modeling Summary for the 2017 Integrated Disposal Facility Performance Assessment," Rep. No. RPP-ENV-58738. Washington River Protection Solutions, Hanford, WA.

Lee, W., and Batchelor, B. (2003). "Reductive capacity of natural reductants," *Environmental Science & Technology* **37**, 535-541.

Lehman, L. L., R. W. Andrews and K. P. Lee (2015). "Integrated Disposal Facility 2017 Performance Assessment Modeling Approach," Rep. No. RPP-ENV-58554. Washington River Protection Solutions, Hanford, WA.

Li, D., and Kaplan, D. I. (2012). "Literature review on the sorption of plutonium, uranium, neptunium, americium and technetium to corrosion products on waste tank liners," Rep. No. SRNL-STI-2012-00040, Savannah River National Laboratory, Aiken, SC.

Lilley, M. S., Powell, B. A., and Kaplan, D. I. (2009). "Iodine, neptunium, plutonium, and technetium sorption to saltstone and cement formulations under oxidizing and reducing conditions," Rep. No. SRNL-STI-2009-00636, Savannah River National Laboratory, Aiken, SC.

Lockrem LL, GA Cooke, and M Johnson (2003). "Cast Stone Technology for Treatment and Disposal of Iodine-Rich Caustic Waste Demonstration Test Plan," Rep. No. RPP-18853, Revision 0, CH2M Hill Hanford Group, Inc., Richland, Washington.

Lockrem, L. L., Cooke, G. A., Clark, B. A., and West, R. (2005). "Cast Stone Technology for Treatment and Disposal of Iodine-Rich Caustic Waste Demonstration-Final Report," Rep. No. RPP-RPT-26725 Revision 0. CH2M Hill Hanford Group, Inc, Richland, WA.

Lukens, W. W., Bucher, J. J., Shuh, D. K., and Edelstein, N. M. (2005). "Evolution of technetium speciation in reducing grout," *Environmental Science & Technology* **39**, 8064-8070.

Macias, A., Kindness, A., and Glasser, F. P. (1997). "Impact of Carbon Dioxide on the Immobilization Potential of Cemented Wastes: Chromium," *Cement & Concrete Research* **27**, 25-225.

Mandel, J. (1964). *The Statistical Analysis of Experimental Data*. John Wiley & Sons. New York. p. 85-93.

McConnell, J. R. D. Rogers, I. L. Larsen, J. D. Jastrow, W. E. Sanford, T. M. Sullivan, and M. Fuhrmann (1997). "Field Lysimeter Investigations: Low Level Waste Database Development Program for Fiscal Year 1996," NUREG/CR-5229, Vol. 9, Idaho National Engineering Laboratory, Idaho Falls, ID.

Meena, A. H., Kaplan, D. I., Powell, B. A., and Arai, Y. (2015). "Chemical stabilization of chromate in blast furnace slag mixed cementitious materials," *Chemosphere* **128**, 247-252.

Meyer, P. D. and R. J. Serne (1999). "Near-Field Hydrology Data Package for the Immobilized Low-Activity Waste 2001 Performance Assessment," Rep. No. PNNL-13035. Pacific Northwest National Laboratory, Richland, WA.

Misson, J., Henner, P., Morello, M., Floriani, M., Wu, T.-D., Guerquin-Kern, J.-L., and Février, L. (2009). "Use of phosphate to avoid uranium toxicity in Arabidopsis thaliana leads to alterations of morphological and physiological responses regulated by phosphate availability," *Environmental and Experimental Botany* **67**, 353-362.

MMES (Martin Marietta Energy Systems, I., EG&G Idaho, Inc., Westinghouse Hanford Company, and Westinghouse Savannah River Company) (1992). "Radiological Performance Assessment for the Z-Area Saltstone Disposal Facility," Rep. No. WSRC-RP-92-1360. Westinghouse Savannah River Company, Aiken, South Carolina.

Molz, F., Demirkanli, D. I., Thompson, S., Kaplan, D. I., and Powell, B. A. (2015). "Plutonium transport in soil and plants: An interdisciplinary study motivated by lysimeter experiments at the Savannah River Site. *In* "Fluid Dynamics in Complex Fractured-Porous Systems" (B. Faybishenko, S. M. Benson and J. E. Gale, eds.), pp. 183-208. John Wiley & Sons, Inc., Hoboken, New Jersey.

Mualem, Y. (1976). "A new model for predicting the hydraulic conductivity of unsaturated porous media," *Water Resour. Res.* **12**, 513–522. doi:10.1029/WR012i003p00513.

Muszer, A. (2006). "Petrographical and mineralogical characteristics of the metallurgical slag from the Dorschl Furnace (Glocow Foundry, Poland)," *Pysicochemical Problems of Mineral Processing* **40**, 89-98.

Myers, G. E. (1971). *Analytical Methods in Conduction Heat Transfer*. McGraw-Hill, New York.

Napier, B. A. (2005). "Soil and Groundwater Sample Characterization and Agricultural Practices for Assessing Food Chain Pathways in Biosphere Models," Rep. No. NUREG/CR-6881, PNNL-15244.

Nimmo, J. R., J. A. Deason, J. A. Izbicki and P. Martin. 2002. "Evaluation of unsaturated zone water fluxes in heterogeneous alluvium at a Mojave Basin Site," *Water Resources Research* **38**, 1215. doi:10.1029/2001WR000735.

NRC (2000). "A Performance Assessment Methodology for Low-Level Radioactive Waste Disposal Facilities. Recommendations of NRC's Performance Assessment Working Group," NUREG-1573, Division of Waste Management, Office of Nuclear Material Safety and Safeguards, U.S. Nuclear Regulatory Commission, Washington, DC.

Oblath, S. B. (1986). "Leach test of 107 liter saltstone blocks at Brookhaven National Laboratory," Rep. No. DPST-86-442. Savannah River National Laboratory, Aiken, SC.

Oblath, S. B. (1989). "Leaching from Solidified Waste Forms under Saturated and Unsaturated Conditions," *Environ. Sci. Technol.* **23**, 1098-1102.

Ochs, M., Mallants, D., and Wang, L. (2016). "Sorption Values for Americium" *In* "Radionuclide and Metal Sorption on Cement and Concrete," pp. 171-182. Springer.

Or, D. and M. Tuller (2000). "Flow in unsaturated fractured porous media: Hydraulic conductivity of rough surfaces," *Water Resources Research* **36**, 1165-1177.

Ozer, B. and M. H. Ozkul (2004). "The influence of initial water curing on the strength development of ordinary portland and pozzolanic cement concretes," *Cement and Concrete Research* **34**, 13-18.

Pabalan, R., Glasser, F., Pickett, D., Walter, G., Biswas, S., Juckett, M., Sabido, L., and Myers, J. (2009). "Review of Literature and Assessment of Factors Relevant to Performance of Grouted Systems for Radioactive Waste Disposal," Rep. No. CNWRA 2009-001. Center for Nuclear Waste Regulatory Analyses, San Antonio, TX.

Papadakis, V. G., C. G. Vayenas, and M. N. Fardis. (1989). "A Reaction Engineering Approach to the Problem of Concrete Carbonation," *AIChE Journal* **35**, 1639-1650.

Parrott, L. J. (1987). "A Review of Carbonation in Reinforced Concrete," Cement and Concrete Association, Buckinghamshire, U.K.

Patton, K., Bruffey, S., Jubin, J., and Walker Jr, J. (2014). "Iodine Loading of NO Aged Silver Exchanged Mordenite," Rep. No. FCRD-SW F-2014-000277, ORNL/LTR-2014/425. Oak Ridge National Laboratory, Oak Ridge, TN.

Phifer, M. A., M. R. Millings and G. P. Flach (2006). "Hydraulic property data package for the e-area and z-area soils, cementitious materials, and waste zones," Rep. No. WSRC-STI-2006-00198 Revision 0. Savannah River National Laboratory, Aiken, SC.

Pierce, E. M., Cantrell, K. J., Westsik, J. H., Parker, K. E., Um, W., Valenta, M. M., and Serne, R. J. (2010). "Secondary Waste Form Screening Test Results: Cast Stone and Alkali Alumino-silicate Geopolymer," Rep. No. PNNL-19505. Pacific Northwest National Laboratory, Richland, WA.

Pierce, E. M., K. M. Krupk, B. P. McGrail, P. F. Martin, E. A. Rodriguez, S. R. Baum, H. T. Schaef, K. N. Geiszler, K. P. Saripalli, L. R. Reed, R. J. Serne, W. J. Shaw (2004). "Waste Form Release Data Package for the 2005 Integrated Disposal Facility Performance." Rep. No. PNNL-14805. Pacific Northwest National Laboratory, Richland, WA.

Pierce, E. M., Mattigod, S. V., Westsik, J. H., Serne, R. J., Icenhower, J. P., Scheele, R. D., Um, W., and Qafoku, N. (2010). "Review of Potential Candidate Stabilization Technologies for Liquid and Solid Secondary Waste Streams," Rep. No. PNNL-19122. Pacific Northwest National Laboratory, Richland, WA.

Pinkston, K. E., Ridge, A. C., Alexander, G. W., Barr, C. S., Devaser, N. J., and Felsher, H. D. (2013). NRC Monitoring of Salt Waste Disposal at the Savannah River Site–13147. WM Symposia, Tempe, AZ.

Pointeau, I., Coreau, N., and Reiller, P. E. (2008). "Uptake of anionic radionuclides onto degraded cement pastes and competing effect of organic ligands," *Radiochimica Acta* **96**, 367-374.

Pointeau, I., Landesman, C., Giffaut, E., and Reiller, P. (2004). "Reproducibility of the uptake of U (VI) onto degraded cement pastes and calcium silicate hydrate phases," *Radiochimica Acta* **92**, 645-650.

Polettini, A., and Pomi, R. (2003). "Modelling heavy metal and anion effects on physical and mechanical properties of Portland cement by means of factorial experiments," *Environmental Technology* **24**, 231-239.

Pollock J, Weber KA, Lack J, Achenbach LA, Mormille MR, Coates JD. (2007). "Alkaline iron (III) reduction by a novel alkaliphilic, halotolerant, *Bacillus sp.* isolated from salt flat sediments of Soap Lake," *Applied Microbial and Cell Physiology* 77: 927-934.

Prindiville, K. A. (2016). "Inventory Data Package for the Integrated Disposal Facility Performance Assessment." Rep. No. RPP-ENV-58562. Washington River Protection Solutions, Hanford, WA.

Pruess, K. 1998. “On water seepage and fast preferential flow in heterogeneous, unsaturated rock fractures,” *Journal of Contaminant Hydrology* **30**, 333–362.

Rai, D., Sass, B. M., and Moore, D. A. (1987). “Chromium(III) Hydrolysis Constants and Solubility of Chromium(III) Hydroxide,” *Inorganic Chemistry* **26**, 345-349.

Rao, L., Zanonato, P. L., and Bernardo, P. D. (2005). “Interaction of Actinides with Carboxylates in Solution,” *Journal of Nuclear and Radiochemical Sciences* **6**, 31-37.

Razzell, W. (1990). “Chemical fixation, solidification of hazardous waste,” *Waste Management & Research* **8**, 105-111.

Reardon, E. J. (1992). Problems and Approaches to the Prediction of the Chemical Composition in Cement/Water Systems. *Waste Management* **12**, 221-231.

Reigel, M. M., and Hill, K. A. (2016). “Results and Analysis of Saltstone Coress Taken from Saltstone Disposal Unit Cell 2A,” Rep. No. SRNL-STI-2016-00106. Savannah River National Labortory, Aiken, SC.

Reigel, M. M., B. R. Pickenheim and W. E. Daniel (2012). “Process Formulations and Curing Conditions that Affect Saltstone Properties,” Rep. No. SRNL-STI-2012-00558 Rev. 0. Savannah River National Labortory, Aiken, SC.

Richards, B. G. (1965). “Measurement of free energy of soil moisture by the psychrometric technique using thermistors,” *In* “Moisture Equilibria and Moisture Changes in Soils Beneath Covered Areas: A Symposium,” 39-46, Butterworths, Australia.

Richards, L.A. (1931). “Capillary conduction of liquids through porous mediums,” Physics **1,** 318–333.

Rizoulis, A., Steele, H.M., Morris, K. and Lloyd, J.R. (2012). “The potential impact of anaerobic microbial metabolism during the geological disposal of intermediate-level waste,” *Mineralogical Magazine* **76**, 3261-3270.

Roberts, K. A., and Kaplan, D. I. (2009). “Reduction Capacity of Saltstone and Saltstone Components,” Rep. No. SRNL-STI-2009-00637, Rev 0, Savannah River National Laboratory, Aiken, SC.

Rockhold, M. L., M. J. Fayer and P. R. Heller (1993). “Physical and Hydraulic Properties of Sediments and Engineered Materials Associated with Grouted Double-Shell Tank Waste Disposal at Hanford,” Rep. No. PNL-8813. Pacific National Laboratory, Richland, WA.

Rockhold, M. L., Z. F. Zhang, P. D. Meyer and J. N. Thomle (2015). “Physical, Hydraulic, and Transport Properties of Sediments and Engineered Materials Associated with Hanford Immobilized Low-Activity Waste,” Rep. No. PNNL-23711, RPT-IGTP-004, Rev. 0. Pacific National Laboratory, Richland, WA.

Rumynin, V. G., Konosavsky, P. K., and Hoehn, E. (2005). “Experimental and modeling study of adsorption-desorption processes with application to a deep-well injection radioactive waste disposal site,” *Journal of Contaminant Hydrology* **76**, 19-46.

Sahmaran, M. and I. O. Yaman. 2008. “Influence of transverse crack width on reinforcement corrosion initiation and propagation in mortar beams,” *Canadian Journal of Civil Engineering* **35**, 236-245.

Samson, E., P. Henocq, J. Marchand (2009). *Chemical degradation review*. DOE-EM Cementitious Barrier Partnership report Rep. No. CBP-TR-2009-002-C4, Rev. 0. Simco Technologies Inc., Quebec, Canada.

Sarott, F. A., Bradbury, M. H., Pandolfo, P., and Spieler, P. (1992). “Diffusion and Adsorption Studies on Hardened Cement Paste and the Effect of Carbonation on Diffusion Rates,” *Cement Concr. Res* **22**, 439-444.

Savannah River Remediation LLC (2009). “Performance Assessment for the Saltstone Disposal Facility at the Savannah River Site,” Rep. No. SRR-CWDA-2009-00017 Rev. 0. Aiken, SC.

Savannah River Remediation LLC (2013). “FY2013 Special Analysis for the Saltstone Disposal Facility at the Savannah River Site,” Rep. No. SRR-CWDA-2013-00062, Rev. 2, Savannah River Remediation, Aiken, SC.

Savannah River Remediation LLC (2014). “FY2014 Saltstone Core-Drilling Mock-Up Summary,” Rep. No. SRR-CWDA-2014-00059 Rev. 0. Aiken, SC.

Savannah River Remediation LLC (2015). “Savannah River Site Liquid Waste Facilities Performance Assessment Maintenance Program,” Rep. No. SRR-CWDA-2015-00152 Rev. 0. Aiken, SC.

Scheele, R. D., Burger, L. L., and Matsuzaki, C. L. (1983). “Methyl Iodide Sorption by Reduced Silver Mordenite,” Rep. No. PNL-4489S. Pacific National Laboratory, Richland, WA.

Scheele, R., Wend, C., Buchmiller, W., Kozelisky, A., and Sell, R. (2002). “Preliminary Evaluation of Spent Silver Mordenite Disposal Forms Resulting from Gaseous Radioiodine Control at Hanford’s Waste Treatment Plant,” Rep. No. PNWD-3225, WTP-RPT-039. Pacific Northwest National Laboratory, Richland, WA.

Seaman, J. C. (2015). “Chemical and Physical Properties of ^{99}Tc-Spiked Saltstone as Impacted by Curing Duration and Leaching Atmosphere,” Rep. No. SREL DOC No. R-15-0003. Savannah River Ecology Laboratory, Aiken, SC.

Seitz, R. R. and J. C. Walton (1993). “Modeling Approaches for Concrete Barriers Used in Low-Level Waste Disposal,” Rep. No. NUREG/CR-6070, Idaho National Engineering Laboratory, Idaho Falls, ID.

Serne, R. J., Lokken, R. O., and Criscenti, L. J. (1993). “Characterization of Grouted Low-Level Waste to Support Performance Assessment,” *Waste Management* **12**, 271-287.

Serne, R. J., A. V. Mitroshkov, J. N. Serne, B. N. Bjornstad, V. L. LeGore, G. V. Last, H. T. Schaef, M. J. O’Hara, S. C. Smith, B. A. Williams, C. F. Brown, C. W. Lindenmeier, D. C. Lanigan, K. E. Parker, J. M. Zachara, D. G. Horton, I. V. Kutnyakov, D. B. Burke, R. E. Clayton (2002). “Characterization of Vadose Zone Sediment: Uncontaminated RCRA Borehole Core Samples and Composite Samples,” Rep. No. PNNL-13757-1. Pacific Northwest National Laboratory, Richland, WA.

Serne, R. J., Westsik, J. H., Williams, B. D., Jung, H., and Wang, G. (2015). "Extended Leach Testing of Simulated LAW Cast Stone Monoliths," Rep. No. PNNL-24297, RPT-SLAW-001, Rev. 0. Pacific Northwest National Laboratory, Richland, WA.

Shafiq, N. and J. G. Cabrera (2004). "Effects of initial curing condition on the fluid transport properties in OPC and fly ash blended cement concrete," *Cement and Concrete Research* **26**, 381-387.

Shuh, D. K., Edelstein, N. M., Burns, C. J., Lukens, W. W., Bucher, J. J., Fickes, M. G., and Scott, B. L. (2000). "Research Program to Investigate the Fundamental Chemistry of Technetium," Rep. No. EMSP-60296, Lawrence Berkeley National Laboratory, Berkeley, CA.

SIMCO Technologies Inc. (2010). "Task 6 – Characterization of a Wasteform Mixture," Report for Washington Savannah River Company, Subcontract no. AC48992N," Simco Technologies Inc., Quebec, Canada.

SIMCO Technologies Inc. (2012). "Washington Savannah River Company Subcontract AC81850N Report – Vault Concrete Characterization," SIMCO Technologies Inc., Quebec, Canada.

Sinclair, A. J. (1976). *Applications of Probability Graphs in Mineral Exploration. Vol 4*. The Association of Exploration Geochemists. Vancouver, Canada.

Smith, R. W., and Walton, J. C. (1993). "The role of oxygen diffusion in the release of technetium from reducing cementitious waste forms," *Mat. Res. Soc. Symp. Proc.* **294**, 247-253.

Smith, S. L., Rizoulis, A., West, J. M., and Lloyd, J. (2015). "The microbial ecology of a hyper-alkaline spring, and impacts of an alkali-tolerant community during sandstone batch and column experiments representative of a geological disposal facility for intermediate level radioactive waste," *Geomicrobiology Journal*.

Smith, S. L. Rizoulis, A., West, J. M. and Lloyd, J.R. (2016). "The microbial ecology of a hyper-alkaline spring, and impacts of an alkali-tolerant community during Sandstone batch and column experiments representative of a geological disposal facility for Intermediate-Level radioactive waste," *Geomicrobiology Journal*, DOI:10.1080 /01490451.2015.1049677.

SRNS (2013). "Savannah River Site Environmental Report for 2013," Rep. No. SRNS-STI-2014-00006. Savannah River Nuclear Solutions, LLC, Savannah River Site, Aiken SC 29808.

Stefanko, D. B. and C. A. Langton (2011). "Tanks 18 and 19-F Structural Flowable Grout Fill Material Evaluation and Recommendations," Rep. No. SRNL-STI-2011-00551 Rev. 0. Savannah River National Laboratory, Aiken, SC.

Stroes-Gascoyne, S. and West, J.M. (1996). "An overview of microbial research related to high-level nuclear waste disposal with emphasis on the Canadian concept for the disposal of nuclear fuel waste," *Canadian Journal of Microbiology* 42: 349-366.

Stumm, W., and Morgan, J. J. (2012). *Aquatic chemistry: chemical equilibria and rates in natural waters*, John Wiley & Sons.

Sugiyama, D., and Fujita, T. (1999). “Sorption of radionuclides onto cement materials altered by hydrothermal reaction,” *In* “MRS Proceedings” **556**, 1123. Cambridge Univ Press.

Surasani, V.K., Li, L., Ajo-Franklin, J.B., Hubbard, C., Hubbard, S.S, and Wu Y. (2013). “Bioclogging and permeability alteration by *L. mesenteroides* in a sandstone reservoir: a reactive transport modelling study,” *Energy & Fuels* **27**: 6538-6551.

Svensson, M., Allard, B., and Düker, A. (2006). “Formation of HgS—mixing HgO or elemental Hg with S, FeS or FeS 2,” *Science of The Total Environment* **368**, 418-423.

Svensson, M., and Allard, B. (2007). “Diffusion tests of mercury through concrete, bentonite-enhanced sand and sand,” *Journal of Hazardous Materials* **142**, 463-467.

Svensson, M., and Allard, B. (2008). “Leaching of mercury-containing cement monoliths aged for one year,” *Waste Management* **28**, 597-603.

Termkhajornkit, P., T. Nawa and K. Kurumisawa (2006). “Effect of water curing conditions in the hydration degree and compressive strengths of fly ash-cement paste,” *Cement & Concrete Composites* **28**, 781-789.

Thornton, E. C. (1997). “Origin of increased sulfate in groundwater at the ETF disposal site,” Rep. No. PNNL-11633 / UC-502. Pacific National Laboratory, Richland, WA.

Thorson, M. R. (2008). "Basis of Recommendation for Use of Spherical Resorcinol Formaldehyde Resin as the Primary Cesium Ion Exchange Resin in the WTP," Rep. No. 24590-WTP-RPT-RT-07-005, Rev 0. River Protection Project, Waste Treatment Plant, Richland, WA.

Tits, J., Fujita, T., Tsukamoto, M., and Wieland, E. (2008). “Uranium (VI) uptake by synthetic calcium silicate hydrates,” *In* "MRS Proceedings" **1107**, 467. Cambridge Univ Press.

Tits, J., Wieland, E., Dobler, J.-P., and Kunz, D. (2003). “The uptake of strontium by calcium silicate hydrates under high pH conditions: an experimental approach to distinguish adsorption from co-precipitation processes,” *In* "MRS Proceedings" **807**, A101. Cambridge Univ Press.

Tits, J., Wieland, E., Müller, C., Landesman, C., and Bradbury, M. (2006). “Strontium binding by calcium silicate hydrates,” *Journal of Colloid and Interface Science* **300**, 78-87.

Um, W., Jung, H. B., Wang, G., Westsik, J. H., and Peterson, R. A. (2013). “Characterization of Technetium Speciation in Cast Stone,” Rep. No. PNNL-22977. Pacific Northwest National Laboratory.

Um, W., Valenta, M. M., Chung, C.-W., Yang, J., Engelhard, M. H., Serne, R. J., Parker, K. E., Wang, G., Cantrell, K. J., and Westsik Jr, J. (2011). “Radionuclide Retention Mechanisms in Secondary Waste-form Testing: Phase II,” Rep. No. PNNL-20753. Pacific Northwest National Laboratory, Richland, WA.

Um, W., Williams, B. D., Snyder, M. M. V., and Wang, G. (2016). “Liquid Secondary Waste Grout Formulation and Waste Form Qualification,” Rep. No. RPT-SWCS-005, Rev A. Pacific Northwest National Laboratory, Richland, WA.

Um, W., Yang, J.-S., Serne, R. J., and Westsik, J. H. (2015). "Reductive Capacity Measurement of Waste Forms for Seconday Radioactive Wastes," *Journal of Nuclear Materials* **467**, 251-259.

Valocchi, A. J. (1985). "Validity of the local equilibrium assumption for modeling sorbing solute transport through homogeneous soils," *Water Resources Research* **21**, 808-820.

Valsami-Jones, E., and Ragnarsdöttir, K. Y. (1997). "Solubility of Uranium Oxide and Calcium Uranate in Water, and Ca (OH) 2-bearing Solutions," *Radiochimica Acta* **79**, 249-258.

van Genuchten, M. T. (1980). "A closed-form equation for predicting the hydraulic conductivity of unsaturated soils," *Soil Science Society America Journal* **44**, 892-898.

VanLoon, L. R., and Glaus, M. A. (1998). "Experimental and Theoretical Studies on Alkaline Degradation of Cellulose and its Impact on the Sorption of Radionuclides," Rep. No. PSI Berisht 98-07. Paul Scherrer Institute, Villigen, Switzerland.

Wada, K. (1985). "The distinctive properties of Andosols," *In* "Advances in soil science", 173-229. Springer.

Walpole, R. E. and R. H. Myers. (1978). *Probability and statistics for engineers and scientists; 2nd edition*. MacMillan, New York.

Walton, J. C. (1992). "Performance of intact and partially degraded concrete barriers in limiting mass transport," Rep. No. NUREG/CR-5445. Nuclear Regulatory Commission, Washington, DC.

Walton, J. C., L. E. Plansky, and R. W. Smith (1990). "Models for Estimation of Service Life of Concrete Barriers in Low-Level Radioactive Waste Disposal," Rep. No. NUREG/CR-5542. Nuclear Regulatory Commission, Washington, DC.

Wang, D., Jin, Y., and Jaisi, D. P. (2015). "Effect of Size Selective Retention on the Cotransport of Hydroxyapatite and Goethite Nanoparticles in Saturated Porous Media," *Environmental Science & Technology*.

Wang, L., Martens, E., Jacques, D., Decanniere, P., Berry, J., and Mallants, D. (2009). "Review of sorption values for the cementitious near field of a near surface radioactive waste disposal facility," Rep. No. NIRAS-MP5-03/NIROND-TR-2008-23E. ONDRAF/NIRAS, Mol, Brussels.

Wang, J. S. Y., and T. N. Narasimhan (1985). "Hydrologic Mechanisms Governing Fluid Flow in a Partially Saturated, Fractured, Porous Medium," *Water Resources Research* **21**, 1861-1874.

Wang, K., D. C. Jansen, S. P. Shah and A. F. Karr (1997). "Permeability study of cracked concrete," *Cement and Concrete Research* **27**. 381-393.

Waste Management Federal Services of Hanford, Inc. (1998). "Specification for Concrete Encasement for Contact-Handled Category 3 Waste," HNF-1981 Rev. 0.

Wellman, D. M., Mattigod, S. V., Arey, B. W., Wood, M. I., and Forrester, S. W. (2007). "Experimental limitations regarding the formation and characterization of uranium-mineral phases in concrete waste forms," *Cement and Concrete Research* **37**, 151-160.

West, J. M., Coombs, P., Gardner, S .J. and Rochelle, C. A. (1995). "The microbiology of the Maqarin site, Jordan – a natural analogue for cementitious radioactive waste repositories," *Materials Research Society Symposium Proceedings* **353**, 181-188.

West, J. M., McKinley, I. G. and Bateman, K. (2008). "The microbiology of redox processes – development of a redox model," British Geological Survey Open Report OR/08/076.

West, J. M., McKinley, I. G., and Stroes-Gascoyne, S. (2009). "Implications of microbial redox catalysis in analogue systems for repository safety cases," *In* "ASME 2009 12th International Conference on Environmental Remediation and Radioactive Waste Management", pp. 833-838. American Society of Mechanical Engineers.

West, J., McKinley, I., and Bateman, K. (2008). "The microbiology of redox processes: development of a redox model," Rep. No. Open Report OR/08/076. British Geological Survey, Keyworth, Nottingham.

Westsik Jr, J., Cantrell, K. J., Serne, R. J., and Qafoku, N. (2014). "Technetium Immobilization Forms Literature Survey," Rep. No. PNNL-23329, EMSP-RPT-023. Pacific Northwest National Laboratory, Richland, WA.

Westsik, J. H., Piepel, G. F., Lindberg, M. J., Heasler, P. G., Mercier, T. M., Russell, R. L., Cozzi, A., Daniel, W. E., Eibling, R. E., and Hansen, E. (2013). "Supplemental Immobilization of Hanford Low-Activity Waste: Cast Stone Screening Tests," Pacific Northwest National Laboratory, Richland, WA.

Wieland, E., and Van Loon, L. R. (2003). "Cementitious Near-Field Sorption Data Base for Performance Assessment of an ILW Repository in Opalinus Clay," Rep. No. PSI Bericht 03-06. Paul Scherrer Institut, Villigen, Switzerland.

Wieland, E., Tits, J., Kunz, D., and Dähn, R. (2007). "Strontium uptake by cementitious materials," *Environmental Science & Technology* **42**, 403-409.

Wilson, L. G. (1980). "Monitoring in the vadose zone: A review of technical elements and methods," Rep. No. EPA-600/7-80-134. Environmental Protection Agency, Washington, DC.

WRPS (2009). "Hanford Tank Waste Operations Simulator (HTWOS) Model Design Description," Rep. No. RPP-17152, Rev. 1, Washington River Protection Solutions, LLC/AEM Consulting LLC, Richland, WA.

WRPS (2015). "Hanford Tank Waste Operations Simulator (HTWOS) Version 8.1 Design Description," Rep. No. RPP-17152, Rev. 12, Washington River Protection Solutions, LLC/AEM Consulting LLC, Richland, WA.

Yabusaki, S. B., G. Wang, R. J. Serne, J. H. Westsik, Jr. and M. L. Rockhold (2015). "Technical Approach for Determining Key Parameters Needed for Modeling the Performance of Cast Stone for the Integrated Disposal Facility Performance Assessment," Rep. No. PNNL-24022, RPT-SWCS-001, Rev. 0. Pacific Northwest National Laboratory, Richland, WA.

Yonkofski, A. J. (2015). "Description of the Natural System for the Integrated Disposal Facility Performance Assessment," Rep. No. RPP-ENV-58427 Rev. 0.

Zainoun, K., Puziewicz, J., and Bril, H. (2003). “Primary Pb-Zn-bearing phases in pytometallurgical slag from Swietochlowice (Upper Silesia, Poland),” *Mineralogical Society of Poland - Special Papers* **23**.

Zurmuhl, T. and W. Durner. (1998). “Determination of Parameters for Bimodal Hydraulic Functions by Inverse Modeling,” *Soil Sci. Soc. Am. J.* **62**, 874–880.

Appendix A. Hydraulic and physical property data

Mix #	Dry bulk Density, gm/cm^3	Water Exchangeable Porosity	Saturated Hydraulic Conductivity, cm/s	Reference
1	1.79	0.269	2.80E-08	Dixon and Phifer, 2007a
1	1.78	0.277	2.50E-08	Dixon and Phifer, 2007a
1	1.78	0.265	2.90E-08	Dixon and Phifer, 2007a
1	1.8	0.275	9.40E-09	Dixon and Phifer, 2007a
1	1.81	0.268	6.80E-09	Dixon and Phifer, 2007a
1	1.81	0.257	2.70E-08	Dixon and Phifer, 2007a
2	1.86	0.219	1.00E-08	Dixon and Phifer, 2007a
2	1.81	0.275	8.50E-08	Dixon and Phifer, 2007a
2	1.81	0.275	1.00E-08	Dixon and Phifer, 2007a
2	1.8	0.271	5.20E-08	Dixon and Phifer, 2007a
2	1.8	0.278	4.30E-08	Dixon and Phifer, 2007a
2	1.81	0.277	1.70E-08	Dixon and Phifer, 2007a
3	1.84	0.19	8.20E-09	Dixon and Phifer, 2007a
3	1.88	0.25	9.50E-09	Dixon and Phifer, 2007a
4	1.82	0.23	1.00E-08	Dixon and Phifer, 2007a
4	1.86	0.25	1.50E-08	Dixon and Phifer, 2007a
4	1.86	0.24	1.40E-08	Dixon and Phifer, 2007a
4	1.85	0.24	1.30E-08	Dixon and Phifer, 2007a
5	2.06	0.186	6.30E-09	Dixon and Phifer, 2007a
5	1.94	0.214	5.50E-09	Dixon and Phifer, 2007a
5	1.92	0.225	6.60E-09	Dixon and Phifer, 2007a
5	1.94	0.211	8.10E-09	Dixon and Phifer, 2007a
12	2.14	0.15	1.60E-08	Dixon and Phifer, 2007a
12	2.01	0.17	3.10E-08	Dixon and Phifer, 2007a
12	2.05	0.19	6.00E-08	Dixon and Phifer, 2007a
12	2.04	0.16	3.30E-08	Dixon and Phifer, 2007a
6	2.03	0.115	6.70E-08	Dixon and Phifer, 2007b
6	2.04	0.129	7.90E-08	Dixon and Phifer, 2007b
6	2.02	0.126	2.90E-08	Dixon and Phifer, 2007b
6	2.03	0.134	6.70E-08	Dixon and Phifer, 2007b
6	2	0.118	5.30E-08	Dixon and Phifer, 2007b
6	2.08	0.128	1.10E-08	Dixon and Phifer, 2007b
7	2.09	0.145	8.90E-08	Dixon and Phifer, 2007b
7	2.1	0.154	3.10E-08	Dixon and Phifer, 2007b
7	2.04	0.147	9.30E-08	Dixon and Phifer, 2007b
7	2.02	0.171	1.50E-08	Dixon and Phifer, 2007b
7	2.13	0.136	1.90E-07	Dixon and Phifer, 2007b
7	2.07	0.173	2.60E-08	Dixon and Phifer, 2007b

Mix #	Dry bulk Density, gm/cm^3	Water Exchangeable Porosity	Saturated Hydraulic Conductivity, cm/s	Reference
8	1.99	0.153	7.20E-08	Dixon and Phifer, 2007b
8	2.03	0.168	1.70E-08	Dixon and Phifer, 2007b
8	2.02	0.153	6.20E-08	Dixon and Phifer, 2007b
8	1.99	0.216	1.50E-08	Dixon and Phifer, 2007b
8	2.01	0.137	1.70E-08	Dixon and Phifer, 2007b
8	2.04	0.175	3.20E-08	Dixon and Phifer, 2007b
9	1.92	0.21	2.30E-08	Dixon and Phifer, 2007b
9	1.91	0.245	3.60E-08	Dixon and Phifer, 2007b
9	1.93	0.205	1.20E-08	Dixon and Phifer, 2007b
9	1.92	0.232	1.80E-08	Dixon and Phifer, 2007b
9	1.91	0.205	6.50E-08	Dixon and Phifer, 2007b
9	1.93	0.236	4.50E-09	Dixon and Phifer, 2007b
9a	1.9	0.235	9.60E-09	Dixon and Phifer, 2007b
9a	1.86	0.233	9.70E-09	Dixon and Phifer, 2007b
9a	1.9	0.237	9.60E-09	Dixon and Phifer, 2007b
9a	1.93	0.229	1.10E-08	Dixon and Phifer, 2007b
9a	1.9	0.234	6.70E-09	Dixon and Phifer, 2007b
9a	1.92	0.229	7.20E-09	Dixon and Phifer, 2007b
10	1.82	0.241	1.93E-08	Dixon and Phifer, 2006
10	1.87	0.205	2.60E-08	Dixon and Phifer, 2006
10	1.87	0.236	8.40E-05	Dixon and Phifer, 2006
10	1.86	0.216	4.80E-05	Dixon and Phifer, 2006
10	1.77	0.233	1.25E-06	Dixon and Phifer, 2006
10	1.83	0.213	1.38E-04	Dixon and Phifer, 2006
10	1.56	0.4	2.30E-04	Dixon and Phifer, 2006
10	1.85	0.28	4.30E-04	Dixon and Phifer, 2006
10	1.98	0.23	1.90E-06	Dixon and Phifer, 2006
11		na	3.42E-06	Dixon and Phifer, 2006
11			1.40E-06	Dixon and Phifer, 2006
11	1.85	0.31	1.90E-06	Dixon and Phifer, 2006
13			2.10E-09	Stafanko and Langton, 2011
13	1.97	0.21	3.10E-10	Stafanko and Langton, 2011
14	1.98	0.21	3.50E-10	Stafanko and Langton, 2011
15	1.04	0.56	1.40E-08	Dixon et al., 2008
15	1.05	0.56	5.90E-10	Dixon et al., 2008
15	1.04	0.56	2.00E-09	Dixon et al., 2008
15	1.05	0.55	1.11E-09	Dixon et al., 2008
15	1.08	0.57	7.20E-11	Dixon et al., 2008
15	1.06	0.56	1.10E-10	Dixon et al., 2008

Mix #	Dry bulk Density, gm/cm^3	Water Exchangeable Porosity	Saturated Hydraulic Conductivity, cm/s	Reference
16	0.98	0.58	5.40E-09	Dixon et al., 2008
16	0.98	0.58	2.10E-09	Dixon et al., 2008
16	0.98	0.58	2.70E-10	Dixon et al., 2008
16	0.95	0.59	1.10E-09	Dixon et al., 2008
16	0.96	0.6	8.80E-10	Dixon et al., 2008
16	0.97	0.61	6.40E-10	Dixon et al., 2008
17	1.01	0.58	1.20E-08	Dixon et al., 2008
17	1	0.59	3.40E-08	Dixon et al., 2008
17	1.02	0.6	2.00E-09	Dixon et al., 2008
17	1	0.59	1.20E-09	Dixon et al., 2008
17	1.01	0.58	2.00E-09	Dixon et al., 2008
17	1	0.59	8.80E-08	Dixon et al., 2008
20	0.98	0.6	5.30E-09	Dixon and Phifer, 2007c
21	1.32		3.60E-09	Joyce, 2016
21	1.32		2.70E-09	Joyce, 2016
21	1.32		5.60E-09	Joyce, 2016
22	1.26		3.40E-09	Joyce, 2016
22	1.27		3.00E-09	Joyce, 2016
22	1.27		6.50E-09	Joyce, 2016
22	1.35		2.40E-09	Arthur, 2015
22	1.37		1.50E-09	Arthur, 2015
23	1.07		5.52E-09	Rockhold et al., 1994
23	1.12		1.10E-08	Rockhold et al., 1994
23	1.11		5.22E-08	Rockhold et al., 1994
24	1.072	0.578	2.30E-09	Dixon et al., 2010
24	1.07	0.576	1.10E-09	Dixon et al., 2010
24	1.077	0.578	2.40E-09	Dixon et al., 2010
16	0.964	0.64	1.20E-09	Dixon et al., 2010
16	0.958	0.635	9.90E-09	Dixon et al., 2010
16	0.963	0.633	8.80E-09	Dixon et al., 2010
16	0.95	0.636	9.60E-09	Dixon et al., 2010
16	0.951	0.637	2.10E-09	Dixon et al., 2010
16	0.951	0.637	1.10E-09	Dixon et al., 2010

This page intentionally left blank

Appendix B. Plots of water retention curve data and subsequent van Genuchten curves for various paste and mortar mixes.

The following figures illustrate the experimental data underlying the water retention curves shown in Figure 6-5 , from which the recommended mortar and paste curves in Figure 6-6 are derived. Table 6-1 provides a key to the mix identifiers and source references, from which these Appendix B figures were reproduced.

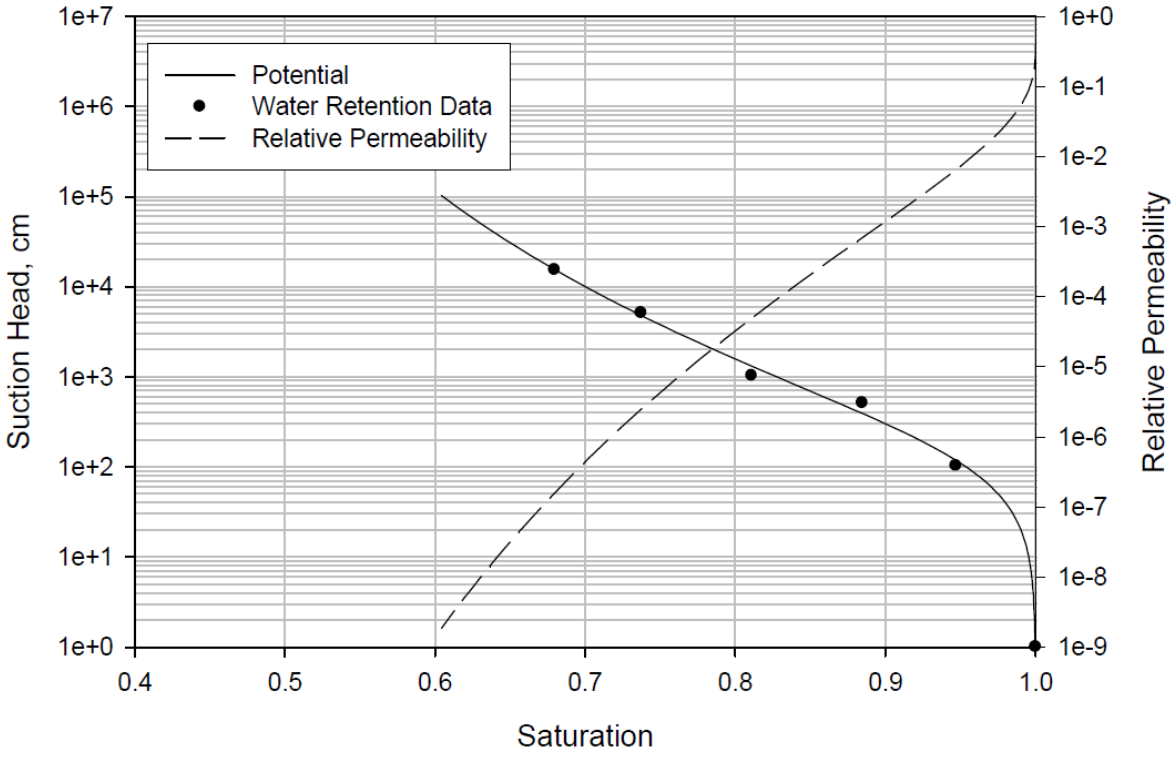

Figure B-1. WCR data and subsequent van Genuchten curve for Mix 3 Sample 1.

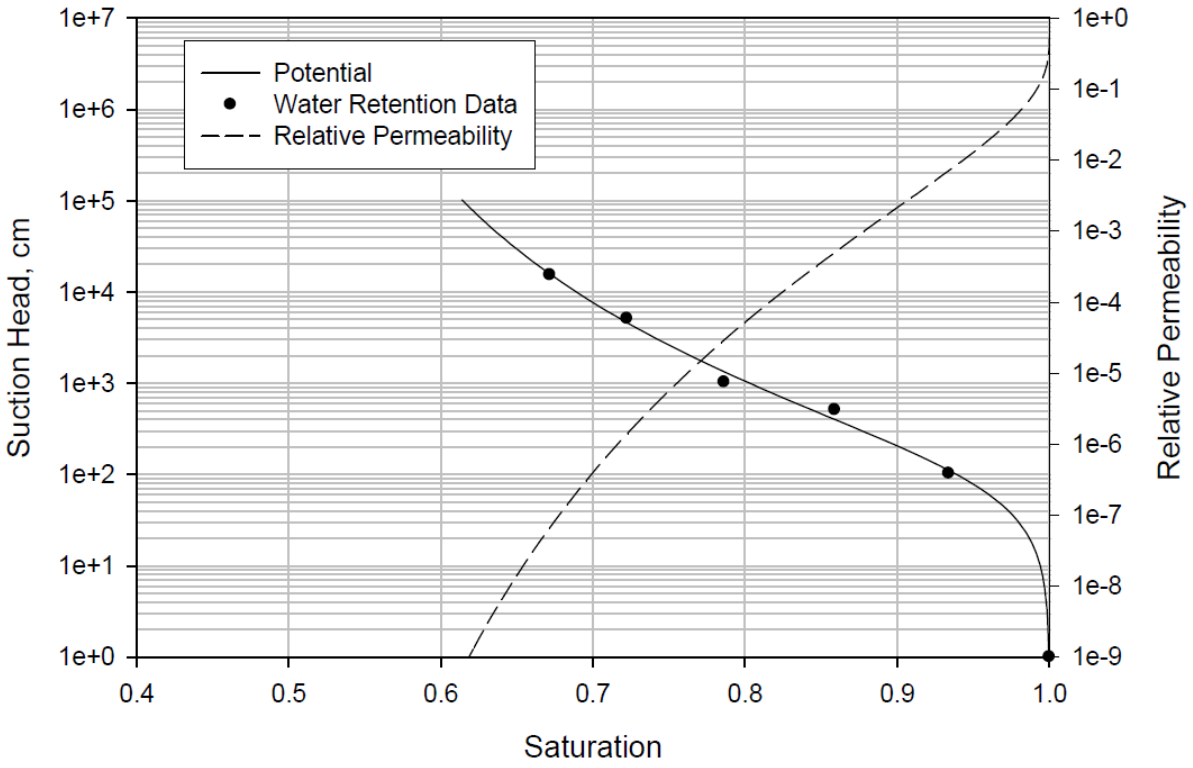

Figure B-2. WCR data and subsequent van Genuchten curve for Mix 3 Sample 2.

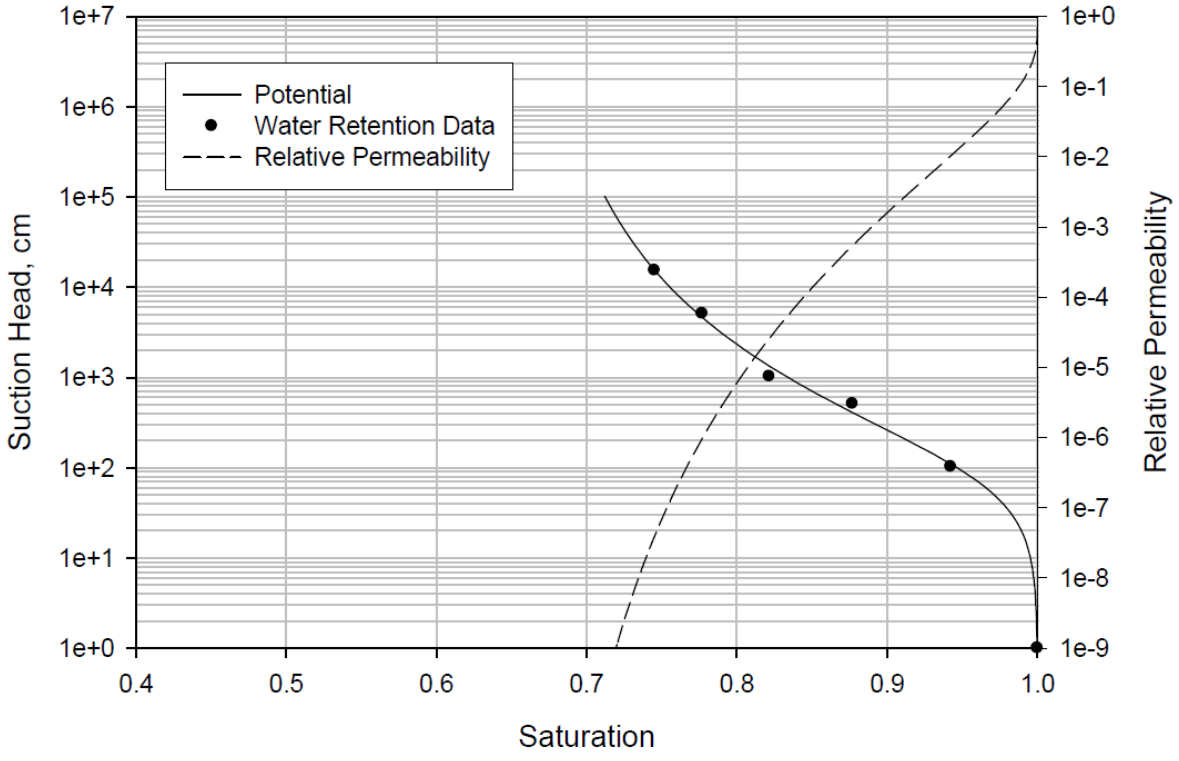

Figure B-3. WCR data and subsequent van Genuchten curve for Mix 3 Sample 3.

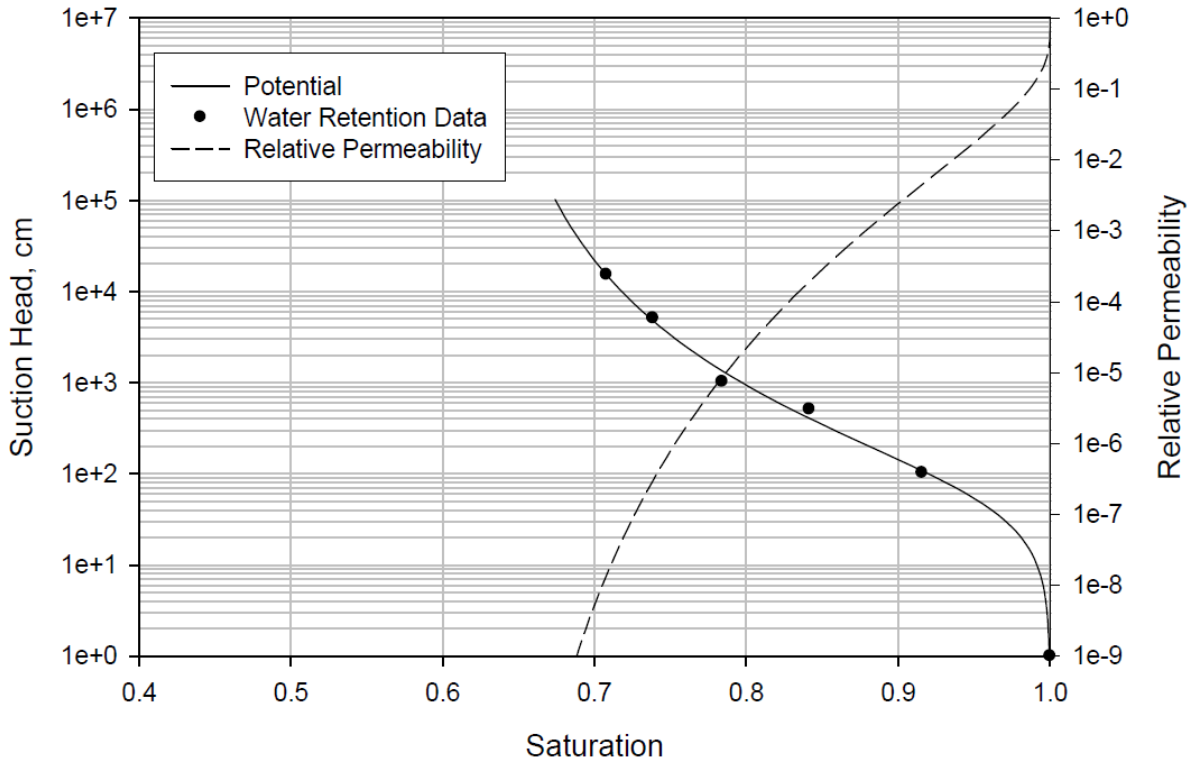

Figure B-4. WCR data and subsequent van Genuchten curve for Mix 5 Sample 1.

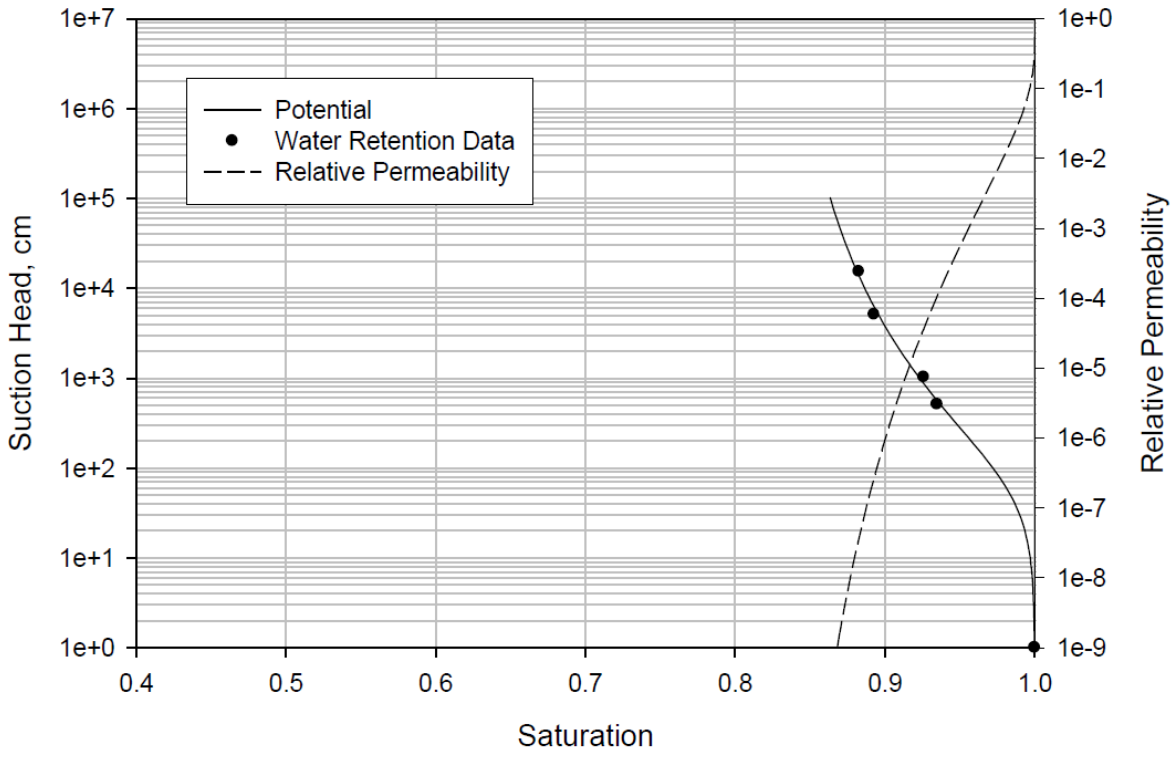

Figure B-5. WCR data and subsequent van Genuchten curve for Mix 5 Sample 2.

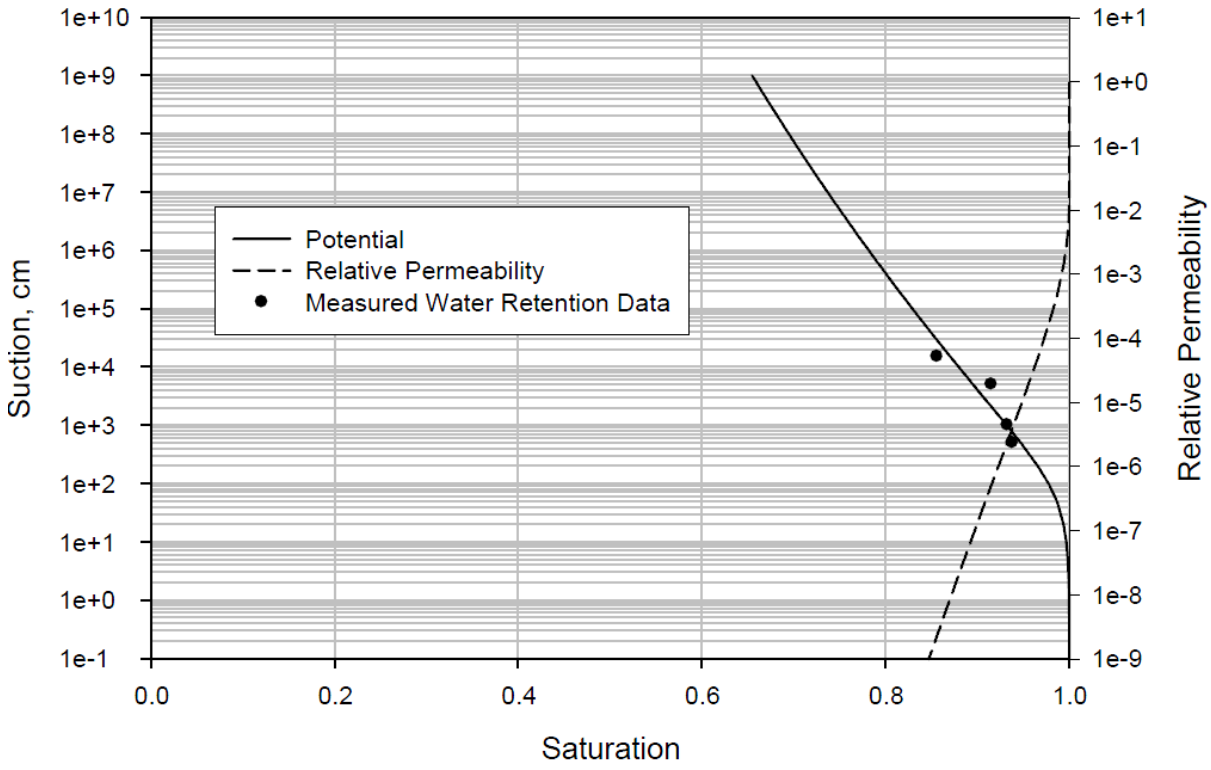

Figure B-6. WCR data and subsequent van Genuchten curve for Mix 9.

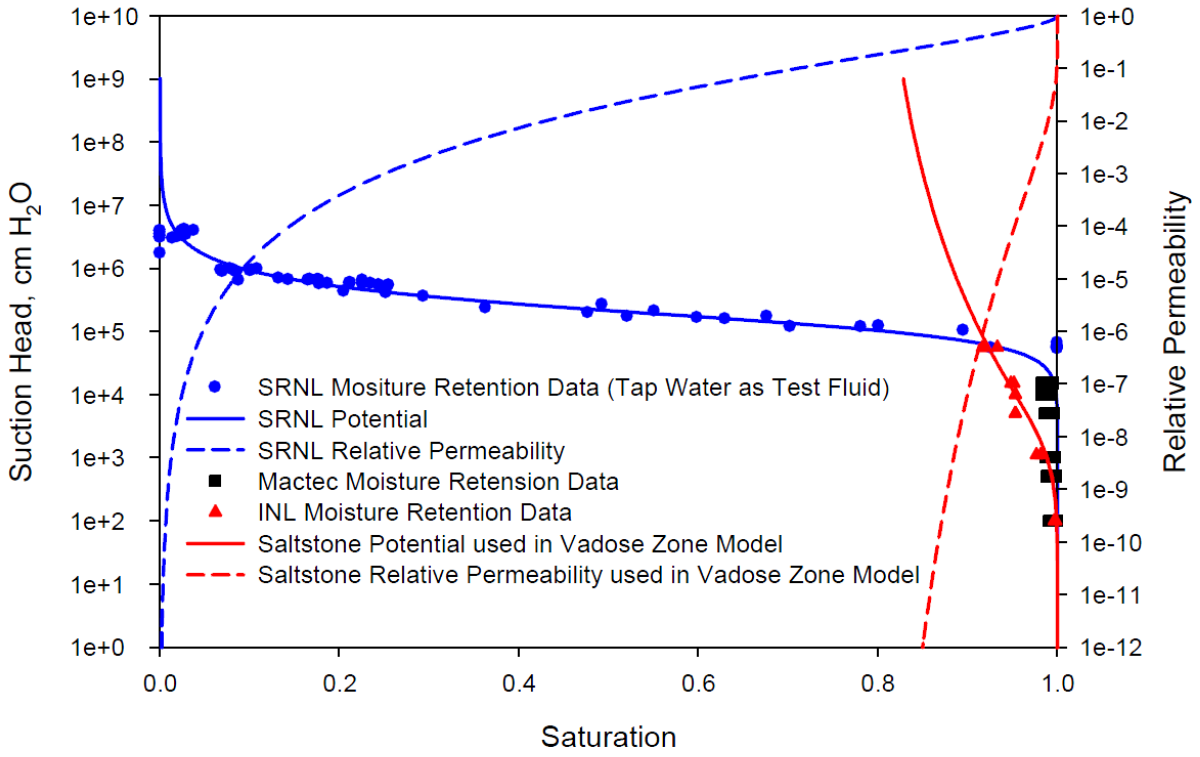

Figure B-7. WCR data and subsequent van Genuchten curve for Mix 16a.

Appendix C. Iodine Species Desorption from Activated Carbon – Granular or Powdered

This Appendix is a Letter Report provided by R. Jeffrey Serne (Pacific Northwest National Laboratory)

Letter Report on Iodine Species Desorption From Activated Carbon-Granular or Powdered

Introduction

Two key issues have been raised by the IDF PA modeling team. The first issue is finding desorption K_d values for iodine species that appear to be captured in powdered or granular activated carbon (GAC) beds within the WTP secondary off-gas scrubber equipment. Current WTP flow-sheet projections suggest that significant quantities of ^{129}I will be captured in the GAC beds that possibly will be encapsulated in grout waste packages that are then disposed of in the IDF as solid secondary wastes. If this is the ultimate disposal pathway for this ^{129}I waste form, then the release of ^{129}I species from the grouted solid secondary waste forms will need to be considered in future IDF PAs. Two conceptual release models are possible for this ^{129}I-laden waste form, desorption K_d values or effective diffusion coefficients, D_e, values. This letter report presents the findings for this issue.

The second issue raised by the IDF modeling team is interest in understanding why the effective diffusion coefficients (D_e) values for ^{129}I and ^{99}Tc through concrete as measured using half-cell through diffusion and standard monolith total immersion tests differ so much from the effective diffusion coefficients (D_e) values for ^{129}I and ^{99}Tc in Cast Stone and grout waste forms as measured in standard semi-dynamic leach tests such as ANS16.1, ASTM-1308, and EPA 1315 leach tests. These issues will be covered in a second letter report.

Release of 129I from Grout Encapsulated GAC

Current WTP flow-sheet projections suggest that significant quantities of ^{129}I will be captured in the GAC beds that possibly will be encapsulated in grout waste packages that are then disposed of in the IDF as solid secondary wastes. If this is the ultimate disposal pathway for this ^{129}I waste form, then the release of ^{129}I species from the grouted solid secondary waste forms will need to be considered in future IDF PAs.

A literature search did not find any articles that addressed release of ^{129}I from GAC or any form of activated carbon that had been encapsulated in grout. There is some literature on the adsorption of iodine species--- iodide, iodate, dissolved free I_2, and dissolved organic bound iodine--- onto activated carbon from contaminated groundwater and other natural waters (river, lake and seawater) and desorption of ^{129}I loaded onto activated carbon. Specific information on iodine species adsorption onto activated carbon is present below. The source of the ^{129}I in the

desorption tests was contaminated groundwater from the Savannah River Site (SRS) and details are also described below.

Available Literature on Iodine Adsorption onto Activated Carbon

Kuboa et al. (2013) studied the removal of various iodine species added to various filtered (to remove suspended solids) river[10] and seawater onto activated carbon. They used ^{131}I tracer in the iodide form as (obtained from vendor) spiked into the natural waters. The AC was derived from coconut husks. The test conditions included adding variable amounts (0.25 to 5 g) of the AC to 200 mL of ^{131}I-spiked water for 1 hr at room temperature. The slurries were then filtered through a quantitative filter paper, No. 5B, and the filtrate gamma radiocounted and compared to the initial solution to obtain the removal ratio of the ^{131}I tracer from solutions using the following equation:

Removal ratio = 1- (Specific activity in filtrate/Specific activity in the initial solution).

The results of this short-term adsorption test showed that ^{131}I in the iodide form was partially removed (from 40 to 60%) from the river water as the AC mass contacting the 200 mL was increased from 1 to 5 g. But iodide was not removed (<10% at 5g AC) from seawater.

Navarrete et al. (2002) studied the retention of carrier-free radioactive ^{131}I (6.4E-04 µg/L; parts per trillion) as iodide in dilute NaOH onto small activated carbon filters (50 mg) from deionized water pH adjusted with either nitric acid or ammonium hydroxide to pH values between 1 and 11. Retention of iodine species (iodide, iodate, and dissolved I_2) is approximately 100% at pH values of 4–6, while no retention of trace concentrations of iodine species occurs after pushing solution through an activated carbon filter from very acidic (pH 1 to 2) or from very basic solutions (pH values >11), respectfully. As shown in Figure 1, there was some adsorption of iodine species at pH values between 2 and 10, respectively. In order to change the oxidation state of the iodine tracer, to evaluate adsorption changes with changes in iodine speciation, a few drops of 30% hydrogen peroxide (H_2O_2) were added to the solutions to create iodate and in separate tests 20 mg of soluble starch was added to create dissolved I_2. After these supposed changes in starting iodine speciation, the Iodine removal results yielded no variation when the different iodine species were contacted with the small AC filters. The results were quite reproducible when the experiment was repeated three times. However, this article doesn't present any details on the contact time between the iodine solutions with the activated carbon nor is there proof that the hydrogen peroxide and starch additions converted iodide to iodate and free I_2 before the solutions were flushed through the small AC filters. The simple solutions used were very dilute such that little information can be gleaned on competitive effects of other dissolved

[10] No river water composition was provided in the journal article. The sampling location was around Tone-Ohzeki, which was a weir across the Tone River between Gunma and Saitama prefectures (located about 200 km south-west of the Fukushima nuclear power plants. Samples were collected June 24, 2011.

cations and anions besides nitrate, sodium and ammonium present in the pH adjusted solutions. In addition, low iodine adsorption onto other common geologic solids at low pH (~1.0) condition is not usual, because anionic solutes like iodide or iodate generally show increasing adsorption as pH decreases. No specific explanation for observing no iodine species adsorption at pH of 1 was addressed by Navarrete et al. (2002).

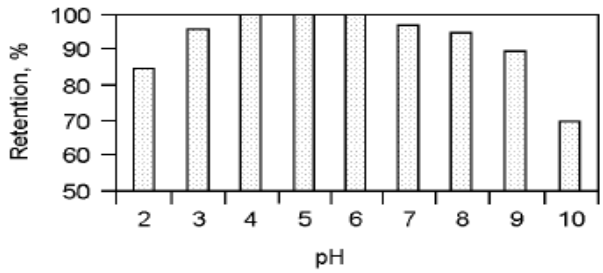

Fig. 1. Iodine trace retention by activated carbon vs. pH of filtered solution

From Navarrete et al. (2002)

Kosaka et al. (2012) studied removal of ^{131}I from water treatment plants, river and pond waters that had been contaminated by fallout from the Fukushima accident onto granular activated carbon (GAC) and powdered activated carbon (PAC).

^{131}I in raw water at two water purification plants was considered to be present in dissolved forms. ^{131}I was partially removed by AC without pre-chlorination. No clear effects of pre-chlorination were observed in this study of water at drinking water purification plants. From the occurrence of ^{131}I at water purification plants, it was shown that ^{131}I was not removed by coagulation/flocculation/sedimentation and filtering through sand filters and thus was considered to be in the dissolved state. ^{131}I from the Fukushima accident, present in river and pond waters, was removed by GAC and PAC through sorption of dissolved iodine species. Removal percentages ranged from 30% to 40% at pH ranges of 6.9 to 7.5, although ^{131}I was not removed in some cases. That is, at different dates the contaminated water seemed to exhibit variable ^{131}I removal rates. The authors suggested that the variable ^{131}I removal rates likely indicated changes in iodine speciation including iodine association with humic substances and inorganic suspended solids, which did not readily get retained on the AC.

Laboratory-scale experiments indicated that the removal percentages of ^{131}I in river and pond waters using 25 mg dry/L of PAC (PAC-1) were 36% and 41%, respectively. These levels were increased by first treating the waters by chlorination. After chlorination the ^{131}I removal percentages for the 25 mg dry/L of PAC increased to 59% for river water and 48% for pond water. Thus the impacts of chlorination differ between full-scale testing at water purification plants and laboratory-scale tests. When varying the mass of PAC in the laboratory tests removal percentages of ^{131}I in river water at 2.5, 5, 10, 25, and 50 mg dry/L of PAC were 11%, 11%, 9%,

36%, and 71%, respectively. Removal percentages in pond water at 10 and 25 mg dry/L of PAC were 13% and 41%, respectively.

The removal percentages of ^{131}I at reaction times of 5, 10, and 30 min with PAC were 36%, 48%, and 48%, respectively. That is, the removal percentages at reaction times of 10 and 30 min were similar under the conditions used in this study.

The environmental water associated with the explosion at a nuclear power plant was considered to contain various forms of ^{131}I, including $^{131}I^-$ and various types of organic ^{131}I. It was reported that the removal percentage of radioactive iodomethane ($CH_3{}^{131}I$), one of the organic I forms detected in air after the accident at the Chernobyl nuclear power plant (Noguchi and Murata, 1988), in humic substance solution (5.98 mg C/L, pH 6.5) by 100 mg/L of AC with a reaction time of 2 days was 92% (Summers et al., 1988). The proportion of $^{131}I^-$ (iodide form) in pond waters was around 30% under the assumption that among the ^{131}I species only $^{131}I^-$ was removed by Ag^+ in companion speciation investigations.

Other laboratory studies indicated that ^{131}I removal by PAC increased with chlorination of the river and pond waters, while the effects of the chlorination were higher at lower PAC concentrations. That is, chlorination aids iodine removal when low concentrations of PAC are used but increasing the concentration of PAC can also increase ^{131}I removal.

I^- reacts rapidly with chlorine and transforms mainly into HOI at neutral pH. The sorption capacities of $HO^{131}I$ and $^{131}I_2$ with AC have been reported to be higher than that of $^{131}I^-$ (iodide form) by 15 and 60-fold, respectively (Mandic et al., 1996). In addition, it has also been reported that I^- or organic I was formed when HOI reacted with natural organic matter (NOM) in environmental waters (Bichsel and von Gunten, 1999). It was presumed that removal of organic ^{131}I by PAC was higher than $^{131}I^-$ as in the case of $CH_3{}^{131}I$ (Summers et al., 1988). Therefore, it was considered that a combination of chlorination and PAC was effective for $^{131}I^-$ removal among ^{131}I species because of the formation of $HO^{131}I$. ^{131}I HOI transformed by chlorination of I^- is further transformed into IO_3^- by reaction with chlorine (Lettinga, 1972; Bichsel and von Gunten, 1999). The transformation yield of IO_3^- depends on chlorination conditions, such as pH, chlorine concentration, and reaction time. It was reported that the distribution coefficients of $^{131}IO_3^-$ for active charcoal at pH 6 to 8 were lower than those of $^{131}I^-$ by one or two orders of magnitude (Ikeda and Tanaka, 1975).

Parker et al. (2014) performed batch iodine species adsorption K_d tests on six activated carbon samples obtained from vendors shown in Table 1. The vendors supplied the following (see Table 2) iodine loading but without more details on how these iodine loading capacities were determined. The solution used by Parker et al. (2014) to measure iodine adsorption was a contaminated groundwater (299-W19-36) from the Hanford Site 200-W Area. This well water is in an ^{129}I plume that generally contains ~3.5 pCi/L (0.0198 µg ^{129}I/L). The water also contains between 7.9 and 11 µg/L total stable I dependent on sampling date. It is not known if the stable

iodine is natural occurring or also Hanford waste impacted because there are few other measurements of total natural iodine for Hanford groundwaters. Suffice it to say that the stable iodine concentration far exceeds the mass concentration of ^{129}I in the groundwater from well 299-W19-36.

Table 1. Activated Carbon Samples Used in Batch Adsorption Tests

Product Name	Source Material	Vendor
Calgon Filtrasorb 400	Bituminous coal	Calgon Carbon Corporation, Pittsburgh, PA
Carbon Resources 1240A	Sub-bituminous coal	Carbon Resources, Oceanside, California
General Carbon GC20X50	Bituminous coal	General Carbon Corporation, Paterson, New Jersey
Siemens[(a)] AC1230AWC	Coconut shell	Siemens Corporation, Warrendale, Pennsylvania
Norit GAC830 M1871	Coconut shell	Norit Americas, Inc, Marshall, Texas
Norit GCA830 M1917	Bituminous coal	Norit Americas, Inc, Marshall, Texas

(a) As of August 2014, this material is no longer sold by Siemens. This material is now known as AquaCarb 1230AWC and is available from Evoqua Water Technologies, Alpharetta, GA.

Table 2. Iodine Loading Capacities for the Activated Carbons Studied

Carbon Material	mg Iodine/g Material
Calgon Filtrasorb 400	1000
Carbon Resources 1240A	1000
General Carbon GC20X50	950
Siemens AC1230AWC	1100
Norit GAC830 M1871	920
Norit GCA830 M1917	920

The speciation of ^{129}I iodine in one of the Hanford Site ^{129}I groundwater plumes[11] has been previously demonstrated, un-expectantly, to be dominated by the presence of iodate (IO_3^-), ~75%. iodide (I^-), the expected dominant groundwater species based on thermodynamic considerations, only accounted for 1% to 2% of the total iodine concentration (Santschi et al. 2012). Organo-iodine comprised approximately 26% of the iodine speciation in the groundwater, which has exceedingly low concentrations of soil organic matter.

Batch sorption tests were conducted by Parker et al, (2014) where a mass of AC and the appropriate amount of groundwater (GW) were placed into poly bottles of the appropriate size for a given solution-to-solid ratio (varied from 100 to 50,000 mL GW-to- dry g of AC). The poly bottles were sealed and placed on a shaker table set at 60 rpm to ensure the sorption materials and groundwater remained well mixed for a 24-hour period. All sorption tests were conducted at room temperature. After the 24-hour contact time, the poly bottles were removed from the shaker

[11] Note that the ^{129}I GW plume characterized by Santschi et al. (2012) is from a different source quite a distance to the north of the well 299-W19-36 used in Parker et al. (2014). Thus, there is perhaps no correlation of the iodine speciation in well 299-W19-36 with the 7 wells that Santschi et al. (2012) characterized.

table and the AC was allowed to settle for 30 minutes. A 0.45 μm syringe filter was then used to separate the groundwater from the AC sorbent. A 5 mL aliquot of the filtered GW was analyzed for total iodine by ICP-MS.

Data from the Carbon Resources 1240A sorption tests for solution-to solid ratios (100 to 5000 mL/g) for this groundwater (which contains 317 mg/L nitrate) indicate the iodine loading ranged from 0.23 μg/g to 6.43 μg/g, respectively. The comparable iodine K_d values ranged from 31.2 to 757.7 mL/g over the same solution-to-solid ratios. The K_d values increased systematically as the solution to solid ratio increased suggesting that the AC per gram was capable of adsorbing more iodine as the total volume of GW contacting it was increased. The iodine loading values are much lower than the stated maximum loading shown in Table 2 (~1000 mg/g) suggesting that other solutes in the groundwater compete for available adsorption sites on the AC or that 24 hr of contact is too short to maximize iodine adsorption.

The sorption of total iodine from this GW that was spiked with additional nitrate (the most common contaminant that is also in the plume) to reach 1400 mg/L nitrate onto Carbon Resources 1240A shows iodine loading values of 0.2 to 4.33 μg/g and iodine K_d values of 26.4 to 479.9 mL/g over the selected solution-to-solid range. The total iodine sorption values are lower in the high nitrate water than in the as-sampled GW, again suggesting potential competition by common GW anions for active sorption sites on the AC.

When the six AC samples were contacted with the "as sampled" GW at a solution-to-solid ratio of 1000 mL/g dry, the iodine K_d for the 24 hr contact ranged from 162 to 226 mL/g. When the GW (2000 mL) was first treated with the oxidizing agent (2.5 mL of 5% sodium hypochlorite) stirred at 600 rpm for three minutes to convert the iodine to iodate, the iodine K_d values ranged from 24 to 176 mL/g for the six AC samples. When 4000 mL of the GW has treated with reducing agents (25 mL 1M hydroxylamine hydrochloride and 10 mL of 1M sodium bisulfite) and stirred at 600 rpm for 45 minutes with the final pH adjusted to 6.5 with sodium hydroxide to convert all the iodine to iodide before performing the batch adsorption tests, the final iodine K_d values ranged from 29 to 131 mL/g. These batch K_d results show that iodine speciation plays an important role in the ability of AC to adsorb iodine. Oxidizing the iodine in the Hanford GW to iodate and reducing the iodine in the Hanford GW both resulted in slightly lower K_d values compared to the "as-sampled" GW that had a mixed iodine speciation.

Because the solution to solid ratio was so high and the contact time was relatively short in Parker et al. (2014) studies, not enough sorption occurred to get precise K_d values. The authors were not confident that their total iodine measurements in the starting GW and final effluents were accurate enough to calculate K_d values unless there was at least a 15% reduction in the total iodine in effluent compared to influent. For the solution-to-solid ratio of 1000 mL/g used in most of the tests the minimal reportable K_d value would be 176 mL/g. I elected to calculate iodine K_d values for all the tests seeing as all the effluents iodine concentrations were lower than the influent concentrations **and** precision between replicate analyses of the "as sampled" GW

and post treatment (to convert to iodate or iodide) was 1% and 3.05%, respectively, was much better than the 15% criteria used by the authors.

It appears to me that each of the six commercially purchased AC samples do adsorb iodide, iodate, and any other iodine species from the Hanford groundwater when the AC is contacted at a solution-to-solid ratio of 1000 mL/g ratio for at least 24 hrs. The resultant iodine K_d values ranged from 20 to 230 mL/g dependent on iodine species in the groundwater and the AC source. For tests at higher solution-to-solid ratios, iodine K_d were as high as 800 mL/g. There was no clear trend in the ability of the six AC source materials to adsorb iodine from the Hanford groundwater amongst all the batch adsorption tests. It has been observed that several of these AC materials do adsorb ^{129}I as well as ^{99}Tc and carbon tetrachloride from contaminated groundwaters treated at the 200-W pump and treat facility.

Velichkina et al. (2014) studied two AC to remove residual iodine from waste solution generated from the production of nuclear-grade zirconium for use in the nuclear industry. After zirconium refining by the iodide method, iodinated circulating solution is used for cleaning apparatus and washing off reusable shavings. At production plants, iodine is precipitated from a circulating solution with potassium permanganate in the presence of sulfuric acid and then the pulp is filtered. After the filtration, the remaining iodine is in the form of free I_2. After the iodine precipitation, the solution has the following chemical composition (mg/L): Na 23.0, K 73.0, Fe 4.8, Ca 11.7, Zn 0.08, Cd < 0.01, Ni 0.4, Co < 0.03, Mn 167.0, Mg 15.0, Cu < 0.01, and I_2 200–600. Unfortunately they never give a pH for the waste solution. It is likely high acid where I_2 dominates. So contact with these GACs could be adsorbing only aqueous I_2 species.

Extraction of iodine from this brine waste was tested using two different GAC materials. Details on the first GAC (SKT-6a) include that it is derived from peat; has a 0.5–2.8 mm grain size, specific surface area of 1200–1500 m^2/g; micro-pore volume of 0.15–0.25 cm^3/g, bulk density of 420 g/L, and a max I_2 sorption of 0.117 g/g from solution containing 0.15 g I/L. The second GAC was VSK-400 derived from fruit or nut pits with very similar grain size, bulk density, iodine sorption capacity but higher micro-pore volume of 0.4 cm^3/g.

The waste brine was placed in a vessel with a stirrer, 1 g of GAC was added then the vessel was hermetically closed with a lid, and the sorption was allowed to proceed for up to 50 hr. Samples of the solutions were taken after certain intervals of time, and the concentration of iodine in them was determined. VSK-400 AC reached steady state I_2 sorption in 5 hrs. In dynamic column loading test the capacity to adsorb I_2 decreased (from 0.34 to 0.06 g I_2 per g of GAC) as the contact time dropped from 13 minutes to 2.6 min.

In another lab study they determined iodine desorption from VSK-400, saturated with iodine from model solutions, in the static mode for 5 h using various desorbing agents: 0.5 N sodium sulfite (Na_2SO_3), 0.5 N sodium hydroxide (NaOH), 0.5 N NH_4OH, and 0.5 N NaOH + 0.5 N Na_2SO_3. The VSK-400 GAC was found to be more universal sorbent, ensuring efficient

desorption of iodine with various agents, such as alkali, sulfite, and ammonia, whereas other GACs that were tested released sorbed I_2 only when the desorption solution contained sulfite.

Other tests showed that under the chosen conditions, sorption of iodine was complete, no iodine remains in the filtrates. For VSK-400, the capacity to remove iodine is 0.321 g g^{-1}. Under the chosen conditions the desorption with a solution containing 0.5 N NaOH + 0.5 N Na_2SO_3 ensured a 96% release of iodine. The VSK-400 activated carbon tested in eight full sorption-desorption cycles retains its iodine sorption capacity, does not change its particle size distribution, and does not lose its iodine sorption selectivity.

Iodine Desorption From Activated Carbon

Kaplan and Serkiz (2000) and Kaplan et al. (1999) studied desorption of ^{129}I from AC used in three SRS liquid waste treatment facilities---Effluent Treatment Facility and the F-Area and H-Area Groundwater Treatment Facilities. The AC materials were purchased from the Calgon Carbon company (Pittsburgh, PA.) and did not contain any special treatment such as Ag impregnation, which is known to enhance removal of iodine species. The exact type of AC purchased from Calgon Carbon was not pursued for this literature search. The three SRS liquid treatment facilities are no longer in operation. The contaminant-laden AC carbon from these three facilities were characterized to determine their ^{129}I contents and then subjected to both batch and flow-through column desorption testing using two leachants. One leachant was a simulated acid rain (dilute solution consisting of 0.0012 M sulfuric acid and 0.0009 M nitric acid with pH ~3. The second leachant was a simulated cement paste pore water consisting of 0.006 M Ca, 0.025 M K, 0.087 M Na, 0.003 M CO_3, and 0.117M OH with a caustic pH that was not specified but likely ~12.

The starting ^{129}I concentrations (pCi/dry g) on the three AC materials were ETF Carbon= 495; F-Area Carbon = 536 ± 34, and H-Area Carbon= 89 ± 4. The batch desorption tests consisted of placing five grams of ^{129}I-laden AC in a bottle containing 475-mL of either the acid rain or cement paste pore water simulants. The bottles were then reacted for seven days with gentle mixing once per day for 30-sec to re-suspend the slurry. After the 7-d contact, the effluent solutions were decanted and filtered through 0.45-µm membranes. The filtered effluents were then subjected to an AgI wet chemical separation procedure with the $Ag^{129}I$ precipitate counted on a low energy X-ray-gamma detector. The initial ^{129}I content of the AC was determined by a similar procedure (counting AC solids directly on a planar X-ray/low gamma ray detector). Batch desorption ^{129}I K_d values were determined from knowledge of the starting ^{129}I mass in the AC and the ^{129}I mass released into the batch effluents using equation 1.

$$K_d = \frac{(I_{solid} \times M_{solid}) - (I_{aq(final)} \times V_{aq})}{\frac{M_{solid}}{I_{aq(final)}}} \quad \text{(Eq. 1)}$$

Where I_{solid} is the ^{129}I concentration in the starting AC (g/g)
$I_{aq(final)}$ is the ^{129}I concentration in the filtered effluent (g/mL)
M_{solid} is the dry mass of AC used in the batch desorption test (g)
V_{aq} is the volume of leachant used in the batch test (mL).

For the flow-through column leach tests ten-mL of "as-received" AC waste material were placed into 20-mL plastic columns with small glass wool plugs on the top and bottom of the sorbent material. The columns were then flushed in up-flow mode (to minimize channeling, air-filled voids, and preferential flow) with either the acid rain or cement pore-water simulants. In the 1999 study the influent flow rate was 5 mL/min (residence time 0.8 min) and in the 2000 study the flow rate was reduced to 15 ± 0.25 mL/hr (residence time of the leachant in the column was approximately 10 minutes) for the F-Area and H-Area AC and 300 ± 15 mL/hr (residence time within the column was approximately 2 minutes) for the ETF AC. For all the column experiments effluents were collected in 1-L containers and each 1-L of effluent was well mixed and ^{129}I measured by the wet chemical procedure mentioned above. Between 13 and 20 L of either of the two leachants were flushed through the small 10-mL AC packed columns over periods of two months (the column tests were stopped each weekend due to radiological safety concerns). 20 L represents >5000 pore volumes, the amount of liquid that is expected to pass through the waste in about 1100 years for burial conditions at SRS.

Column desorption K_d values were calculated for several of the 1-L batches of effluents using a mass balance approach that starts with the initial ^{129}I concentration on the AC solid and starting AC mass and then subtracting out the ^{129}I mass leached in each 1-L batch of effluent to get the value of ^{129}I remaining in the packed AC at any time during the flow through test. The flow through column K_d value at any time (1-L increments) during the test is then the ratio of ^{129}I remaining in the packed AC divided by the ^{129}I in the current 1-L packet of effluent normalized by the volume (1000 mL) in each batch of effluent and the mass (X g) of AC packed in the column.

The batch desorption tests provide a maximum leach rate, or low desorption K_d value compared to the column K_d based on the much longer leaching time for the batch tests (7 days “residence time” for batch tests vs. 0.8 to 10 minutes residence time for each pore volume of leachate in the column tests).[12]

[12] Note there are errors in portions of the text in Kaplan et al. (1999) regarding flow rate and residence time for the two solutions used to leach the AC. The correct values are 5 mL/min flow rate and residence time 0.8 min.

The ^{129}I desorption K_d results for the cement paste pore water are most relevant for disposal of grout encapsulated AC solid secondary wastes in IDF. Key conclusions from Kaplan and Serkiz (2000) and Kaplan et al. (1999) follow.

For the cement paste pore-water simulant, the reasonably conservative ^{129}I desorption K_d values were 600 mL/g for ETF AC, 880 mL/g for F-Area AC, and 320 mL/g for H-Area AC. The activated carbon K_d value measured in the cement leachate simulant was more than two orders-of-magnitude less than the K_d value measured in the acid rain simulant.

The acid-rain simulant desorbed appreciably less ^{129}I (i.e., had greater ^{129}I desorption K_d values) than the cement paste simulant. Reasonably conservative ^{129}I desorption K_d values in a simulated acid rain environment are 7400 mL/g for ETF Carbon, 132,500 mL/g for F-Area AC, and 58,100 mL/g for H-Area AC.

The flow-through column desorption tests showed a general tendency for the AC solids to release contaminants more readily in early leaching volumes. That is, ^{129}I desorption K_d values generally increased sharply as the amount of leachate that passed through the column increased. For example, after ~3-L of effluent (equivalent to ~240-yr through SRS buried solid wastes encapsulated in grout) had been introduced into the AC packed columns, the ^{129}I desorption K_d values increased appreciably, often increasing more than an order of magnitude. This increase was attributed to the more readily extractable species of ^{129}I being leached from AC materials first, leaving the more strongly sorbed ^{129}I species more strongly sequestered in the AC.

The ^{129}I desorption K_d values of the activated carbon varied, depending on the source of the waste. This might be caused by chemical differences in the liquid waste streams being processed, different process times in the three facilities, or to the differences in the treatment trains. It may also be attributed to different batches/sources for the activated carbon used in the three facilities, which were known to vary over time. Specifically, activated carbon ^{129}I desorption K_d values were generally greater for the F-Area and ETF facility AC than for the H-Area AC when leached in cement paste pore water simulant.

The contact time used in these two studies was appreciably less than that expected under SRS disposal field conditions. The problem with a shorter contact times is that they tend to overestimate actual ^{129}I desorption K_d values; however the recommend ^{129}I desorption K_d values mentioned above are considered to be reasonably conservative for future SRS burial ground PA predictions.

Adsorption of Iodine on Black Carbon

Choung et al. (2013) studied the adsorption of iodide and iodate present in 0.001 M sodium nitrate solutions at several pHs onto a black carbon (BC). The black carbon was generated by pyrolyzing heartwood of a pine tree (Gangneung, Korea) that had been cut into 1 cm^3 blocks that were oven-dried at 105 °C overnight. Then the heartwood blocks were placed in a tube furnace under a constant nitrogen flow ~0.1 L min−1, and pyrolized for 30 min at final temperature 600 °C with increasing temperature rate, 10 °C min−1. The produced-char was pulverized, and

sieved to isolate the 75−150 μm size fraction. This process is somewhat similar to creating activated carbon but the temperature and length of time for the pyrolysis are lower and shorter, respectively. The BET specific surface area of the black carbon was only 3.85 m^2/g in comparison to most AC's, which have specific surface areas of ~1000 m^2/g. The black carbon adsorbed both iodide and iodate from pH=3. Iodate sorption kinetics were faster than iodide. However, the K_d values for iodide were much higher (800 to 1000 mL/g) than for iodate (15 to 20 mL/g). These results were explained and supported by hypothesizing that molecular dimension and steric effects were controlling the amount and kinetics of adsorption. Because iodate has trigonal pyramidal molecular geometry with approximately a two times larger molecular size (>4 Å) than iodide, iodate does not penetrate into micropores in the black carbon as readily as iodide. Thus, the observed rapid uptake rate for iodate on the BC may be attributed to predominant outer surface reaction rather than access to micropores in the BC that iodide can enter.

Iodide and iodate uptake by BC was dependent on pH conditions. The measured K_d value for iodide was 1700 mL/g under highly acidic conditions (pH < 3), decreased to 410 mL/g near neutral pH~6 and 39 mL/g under alkaline condition (pH ~8) at low dissolved iodide concentrations, of ≈ 10 μg/L. Similarly, iodate uptake onto BC was lowered with increasing pH. Previous BC studies showed that BC has high amounts of surface positive charge at low pH that attracts anions such as iodide and iodate.

XANES spectra for the BC loaded with iodide shows an intermediate peak position between iodide and iodate reference materials. The BC material seems to act as an oxidizing agent for iodide based on the XANES spectra. The BC iodate XAFS spectra was not collected for XANES analysis. However, the authors speculate that the BC is likely to play more important role as oxidizing agent than reducing agent because of approximately more than 1 order of magnitude lower iodate uptake compared to iodide uptake. The EXAFS spectra of the iodide-laden BC yielded an atomic distance for the I to C bond closest to the distance for aromatic carbon-iodide reference materials than the distance for aliphatic carbon-iodide bonds. This result is consistent with chemical composition of the BC used in this study, which predominantly consisted of aromatic carbon species based on ^{13}C NMR analysis.

Literature on X-Ray Absorption Spectroscopy of Iodine Species in Solids Relevant to Cementitious Waste Forms and Geologic Media

Bonhoure et al. (2002) studied the sorption of iodine species (I^-/$IO3^-$) by hardened cement paste (HCP) and a calcium silicate hydrate (CSH) phase under highly alkaline conditions using X-ray absorption spectroscopy (XAS).

They suggest that iodine is expected to exist predominantly as iodide (I^-) in cement systems except under oxic conditions, where iodate (IO_3^-) may be the dominant species. They cite several studies that indicated the potential of individual cement minerals to immobilize I^- and

IO_3^- [see Atkins and Glasser (1990, 1992); Brown and Grutzeck (1985); Toyohara et al. (2000)], e.g., CSH, sulfoaluminates such as AFm (monosulfate: $3CaO{\cdot}Al_2O_3{\cdot}CaSO_4{\cdot}12H_2O$) and Aft (ettringite: $3CaO{\cdot}Al_2O_3{\cdot}3CaSO_4{\cdot}32H_2O$), and, most recently, tetracalcium aluminate hydrate ($4CaO{\cdot}Al_2O_3{\cdot}XH_2O$ (X = 13to 19)). AFm was reported to exhibit the highest potential for I^- sorption [Atkins and Glasser (1990) and Brown and Grutzeck (1985)]. Substitution of SO_4^{2-} by I^- is considered to be the predominant uptake process where $CaSO_4$ is replaced by CaI_2. The greater affinity of CSH phases for IO_3^- over I^- was observed and interpreted as being due to direct bonding between CSH and IO_3^- or to the precipitation of a Ca-IO_3^- containing solid precipitates.

Bonhoure et al. (2002) prepared their HCP from commercial sulfate-resisting cement (Type CPA 55 HTS, Lafarge, France). Their CSH gel was prepared using a standard procedure [Atkins et al. 1991]. The CSH gel was found to have a $CaO:SiO_2$ (C : S) ratio of 0.95±0.05 using SEM/EDS.

Uptake kinetics for I^- and a sorption isotherm for I^- were determined on HCP material in an artificial cement pore water (ACW, pH 13.3) at a solid to liquid (S/L) ratio of 25 mg/L. The cement paste suspensions were pre-equilibrated for 28 days prior to adding ^{125}I tracer solution with $[I]_{tot} = 10^{-8}$ M to the cement suspensions. The suspensions were then shaken end-over-end for, at a maximum, 180 days. For the isotherm experiments, ^{125}I containing stock solutions were added to the suspensions to give total iodide concentrations ranging from 10^{-9} M to 5×10^{-4} M. These samples were shaken end-over-end for 7 days. After equilibration (isotherm) or appropriate time periods (kinetics), the suspensions were centrifuged (60 min at 95,000 g). For radionuclide assay, 2 ml aliquots of the supernatant solution were mixed with 2 ml of a scintillation cocktail and measured by LSC.

I^- uptake by HCP was significant under the given experimental conditions, with iodide K_d values ranging from ~100 to 200 mL/g in the kinetic study and from 20 to 150 mL/g in the isotherm study. Note that iodide K_d values deduced from the sorption isotherm were found to be about a factor of two lower (equilibration time = 7 days) than the K_d values determined after 180 days equilibration. **The sorption isotherm had a slope of 0.87 indicating decreasing iodide adsorption K_d values with increasing I^- concentration**. These sorption results corroborate earlier findings that HCP and cement minerals tend to be more reactive towards I^- and IO_3^- than most geological materials.

XAS samples were prepared by mixing 1 g of solid material (HCP or CSH) with 40 mL ACW, pre-equilibrating the suspensions (HCP: 28 days/CSH: 14 days), adding stable I^- or IO_3^- solutions ($[I]_{tot} = 10^{-3}$ M and 10^{-2} M), respectively and equilibrating the suspensions again for 28 days. After centrifugation and decanting the ACW, the residual wet paste was used for the XAS measurements. A key finding of the XAS characterization of the solids was that redox reactions do not influence sorption processes in the cementitious systems studied here as there was no change of oxidation states observed upon uptake of the either the iodine species (either I^- or IO_3^-) by HCP or CSH. That is, HCP and CSH contacted with I^- bearing ACW showed XANES

spectra for only I^- and likewise HCP and CSH contacted with IO_3^- bearing ACW showed only IO_3^- in the residual solids. Thus there were no changes in iodine speciation over the 14 to 28-d contact times for the two solids immersed in iodine-spiked ACW.

In summary, these cited articles suggest that AC can sorb all common iodine aqueous species (iodide, iodate, and dissolved I_2) from various aqueous solutions with K_d values generally ranging from 20 to at least 800 mL/g. The sorption kinetics are relatively fast (minutes to a few days) to reach steady state residual solution concentrations. Desorption tests conducted by Kaplan et al. (1999) and Kaplan and Serkiz (2000) on ^{129}I-laden ACs showed relatively conservative ^{129}I desorption K_d values between 320 and 880 mL/g when the ^{129}I-laden ACs were leached with a simulated cement pore water with caustic pH similar to expected grout leachates from cementitious waste forms and grout encapsulated solid secondary wastes.

Questions Posed by IDF PA Team Regarding ^{129}I Sequestered by AC

1. *Is ^{129}I somehow physically 'trapped' within AC rather than simply chemisorbed on surfaces?*

None of the literature cited above discusses the sorption mechanism(s) that controls ^{129}I (or iodine in general) on AC. However the fact that Parker et al. (2014) found that increasing the nitrate concentration in the Hanford groundwater resulted in a reduction of iodine adsorption K_d values onto AC and the fact that Kuboa et al. (2013) found that iodine species could be removed from river water but not from seawater by AC suggests that the iodine adsorption mechanism is sensitive to competing solutes and thus likely a relatively weak chemisorption process based on electrostatic attraction between charged iodine species and AC surfaces. Further Navarrete et al. (2002) found that the pH of the iodine bearing solution impacted the percentage removal by AC, which also suggests chemisorption processes more so than physical trapping.

Finally several articles suggest that the surface charge of AC is an important attribute that controls iodine species (iodide and iodate anions) adsorption tendencies. Sánchez-Polo et al. (2006, 2007) and Hoskins et al. (2002) discuss the importance of the AC's pH_{pzc} (pH at which the surface charge becomes zero) in determining iodine species adsorption tendencies. There are attractive electrostatic interactions between the positively charged carbon surface, when the pH of the solution is less than the pH_{PZC} of the AC, and the negatively charged halide anions, favoring the halide adsorption process. These articles report that the pH_{PZC} values of the virgin GACs are generally between 8.5 and 10.0, indicating positive surface characteristics at acidic to slightly alkaline pH values leading to favorable sorption of anions such as iodide and iodate from solutions with pH values at or below the pH_{PZC}.

2. *One worry from the zero-point of charge/ iodine sorption aspect you mentioned; so encasing GAC in cement might not seem such a wise choice?*

Yes, cement pore water will be at pH values above the pH_{pzc}, so AC surface sites will become negative in cement-dominated pore water and theory says anions will be repelled. However, the two Kaplan SRNL reports cited above still show ^{129}I stayed relatively well sorbed when iodine-laden AC was leached with simulated cement pore water. The desorption K_ds were still above 300 mL/g for contact times up to 7 days. Most of the other literatures address adsorption onto clean AC from simple solutions with no mention of desorption by caustic solutions. Thus, I recommend a full system analysis, which considers time needed to degrade a cement box that encapsulates ^{129}I loaded AC and subsequent cement leachate driving iodine desorption, is needed. It would be prudent to also separately study, iodide- and iodate-laden spent AC desorption in cement leachate under both oxidizing and reducing conditions to gather data on all near-field disposal.

One idea would be to use the Ag-impregnated AC from the very beginning to capture ^{129}I from WTP off-gas. I don't think high pH solution will desorb iodine from silver impregnated AC because the iodine is precipitated as AgI (or at least there is a strong chemical bonding between Ag and I), which won't be more soluble at high pH. [13]

3. *I have not found any study in which the actual chemical form of iodine in carbon filters has been determined; it could be as I_2 or dissociated atomic I, as opposed to I^- or IO_3^-. The same EXAFS technique that PNNL used to look at oxidation of Tc-cement could be used for this purpose.*

I agree that XAS, especially XANES, can determine iodine species valence states. I reviewed several XAS articles that discuss characterization of iodine. For example Fuhrmann et al. (1998), Bonhoure et al. (2002), Reed et al. (2002), Schlegel et al. (2006), Kodama et al. (2006) and Choung et al. (2013). It is clear that using iodine K-edge lines yields better XAS data than using L-III edge lines because of the K-edge lines show higher energy (less self-absorption issues) and less interferences from other elements. Our XAS expert (Wayne Lukens-LBNL) has done iodine XAS for simulated waste glass and investigated iodine speciation XAS analyses on a Cast Stone sample in January 2016. Wayne believes that he can get good XANES iodine speciation information if the solid sample contains at least 20 ppm total iodine. I K-edge EXAFS is much more difficult. I K-edge EXAFS are greatly broadened by the short core-hole lifetime. In addition, except for iodate, the EXAFS of all of the iodine species are weak and will have large Debye-Waller parameters, both of which limit the usable range of the data. So if someone could provide AC carbon samples with at least 20 ppm total iodine, XANES spectra could be obtained and the valence states of the sequestered iodine could be established. Valence state information would likely establish the species iodide (-1), iodate (+5), free iodine I_2 (0). In

[13] I think this is true but suggest IDF PA team do a complete geochemical speciation-saturation index calculation for AgI in various types of pore waters at various pHs.

addition, iodine species can be determined by X-ray photoelectron spectroscopy (XPS) on AC surfaces. We likely need AC samples with higher than 20 ppm total iodine to effectively use XPS, but XPS analysis can be easy to perform.

4. *Carbon has an incredibly high surface area; 1 gm has a surface area of 5,500 square meters (size of a football field); I am trying to figure out what this information would mean with respect to 'sorption' testing*

For sure activated carbon has high specific surface areas (reviewed literature generally shows SA values between 1000 and 2000 m^2/g; not your value of 5500) and if the iodine species sorption is either physical or chemical both would give high K_ds per gram. Also the individual grains of activated carbon are quite small so diffusion of sorbed material out of "nano" and "micro" pores should not take long if there are no steric size issues. In a sense, Kaplan's packed AC columns results show that early effluents yield a much lower ^{129}I desorption K_d than later effluents. This is explained as having the readily desorbable (low energy sites) iodine coming off first from the exterior surface and less desorbable (more resistant from interior higher energy sites) releasing iodine later in the process. Also Kaplan's batch desorption K_ds (7 day contact time) are larger than the column desorption K_ds (that had contact times that varied from only 0.8 to 10 minutes). The lower desorption K_ds from the batch test result from the longer contact time that allows the cement pore water more time to desorb ^{129}I off AC surface sites before the solution is removed from the AC by centrifugation, decanting and filtration.

Also note that Kaplan's iodine desorption K_ds for cement leachate are much lower than for the "acid rain" leachate. EPA acid rain leachate is a very dilute nitric/sulfuric acid solution and not as aggressive at desorbing anions from AC with net positive surface charge at the acid rain pH of 3. The cement pore water (with higher competing ions and caustic pH between 12 and 13) would strip sorbed anions as the AC net surface charge trends to negative values and tends to repel anions.
The point is that Kaplan's I desorption K_ds for cement leachate are in the range of hundreds to mid thousands mL/g: more reasonable than the values for acid rain. Assuming that the Hanford WTP off-gas spent activated carbon secondary wastes will be cement encapsulated, the Kaplan ^{129}I desorption K_d data for the cement leachate would be most relevant. Albeit performing longer term desorption tests than Kaplan's 7-d batch contacts would be useful to see how low the ^{129}I desorption K_d might go.

5. *There seems a lot of strangeness in the Kaplan results for the packed AC column of these tests (an early, faster release of I-129, followed by a slower release of I-129 possibly representing a different location/ bonding/ site)?*

I agree with Kaplan's explanation of the packed AC column leach results showing the early, faster release of ^{129}I, followed by a slower release of ^{129}I at later times. Kaplan states:

"The increase in ^{129}I desorption K_d value at later pore volumes is attributed to the more readily extractable ^{129}I being leached from AC materials first, leaving the more strongly sorbed ^{129}I species more strongly sequestered in the AC after the early leaching stage."

I have seen this same trend for most contaminants leaching from contaminated sediments that were leached in similar flow-through tests and even from grout monoliths leached in the semi-dynamic (intermittent solution exchange test protocols). So the trend can be explained by the multiple adsorption site conceptual model with varying adsorption site binding energies or to the wash-off conceptual model where direct diffusion from near-surface pores that are in intimate contact with the leachant cause early high effective diffusion coefficients to be measured. Thus either desorption or diffusion based conceptual models can explain the observed higher release in the early stage of contact with leachants.

6. *INTERA PA team's thought, given the limited SRS AC solids characterization, is that most of the I-129 in the AC is in a form that is highly insoluble (AgI? or some strange iodate?), or is physically trapped (as I_2?)*

Dan Kaplan confirmed via email that the three AC materials in use in 1999 to 2000 at their ETF, F-Area and H-Area treatment facilities was "normal" AC supplied by the Calgon Carbon Company; there was no Ag or other specialized treatment performed on the AC.

I also asked if all three facilities are still operating and using AC. Dan replied that these three facilities are no longer operational and no ^{129}I-laden spent AC is available for further testing or characterization.

The ACs used at the Hanford 200-W pump and treat are also not Ag-impregnated but appear to capture ^{129}I, ^{99}Tc as well as the main contaminant of interest, carbon tetrachloride. Several of the AC articles reviewed used AC impregnated with Ag to specifically sequester iodine species (see Sánchez-Polo et al. (2006, 2007), Qafoku et. al. (2015), and especially Hoskins et al. (2002)). The latter article presents a very detailed comparison between regular AC and silver-impregnated AC. Some key findings follow. The aqueous solutions used by Hoskins et al. (2002) were dilute sodium chloride (ionic strength ranged between 0.05 and 0.09 M) and pH values were maintained using potassium mono and/or dibasic phosphate buffers. At pH values of 7 and 8 there was a marked increase in iodide removal for the 1.05% silver-impregnated activated carbon (SIAC) over that of its virgin GAC, while their performances were similar at a pH of 5. When the moles of Ag in the SIAC is smaller than the moles of total iodine, silver iodide precipitation occurred until all available silver had reacted, and additional iodide was removed from solution by pH-dependent adsorption to the GAC. Under this condition, silver leaching did not occur while iodide leaching increased with increasing pH. These findings suggest that in the presence of silver on activated carbon, the uptake is initially controlled by precipitation[14] of silver iodide. After all the available silver is consumed by precipitation with iodide, additional uptake will

[14] It is also plausible that there is also strong covalent Ag-I bonding, especially when the SIAC has conditions below discrete AgI solubility limits.

occur as a result of adsorption by the GAC, a pH-dependent phenomenon. Additionally, the iodide uptake decreased with increasing pH for virgin GAC, while iodide uptake by SIAC was less pH-and concentration-dependent.

Qafoku et al. (2015) also studied the removal of trace quantities of iodide (0.6 to 6 ppm) spiked into two solutions, deionized water and a highly saline, caustic Hanford low-activity tank waste (7.8 M sodium nitrate based) simulant. Batch adsorption tests were performed at a solution to solid ratio of 100:1 mL/g. Each test was conducted at room temperature in an anoxic chamber containing N_2 with a small amount of H_2 (0.7%) to maintain anoxic conditions. The Ag-impregnated activated carbon (wt % Ag and type of activated carbon not specified) was obtained from Prominent Systems, Inc. (City of Industry, CA). The Ag-impregnated activated carbon had a specific surface area of 1193 m^2/g as measured by BET. The observed batch adsorption K_d's for iodide onto this Ag-impregnated activated carbon for iodide traced deionized water were generally ≥ 10,000 mL/g but for the iodide traced 7.8 Na tank waste simulant were ≤10 mL/g. Thus one key observation based on the limited iodide adsorption-desorption studies reviewed is that iodide adsorption onto both virgin AC and SIAC is high for low ionic strength solutions but much lower for high ionic strength (>5 M) and highly caustic high ionic strength solutions. Qafoku et al.'s data do raise a concern that very high (>5 M; mostly Na, nitrate) and very caustic pH (>12) might significantly reduce the amount ^{129}I that is sorbed to AC. Thus the positive results shown by Hoskins et al. (2002) need more study.

I speculate that the ionic strength of grout encapsulated solid secondary waste leachates will have a moderate ionic strength (likely <0.3 M) but will have a caustic pH (>12). Thus the ability of either AC or SIAC to retain the iodide needs to be carefully evaluated under various conditions, despite the "good" desorption iodine results of Kaplan and Serkiz (2000).

If the off-gas treatment AC captures iodine from aqueous waste, the likely form for the iodine should be iodide or iodate, based on thermodynamics. If the AC in the off-gas treatment equipment captures volatile iodine in a gaseous form it could be as I_2, which is well captured by AC. However, I did not find any mechanistic information on the process by which AC binds I_2 gas.

7. *Given available information, what conceptual release model do you recommend for release of ^{129}I from activated carbon encapsulated in grout?*

I could find no information on a diffusional release conceptual model or ^{129}I diffusional release from AC that had been encapsulated in grout. I did find desorption ^{129}I K_d data for release from AC and adsorption ^{129}I K_d values for AC that is contacted by low ionic strength solutions (river water, lake water, groundwater) and for seawater and an industrial liquid waste. Thus at this time the ^{129}I desorption K_d conceptual model for AC, based on the desorption tests using simulated cement pore water by Kaplan and Serkiz (2000) and Kaplan et al. (1999), is my recommendation. In the future diffusion-controlled release of I-laden AC that has been

encapsulated in grout should be studied, likely using the standard EPA Method 1315 protocol, to gain more reliable data that quantifies an iodine diffusion coefficient to compare against a desorption controlled conceptual model.

References Cited in the Review of Iodine Sorption-Desorption onto Activated Carbon

(Gray shaded references directly used in this review.)

Atkins M and FP Glasser. 1990. "Encapsulation of radioiodine in cementitious waste forms". Mat. Res. Soc. Symp. Proc. **176**:15-22.

Atkins M and FP Glasser. 1992. "Application of portland cement-based materials to radioactive waste immobilization". Waste Management **12**:105-131.

Atkins M, FP Glasser, and A Kindness. 1991. *A Thermodynamic Model for Blended Cement*. DoE/HMIP/RR/92/005, Aberdeen University, Scotland.

Bichsel Y and U von Gunten. 1999. "Oxidation of iodide and hypoiodous acid in the disinfection of natural waters". Environ. Sci.Technol. **33**:4040-4045.

Bonhoure I, AM Scheidegger, E Wieland and R Dähn. 2002. "Iodine species uptake by cement and CSH studied by I K-edge X-ray absorption spectroscopy." Radiochim. Acta **90**:647–651.

Brown DR and M Grutzeck. 1985. "The synthesis and characterization of calcium aluminate monoiodide". Cem. Concr. Res. **15**:1068-1078.

Bonhoure I, AM Scheidegger, E Wieland and R Dähn. 2002. "Iodine species uptake by cement and CSH studied by I K-edge X-ray absorption spectroscopy." Radiochim. Acta **90**:647–651.

Choung S, W Um, M Kim, and M-G Kim. 2013. "Uptake Mechanism for Iodine Species to Black Carbon." Environ. Sci. Technol. **47**: 10349-10355 dx.doi.org/10.1021/es401570a

Fuhrmann M, S Bajt, and MA A Schoonen. 1998. "Sorption of iodine on minerals investigated by X-ray absorption near edge structure (XANES) and ^{125} I tracer sorption experiments." *Applied Geochemistry*, **13**:127-141.

Hoskins, JS.T Karanfil, and SM Serkiz. 2002. "Removal and sequestration of iodide using silver-impregnated activated carbon". Environ. Sci. Technol. **36:**784–789.

Ikeda N and K Tanaka. 1975. "Column chromatographic separation of radioactive tellurate, tellurite, iodide and iodate by active charcoal. J. of Chromatography **114**:389-395.

Kaplan DI and SM Serkiz. 2000. ^{129}Iodine Desorption from Resin, Activated Carbon, and Filtercake Waste Generated from the F- and H-Area Water Treatment Units. WSRC-TR-2000-00308, Westinghouse Savannah River Company, Aiken, SC.

Kaplan DI, SM Serkiz, and NC Bell. 1999. I-129 Desorption from SRS Water Treatment Media from the Effluent Treatment Facility and the F-Area Groundwater Treatment Facility. WSRC-TR-99-00270, Westinghouse Savannah River Company, Aiken, SC.

Kodama S, Y Takahashi, K Okumura, and T Uruga. 2006. "Speciation of iodine in solid environmental samples by iodine K-edge XANES: Application to soils and ferromanganese oxides." Science of the Total Environment **363**:275–284.

Kosaka K, M Asami , N Kobashigawa, K Ohkubo , HTerada ,N Kishida , and M Akiba . 2012. "Removal of radioactive iodine and cesium in water purification processes after an explosion at a nuclear power plant due to the Great East Japan Earthquake." Water Research **46:** 4397-4404.

Kuboa T, S Fukutani, T Ohta, and Y Mahara. 2013. "Removal of radioactive cesium, strontium, and iodine from natural waters using bentonite, zeolite, and activated carbon." J Radioanal Nucl Chem **296**:981–984.

Lettinga G..1972. Radioactivity and Water Supplies. EUR-4866, Commission of the European Communities (CEC, Brussels, Belgium, 198 p.

Mandic M, Z Vukovic, S Lazic, and S Raicevic. 1996. "Sorption of Hypoiodous Acid on Activated Carbon." Journal of Radioanalytical and Nuclear Chemistry, Articles, 208(2):453-460.

Navarrete M, A Gaudry , L Cabrera, and T Martı´nez. 2002. "Concentration of iodine traces in solution by filtering through activated carbon. "J Radioanal Nucl Chem **251 (2)**:297–298.

Noguchi H and M Murata. 1988. "Physicochemical speciation of airborne I-131 in Japan from Chernobyl". Journal of Environmental Radioactivity, **7**:65-74.

Parker KE, EC Golovich, and DM Wellman. 2014. *Iodine Adsorption on Ion-Exchange Resins and Activated Carbons–Batch Testing.* PNNL-23730 or RPT-DVZ-AFRI-021, Rev.0, Pacific Northwest Laboratory, Richland, WA.

Qafoku N, JJ Neeway, AR Lawter, TG Levitskaia, RJ Serne, JH Westsik, Jr, and MMV Snyder. 2015. Technetium and Iodine Getters to Improve Cast Stone Performance . PNNL-23282 Rev. 1, Pacific Northwest National Laboratory, Richland, WA.

Reed WA, I May,FR Livens, JM Charnock, AP Jeapes, M Gresley, RM Mitchell, and P Knight. 2002. "XANES fingerprinting of iodine species in solution and speciation of iodine in spent solvent from nuclear fuel reprocessing. J. Anal. Atom. Spectrom. **17**: 541–543.

Sánchez-Polo M, J Rivera-Utrilla , E Salhi, and U von Gunten. 2006. "Removal of bromide and iodide anions from drinking water by silver-activated carbon aerogels." Journal of Colloid and Interface Science **300**:437–441.

Sanchez-Polo M, J Rivera-Utrilla,, E Salhi and U von Gunten. 2007. "Ag-doped carbon aerogels for removing halide ions in water treatment." Water Research **41**:1031 – 1037.

Santschi PH, C Xu, S Zhang, Y Ho, HP Li, KA Schwehr, and DI Kaplin. 2012. *Laboratory Report on Iodine (129I and 127I) Speciation, Transformation and Mobility in Hanford Groundwater, Suspended Particles and Sediments*. SRNL-STI-2012-00592, Savannah River National Laboratory, Aiken, South Carolina.

Schlegel ML, P Reiller, F Mercier-Bion, N Barre´, and V Moulin. 2006. "Molecular environment of iodine in naturally iodinated humic substances: Insight from X-ray absorption spectroscopy". Geochimica et Cosmochimica Acta **70**:5536–5551.

Summers RS, F Fuchs, and H Sontheimer. 1988. "The fate and removal of radioactive iodine in the aquatic environment. In:Aquatic Humic Substances, pp. 623-636. Chapter 35.

Toyohara M., M Kaneko, H Ueda, N Mitsutsuka, H Fujihara, T Murase, and N Saito. 2000. "Iodine sorption onto mixed solid alumina cement and calcium compounds". J. Nucl. Sci. Technol. **37**: 970-978.

Velichkina NS, TV Vlasova, A V Kalashnikov, and V Y. Kol'tsov. 2014. "Extraction of Iodine from Mother Liquors Formed as Industrial Waste with Activated Carbons." *Russian Journal of Applied Chemistry*, **Vol. 87**, No. 7, pp. 994−997.

This page intentionally left blank

Appendix D. Comparison of Iodine Geochemical Behavior in Oxidized and Reduced Cementitious Materials

Iodine has been shown to have similar apparent diffusion coefficients in reduced cementitious materials as Na, NO_3^- and NO_2^- (Um et al. 2016), suggesting that its migration through this material is not attenuated. This is contrary to other studies conducted with non-reduced cementitious materials, where iodine was significantly attenuated (Serne et al. 1992; Ochs et al. 2016). Serne et al. (1992) measured effective diffusion coefficients, D_a, in reducing and oxidizing cementitious waste formulations. The oxidized samples had D_a values of 1E-10 to 3E-9 cm^2/s and the reduced samples had D_a values 2E-8 to 8E-8 cm^2/s. The oxidized, but not the reduced samples were attenuated with respect to Na. Also, there have been several studies conducted with non-reduced cementitious materials that have demonstrated measureable iodine sorption via ion exchange and coprecipitation in the salts and mineral phases (Ochs et al. 2016).

One likely factor contributing to this difference in sorption is iodine speciation (Figure D-1). The line separating IO_3^- from I^- represents where these two species exist at 50:50 ratios. In BFS-free material, the Eh is greater than in BFS containing materials, which promotes a relative increase in IO_3^- concentrations. This greater reactivity can be partly attributed to the greater hard-hard ion-ligand coordinate chemistry that can be attributed to iodate compared to iodide. Another attribute of IO_3^- that makes it more reactive in cement chemistry is that it has several similar physical and chemical attributes with carbonate, enabling the opportunity for coprecipitation and solid phase substitution into carbonate phases.

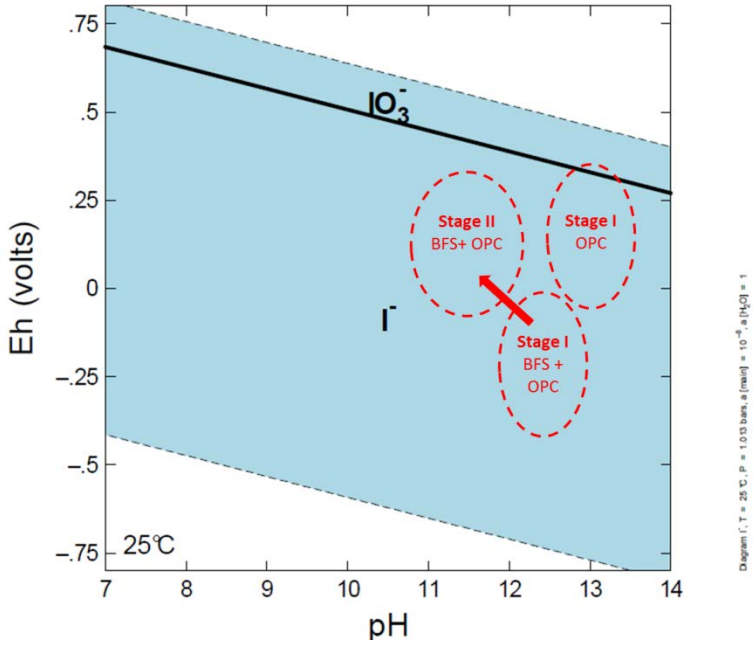

Figure D-1. Iodine speciation and pH-Eh zones where oxidized Stage I (Stage I OPC), reduced Stage I (Stage I BFS+OPC), and reduced Stage II (Stage II BFS+OPC) predominate. Iodine in oxidized cementitious materials is expected to have a greater proportion of IO_3^- than reduced cementitious materials.

This page intentionally left blank

Appendix E. Calculating D_a Values Using K_d Values: Comparison of Measured vs. Calculated Values.

Apparent diffusion coefficients (D_a), describe the rate of diffusion of a COPC through a monolith and accounts for several fundamental processes, including: molecular diffusion coefficient (D_m, which is the diffusion of molecules driven by concentration gradients measured in an open beaker), effective diffusion coefficient (D_e, which is how COPC move through a porous media, without any interactions with the porous media), and retardation (R, which accounts for sorption to the porous media surfaces; it's the ratio of the velocity of water divided by the velocity of the COPC). In turn, R is related to K_d.

$$D_a = \frac{D_e}{R}$$

$$R = 1 + \frac{\rho_b K_d}{\eta}$$

where ρ_b and η are bulk density and porosity. Below are D_a values estimated using the above equations, and K_d, ρ_b, and η values (Table E-2).

Table E-1. Apparent Diffusion Coefficients for Stage I (D_a; cm^2/s): Oxidizing and Reducing Cementitious Materials

COPC	Reducing			Oxidizing			Comments
	Best	Min	Max	Best	Min	Max	
Cr	8E-14	8E-15	9E-13	3E-09	1E-09	1E-08	Reducing: Min and Max values from Cantrell et al. (2016) and Best value is the geometric mean of the Min and Max. Oxidizing: D_a values were based on K_d values; calculations presented in Table E-2.
Cs	3E-09	1E-09	2E-08	3E-09	1E-09	2E-08	Reducing and Oxidizing: D_a values were based on K_d values; calculations presented in Table E-2.
Hg	2E-11	6E-12	1E-10	4E-11	1E-11	2E-10	Reducing and Oxidizing: D_a values were based on K_d values; calculations presented in Table E-2.
I	4E-09	2E-09	1E-08	1E-09	6E-10	3E-08	Oxidizing: Under oxidizing conditions iodine tends to bind to cementitious materials more strongly (See Appendix D). D_a values were based on K_d values; calculations in Table E-2. Reducing: Based on Cantrell et al. (2016), assumed no sorption. $D_a = D_e$.
N	4E-09	2E-09	1E-08	4E-09	2E-09	1E-08	Reducing and Oxidizing: Based on Cantrell et al. (2016), assumed no sorption. $D_a = D_e$.
Sr	1E-11	3E-12	6E-11	1E-10	3E-11	6E-10	Sr binds to cement by substituting for Ca in various cementitious phases. It can also form sparingly soluble phases when sulfate is present in sufficient concentrations. Reduced and Oxidized: Sr typically has a moderately low K_d in cementitious environments, however when sulfate concentrations are high, $SrSO_4$ precipitates, as was likely the case here. $SrSO_4$ has a solubility of 3.2E-07 M (strontium sulfite solubility product is even lower, $SrSO_3$ k_s = 4E-08 M). Additional research needs to be performed with actual SDF samples because Sr solubility is not detected when Sr is simply added to saltstone. Large Sr sorption noted under reducing conditions also. Almond and Kaplan (2011) measured desorption K_d values from actual Saltstone cores recovered from the Saltstone Disposal Facility that were 5728 mL/g under oxidizing conditions and 737 mL/g under reducing conditions (sulfate converted to sulfide which does not bind Sr as well). Sr D_a values were calculated based on the K_d values. K_d values under reducing conditions are greater than under oxidizing conditions because the Sr was observed to precipitate as a sulfide (See Tables 8-4 and 8-5).
Tc	3E-11	6E-12	2E-10	4E-09	2E-09	1E-08	Reduced: Min and Max values from Cantrell et al. (2016) and Best value is the geometric mean of the Min and Max. Oxidized: Based on the assumption that no sorption occurs. D_a values set to the N D_a values reported by Cantrell et al. (2016).
U	2E-16	6E-17	6E-16	6E-12	3E-12	6E-11	Reduced: Min and Max values from Cantrell et al. (2016) and Best value is the geometric mean of the Min and Max. Oxidized: D_a values were based on K_d values; calculations presented in Table E-2.

[(a)] EPA 1315 tests are conducted under conditions that would best be described as Stage I. There is not data appropriate to estimate Stages II and Stages III values. Therefore, it will be assumed that D_a values remain constant. While it is reasonable to expect the D_a values to change with cement aging, there is not sufficient data to create such a data set.
[(b)] To make the data set consistent with the measured D_a values (as reviewed in Cantrell et al. (2016; "Secondary Waste Fly Ash-Based Cast Stone"), all D_a values estimates were based on Stage I K_d values.

Table E-2. Apparent Diffusion Coefficients Estimated by Recommended K_d Values.

COPC	Best/Min/Max	Redox	K_d (mL/g)	R (unitless)	Best/Min/Max	Calc D_a (cm^2/s)
Cr	Best	Ox	3	15	Best	2E-09
	Min	Ox	0.3	2	Max	1E-08
	Max	Ox	6	30	Min	1E-09
Cs	Best	Ox	2	11	Best	3E-09
	Min	Ox	0.2	2	Max	2E-08
	Max	Ox	4	20	Min	1E-09
Hg	Best	Ox	300	1447	Best	2E-11
	Min	Ox	30	146	Max	2E-10
	Max	Ox	600	2893	Min	1E-11
I	Best	Ox	4	20	Best	1E-09
	Min	Ox	0	1	Max	3E-08
	Max	Ox	10	49	Min	6E-10
Sr	Best	Ox	90	435	Best	7E-11
	Min	Ox	10	49	Max	6E-10
	Max	Ox	200	965	Min	3E-11
Tc	Best	Ox	0.8	5	Best	6E-09
	Min	Ox	0	1	Max	3E-08
	Max	Ox	2	11	Min	3E-09
U	Best	Ox	1000	4821	Best	6E-12
	Min	Ox	100	483	Max	6E-11
	Max	Ox	2000	9641	Min	3E-12
Hg	Best	Red	500	2411	Best	1E-11
	Min	Red	50	242	Max	1E-10
	Max	Red	1000	4821	Min	6E-12
Sr	Best	Red	1000	4821	Best	6E-12
	Min	Red	100	483	Max	6E-11
	Max	Red	2000	9641	Min	3E-12

[a] Estimates used in Table E-1

Table E-3. Comparison of Measured Caststone D_a Values Reported by Cantrell et al. (2016) with D_a Estimated Using K_d Values.

COPC		Recommended Reducing K_d Stage I[c] (cm^3/g)	Best Density/Best Porosity[a]	*R*		$D_a(calc)$[b] (cm^2/s)	D_a Cantrell et al. (2016)[d] (cm^2/s)	Is $D_a(calc)$ within an order of magnitude of measured D_a values?
Cr	Best	1000	4.82	4821	Best	6E-12	8E-13	Yes, $D_a(calc)$ is larger (pessimistic-bias)
Cr	Min	100	4.82	483	Max	6E-11	8E-15	No, $D_a(calc)$ is larger (pessimistic-bias)
Cr	Max	2000	4.82	9641	Min	3E-12	9E-13	No, $D_a(calc)$ is larger (pessimistic-bias)
Tc	Best	1000	4.82	4821	Best	6E-12	3E-11	No, $D_a(calc)$ is larger (pessimistic-bias)
Tc	Min	100	4.82	483	Max	6E-11	6E-12	
Tc	Max	2000	4.82	9141	Min	3E-12	2E-10	Yes
U	Best	5000	4.82	24101	Best	1E-12	2E-16	No, $D_a(calc)$ is larger (pessimistic-bias)
U	Min	1000	4.82	4821	Max	6E-12	6E-17	
U	Max	10000	4.82	48201	Min	6E-13	6E-16	No, $D_a(calc)$ is larger (pessimistic-bias)

[a] Best bulk density = 1.59 g/cm^3; Best porosity = 0.33
[b] D_e = 3E-8 cm^2/s; used to calculate D_a from *R*.
[c] K_d values from Table 8-4 and Table 8-5.
[d] D_a values were taken from Table 3.1 – "Secondary Waste Fly Ash-Based Cast Stone" (Cantrell et al. 2016).

This page intentionally left blank

Distribution:

T. B. Brown, 773-A
B. T. Butcher, 773-42A
M. E. Cercy, 773-42A
A. D. Cozzi, 999-W
D. A. Crowley, 773-43A
K. L. Dixon, 773-42A
D. E. Dooley, 773-A
A. P. Fellinger. 773-42A
S. D. Fink, 773-A
G. P. Flach, 773-42A
C. C. Herman, 773-A
D. T. Hobbs, 773-A
E. N. Hoffman, 999-W
J. E. Hyatt, 773-A
D. I. Kaplan, 773-42A
K. M. Kostelnik, 773-42A
W. P. Kubilius, 999-W
D. Li, 773-42A
B. B. Looney, 773-42A
D. A. McGuire, 773-42A
R. L. Nichols, 773-42A
T. O. Oliver, 773-42A
F. M. Pennebaker, 773-42A
R. R. Seitz, 773-42A
G. N. Smoland, 773-42A
A. L. Washington, 773-42A
W. R. Wilmarth, 773-A
Records Administration (EDWS)

Washington River Protection Solutions
P. A. Cavanah
K. P. Lee
D. J. Swanberg

DOE – Office of River Protection
G. L. Pyles

Pacific Northwest National Laboratory
G. Smith
J. H. Westsik, Jr.
R. J. Serne

Intera
R. Andrews
M. Apted
R. Arthur
B. Paris
R. Senger